CRUSHING

CRACKING

ICE STRUCTURE INTERACTION AT THE WEST COAST OF SWEDEN

A comparison of existing guidelines and simplified finite element analyses

Master's thesis in the Master's Programme Structural Engineering and Building Technology

LINNÉA PERSSON
MAJA SWERRE

ICE STRUCTURE INTERACTION AT THE WEST COAST OF SWEDEN

A comparison of existing guidelines and simplified element analyses

Master's Thesis in the Master's Programme Structural Engineering and Building Technology

LINNÉA PERSSON

MAJA SWERRE

Department of Architecture and Civil Engineering
Division of Structural Engineering
Concrete Structures
CHALMERS UNIVERSITY OF TECHNOLOGY
Gothenburg, Sweden 2018

ICE STRUCTURE INTERACTION AT THE WEST COAST OF SWEDEN
A comparison of existing guidelines and simplified element analyses
Master's Thesis in the Master's Programme Structural Engineering and Building Technology
LINNÉA PERSSON
MAJA SWERRE

Department of Architecture and Civil Engineering
Division of Structural Engineering
Concrete Structures
Chalmers University of Technology
SE-412 96 Göteborg
Sweden
Telephone: + 46 (0)31-772 1000

Cover:
Illustration of the two studied failure modes of the ice sheet, i.e. crushing and cracking
Department of Architecture and Civil Engineering
Göteborg, Sweden, 2018

I

ICE STRUCTURE INTERACTION AT THE WEST COAST OF SWEDEN

A comparison of existing guidelines and simplified finite element analyses

Master's thesis in the Master's Programme Structural Engineering and Building Technology

LINNÉA PERSSON
MAJA SWERRE
Department of Architecture and Civil Engineering
Division of Structural Engineering
Concrete Structures
Chalmers University of Technology

ABSTRACT

Structures in water need to be designed to resist ice loads, and the Swedish standards and guidelines that exist today to support the determination of these loads are insufficient. Thus, the industry has an interest in developing these standards to simplify the design of structures and find a general determination of ice loads. The aim of this work was to investigate how different column configurations in the Swedish west coast marine environment are influenced by ice load, by a comparison between simplified finite element analyses and current Swedish guidelines.

A literature study reviewed the main physical properties of ice and how these could be translated into ice loads. Ice structure interactions were also studied, together with how these have been modelled before, in order to find a realistic but simplified way to model the interaction using finite element analyses. Two different finite element models were set up: ice interaction with one single column and ice interaction with multiple columns, where the columns were considered to be infinitely stiff. The studied failure modes for both models were cracking and crushing of the ice sheet.

The results from the analyses showed that larger column widths generated larger ice loads. The distance between the columns influenced the governing failure mode; a larger distance resulted in crushing, whereas a smaller distance resulted in cracking and a smaller ice load. The range of numerical results was 12 – 630 kN. The design values from the guidelines also showed a wide range of ice loads, between 2 – 1 680 kN, as well as a high dependency of the column width. Some of the analytically calculated ice loads gave very high and conservative values in comparison with the numerical results, while others gave constantly lower loads. Some values from the guidelines were constant, and thus showed sporadic agreement with different FE results. The analytical design that, generally, agreed with the FE results was one from Vägverket (1987) which is based on the crushing strength, the impact area, and a shape factor depending on the aspect ratio.

Key words: Abaqus, Cracking, Crushing, Failure of Ice, Ice loads, West coast of Sweden, XFEM

Interaktioner mellan is och konstruktioner på Sveriges västkust

En jämförelse mellan svenska rekommendationer och förenklade finita elementanalyser

Examensarbete inom masterprogrammet Konstruktionsteknik och byggnadsteknologi

LINNÉA PERSSON
MAJA SWERRE
Institutionen för Arkitektur och samhällsbyggnadsteknik
Avdelningen för Konstruktionsteknik
Betongbyggnad
Chalmers tekniska högskola

SAMMANFATTNING

Konstruktioner i vatten måste dimensioneras för att motstå islaster och de svenska standarder och rekommendationer som finns idag för att bestämma dessa islaster är otillräckliga. Därför finns det ett intresse från samhällsbyggnadsbranschen att utveckla dessa standarder för att förenkla dimensioneringen av konstruktioner i vatten samt att hitta ett mer generellt sätt att bestämma islaster på. Syftet med denna studie var därför att undersöka hur olika pelarkonfigurationer, i vattnet utanför Sveriges västkust, påverkas av islaster, genom att göra en jämförelse mellan förenklade finita elementanalyser och nuvarande svenska rekommendationer.

Genom en litteraturstudie fastställdes isens fysiska egenskaper och hur dessa egenskaper kan omvandlas till islaster. Olika interaktioner mellan is och konstruktioner studerades också, tillsammans med hur dessa tidigare har analyserats i finita elementprogram för att kunna skapa en förenklad, men realistisk, finita elementmodell. Två olika modeller skapades och studerades. En modell där ett isflak stöter samman med en pelare och en modell där ett isflak stöter samman med ett flertal pelare. Samtliga pelare, i båda modellerna, antogs vara oändligt styva. De studerade brottmoderna var uppsprickning och krossning av isflaket.

Resultaten från analyserna visade att en större pelarbredd genererade en större islast. Brottmoden påverkades av avståndet mellan pelarna, där ett större avstånd resulterade i krossning av isflaket medan ett mindre avstånd resulterade i uppsprickning samt en lägre islast. Spannet av de numeriska resultaten var 12 – 630 kN. Dimensioneringsvärdena, enligt befintliga standarder och rekommendationer, gav en stor variation av islaster, mellan 2 – 1 680 kN, där lasten influerades av pelarbredden. I en jämförelse med de numeriska resultaten var några av de analytiska värdena stora och konservativa medan andra genererade lägre värden. Vissa av islasterna från rekommendationerna var konstanta, och visade därmed sporadisk överenstämmelse med olika FE resultat. En av islasterna, enligt dimensioneringsrekommendationen från Vägverket (1987), gav generellt bäst överenstämmelse och den är baserad på isens krosshållfasthet dess sammanstötningsarea samt en formfaktor som i sin tur beror på relationen mellan isens tjocklek och pelarens bredd.

Nyckelord: Abaqus, isens brottmod, islaster, krossning, sprickning, Sveriges västkust, XFEM

II

Contents

Preface

This Master's Thesis was carried out during the spring of 2018 at the Department of Civil and Environmental Engineering, Division of Structural Engineering at Chalmers University of Technology.

The initial aim and main purpose of the thesis's was proposed by Mr Emil Lindqvist at ÅF Infrastructure, who was supervisor of the thesis. Therefore, a thank is directed towards Emil Lindqvist for his guidance and support throughout the work. A thank is also addressed to ÅF's department of Infrastructure in Gothenburg for the possibility to carry out our Master's Thesis at their office, for the nice conversations during the breaks and the motivation given from all employees.

A particular thank is directed to our examiner Professor Karin Lundgren at the Division of Structural Engineering at Chalmers University of Technology, for all your commitment and comments, guidance and support you have given us with such carefulness throughout the thesis.

Next, we would like to thank our opponents, Michaela Munther and Josefine Runebrant, who with fresh eyes gave new inputs during the process, helping us improve our work while enjoying a "fika".

Finally, we would like to thank each other for time we spent on this Master's thesis, it would not have been the same otherwise. Also, a huge thanks to our fellow students at the masters programme Structural Engineering and Building Technology, we are finally there!

Gothenburg, June 2018

Linnea Persson

Maja Swerre

Notations

Abbreviations and explanations of words

Aspect ratio	A ratio of the structure width divided by the ice thickness
Brine	Liquid water with high salinity
Brine channel	Vertical channels of brine in ice created when salt is expelled during the formation of sea water ice
CPS4R	A 4-node bilinear plane stress quadrilateral, reduced integration, hourglass control
EKS10, BFS 2015:6	National board of housings design rules, given out by Boverket
ICE-1	Natural occurring ice on Earth
Ice floe	A sheet of ice floating in water
Ice sheet	Glacial ice which covers more than 50 000 km^2
In-situ ice	Ice before its subjected to any load
MHW	Mean High Water, average of the years highest water level
MLW	Mean Low Water, average of the years lowest water level
Nlgeom	Nonlinear geometries
NVF	Nordic Road Engineering Association
Pure ice	Ice without imperfections e.g. air, objects or chemicals
SOU1961	State load regulations of 1960th
TDOK 2016:0203	Guideline of bridge design from Trafikverket
TDOK 2016:0204	Requirement of bridge design from Trafikverket
Trafikverket	Swedish Transport Administration
TRVFS	Swedish Transport Administrations statutes
VV 1987:43	Ice pressure against bridge support, from (Vägverket, 1987)
Vägverket	Swedish Road Administration (predecessor to the Swedish Transport Administration)
XFEM	Extended finite element method

Roman upper case letters

A	Area of an ice floe	m^2
C_1	Shape factor w.r.t. aspect ratio	-
C_2	Shape factor w.r.t. sharp edge	-
C_3	Shape factor w.r.t. inclination of edge	-
C_d	Reduction factor for wind and current	-

E	Young's modulus	Pa
G_F	Fracture energy	N/m
H	Height of the modelled ice sheet	m
I_1	Ice load from fixed ice cover perpendicular to the water flow	N
I_2	Ice load from a moving ice sheet parallel to the water flow	N
$I_{h,w/c}$	Horizontal ice pressure induced by wind or current	N
$I_{h,crush}$	Maximal static horizontal ice load with regard to the crushing strength of ice	N
L_1	Distance to first adjacent support	m
L_2	Distance to second adjacent support	m
L_{tot}	Total length of the modelled ice sheet	m
R_1	Ratio of the height divided by the total length	-
R_2	Ratio of the distance between columns divided by the column width	-
U	Free stream velocity	m/s

Roman lower case letters

a	Structure/column height	m
b	Structure/column width	m
i_1	Distributed ice load perpendicular to the water flow	N/m
i_2	Distributed ice load parallel to the water flow	N/m
k_1	Shape factor w.r.t. the shape of the column	-
k_2	Contact factor w.r.t. the movement of ice	-
k_3	Aspect ratio factor	-
l	Distance between columns	m
t	Ice thickness	m
v	Velocity of ice sheet	m/s

Greek lower case letters

α	Edge inclination	°/rad
β	Support inclination	°/rad
$\dot{\varepsilon}_{D/B}$	Transition strain rate between ductile and brittle behaviour	s^{-1}
ε_{pl}	Plastic strain	-
ρ	Density	kg/m^3
σ_c	Compressive/crushing strength	Pa
σ_t	Tensile strength	Pa
σ_y	Yield stress	Pa
v	Poisson's ratio	-

1   Introduction

Bridge supports, pier columns and other structures in water can be subjected to ice loads. These ice loads will cause forces on the structures which could lead to failure. The magnitude and the action of the ice loads are influenced by parameters such as structure type, structure shape, type of ice formation, thickness of the ice cover and angles between ice loads and structures. Furthermore, the local environment will decide type of formation and thereby the ice action. Therefore, parameters such as salinity in the water, temperature in the water and in the ice are important aspects to consider when designing a structure against ice loads (Bergdahl, 1977). Due to the number of influencing parameters there is a high uncertainty when it comes to predict the magnitude of the ice load (Chandrasekaran, 2015).

In Sweden there are certain rules given in documents that needs to be followed when designing against ice loads. The first three documents are requirements that needs to be followed by law, see Figure 1-1. These are Eurocode (EN 1991, 2003) together with *National board of housings design rules* (EKS10, BFS 2015:6) (Boverket, 2016), applied for structures in general, and *Swedish Transport Administrations statutes* (TRVFS 2011:12) (Trafikverket, 2011), applied for bridges. In addition to these, there are certain requirements and guidelines for specific structures which are exposed to ice loads, see Figure 1-1. For bridges, there are two guidelines published by Swedish Transport Administration (Trafikverket) which are called *Requirements Bridge Design* (TDOK 2016:0204) and *Guideline Bridge Design* (TDOK 2016:0203). For hydropower dams there is a guideline published by Svensk Energi called *RIDAS 2012, Power companies guidelines for dam security* (RIDAS, 2012a).
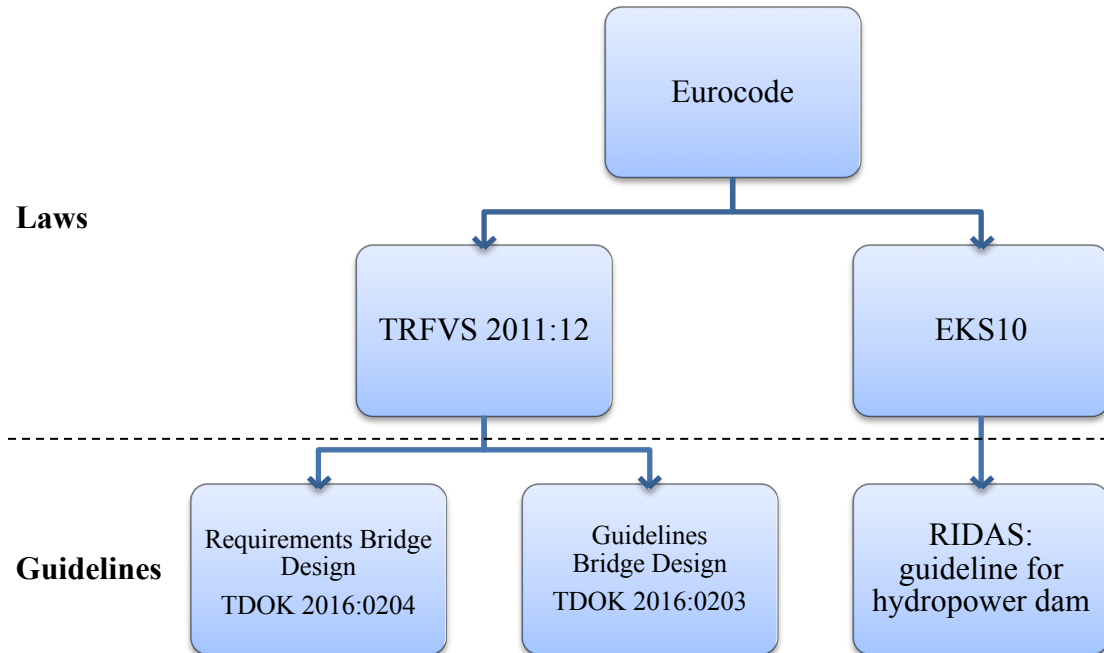
Figure 1-1.   Overview of design rules and guidelines concerning ice loads in Sweden today for bridges and hydropower dams.

In *Eurocode 1: Actions on Structures* (EN 1991, 2003), no guidance on the magnitude of ice pressure is given, neither concerning the effect on the structure nor on the design values of ice. Instead the reader is referred to its country's national annex, in Sweden: EKS10, BFS 2015:6 (Boverket, 2016) and TRVFS (Trafikverket, 2011). These Swedish annexes do not give any guidance either and refer further to the documents: *Requirements Bridge Design* (TDOK 2016:0204), *Guideline Bridge Design* (TDOK 2016:0203) and RIDAS. In TDOK 2016:0204 a minimum design value of the ice pressure is given (Trafikverket, 2016a). In TDOK 2016:0203 it is stated that the value in the requirement could only be used for some specific cases (Trafikverket, 2016b). Otherwise, the ice load should be investigated separately with respect to local climate and conditions together with the geometry and location of the structure. The reader is then referred to a document published by Swedish Road Administration (Vägverket), called *Ice pressure against bridge supports* (VV 1987:43), which states how to determine the ice pressure for some common cases, see Section 4.4 (Vägverket, 1987). In RIDAS (2012b) an ice pressure intensity is given as 50–200 kN/m depending on geographical location, altitude and local conditions. It also states that the ice thickness should be set to either 0.6 meter or 1.0 meter, depending on geographical location. Furthermore, RIDAS also mentions that the ice pressure could be higher depending mainly on local conditions.

To conclude, there are no standard or guideline on how ice loads generally should be predicted in Sweden today. Instead all design cases should be investigated separately if they are not case specific which could simplify the calculations. Thus, there is a need for a guideline of how ice loads magnitude can be predicted for columns in water with different distances between them in Swedish climate. Accordingly, this thesis investigates how these ice loads can be determined.

1.1 Aim and objectives

The aim of this study was to investigate how structures in the Swedish west coast marine environment are influenced by ice loads.

To answer the aim, the following questions were formulated:

- Which are the main physical properties of ice and how can ice loads be described with these?
- Which parameters affect the ice load and should be included when modelling it?
- Can ice be modelled in a realistic way using finite element (FE) analyses in order to compare the effects of ice load on different configurations of columns?
- What are the differences between modelled ice loads and the design values according to the Swedish guidelines?

1.2 Method

This study was divided in four different parts:
- literature study,
- finite element (FE) analyses,
- analytical calculations, and
- comparison between the three.

In the literature study, previous research and information about ice and its properties were studied. This included its material and mechanical properties, different formations of ice as well as influencing parameters on ice and its failure modes. How ice structure interactions has been modelled using FE analysis in previous studies was also collected in order to be able to model it in a realistic way.

The FE analyses were performed in a FE program called Abaqus/CAE 2017. Two different models were set up in order to simulate the interaction between an ice sheet and structures in water. The first models simulates when ice interacted with one single column, shown in Figure 1-2 a). The second model, shown in Figure 1-2 b), simulated when ice interacted with multiple columns. In order to limit the model size, and thereby also the computer time, only two columns were modelled together with the use of symmetry lines.

a) Single column
b) Multiple columns
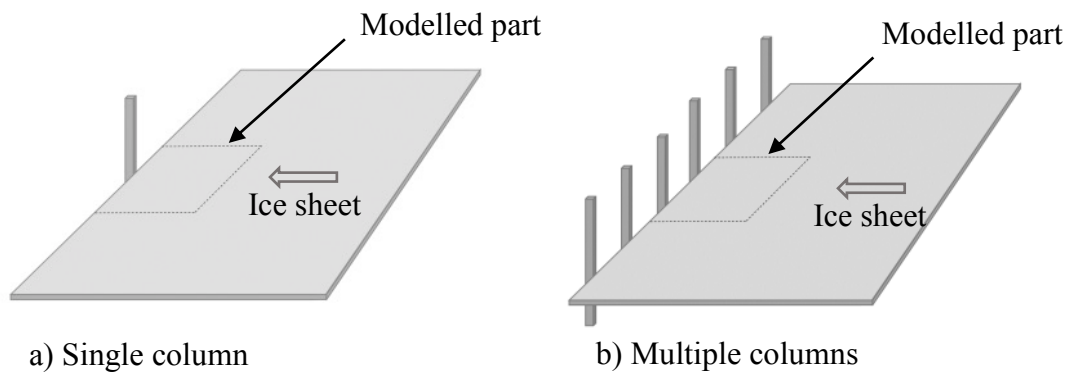
Figure 1-2.   *Ice interaction with a) single column b) multiple columns.*

For both models, the ice was the only modelled and analysed part. The columns were instead acting as loads on the ice sheet and considered to be infinitely stiff. This led to that the ice was not modelled as the moving object, as in reality, but instead the columns worked as a load which increased gradually until failure. The same material model of the ice was used for all analyses; an elastic-perfectly plastic material model, see Section 5.3.

Analytical calculations were done for all configurations in this study by using Swedish standards and guidelines that include ice loads. The analytical calculations were performed in MathCad with the same input values as in the FE analyses, as far as possible. Finally, the results from the FE analyses were compared with the analytical calculations, according to Swedish guidelines. The comparison was performed in order to conclude whether the values given in the guidelines were reasonable for the configurations which were simulated, but also to see if the ice sheet was modelled in a realistic manner with respect to the models limitations.

1.3   Limitations

The focus in the study was on ice at the Swedish west coast. Previously performed studies of the different properties of ice were investigated but no experiments were conducted on ice in this area. However, during modelling and analyses of the ice sheet, all parameters were set to realistic values with regard to the ice at the west coast with support from both research and guidelines.

The treated standards and guidelines in this study were:
- Eurocode (EN 1991, 2003),
- *Requirement Bridge Design*, TDOK 2016:0204 (Trafikverket, 2016a),
- *Guideline Bridge Design*, TDOK 2016:0203 (Trafikverket, 2016b),
- *Ice pressure against bridge supports*, VV 1987:43 (Vägverket, 1987),
- *RIDAS* (RIDAS, 2012a),
- *Recommendations for design of offshore foundations exposed to ice loads* (Fransson and Bergdahl, 2009), and
- *Eurocode for design of concrete dam* (Andersson *et al.*, 2016).

Standards and guidelines from other countries were not considered in the study.

The study was limited to two different cases of quadratic column configurations. The first case was an ice interaction with one single column, which acted as a reference case to confirm that the modelled ice responded in a correct manner. The second case was an ice interaction with multiple columns. How an ice sheet would interact with other type of configurations and structures was not treated. Only the horizontal ice load during an interaction was studied and the influence of a shoreline, working as an counteracting force, was not taken into consideration.

The studied interactions were only modelled for short term loading, which indicated that the model could only respond correct up to failure and not show the progressive damage after failure. In this study the focus were on two types of failure modes; cracking and crushing. Thus, the modelled ice sheet could not describe other types of failure modes.

2 Configurations and modes of ice

Ice covers approximately 13% of the northern hemisphere (Chatterjee and Chattopadhyay, 2017). Since ice is a geophysical material, different stresses and behaviour will occur depending on both external and internal parameters. The first step to understand action of the ice is to examine the global formation and its internal structure.

Fransson (2009) states that the only natural occurring ice on Earth is known as ICE-1. It consists of hexagonal crystals that can vary in shape and size, from less than one millimetre to several meters wide. Other types of ice have been found in laboratories and consist of different crystal structures and varying densities. Chemically clean water does not freeze until –40°C but because of impurities in the water the freezing point of natural water is 0°C (Fransson, 2009). When freezing, the volume of water increases with 9% which can lead to high pressure if it is confined. Conditions such as water movement, temperature gradient, pressure and absolute temperature influence the quality of ice and determinate its properties.

This chapter explains how ice can form in seawater, fresh water and brackish water. Furthermore, the chapter treats the modes of ice configurations which can form at the Swedish west coast. The chapter also treats its properties as well as the extent and recurrence time.

2.1 Types of ice

Ice can be divided into first- and multiyear ice. First year ice can have several different appearances depending on the condition where it is formed and in which type of water it is formed. Multi-year ice is, by Fransson (2009), defined as ice that has survived two summer seasons, this only occurs at the polar regions. Since multiyear ice only occurs near the polar regions and not at the west coast of Sweden, it will not be treated further in this study. The following sections treat the formation of first year ice in different types of Swedish water climate.

2.1.1 Ice in seawater

When the temperature drops to freezing point in the water and the air temperature is constantly low, ice crystals will form in the water and eventually form a continuous ice cover on the surface (Sand, 2008). This is known as primary ice. In exceptionally calm water this layer can stay intact and reach a thickness of more than 30 centimetres (Fransson, 2009; Timco and Weeks, 2010). Sand (2008) and Timco and Weeks (2010) describe how this ice formation progresses downwards and as salt is excluded, brine channels are formed vertically in between the ice. Brine is water with too high salinity to freeze and it gets trapped in small channels between the ice crystals during the freezing process, known as brine channels. The salt water under the ice is replaced by less salinity water rising from the bottom and the ice formations becomes vertical. This is known as columnar ice and a typical vertical section of this ice type is illustrated in Figure 2-1 (Fransson, 2009).
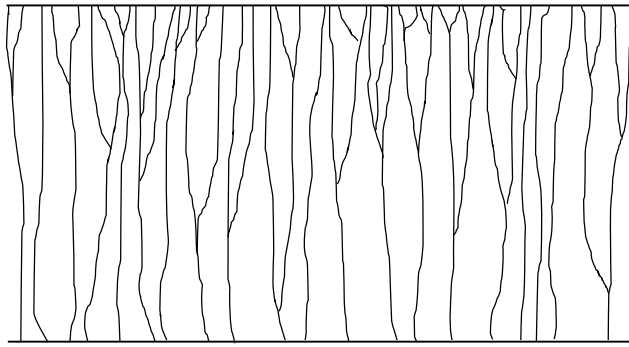
Figure 2-1.   *A typical cross section through the thickness of columnar ice with the brine channels visualised (modified from Bergdahl (1977)).*

Sand (2008) explains how the ice crystals will orient themselves depending on the current. If the water has a variable current the crystals will orientate in all directions in the plane and the ice will then become transversely isotropic. In cases where the current is steady the crystals will orientate in the current direction. (Timco and Weeks, 2010) instead explain the crystal orientation to be parallel to the direction of heat flow.

First year ice in seawater is influenced by the forces it is subjected to (Sand, 2008). Near the shore the ice is often flat and uniform. Further out, currents and wind have a larger impact resulting in ridging and rafting of the ice.

2.1.2   Ice in fresh water

Ice formation in fresh water usually starts with crystals at the surface which progress downwards (Vägverket, 1987; Fransson, 2009). Eventually, the crystals become vertical and can be as long as the thickness of the ice. The difference compared to seawater is that the ice cover has a constant thickness without any brine channels. In flowing fresh water the current prevents the ice sheet to form. Instead ice particles are formed as small rounded ice sheets known as pancake ice, see Figure 2-2 (Vägverket, 1987).
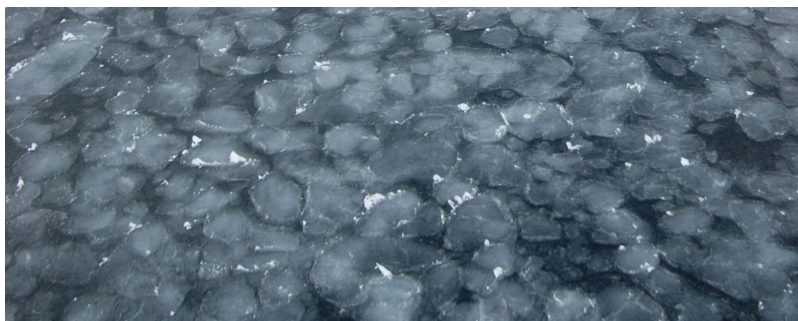
Figure 2-2.   *Pancake ice formed at the west coast of Sweden* (SMHI, 2017a).

2.1.3   Ice in brackish water

Fransson (2009) states that brackish water, as in the Baltic Sea, shows different properties than ordinary sea- and fresh water. In the northern parts of the Baltic Sea, the ice acts more like fresh water ice. Further out, where the salinity is higher, the ice

acts more like seawater ice (Fransson, 2009). Both pancake ice and columnar ice are formed in brackish water. The salt is not expelled from the ice to the same extent as for seawater which makes the ice more saline. Pancake ice is most common and contains more salt than columnar ice. The Swedish meteorological and hydrological institute, SMHI, (2017) describes the forming of pancake ice in brackish water in another way, where it forms several meters under the surface. A colder, less saline, brackish, layer lies above a more saline layer. The brackish water freezes in forms of ice pancakes and then floats up to the surface.

2.2 Modes of ice

As mentioned in Section 2.1, many ice formations exist which leads to a number of possible interactions with structures. Vägverket (1987) divided these interactions, and upcoming ice pressures, in six main categories:
- thermal ice pressure,
- ice pressure caused by water level variation,
- dynamic ice pressure from moving ice,
- ice pressure caused by wind and current,
- pressure from ice ridge, and
- vertical pressure from solid ice.

According to Vägverket (1987) these interactions are the most common ones and are therefore treated in the guideline *Ice pressure against bridge supports*. In this study the interactions possible on the west coast of Sweden has been treated. These are thermal ice pressure, moving ice sheet or floe, ice ridges and ice arching. The section includes the modes, their origin and parameters affecting their magnitude.

2.2.1 Thermal ice pressure

One way for ice to move and cause ice pressure is by thermal expansion or contraction. The expansion or contraction is caused by a temperature variation between the ice and the surrounding air temperature (Vägverket, 1987). Thermal ice pressure only occurs in lake and brackish seas, not in seawater. The reason is that ice with salinities above 5‰, have a negative thermal expansion coefficient, see Section 3.1 (Cox, 1983; Fransson and Bergdahl, 2009).

According to Bergdahl (1977), a thin ice sheet has a surface temperature of 0°C. The definition of a thin ice sheet is that its thickness is less than 100 millimetres (Fransson, 2009). If the air temperature starts to decrease the surface temperature will drop and the ice thickness will increase. The lower ice surface keeps a constant freezing-point temperature. Since the upper surface temperature is lower than the bottom, the ice sheets upper layer will contract and cause tensile stresses, creep and possibly even cracks. Furthermore, Bergdahl (1977) writes that the growth rate of the ice thickness normally is slow which leads to that the ice sheet can recover and deform elastically and/or viscously. However, if the temperature changes rapidly the ice cover will bend and cause tensile and compression stresses due to that free bending is restricted by the water surface. This bending can, if the tensile strength of the ice is reached, cause deep cracks in the ice cover.

Määttänen (1991) states that thermal ice pressure are complex and parameters dependency need to be viewed and related to each other. He mentions that a

structure's shape and size, type of foundation, its rigidity, mass and damping need to be considered in relation to the ice properties. This includes ice type, ice cover thickness, number of cracks and the velocity of the ice cover (if it is a moving ice sheet).

Over the years a lot of research has been made in the subject of influencing parameters on thermal ice pressure (e.g.Bergdahl, 1977; Vägverket, 1987; Sanderson, 1988; Azarnejad and Hrudey, 1998). Bergdahl (1977) performed research on how the physics of ice and snow affected the thermal pressure, and concluded that the magnitude of the thermal ice pressure depends on the following parameters:
- rate of temperature variation,
- ice condition,
- snow condition (mainly snow depth),
- the local climate,
- distance to and shape of the shoreline.

Bergdahl (1977) mentions that one of the most important parameters is the change rate of temperature. If the change rate of temperature is rapid, cracks and high pressures will occur, but if the change rate of temperature is low the ice will be able to handle the creep deformations. Furthermore, Bergdahl (1977) mentions that the change rate of temperature in the ice depends on:
- weather condition;
  - air temperature,
  - wind speed,
  - solar radiation,
  - depth of snow.
- thermal expansion coefficient of the ice,
- thickness of the ice cover,
- rheology of the ice,
- degree of restriction from the shores.

Since the magnitude of thermal ice pressure is affected by all of the parameters above, determination of the thermal ice pressure is complex (Bergdahl, 1977; Määttänen, 1991; Fransson, 2009).

2.2.2 Moving ice sheet or floe

The definition of an ice sheet is, according to (National Snow & Ice Data Center, 2018), a sheet consisting of glacial ice which covers more than $50\,000 \text{km}^2$, e.g. Greenland and Antarctica. However, this definition is not used in any literature concerning the subject, and this study will follow in the same manner, and an ice sheet will be defined as a larger region of ice floating in the water. An ice floe will describe a smaller ice part e.g. spalled of ice from a sheet and finally an ice cover will describe a continuous region of ice.

The driving forces of ice are wind, current and tidal variations (Fransson and Bergdahl, 2009). Which of the driving forces that are dominant depends on the local condition. As an example Fransson and Bergdahl mention that the driving forces in the Gulf of Bothnia is determined by wind, but in the Atlantic both tidal variations and currents influence the moving of ice sheets more than the wind. Another driving force is ships and shipping traffic, especially in waterways (Croasdale, 2012).

The ice pressure from a moving ice sheet, or floe, can act both in vertical and horizontal direction. The main pressure acts in horizontal direction and can be divided into static and dynamic pressure (Fransson and Bergdahl, 2009). The highest theoretical horizontal static pressure is reached right before the sheet starts to move but due to influence of creep deformations and cracks this never happens in reality. Despite these influences, Fransson and Bergdahl (2009) state that the magnitude of the horizontal ice load could be assumed to depend on the compressive strength of the ice, the impact zone and the degree of confinement. The horizontal dynamic ice pressure can result in crushing of the ice sheet if the driving forces are large enough. The magnitude of the pressure depends on the structure width, ice thickness, impact zone and degree of rigidity.

The vertical pressure is normally negligible for larger structures such as bridge columns and wind power foundations (Vägverket, 1987). For smaller structures, such as small piers, the vertical pressure can become relatively large and is therefore important. The magnitude of the vertical pressure on smaller structures depends on the ice cover thickness and will be limited by the shear strength of ice. The vertical force has its maximum value when an even and slow rise of the water level occurs.

In a report published by the US Army Corps of Engineers (2006) it is stated that the failure mechanism of a moving ice sheet depends on the temperature, the velocity of the ice sheet and if the structure is rigid or not. If an ice sheet interacts with a rigid structure the failure will be either brittle for high velocity rate or ductile for low velocity rate. However, if an ice sheet interacts with a non-rigid structure the failure mode could be an intermediate failure mode, a combination of both brittle and ductile failure, see Figure 2-3. To conclude, the three parameters that will affect the magnitude of the horizontal ice pressure are: temperature, velocity of the ice sheet and the level of rigidity of the structure.

Low ice velocity rate ⟶ High ice velocity rate		
Rigid structure	Ductile	Brittle
Flexible structure	Ductile	Alternating ductile or brittle / Brittle

Figure 2-3. *Failure response depending on the rigidity of the structure and the velocity of the ice sheet (modified from US Army Corps of Engineers (2006)).*

2.2.3 Ice ridges

According to Fransson and Bergdahl (2009) water and wind are the driving forces when ice ridges appear as they press together drifting ice into ridges. Ice floes are continuously broken and placed on top of each other. Fransson (2009) describes how this continues until the ridge reaches equilibrium and a new ridge is formed at a new location. Furthermore, he writes that they are often formed in shallow water when the ice floes collide with obstacles. The ridge is divided in the visible part above the water surface, known as the sail, and the much bigger part under the surface, called the keel (Fransson and Bergdahl, 2009). A typical pressure ridge, which forms when the ice sheet is 30 centimetres deep, can have a sail of 2 meters and a keel of 10 meters (Fransson, 2009).

An ice ridge is a strong formation and while small ridges often do not cause any problem larger ones can be of major concern both for structures and shipping. Both the keel and the sail are causing ice pressure on a structure at an ice structure interaction and has therefore a larger contact area than an ice sheets. The risk of a major impact on a structure is high because of the keel. Especially offshore structures and ships which need to navigate through the ice ridges during winter season (Leppäranta and Hakala, 1992; Fransson, 2009). Ice ridges are common in shallow waters and therefore often occur close to shore and in archipelagos (Leppäranta and Hakala, 1992).

2.2.4 Ice arching

An illustration of an ideal arch which could occur during an interaction between two obstacles and an moving ice sheet is presented in Figure 2-4. After impact, cracks starts to initiate in locations where the tensile strength is reached. The location of the cracks is determined by the geometry of the supports and the distance between them. The cracks are illustrated in Step 1. In Step 2, there is a possibility that an arch is formed. The shape and strength of the arch mainly depend on the compressive strength of the ice.

Step 1.   Cracks occur in location where the tensile strength is reached.

ice

Step 2.   The formed ice arch causes a horizontal force which needs to be resisted by the obstacles. The arch is stable if the compressive strength is not reached.

water

ice
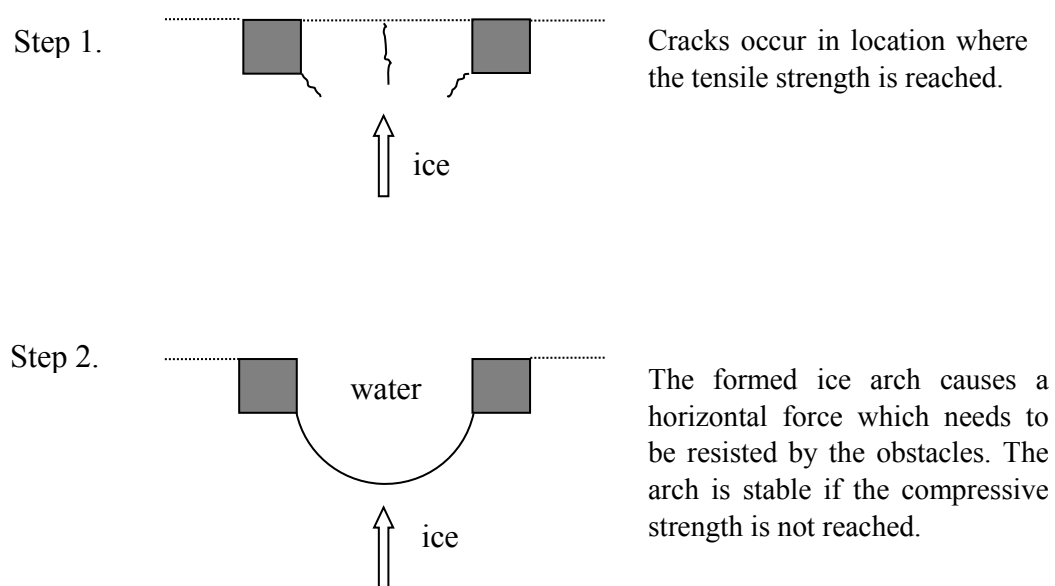
Figure 2-4.   An ideal arch forming between an interaction of two obstacles and a moving ice sheet.

A static ice arch can be formed if the conditions are right, both with the properties of the ice and the external parameters. The main parameter is the uniaxial compressive strength but the exact shape and strength of the arch is more complex, potentially depending on the arch's supports (Olason, 2016). To maintain a stable arch the ice also has to sustain the tensile stresses arising together with the compressive strength (Lemieux *et al.*, 2016).

An ice arch can also arise in channels during melting period due to melting and calving of the ice. The mechanics of the sea arches are according to Shroyer *et al.* (2017) dependent on the internal stresses of the ice. An arch leads to a reduction of flow of ice and water and the occurrence of an arch thereby effects the local water movements. These effects have been observed in Nares Strait between Greenland and Canada (Shroyer *et al.*, 2017). Ice arches can also arise in archipelagos where the islands act as supports of the arches (Olason, 2016). This has been documented both in Kara Sea and the Bay of Bothnia (Goldstein, Osipenko and Leppäranta, 2004).

The arching effect has been observed with fractured ice where ice floes travel and form arches at bridge supports and narrow channels. These observations have led to research, for example by Calkins and Ashton (1975) and Hara *et al.* (1993), where they tried to replicate the behaviour when ice floes create arches. The main objective of this research was to find a distance between the structures where ice arching would not occur with respect to the chosen size of the ice floes. The main result from Calkins and Ashton (1975) was an equation describing when arching occurred or not. The relationship depends on the supply rate and velocity of floes and the distance between two structures or the width of the channel.

Kato and Sodhi (1984) performed a test by interacting laboratory columnar ice with two cylindric formed structures. The objective was to see what influence the distance between the cylinders had on the failure mode and the magnitude of the ice force. They found that when the distance between two structures was less than four to five times the diameter of the structures, the ice force was affected. At wider distances the force was unaffected. One important factor for the type of failure was the velocity; at low velocities the ice would fail in buckling while at high velocities the ice would fail by crushing. When the structures were placed far apart the velocity had no impact on the ice force. Kato and Sodhi (1984) stated that the buckling failure depends on the aspect ratio, structure width divided by ice thickness, and at a high aspect ratio the governing failure mode will be buckling failure. The effect from the aspect ratio was highest when the structures were placed far apart. Then it was also observed that the measured buckling load corresponded to the calculated theoretical buckling. Kato and Sodhi (1984) concluded that the force can be seen as a distributed load if the structures are placed close together. The width is then taken as the distance between the structures together with their diameter. With this approximation the whole ice sheet will buckle in one mode instead of having several buckling zones, see Figure 2-5.
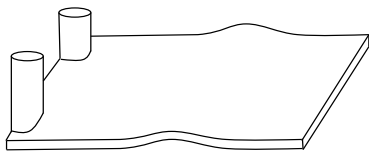
Figure 2-5.   Illustration how an ice sheet could buckle against two circular columns.

2.3   Ice on the west coast of Sweden

The sea Kattegat, on the west coast of Sweden, is saline but also receives brackish water from the Baltic stream. This results in a change of salinity in the water, from 15‰ in the southernmost part to 30‰ in the most northern parts (Tidlund *et al.*,

2017). Since the salinity in the water changes, the properties of the ice between the north and south also change. The thickness and extent, which also varies from year to year, of the ice sheet needs to be determined in order to be able to estimate the properties of the ice and by that also the magnitude of the ice pressure on the west coast.

2.3.1 Thickness and extent of the ice sheet on the west coast

The winter seasons in Sweden can, according to the Swedish Board of Shipping and Navigation, be divided into three classifications: severe, average and easy winters (Sjöfartsverket, 2015; Sjöfartsverket and SMHI, 2017). The main factor is the ice extent and according to definitions a severe winter includes ice coverage in the Bothnia Bay, larger part of the Baltic Sea, part of the west coast and the lake Vänern, see Figure 2-6 (Sjöfartsverket, 2015). During an average winter the Bothnia Bay is covered by ice, as well as the north part of the Baltic Sea, the majority of the coast in the central part of the Baltic Sea and the lake Vänern. An easy winter occurs when the extent of the ice is limited to the Bothnia Bay. Other parameters which are taken into account are the time period of ice coverage and the navigability due to wind and currents as well as local variations. This means e.g. that an easy winter could have ice coverage in other parts than the Bothnia Bay. To simplify, the west coast only have an ice cover during a severe winter (Sjöfartsverket, 2015).

Figure 2-6.   Waters in and around Sweden (modified from Google maps (2018))

Fransson and Bergdahl (2009) published the mean ice thicknesses during a severe, average and easy winter for Swedish water, see Table 2-1 (Sjöfartsverket, 1992). In the table it is shown that ice also was observed at the Swedish west coast during average winters. This can be explained by a different classification of winter seasons (Sjöfartsverket, 1992; Sjöfartsverket, 2015).

Table 2-1. Mean ice thickness in Skagerrak and Kattegat (Fransson and Bergdahl, 2009).

Severe winters [mm]		Average winters [mm]		Easy winters [mm]	
Open sea	Coastal sea	Open sea	Coastal sea	Open sea	Coastal sea
100–200	200–300	Ice free	100–150	Ice free	Ice free

2.3.2 Recurrence time of the sheet of ice on the west coast

Each year, the Swedish meteorological and hydrological institute (SMHI) together with Swedish board of Shipping and Navigation publish a summary of the winter ice season in Swedish water. The last summary is from the ice season 2016/2017 (Sjöfartsverket and SMHI, 2017). In the report a diagram shows the magnitude of maximum ice extent during each winter season from 1900 until 2017, see Figure 2-7. For the last 117 years, from 1900–2017, there has been 28 severe winter seasons, see Section 2.3.1 for definitions. This means that ice has been present on the west coast during 28 winter seasons. An estimation could be that ice will cover the west coast around 10–20% of all winters (Allt om Vetenskap, 2013). However, this do not mean that the whole west coast is covered by ice since the definition of a severe winter is that part of the west coast should be covered by ice.
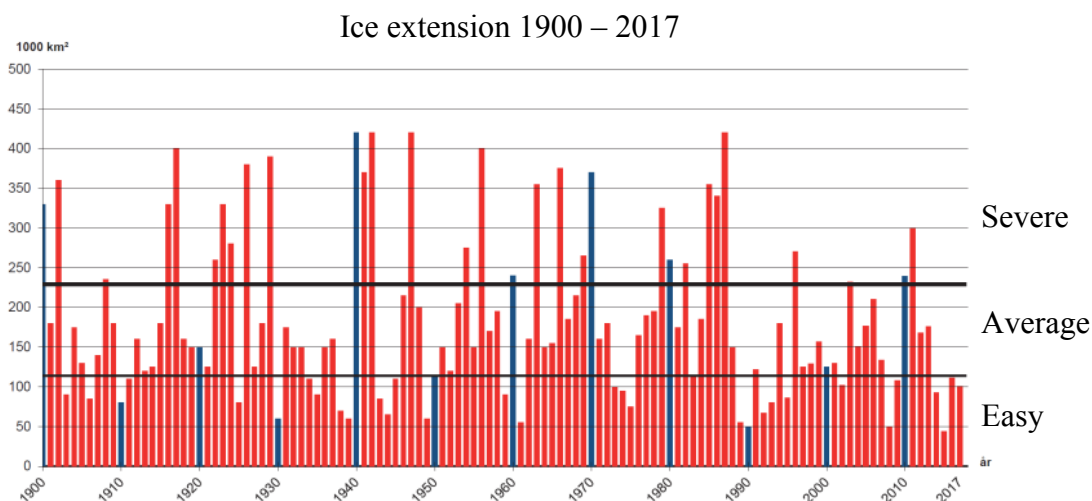
Figure 2-7. Ice extension 1900-2017 (modfied from Sjöfartsverket and SMHI, 2017).

The last severe winter season occurred in 2010–2011. According to SMHI (2011a) extended the ice at the west coast, where a thin ice sheet developed along the coast line of Halland all the way up to the south coast of Norway. From the end of January 2011 to middle of February 2011 was the sea at the west coast, more or less, covered with a solid ice sheet with a thickness of around 300 millimetres (SMHI, 2011b). The channel of Trollhättan and Göta river were also covered by a solid ice sheet with a varied ice thickness, 200 − 500 millimetres. However, SMHI (2011a) mentioned the

most of the ice were not located near the coast lines. The most severe winter, from 1900 until today, was in 1986–1987, where both the Bothnia Bay and Gulf of Bothnia were covered with more than 500 meters thick ice (Allt om Vetenskap, 2013). At the west coast the ice thickness varied between 50–200 millimetre.

3 Capacity and failure of ice

All types of material has a certain capacity which it can handle before it fractures. Since ice is a geophysical material, created by nature with its irregularities, the capacity of ice differs between ice types and formations as well as geographical location and external parameters. Ice can fail in many ways and the failure mode is thereby an important aspect. In this chapter, the material and mechanical properties of ice are treated. Furthermore, the failure of ice and influencing aspects on the failure are brought up.

3.1 Material and mechanical properties of ice

The difference in properties between sea- and fresh water ice are several. Generally, seawater ice has a lower compressive strength compared to fresh water ice (Vägverket, 1987; Sand, 2008). Although Vägverket (1987) implies that there are tests contradicting this and emphasize on the importance of geographical location. Ice properties differ a lot between the west and east cost of Sweden due to the fact that the east coast has brackish water.

Fransson (2009) states that this is why seawater freezes at a lower temperature than freshwater at the same depth, this is explained by the thermal expansion coefficient. Vägverket (1987) states that the thermal expansion coefficient for fresh water ice is positive and around five times higher than for steel. This will entail large pressure and high stresses during a temperature increase. As an example, at a temperature increase of 10°C, an ice sheet that is 100 meters long will increase with 5 centimetres (Vägverket, 1987). For seawater ice the thermal expansion coefficient is negative which will result in an ice volume decrease when the temperature increases (Vägverket, 1987).

However, research has shown that the thermal expansion coefficient for sea ice can be both positive and negative depending on salinity and temperature (Cox, 1983). As an example, an ice with a salinity of 5‰, first expands when cooled until –10°C and starts to contract as the temperature continuous to decrease. Johnson and Metzner (1990) explains the negative thermal expansion coefficient in seawater by a phase change between the brine and the pure ice. This leads to an increase in porosity which will create a negative pressure absorbs water into the brine system. The phenomenon is more evident at warmer temperatures, closer to 0°C, and consequently, the thermal expansion coefficient is of larger magnitude at this temperature, but still negative. At lower temperature, around –20°C the thermal expansion coefficient is almost neglectable (Johnson and Metzner, 1990b). Cox (1983) reject this phenomenon by stating that both the mass and volume will change and sea water ice can never be seen as a closed system, resulting in a non-valid explanation by Johnson and Metzner (1990). Cox (1983) conclusion is that the thermal expansion coefficient for sea water ice is positive, the same as for pure ice.

The following sections start by describing the material properties of ice; the density, elastic properties and friction coefficients. Further, the strength parameters are explained, including their dependence, and typical values.

3.1.1 Density

The density of the ice has big influence on the strength of the ice. Even small changes in density can change the buoyancy profoundly, according to Timco and Weeks (2010). The amount of brine drainage has a significant influence on the density and ice with small brine amount will have a higher density and values more similar to in-situ ice. This type of ice has not been subjected to any loads. Timco and Frederking (1996) calculated the ice density for gas free ice with different salinities at different temperature. At –30°C, the density range was 921-928 kg/m^3 for an ice with salinity of 0–10 ‰. The range increase at higher temperature and at –3°C it is instead 917–940 kg/m^3 for the same salinity conditions. In other words, the density increases with higher salinity at all temperatures although the range becomes larger at higher temperatures. Finally, Timco and Frederking (1996) proposed to use the value 920 kg/m^3 as an estimation for all first-year sea ice if no ice sample can be collected and tested.

3.1.2 Fracture energy

The energy absorbed during fracture of a material is noted as the specific fracture energy. The fracture energy could be used as a damage criterion, e.g. to simulate the brittle cracking behaviour. For ice, among other materials, this damage criterion is based on the "viscoelastic fictitious crack model", developed by Hillerborg, Modéer and Petersson (1976), which still is used by many ice researchers and engineers. Mulmule and Dempsey (1998) used Hillerborg et. al (1976) approach on sea ice and came to the conclusion that the fracture energy can be back-calculated, commonly used value with the back-calculation is G_F = 15 N/m (Weiss, 2001; Lu, Löset and Lubbad, 2012; Lu, Lubbad and Løset, 2015a; Lu *et al.*, 2016). This value is also based on field measurement by Mulmule and Dempsey (1999) where they tried to explain how the magnitude of the fracture energy influence the size of the specimen. Another scientist who investigated in this subject was Weiss (2001) who stated in his article, with information from previous research, that a measured fracture energy increases with increasing specimen size. However, at large scale this effect seems to be insignificant. With that information at hand a reasonable constant value for the fracture energy could be set to 15 N/m.

3.1.3 Elastic properties

According to Sand (2008), the elastic property of ice may be one of the most studied properties. Two different measurements of the elastic properties are possible to perform; static or dynamic. Static tests only measure the strain after the load is applied and until a certain deformation is reached. The negative aspect of this method is that it cannot show the behaviour between the load application and measuring point. This is not of importance if the material is purely elastic, see Figure 3-1 a). However, since ice has a visco-elastic behaviour, see Figure 3-1 b), this has to be taken into account while measuring the elastic properties. On the other hand, dynamic tests measure the propagation of vibrations or the frequencies in small specimens resulting in small displacements (Sand, 2008). The strain in a viscoelastic material consist of three parts; instantaneous elasticity, delayed elasticity (i.e. creep) and flow (Brinson and Brinson, 2015). Since the displacement from the dynamic test are small, everything except the instantaneous elastic effect can be neglected (Sand, 2008; Brinson and Brinson, 2015).
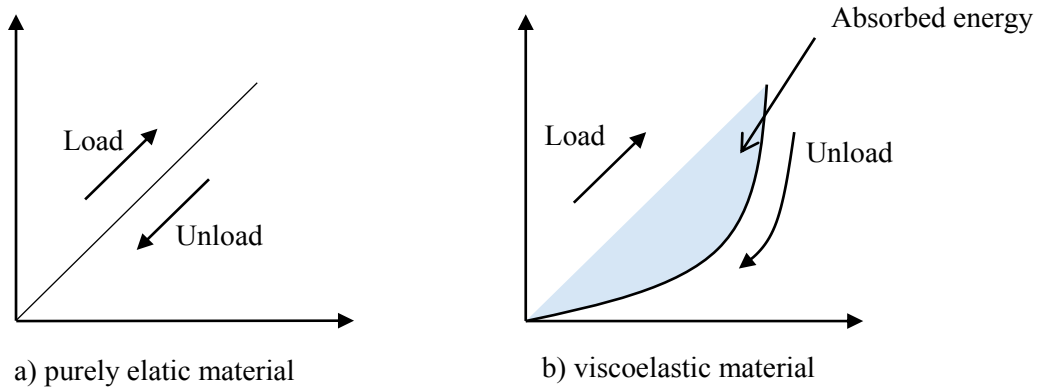
Figure 3-1.   *Idealisation of material response a) purely elastic material b) viscoelastic material* (Brinson and Brinson, 2015).

Since the viscosity and elastic deformation cannot be neglected in the static test, the result will give values from 0.3–10 GPa while dynamic measurements give a smaller range, from 6–10 GPa (Michel, 1978; Cammaert and Muggeridge, 1988; Sanderson, 1988; Sand, 2008). US Army Corps of Engineers (2006) gives similar ranges for the Young's modulus but also states that the values are substantially lower for cracked or deteriorated ice.

The brine volume in the ice influences the elastic modulus profoundly and ice with low brine volume can have an elastic modulus of 9–10 GPa (Timco and Weeks, 2010). On the other hand the scattering of results decreases with increasing brine volume and typical measurement gives values of 1–5 GPa. Furthermore, the porosity in ice has a large influence on the modulus of elasticity. According to Sand (2008), the modulus of elasticity decreases linearly in accordance to the porosity.

According to Eranti and Lee (1986), the salinity of the water has also an influence on the elastic modulus of ice; Young's modulus decreases with a higher salinity. As an example, Eranti and Lee (1986) states that water with a salinity between 15–30‰, would give an Young's modulus of the ice as 5–7 GPa.

The Poisson's ratio can in the same way as for the elastic modulus be determined by static or dynamic loading. Results from such tests also show a big scatter since they are dependent on both stress or strain and temperature. The loading direction relative the grain direction has an influence on the Poisson's value, especially in sea ice which has many different directions and orientations of the grains (Sand, 2008). For pure ice, tests have given a value of 0.30–0.36 (Michel, 1978; Cammaert and Muggeridge, 1988; Sanderson, 1988). A common recommended value for all ice types is 0.30 (Tsinker, 1997).

3.1.4   Compressive strength

The most common test performed on ice is, according to Sand (2008), the uniaxial unconfined compressive test where either a cylindrical or prismatic specimen is tested. Another type of test that could be performed is a confined uniaxial test. An unconfined test fails by longitudinal splitting while a confined test instead fails by spalling or faulting, see Figure 3-2.
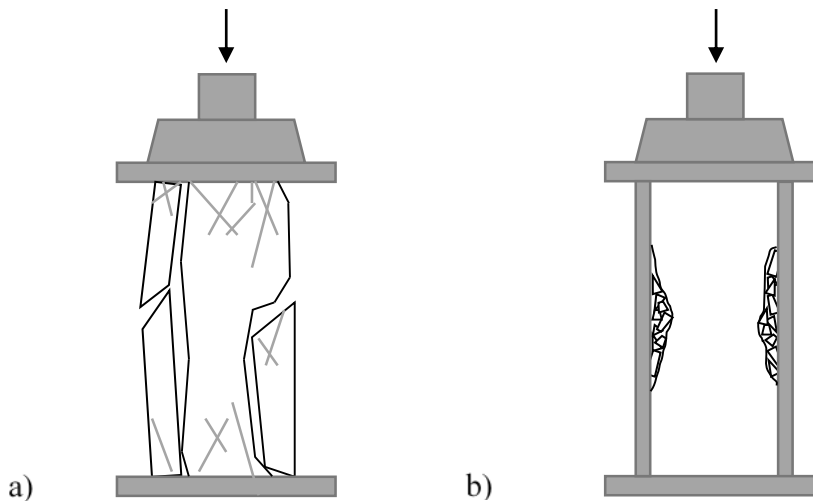
Figure 3-2.   *a) Unconfined compressive test failing by longitudinal splitting, b) confined compressive test failing by spalling.*

The ice generally shows two types of inelastic behaviour during these tests; brittle and ductile. The ductile behaviour can be seen as a rounded peak in the stress-strain curve that displays strain hardening followed by strain softening, as seen in Figure 3-3. The peak displays the highest compressive strength and it decreases with higher salinity and porosity but is almost unaffected by the grain size. At higher strain rates the ice has a brittle behaviour which is displayed by a sudden stop in the stress-strain curve, see Figure 3-3.
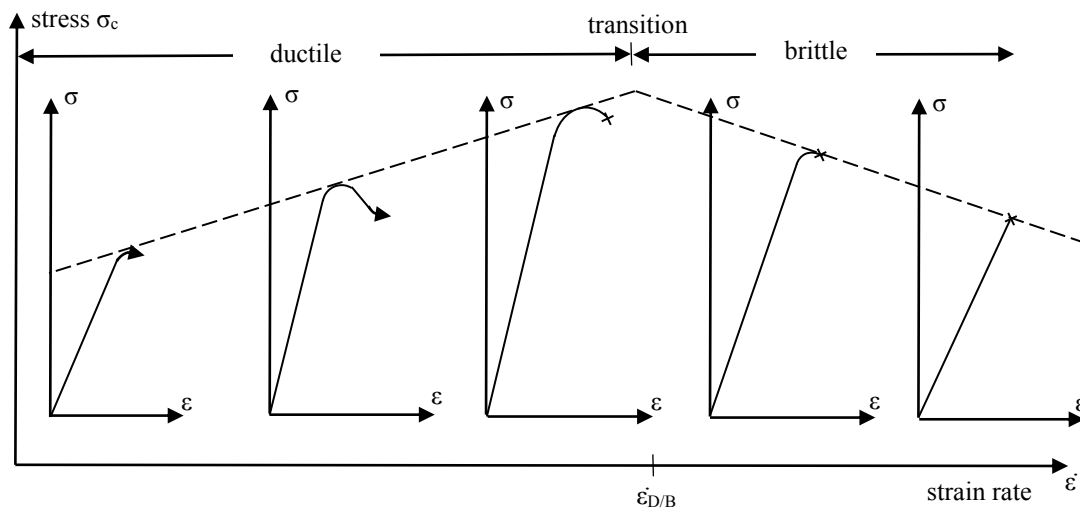
Figure 3-3.   *The different compressive stress-strain behaviour of ice (modified from Sand (2008)).*

The compressive strength of ice increases drastically as the temperature drops but the ice also becomes more brittle in the process (Vägverket, 1987). Sand (2008) writes that the compressive strength can vary between 0.5–12 MPa. The lower values are for ice with low strain rate and high temperature and the higher values are for higher strain rates and low temperatures. As an example, Vägverket (1987) states that the

crushing strength, thereby the compressive strength, of ice at the west coast could be estimated between 0.5–1.4 MPa.

The brittle compressive strength depends on the temperature, strain rate and grain size. It decreases with increasing temperature, increasing strain rate and increasing grain size. The brittle behaviour seems to have no dependence of salinity or porosity, at least at the fixed test temperature. Sand (2008) emphasize the importance of the transition zone since it is where the highest compressive strength is reached. The temperature range where the strain rate transition takes place is –40°C to –5°C and occurs in the ice when the cracks start to propagate.

3.1.5 Tensile strength

Sand (2008) writes that the best way to determine the tensile strength is through a uniaxial direct tension test. The direct test works well for ductile materials but for brittle materials stress concentrations can lead to an early failure. This effect needs to be considered during ice testing and therefore, Sand proposes to use a dumbbell-shaped ice specimen.

The tensile strength of ice is a function of the temperature and brine volume, where the strength will decrease with increasing temperature (Timco and Weeks, 2010), although it is generally not as temperature dependent as the compressive strength of ice (Vägverket, 1987). According to Sand (2008), granular ice fails in tension at about 1 MPa and depends mostly on cracks and grain size. The temperature is also an influencing parameter but Sand (2008) demonstrates that it is of less importance to the tensile strength. In general, the tensile strength of ice is substantially lower than the compressive strength (Vägverket, 1987; Sand, 2008).

Columnar ice is severely dependent on the loading direction in relation to the direction of the grains and brine channels, see Figure 3-4 a). Testing done by Kuehn, Lee, Nixon, & Schulson (1987) shows that the strength increases when the ice is loaded parallel to the columns, see Figure 3-4 b). They also came to the conclusion that the strength, when loading in vertical direction, is three to four times as high compared to when loading in the horizontal direction, see Figure 3-4 c).
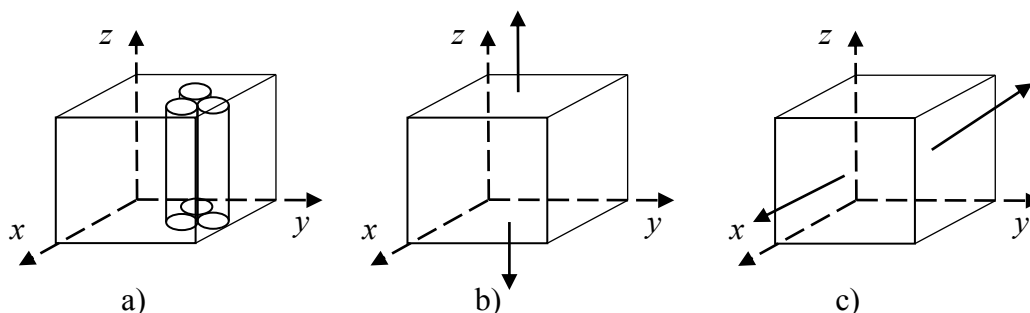
Figure 3-4.   *Coordinate system for an ice cube a) with respect to the structure of columnar ice, b) tension test parallel to the direction of the columns and c) tension test perpendicular to the direction of the columns.(modified from Sand, (2008))*

As an example of tensile strength, Sand (2008) writes about a test where first year columnar ice was loaded in horizontal direction. The ice had a salinity of between 3–6‰. The test gave a tensile strength of 0.7–0.8 MPa at –20°C and a reduced tensile

strength of 0.2–0.3 MPa at –3°C. In this case the temperature is crucial because of the saline water between the ice columns. Timco and Weeks (2010) also second these values by stating that an ice sheet will have a tensile strength between 0.2 and 0.8 MPa in horizontal direction.

First year sea ice creates a column like structure with brine pockets, as described in Section 2.1.1. The minimum strength is reached perpendicular to these pallets or columns, in the horizontal direction, and can further be reduced by brine channels (Bouchat and Tremblay, 2017). When modelling, Bouchat and Tremblay (2017) suggest that the tensile strength should be set to zero since geophysical sea ice generally is cracked and therefore will resist very little tension.

3.1.6　Shear strength

Shear strength of ice is, by Sand's (2008) investigations, not commonly mentioned in literature. Existing results show that it is dependent on temperature, salinity, density and the direction of the grains. In modelling, the shear stress becomes an important parameter as shear could be a governing factor in failure.

Many different measurement methods have been used to determine the shear strength of ice e.g. direct shear, punching or torsion tests (Sand, 2008). In these conventional tests, shear stresses arise in the plane of failure and Sand (2008) states that many methods results in an additional undeterminable normal stresses which arise in that same failure plane. The magnitude of this normal stress is hard to determine leading to an uncertain measurement of the shear strength. According to tests carried out by Frederking and Timco (1986), an asymmetrical four-point bending device for shear stress, see Figure 3-5, generally gives a normal force less than 10% when testing on ice beams. The remaining 90% of the load is handled by shear, and the test is therefore considered to be more reliable than normally conducted single and double shear tests.
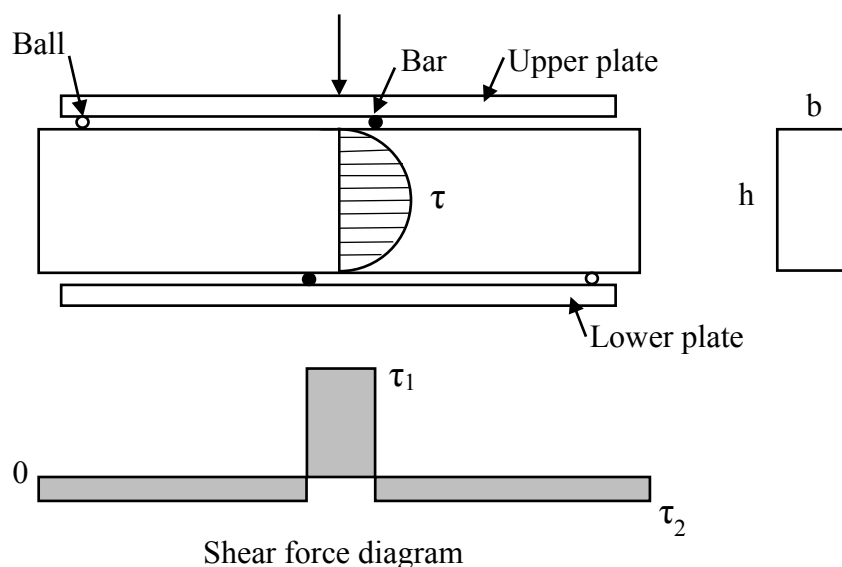
Figure 3-5.　Asymmetric four point loading apparatus and shear force diagram (modified from Frederking and Timco (1986))

The ice tested by Frederking and Timco (1986) was columnar grained sea ice with a salinity of 1.4–2.1‰ with different loading direction with respect to the grain direction. The shear strength obtained gave values between 0.55–0.9 MPa. Their experiments also showed that a higher temperature of –2°C shows ductile behaviour while specimen with a temperature of –12°C shows brittle behaviour and gave a higher shear strength.

3.1.7 Flexural strength

Flexural strength is, according to Sand (2008), an important factor concerning the bearing capacity of ice. It is also one of the more important parameters when deciding the interaction between floating ice and a structure, especially inclined ones. Vägverket (1987) states that the flexural strength is, similar to the tensile strength, not as temperature dependent as the compressive strength of ice. Sand (2008) states that flexural tests most often observes tensile failure.

Sand (2008) writes that flexural strength can be measured in many different ways, but generally ice beams are tested in three- or four point bending tests. He highlights the disadvantage with the test being indirect as well as the complexity of calculating the flexural strength. It originates from the fact that ice is an inhomogeneous, anisotropic and elasto-viscoplastic material. Sanderson (1988) presents experimental values obtained for the flexural strength, 0.5–1.0 MPa for fresh water ice and 0.1–0.8 MPa for seawater ice. As an example, an ice with a salinity of 6.6 ‰ and temperature of –10°C will have a flexural strength of 0.7 MPa according to the empirical formulas stated by Sanderson (1988).

3.1.8 Biaxial and triaxial compressive strength

Sand (2008) starts by proclaiming that there are few studies which have considered biaxial or triaxial behaviour of ice. However, a test performed by Sand (2008) showed that the strength obtained from biaxial and triaxial testing is higher than the one obtained from uniaxial tests. This depends on the effect of confinement pressure which leads to a more ductile behaviour of the ice.

Schulson and Iliescu (2006) have conducted biaxial compressive brittle failure testing on columnar-grained fresh water ice, which is claimed to have the same behaviour as first-year sea ice. The ice is tested at a temperature of –10°C and a strain rate of 3×10^{-3}–6×10^{-3} 1/s and is conducted both across and along the columns. Schulson and Iliescu (2006) conclude that the biaxial strength can be assumed to be equal in both directions since the deviations are insignificant. This is true under low confinement and if the final failure is by shear according to Coulomb's shear criteria.

Triaxial tests on laboratory-grown columnar sea ice at the temperature –20°C with a strain rate of 10^{-5}–10^{-1} 1/s has been conducted by Golding *et al.* (2014). The ice shows a plastic faulting when being loaded rapidly under a high degree of confinement.

3.2 Friction coefficient

Timco and Weeks (2010) used laboratory grown saline ice to determine the friction coefficient of ice against different structures. Both static and kinetic friction were

obtained and it was found that the static friction at the start of motion was five times higher than the kinetic friction for a velocity of 0.1 m/s. The kinetic friction was higher at lower velocities and on rougher material. The variation of the test results was 25–30% at a constant speed independent of the tested material. The friction coefficient was also dependent on the temperature and showed a small increase when the temperature was –2°C compared to –10°C. The average kinetic friction coefficient for sea ice interaction between different materials are displayed in Table 3-1 for different velocities of the ice (Timco and Weeks, 2010). These values correspond, relatively well, to the friction coefficients presented by Fransson and Bergdahl (2009) who suggest the kinetic friction coefficient to be 0.1 for painted steel and 0.15 for concrete and corroded steel.

Table 3-1.   *Average kinetic friction coefficient for interaction between ice and different materials at different velocities (Timco and Weeks, 2010).*

Material	Velocity	Friction coefficient [-]	Velocity	Friction coefficient [-]
Smooth concrete		0.1		0.05
Painted steel		0.1	> 50 mm/s	0.05
Sea ice	10 mm/s	0.1		0.05
Rough concrete		0.2	>100 mm/s	0.1
Corroded steel		0.2		0.1

3.3 Failure modes of ice

Määttänen (1991) writes that the failure of ice is a nonlinear process, from the load build-up to the ultimate failure including the following clearing process. This is seconded by Daley, Tuhkuri and Riska (1998) who also write that the ice failure must be seen as a progressive action. Karna, Frederking and Shkhinek (2011) consider the possible failure modes of ice to be: creep, crushing, bending, buckling and splitting by shear, where crushing is the most common one. Another treated failure mode is radial and circumferential cracking which, according to Määttänen (1991), Sodhi (1998) and Lu, Lubbad and Løset (2015b), could lead to failure but also initiate other failure modes. At an ice structure impact the ice do not fail simultaneously from a single stress peak (Johnston, Croasdale and Jordaan, 1998). Instead small zones will fail with individual peak stresses until global failure is reached. In this chapter different types of failure modes will be presented together with influencing parameters of the failure process. A brief presentation of the limiting processes of ice failure will also be treated as well as how ice can and have been modelled by previous researchers.

An ice sheet can fail locally by microcracking or flaking and globally by crushing or bending (Daley, Tuhkuri and Riska, 1998). The tensile strength is one of the most important parameters, both with regard to local and global failure (Frederking and Timco, 1986). Bhat *et al.* (1991) state that local failure is limited to the surrounding contact zone of the ice or the edge of the ice formation. When an ice formation is split into two pieces and reach global failure, it is called a splitting failure (Bhat *et al.,* 1991). In the following sections a brief introduction to the most common failure modes are treated (Johnston, Croasdale & Jordaan, 1998).

3.3.1 Creep

Ponter & Cocks (1989) have investigated creep behaviour of ice at strain rates in the range of 10^{-7}–10^{-2} s^{-1}. The creep deformations observed in the ice are divided into four categories dependant on the local stress state. The first one have stresses so small that no microcracking is observed and the ice is thereby subjected to pure creep. The next category is when the stresses are large enough to produce microcracks along with the creep of the ice but no progressive crack propagation is observed. The third step is when the microcracking is substantially large that the region can carry small stresses or when a crack has propagated. The last category is when a region is fully cracked and has separated from the original ice region, called a creep slip. This type of creep failure is not common since creep has an anisotropic behaviour and the same stress needs to arise in all directions to achieve a creep slip (Ponter and Cocks, 1989). Duval et al. (1989) second this and state that the strain due to creep will be very small for columnar ice because it has an anisotropic structure, as described in Section 2.1.1. The highest creep values occurs during melting and therefore the risk of creep slip is highest during these circumstances (Ponter and Cocks, 1989).

Bergdahl (1977) explains the creep, when the ice is subjected to constant loading, in three steps according to Figure 3-6. The primary creep changes the substructure of the ice and is highly dependent on the creep stress. In the secondary step the substructure does not change, instead there is a constant deformation rate. In the third, and final, step the deformation rate accelerates until the tensile strength is reached and failure occur. To conclude, the creep has a small influence on the failure mode of ice. It is even stated, by Jordaan & Timco (1988), that the creep at low loading rates can prevent other types of failure in the ice by keeping the energy per unit volume at a low level.
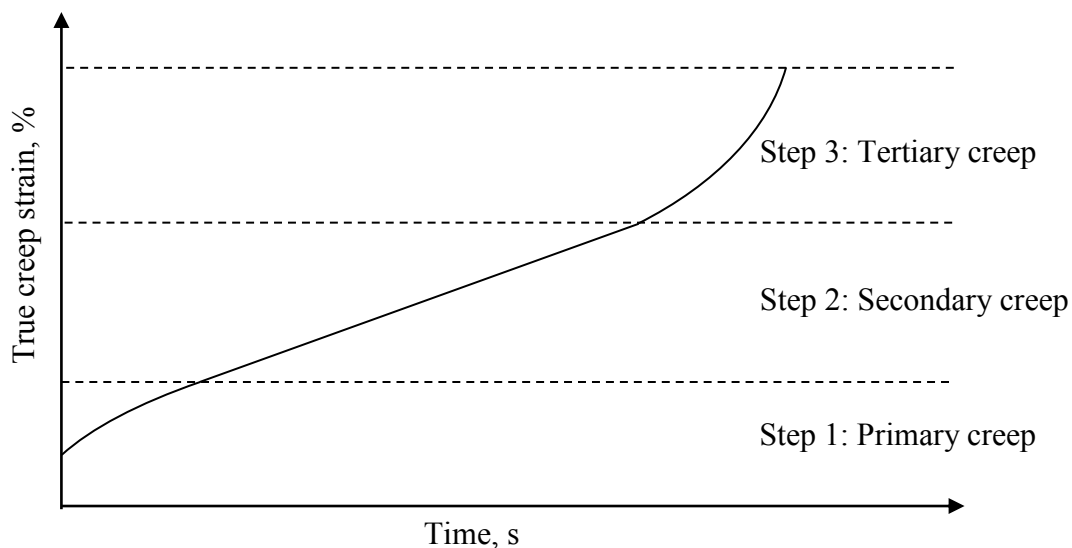
Figure 3-6.   *Definition of the three creep steps for a typical creep curve for a given temperature, (modified from Bergdahl (1977)).*

3.3.2 Crushing

According to Sand, (2008) and Karna, Frederking and Shkhinek (2011), crushing is one of the most common failure modes, especially when it comes to interaction with column-supported structures such as bridge piers and lighthouses. Crushing of ice is observed for a certain combination of aspect ratio and velocity (Timco, 1987; Jordaan and Timco, 1988; Marcellus and Heuff, 1991). In Sand (2008), it is stated that crushing occurs when the aspect ratio is less than six.

According to Jordaan & Timco (1988), crushing is a complex interaction which starts with microcracking in the ice, followed by cracks in maximum shear direction and finally crushing and pulverization of the ice. Marcellus & Heuff (1991) describe crushing failure in the same, somewhat simplified, manor as crushing and pulverisation of ice in front of the structure.

3.3.3 Bending

Bending failure, also known as flexural failure, is mainly observed during interaction with sloping structures since the inclination, between the ice and the structure, reduces the needed ice load to induce failure (Lu *et al.*, 2017; Teo, Poh and Pang, 2017; Wang and Poh, 2017a). When an interaction occurs between a vertical structure and an ice formation a higher ice load is needed to induce failure and therefore other failure modes could occur earlier (Wang and Poh, 2017b). This results in a smaller ice force for bending failure against sloping structures than for e.g. crushing (Karna, Frederking and Shkhinek, 2011). The failure starts by bending of the ice sheet downwards against the structure until the flexural strength is reached and failure occurs (Wang and Poh, 2017b).

3.3.4 Buckling

If an ice sheet is relatively thin or the structure is much wider than the thickness of the ice sheet, the ice is prone to buckle and finally fails when the bending strength of ice is reached (Hendrikse and Metrikine, 2016a). Buckling failure can occur in alliance with crushing and is a common failure mode against offshore structures. The difference between buckling- and bending failure is that the buckling failure leads to large out-of-plane deformations (Marcellus and Heuff, 1991; Hendrikse and Metrikine, 2016b). In the same way as for bending, the force is generally smaller for buckling than for crushing (Karna, Frederking and Shkhinek, 2011).

3.3.5 Splitting

A splitting failure occurs when the tensile strength is reached and the sheet tries to minimize the spread of energy by concentrating it to one central crack. By doing so, the sheet is split into two pieces instead of spalling of smaller pieces (Lu, Lubbad and Løset, 2015a). Up to the point when the splitting crack occurs, the failure mode is considered to be local. The failure mode has been observed in ice structure interactions for finite ice floes with low lateral confinement. Higher confinement can easily prevent splitting failure or substantially increase the splitting load. Test done by Lu *et al.* (2016) shows that the risk of splitting failure will increase as the thickness of the ice increases.

3.3.6 Radial and circumferential cracking

An ice structure interaction could lead to initiation and propagation of radial cracks in the ice sheet (Määttänen, 1991; Marcellus and Heuff, 1991; Sodhi, 1998; Lu, Lubbad and Løset, 2015b). The radial cracks starts at the ice structure interface and orientates perpendicular from this interface, in direction of maximum shear stress. A successive increasing ice force could later lead to circumferential cracks which are coupled to the radial cracks, according to Figure 3-7. Further increase of this will lead to bending failure (Määttänen, 1991).
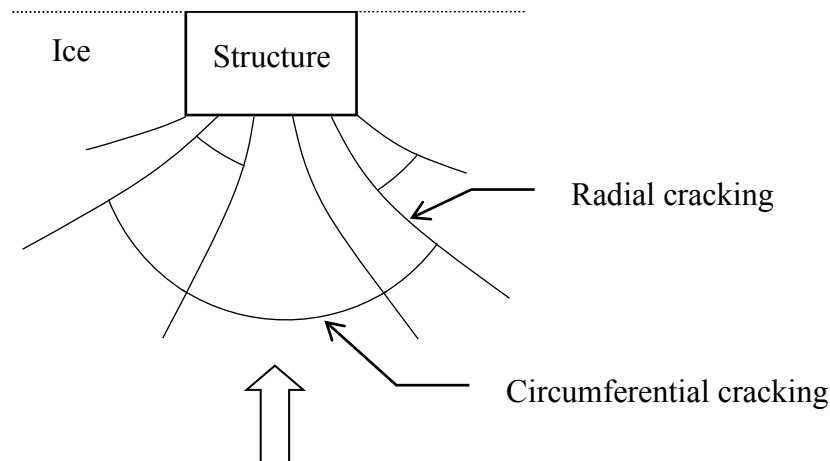
Figure 3-7.   *Illustration of radial and circumferential cracking during an ice structure interaction.*

According to Lu *et al.* (2015b), the load to initiate a radial crack is significantly smaller than the load to initiate circumferential cracks. Therefore, a general assumption is that when the circumferential crack occur the final strength of the ice floe is reached. Lu et al. (2015b) divided the two cracking phenomena in two classifications. The first is a finite size ice floes which only breaks in radial cracking (Sodhi, 1998) and the second is a semi-infinite ice floes which breaks by formations of both radial and circumferential cracking (Lu *et al.*, 2015b). The division has been proven to be a conservative approach.

3.3.7 Influencing parameters of failure mode of ice

As stated previously, the failure mode of ice is a complex and nonlinear process, and it is affected by both the structure and the ice (Jordaan and Timco, 1988; Määttänen, 1991; Daley, Tuhkuri and Riska, 1998; Sand, 2008). The different failure modes, which have been brought up above, depend on many parameters and some of these parameters will be treated below.

One influencing parameter is the ice thickness. In an ice structure interaction most of the ice force is transmitted through a high pressure zone which tend to appear in the most confined parts of the ice sheet (Johnston, Croasdale and Jordaan, 1998; Jordaan, 2001). The interaction zones are often reduced by spalling which will result in a narrow pressure band with high strength ice, see Figure 3-8. Fracture have a tendency

to occur in the weak parts of the ice and the high pressure zones will govern the global response of the ice formation (Jordaan, 2001). Since not the whole impact area is active during the interaction, but only the high pressure zone, a conclusion can be made that models and laboratory tests in some cases uses a too large area when calculating or predicting the impact force between the ice and the structure.
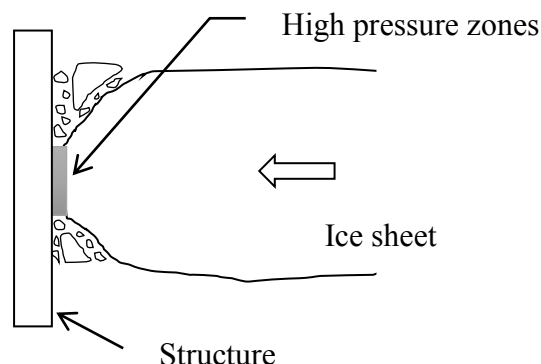
Figure 3-8. *Illustration of the spalling and high pressure zone from a section view (from Jordaan, 2001).*

The failure modes dependence on the strain rate has been investigated by many researchers (as example Marcellus and Heuff, 1991; Azarnejad and Hrudey, 1998; Schulson, 2000). The results, with respect to the failure response, from these research can be seen in Table 3-2.

Table 3-2. *Strain rates related to different failures according to three research.*

	Thermal failure [s^{-1}]	Ductile failure [s^{-1}]	Brittle failure [s^{-1}]
Schulson (2000)	-	$<10^{-7}$	$\sim 10^{-7}$–10^{-1}
Marcellus and Heuff (1991)	-	$<10^{-4}$	$\sim 10^{-2}$
Azarnejad and Hrudey (1998)	10^{-8}–10^{-7}	-	-

Azarnejad and Hrudey (1998) performed a numerical study on thermal ice loads and claims that the strain rate has to be in the range of 10^{-8}–10^{-7} s^{-1} in order to ensure that the govern action will be thermal ice failure. Schulson (2000) have instead studied the brittle failure of ice and states that the brittle failure regime generally can be considered within strain rates of $\sim 10^{-7}$–10^{-1} s^{-1}. Creep and ductile failure will be governing when the strain rate is $<10^{-7}$ s^{-1}. Marcellus and Heuff (1991) have studied the role of fracture during ice failure and write that the failure will be completely ductile for strain rates $<10^{-4}$ s^{-1}. For higher strain rate, $\sim 10^{-2}$ s^{-1}, the failure will be brittle. To conclude, Schulson (2000) assumed a larger range of strain rate for the brittle regime than Marcellus and Heuff (1991), compare $\sim 10^{-7}$–10^{-1} s^{-1} with 10^{-4}–10^{-2} s^{-1}. Due to the larger range it can be assumed that the definition of strain rate in experiments and models is a highly important parameter when it comes to which failure mode of ice that will be investigated.

Yasui, Schulson and Renshaw (2017) have in later research performed compressive tests on ice cylinders at different strain rates in order to illustrate both brittle and ductile behaviour. Their results are seen in Figure 3-9.

10⁻⁵	10⁻⁴	10⁻³	10⁻²	10⁻¹	(5-6)x10⁻¹

◄——————— Ductile ———————► ◄——————— Brittle ———————►
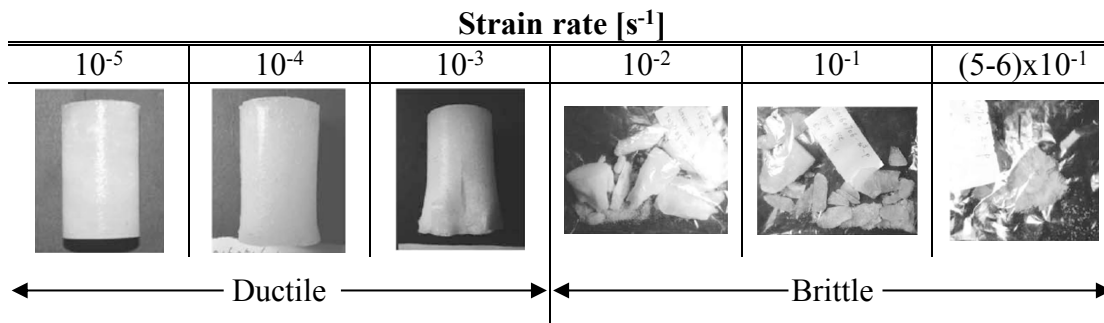
Figure 3-9.   Experimental behaviour of ice at different strain rates (modified from Yasui, Schulson and Renshaw (2017)).

Timco (1987) succeeded to find an empirical relation between failure modes, indentation rate (the velocity divided by the width of the structure) and aspect ratio, see Figure 3-10. The chart depends on given external parameters: the width of the structure, the thickness of the ice and the velocity. However, the failure mode of ice depends, not only, on these but also on the ice properties and temperature which is considered to be a weakness of Timco's chart (Daley, Tuhkuri and Riska, 1998). Another weakness is that it lacks the potential to see various failure modes which follow each other (Daley, Tuhkuri and Riska, 1998). To conclude, this means that the same failure mode will always be expected for the same external conditions; this is in contradiction with experiments and the fact that ice is a geophysical material with flaws and irregularities. Nevertheless, the chart in Figure 3-10 is useful and have been used by researchers to continue the work with finding an improved relationship between the different failure modes of ice.

v – velocity of ice, b – column width, t – thickness of ice
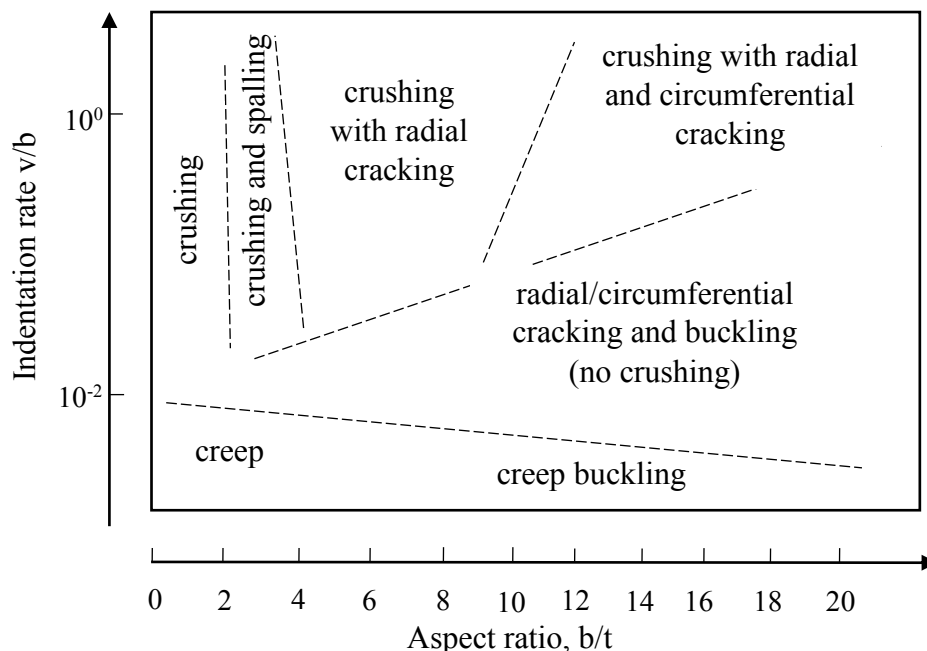
Figure 3-10.   Chart of failure modes and its dependence on the aspect ratio and indentation rate (Modified from Timco (1987) and Daley, Tuhkuri and Riska (1998)).

In line with the work performed by Timco (1987), Marcellus and Heuff (1991) also expressed the failure mode of an ice sheet as a function of the aspect ratio. In the article they state that these relations have been showed before, not only by Timco (1987) but also by Blanchet *et al.* (1988). Marcellus and Heuff (1991) summarized Blanchet's *et al.* (1988) work of how the failure mode can be described as a function of the aspect ratio and the ice thickness. Blanchet *et al.* (1988) based their work on laboratory made first- and multiyear ice. In Table 3-3 Marcellus and Heuffs (1991) overview of Blanchet *et al.* (1988) research is summarized.

Table 3-3. *Failure modes in relation to the aspect ratio and ice thickness (Marcellus and Heuff, 1991).*

Aspect ratio [-]	Ice thickness, t [m]	Failure mode
b/t < 5	All	Crushing
5 < b/t < 20	t < 0.75	Flexural
20 < b/t	t < 0.75	Buckling
50 < b/t	t < 0.25	Buckling
	0.25 < t < 0.75	Buckling and flexural
b/t > 0.75	t > 0.75	Gradual change in failure mode, result of ice width and load scenario
b/t > 5	t ~ 1	Flexural, mainly
	t ~ 3	Crushing and flexural
	t > 3	Crushing, mainly

To conclude, both Timco (1987), Marcellus and Heuff (1991) and Blanchet *et al.* (1988) worked on the same approach; the failure mode of ice can be described as a function of the aspect ratio. One major difference between the two results is the fact that Blanchet *et al.* (1988) did not include the strain rate, which is a highly important parameter that needs to be considered.

3.3.8 Limiting processes of ice failure

The failure of ice has different limiting processes which will govern the failure mode (Karna, Frederking and Shkhinek, 2011). The limiting processes can be divided into four categories; limiting stress, limiting force, limiting momentum and limiting energy, see Figure 3-11. Three of the four limiting categories are discussed by Palmer and Croasdale (2013): limiting stress, limiting force and limiting momentum. The fourth category, limiting energy, is similar to limiting force but can also be seen as a combination of the other three actions.
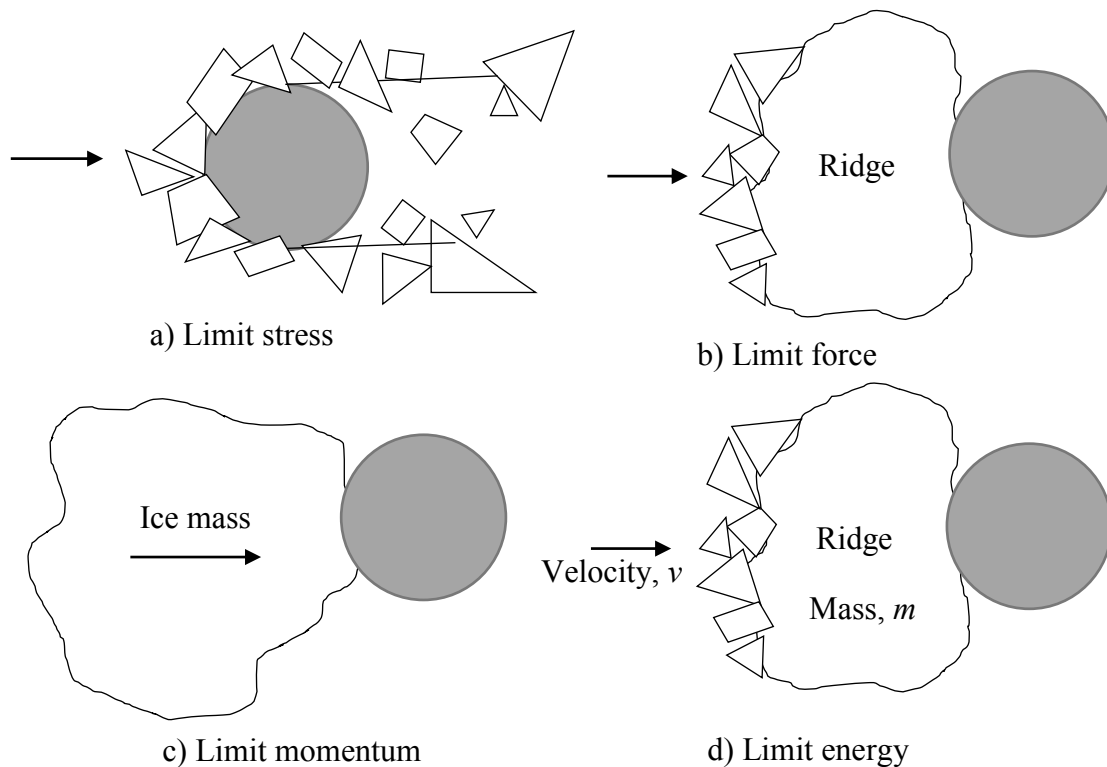
Figure 3-11. *The four limiting categories: a) limiting stress, b)limiting force, c) limiting momentum and d) limiting momentum (Karna, Frederking and Shkhinek, 2011; Palmer and Croasdale, 2013a).*

The first category is when stress is the limiting factor. The ice often consists of a solid sheet which moves and interact with a structure (Palmer and Croasdale, 2013b). During the interaction the ice does not have sufficient energy to generate stresses across the entire width of the structure. The result is that the ice sheet breaks into smaller pieces (Karna, Frederking and Shkhinek, 2011). The pieces can either clear out and be carried away with the current or pile up against the structure and form a rubble field (Palmer and Croasdale, 2013b). The second category is when the force is the limiting factor. This can happen when an ice cover is driven by wind and/or currents. The driving forces is insufficient for the ice to break against the structure but big enough to stop the ice from developing around it (Karna, Frederking and Shkhinek, 2011). The third category is when the limiting factor is caused by a momentum force. This momentum force is twisting and moving the ice formation around the structure without any impact on either the ice sheet or the structure (Palmer and Croasdale, 2013b). This is likely to occur when an ice formation interacts with structures in calm waters (Karna, Frederking and Shkhinek, 2011). The last category is when the energy is the limiting factor which often occurs when ridges or bigger ice floes interact with a structure. The impact is similar to the limit force but also depends on the amount of released kinetic energy which in its turn depends on the mass and velocity of the ice formation. All, or some, of these four limiting processes can occur at the same time. This indicates that it is not always clear which limiting process that govern the failure and it is therefore not clear which failure mode that will occur.

3.4   Modelling of ice failure

An ice structure interaction can be described in many ways, and how it is described is an important factor when modelling and predicting ice loads. One physical model which corresponds well to the reality was set up by Määttänen (1991). He explained that it could be divided into three parts: the structure, the ice and the ice failure including the clearing process. Furthermore, he explained that the structure and the ice failure, including the clearing process, can be described with mathematical models which are a simplification of reality. However, the challenge is to describe the constitutive model of ice with its visco-elasto-plastic behaviour including cracking during an interaction, described in Section 3.3.6. Määttänen (1991) stated that the constitutive models of ice that existed was not fully reliable.

Kolari, Kuutti and Kurkela (2009) accentuate, in the same manner as Määttänen (1991), two criteria that need to be fulfilled to obtain reliable results from numerical simulations of ice. Firstly, the model must predict a correct stress-strain behaviour at failure. Secondly, the failure mode needs to correspond to the failure mode seen in experimental tests. They claim that these criteria are rarely completely met since ice have different failure mechanisms in different situations. In FE analysis the correct failure mode is hard to predict.

During FE analysis one element which has reached failure can, in some cases, be removed before the analysis proceeds. The removal of failed elements then continues until the model has reached global failure. If the failed elements instead are kept in the analysis, global failure could be reached when the first element has failed. Kolari, Kuutti and Kurkela (2009) note in their article that none of these two scenarios are desirable when ice is modelled. The main reason is that ice has brittle behaviour which means that when it fails it will go from a continuous material to a discontinuous. This needs to be considered since the discontinuous elements are still a part of the ice interaction. This behaviour is also explained by Daley, Tuhkuri and Riska (1998) who state that the ice load depends on the progressive sequences after failure. Since ice failure change the geometry of the ice sheet, the geometry needs to be adjusted continuously through the analysis to show a reliable interaction and failure mechanism. Karna, Frederking and Shkhinek (2011) state the same thing and second it by saying that broken ice will remain broken and can never be completely intact again.

4 Calculation of ice loads according to standards and guidelines

As mentioned in Chapter 1, there are certain laws, requirements and guidelines that needs to be followed when designing structures in Sweden. The overview of in which order these standards and guidelines should be followed when designing bridges against ice loads are presented in Figure 4-1. The figure represents the requirements and guidelines that should be followed if the Swedish Transport Administration is the client and if nothing else is stated in the commission. Of course other clients such as municipality or private actors can state that Trafikverket's requirements and guidelines should be followed but they could also state their own requirements.
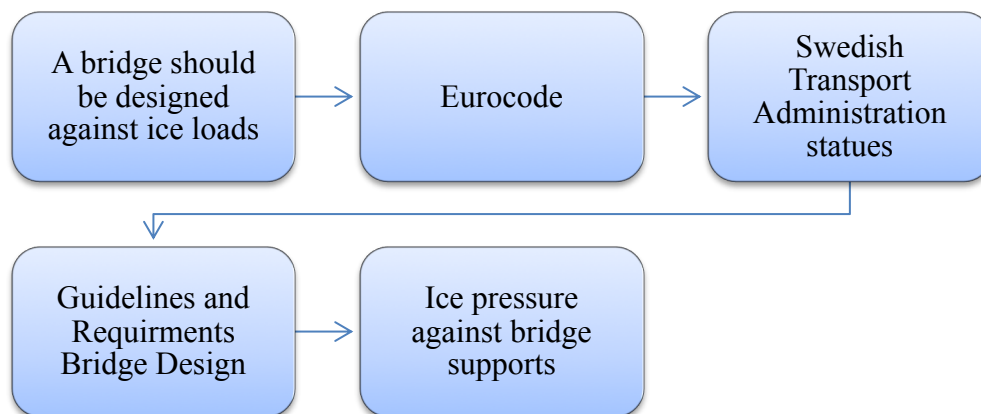
Figure 4-1.   *Overview of in which order the standards and guidelines that should be followed when designing against ice loads if Swedish transport administration is the client.*

In the 1990th, the hydropower companies in Sweden came to the conclusion that the available guidelines of designing dams safely, including estimations of ice loads, were not sufficient. This resulted in *RIDAS* (RIDAS, 2012a) which is the hydropower companies guideline for dam security and is given out by Svensk Energi, which most of the Swedish hydropower companies are a part of.

In the sections below, a brief introduction will be presented of what is stated in the standards mentioned above concerning ice loads.

4.1 Eurocode

Eurocode is divided into ten parts which treat different aspects of the design process. In *Eurocode 1991: Actions on structures* (EN 1991, 2003) all loads and load combinations which a designer needs to consider during design are stated. Ice loads are mentioned in part 1991-1-3 in paragraph 1.1.8 where it is stated that the paragraph does not give any guidance on ice loading (EN 1991-1-3, 2003). In the document it is stated that this is a unique aspect of snow loading and therefore needs to be treated separately by each countries national annex, see Section 4.2.

4.2 Swedish Transport Administration statues, TRVFS 2011:12

The *Swedish Transport Administration statues* (TRVFS 2011:12) is an national annex to Eurocode published by Trafikverket (Trafikverket, 2011). The annex makes it possible to use Eurocode when designing structures in Sweden which are subjected to traffic. *EKS10* (BFS 2015:6) is the counterpart applied for buildings (Trafikverket, 2011; Boverket, 2016). As in Eurocode, no guidance or requirements are given concerning ice loads in any of the two documents (Trafikverket, 2011).

4.3 Requirements and guidelines of bridge design, TDOK 2016:0204 and TDOK 2016:0203

Except following Eurocode and TRVFS or EKS10 (there are two documents published by Trafikverket that also need to be followed if it is stated in the commission. These are *Requirements of Bridge Design* (Trafikverket, 2016a) and *Guidelines of Bridge Design* (Trafikverket, 2016b). In both documents, the appliance and magnitude of ice loads in bridge design is mentioned.

In the requirements, it is stated that any support which is located in the water should be designed against ice loads (Trafikverket, 2016a). The ice load should be assumed to act at mean high water level (MHW) and mean low water level (MLW). The magnitude of the ice load should be investigated separately, but a minimum value is set to 200kN acting as a point load, in either longitudinal or transversal direction. Also stated in the requirements is that the ice load cannot act in both directions at the same time. See Figure 4-2 for an overview of how the ice load should be applied. Finally, it is stated that Trafikverket and other clients always have the choice to state how they want to design their bridge against ice loads; both when it comes to the magnitude of the ice load, where the ice load should be applied, and in which direction. The client can even chose to not design the bridge against ice loads at all (Trafikverket, 2016a).

$\geq$ 200 kN

$\leq$ 200 kN
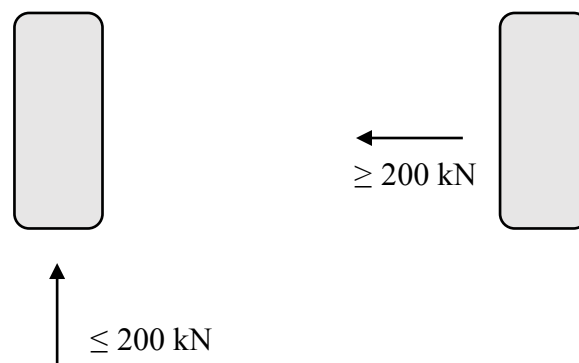
Figure 4-2.   Example of how the ice load should be applied in the longitudinal (left) and transversal (right) direction. The ice load cannot act in both directions simultaneously.

All the requirements and minimum values given in TDOK 2016:0204 could, according to the guidelines (TDOK 2016:0203), be used if the following statements are true (Trafikverket, 2016b).
- The ice thickness at the location of the bridge is not expected to be thick.
- The ice cover is not affected by currents.
- No moving or driving ice is present.

If some of the three statements above is true the guideline states that the ice pressure should be investigated separately with respect to local conditions. Guidance on how the magnitude and mode of the ice pressure should be determined are given in *Ice pressure against bridge support* (Vägverket, 1987; Trafikverket, 2016b), see Section 4.4.

4.4 Ice pressure against bridge supports (VV 1987:43)

The guideline *Ice pressure against bridge supports* (VV 1987:43) is mainly based on design values which have been used over the years (Vägverket, 1987). In the preface it is stated that the guideline has originated without any actual knowledge of the formation of ice and its actions. Instead, the guideline relies on empirical values of the ice load since it has been used for many years. VV 1987:43 is also based on publications from Nordic Road Engineering Association (NVF), *State load regulations of 1960th* (SOU1961:12, 1960) as well as Canadian and Russian standards from the time of writing (Vägverket, 1987).

In the guideline, a standard support in water has been used in order to illustrate certain ice actions and ice load configurations, see
Figure 4-3.
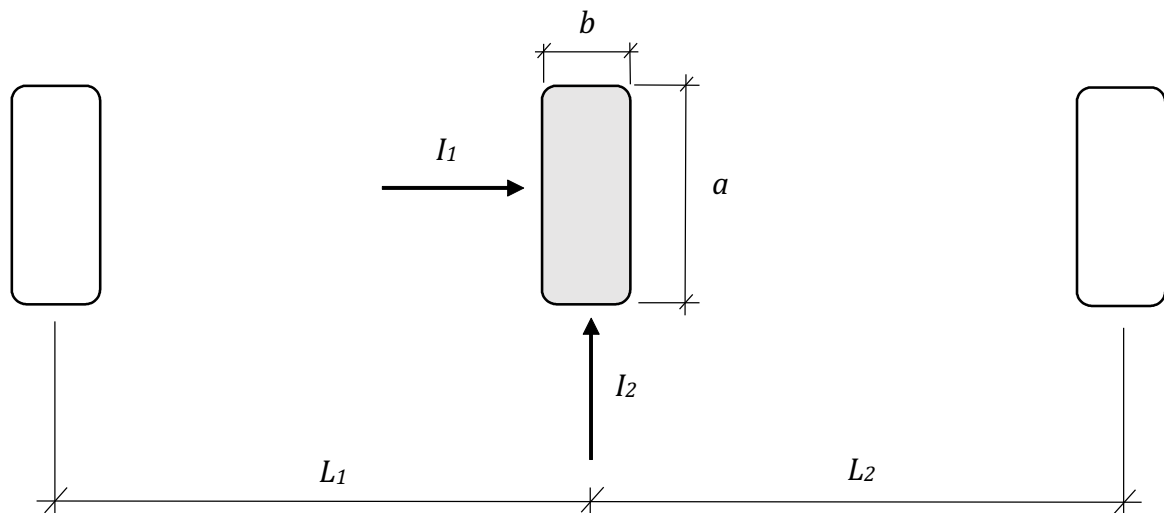
Figure 4-3. *Denotation of ice loads, I_1 and I_2, and distances, L_1, L_2, a and b, through a standard section (modified from Vägverket (1987)).*

The load, perpendicular to the water flow, from a fixed ice cover can, according to VV 1987:43, be estimated to:

$$I_1 = i_1 a \tag{4-1}$$

where,
i_1 distributed ice load perpendicular to the water flow in [N/m], and
a column height [m], $a \geq 4$ meter.

For fresh water ice the distributed ice load, i_1, is generally 50–300kN/m (Vägverket, 1987). If the support height is smaller than 4 meter, VV 1987:43 suggest that a should be set to 4 meter.

If there is a high amount of water level variation the ice cover could break up and create an arch between the supports or between the shore and the support. The distributed load, i_1, from this effect could then be estimated to 200kN/m. The distributed load can then be assumed to act against one support or many supports over several spans.

As mentioned in Section 2.2, a horizontal dynamic ice load can arise due to a moving ice sheet which is caused by the driving force from wind, current or tidal variations. According to VV 1987:43, the magnitude of this ice load parallel to the water flow can be estimated according to:

$$I_2 = \frac{i_2(L_1 + L_2)}{2} \tag{4-2}$$

where,
i_2 distributed ice load parallel to the water flow in [N/m], and
L_1, L_2 distance to adjacent support [m], see Figure 4-3.

Generally, the distributed ice load, i_2, varies between 10–30kN/m for all ice types (Vägverket, 1987). If there is a risk of larger ice sheets to be present, the ice load can also, according to VV 1987:43, be estimated as:

$$I_2 = C_1 \sigma_c b t \tag{4-3}$$

where,
C_1 shape factor depending on the aspect ratio [-], see Table 4-1,
σ_c crushing strength of the ice [Pa],
b column width [m], and
t ice thickness [m].

Table 4-1.   *Values of the shape factor C_1 with respect to the aspect ratio (Vägverket, 1987).*

Aspect ratio b/t	Shape factor C_1 [-]
0.5	1.8
1.0	1.3
1.5	1.1
2.0	1.0
3.0	0.9
≥ 4.0	0.8

VV 1987:43 states that the crushing strength of ice can be estimated with respect to where the ice is located and the driving forces that are governing the action of the ice. As an example, the ice on the Swedish west coast can be estimated to have a crushing strength of 500kPa and the rivers in the north of Sweden a crushing strength of 700kPa. If solid ice is present together with large currents, the crushing strength could be as high as 1400kPa (Vägverket, 1987).

If a support has a sharp and/or inclined edge, see Figure 4-4, the ice load can be estimated according to:

$$I_2 = C_1 C_2 C_3 \sigma_c bt \qquad (4\text{-}4)$$

where,

C_1 shape factor depending on the aspect ratio [-], see Table 4-1,
C_2 shape factor for sharp edge [-], see Table 4-2,
C_3 shape factor for inclined edge [-], see Table 4-3,
σ_c crushing strength of the ice [Pa],
b column width [m], and
t ice thickness [m].

a) From above   b) From the side
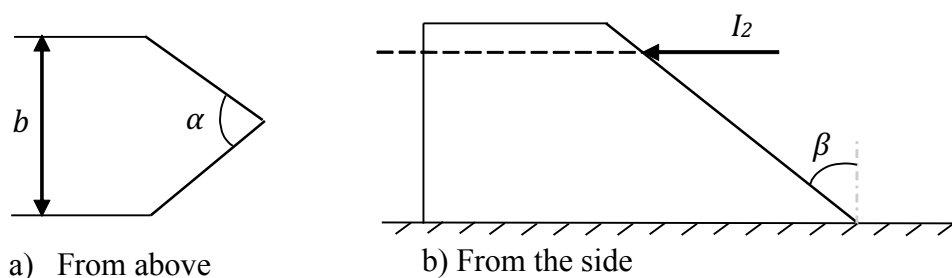
Figure 4-4.   *Support with a sharp and/or inclined edge a) sharp edge b) a inclined support*

The shape factors C_2 and C_3 are presented in Table 4-2 and Table 4-3. The factors will reduce the magnitude of the ice pressure depending on how much the support is inclined or how sharp the edge is, see Figure 4-4. The total reduction due to C_2 and C_3 should not be more than 0.5 (Vägverket, 1987).

Table 4-2.   *Values of the shape factor C2 with respect to sharp edge (Vägverket, 1987).*

α	C_2
45°	0.54
60°	0.59
75°	0.64
90°	0.69
120°	0.77
180°	1.00

Table 4-3.   *Values of the shape factor C3 with respect inclination of the edge (Vägverket, 1987).*

β	C_3
0–15°	1.00
15–30°	0.75
30–45°	0.50

4.5 RIDAS

As mentioned before, RIDAS (2012a) is a guideline given out by *Svensk Energi* which consists of a number of Swedish hydropower companies (RIDAS, 2012a). The guideline was set up with the aim to develop the recommendations and guidelines within dam security department. The first edition was published in 1997, and it has been updated three times since then.

In the document it is stated that the horizontal distributed ice load can be assumed to be 50–200kN/m (RIDAS, 2012b). The exact value depends on geographical location, altitude and local conditions around the dam. As an estimation, 50kN/m can be assumed in south of Sweden for dams at low altitudes, 100kN/m can be assumed in the east and middle part of Sweden, and 200kN/m can be assumed north of Karlstad–Stockholm, see Figure 4-5 a). These estimations are not definite values since the ice load affected by local conditions could lead to significantly higher or lower magnitudes (RIDAS, 2012b). Parameters that could influence are the ice thickness, the resistance from the shores during temperature changes and potential unsymmetrical loading. However, RIDAS (2012) does not mention what the magnitude of the ice pressure should be if this is the case. The magnitude of the ice thickness is, according to RIDAS (2012), 0.6 meter for the southern part of Sweden and 1.0 meter in the northern part, see Figure 4-5 b). However, these are only benchmark values and should not be taken as the true values.
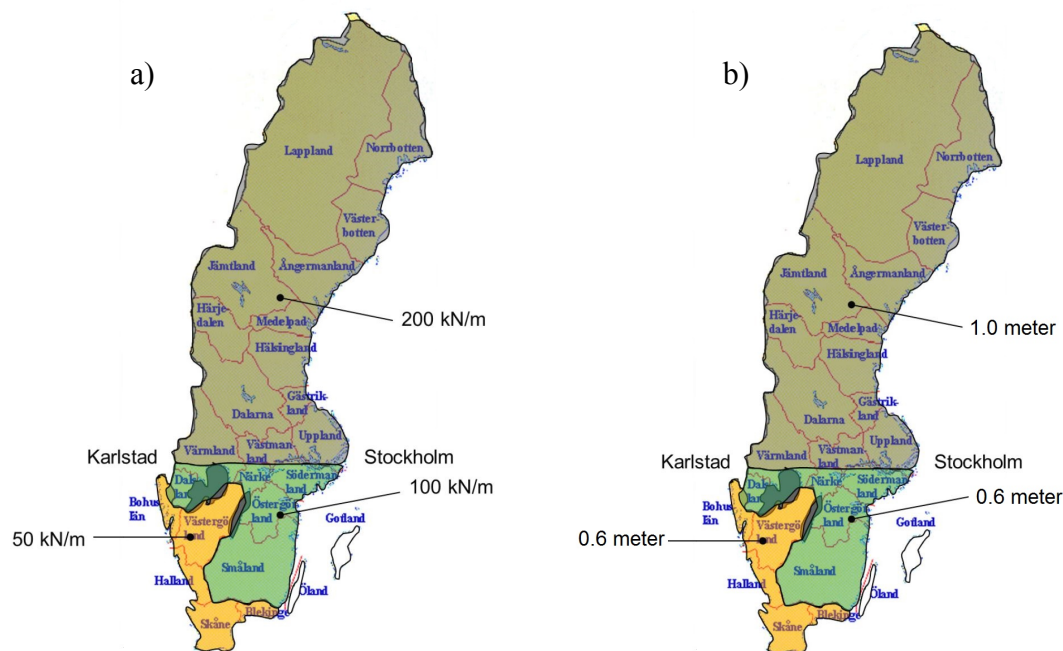
Figure 4-5.   *a) Values of the ice pressure according to* RIDAS(2012). *b) Assumed ice thicknesses according to* RIDAS(2012). *Modified from* Malm *et al.* (2017).

RIDAS (2012) mentions the arching effect which should be considered in dams in front of the defer openings if ice prevention has been installed, for example heating coils. The ice load which could have acted on the opening is instead transformed into two point loads acting on either side of the opening.

4.6 Other recommendations

Over the years, researchers have tried to clear out the issues regarding ice load and how it should be estimated. Research has shown that it is relatively easy to calculate the ice load if the ice conditions are well known and defined (Fransson and Bergdahl, 2009). However, the hard task is to define these conditions. Therefore, a brief information will be given of two other recommendations and design regulations which consider ice loads.

4.6.1 Recommendations for design of offshore foundations exposed to ice loads

Recommendations for design of offshore foundations exposed to ice loads was written by two Swedish pioneers within ice loads, Fransson and Bergdahl (2009). The guideline is an update of earlier recommendations written by Bergdahl (2002). The updated recommendation now consider the experienced damage on offshore structures in both Sweden and Finland as well as it comments and reflects the Canadian and Russian standards (Fransson and Bergdahl, 2009). Similar to VV 1987:43, this recommendation also stresses on that the practical design rules, used today, is based on no prior knowledge of ice mechanics. Since more than 20 years has passed since it was published, the guideline also emphasize the empirical value of this design rule. No larger damage on bridge supports has been reported over the years and therefore the recommended values can be assumed to be reliable and conservative.

Firstly, Fransson and Bergdahl (2009) treats the thermal ice pressure. No difference is made here compared to VV 1987:43 which means that the ice load can be calculated as in (4-1). Secondly, they treat the horizontal ice load caused by a moving ice sheet. Here, it is also estimated in the same way as in VV 1987:43 and it can be calculated according to (4-3). However, some differences are made regarding the crushing strength of the ice, since the recommendation is referred to offshore foundations in the Baltic Sea. Thirdly, the ice loads which are induced by wind or current are treated (Fransson and Bergdahl, 2009). This part is not included in VV 1987:43 and the ice load could be estimated as:

$$I_{h,w/c} = C_d \rho \frac{U^2}{2} A \tag{4-5}$$

where,
C_d 0.004 for wind and 0.006 for current,
ρ 1.3 kg/m³ for wind and 1 000 kg/m³ for current,
U free stream velocity at 10 meters above ice surface or free stream at one meter below the ice lower surface [m/s], and
A area of the ice floe [m²].

Fransson and Bergdahl (2009) also suggest a calculation for a maximal static horizontal ice load on a vertical structure with the crushing strength of ice as an starting point:

$$I_{h,crush} = bt\sigma_c k_1 k_2 k_3 \tag{4-6}$$

where,

b   column width [m],

t   ice thickness [m],

σ_c crushing strength of ice [Pa],

k_1 shape factor concerning the shape of the column [-], see Table 4-4,

k_2 contact factor concerning the movement of the ice, see Table 4-5,

k_3 aspect ratio factor [-]:

$$k_3 = \sqrt{1 + 5t/b} \qquad \begin{cases} t/b \leq 1 \ \rightarrow \ 1 \leq k_3 \leq 2.5 \\ \ \ t/b > 1 \ \rightarrow \ k_3 = 2.5 \end{cases} \qquad (4\text{-}7)$$

Table 4-4.   *Values of the shape factor k_1 with respect to column width (Fransson and Bergdahl, 2009).*

Shape of column	k_1
Rectangular	1.0
Circular	0.9

Table 4-5.   *Values of the contact factor k_2 with respect to the movement of the ice (Fransson and Bergdahl, 2009).*

Movement of the ice	k_2
Continuously moving	0.5
Frozen to the foundation at start of movement	1.0
Ice locally increased around the foundation	1.5

4.6.2 Eurocode for design of concrete dam

Andersson *et al.* (2016) aimed to develop how Eurocode, together with RIDAS, could be used during design of concrete dams by suggesting ice loads. It is important to note that the report is not a recommendation of how to design concrete dams, but rather a suggestion on how to implement Eurocode on Swedish concrete dams since the design differ from other structures. Andersson *et al* (2016) mention that the characteristic value of the ice load is determined according to Table 4-6. If the ice thickness will never be over 0.4 meter, the design due to ice loads can be neglected (Andersson *et al.*, 2016).

Table 4-6.   *Characteristic distributed ice loads and ice thickness based on average yearly maximum ice thickness (Andersson et al., 2016).*

Ice thickness [m]	Characteristic distributed ice load [kN/m]
0.4	85
0.6	180
0.8	215
1.0	245
1.2	280

5 Modelling

The FE analyses were performed in Abaqus/CAE 2017. The modelling was limited to Abaqus standard version which is ideal for static loading and low–speed dynamic interactions (SIMULIA, 2018). The material model in the standard version is limited to describe yielding. Consequently, it cannot describe ice and its non-simultaneous failure modes. Many researchers stress on the importance of this phenomenon, see e.g. Johnston, Croasdale and Jordaan (1998), Kolari, Kuutti and Kurkela (2009) and Karna, Frederking and Shkhinek (2011). Another aspect to consider is that the ice structure interaction is caused by driving forces such as wind and current, which are high–speed dynamic interactions (Määttänen, 1991). Thereby, the analyses were limited to only show the ice behaviour until either cracking or crushing occurs.

In Abaqus, no units are defined as default and therefore it is the users decision to decide which units that are used in the models, see Table 5-1. It is important to be consequent and use the same units in all parts of the models to avoid errors in the results. A more detailed description of the modelling is presented in Appendix A.

Table 5-1.   Quantities and units used in Abaqus.

Quantity	SI - unit
Length	mm
Force	N
Stress	N/mm^2

In the following sections, the modelling of ice structure interactions in Abaqus are treated. The content in the sections are: introduction of the models, element properties, material model, extended finite element method, solution method as well as definition of boundary- and loading conditions.

5.1 Introduction of models

One aim with this study was to simulate the interaction between a large ice sheet and structures in water, e.g. bridge or pier supports, see Section 1.2. To limit the amount of possible cases, two different models were created: Model S – single column, see Figure 5-1, and Model M – multiple columns, see Figure 5-2. The ice sheet was reduced to a smaller area in order to achieve a manageable model size and minimize the computer time. The ice was the only modelled and analysed part whereas the columns were considered as infinitely stiff and instead acted as loads on the ice. The ice was modelled fixed, instead the columns worked as an increasing load, or increased prescribed displacement. The effects were the same as if the ice sheet would be the moving object. In Model S, the interaction between a single column and an ice sheet was simulated and in Model M, the interaction between an ice sheet with multiple columns were simulated. However, only two columns were represented in the FE model, see Figure 5-2.
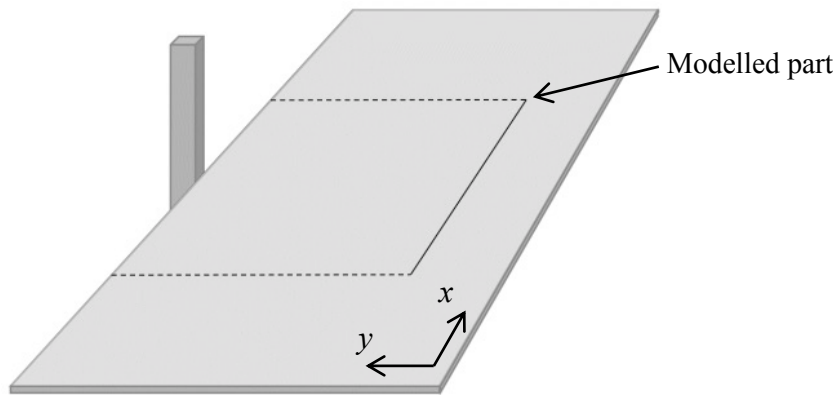
Figure 5-1.   Sketch of Model S – singe column with the modelled part marked.
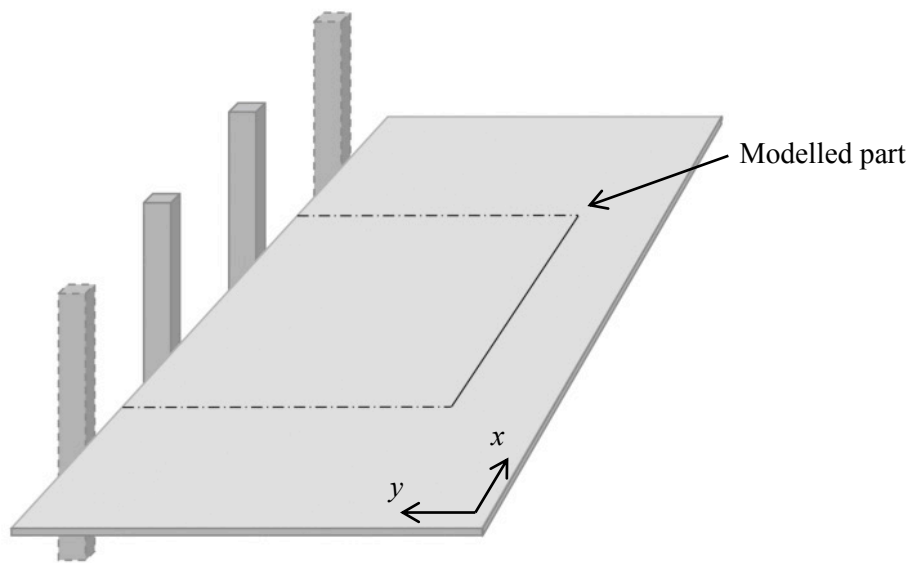
Figure 5-2.   Sketch of Model M – multiple columns with the modelled part marked.

5.2   Element properties

The element type that was used in all models, to simulate the ice, was a bilinear 4-node quadrilateral plane stress element, see Figure 5-3 (SIMULIA, 2014). The notation of the element in Abaqus is CPS4R. By the usage of plane stress element, out-of-plane normal- and shear stresses are equal to zero. To save computer time, reduced integration was implemented together with enhanced hourglass control in order to minimize the loss of zero-energy in the elements. Plane stress elements were chosen since the type is recommended to be used when the thickness of the modelled part is smaller compared to its lateral dimensions as well as the limitation due to XFEM, see further Section 5.4. The plane stress thickness was set to 1 millimetre; thus the results from Abaqus were given per millimetre thickness.
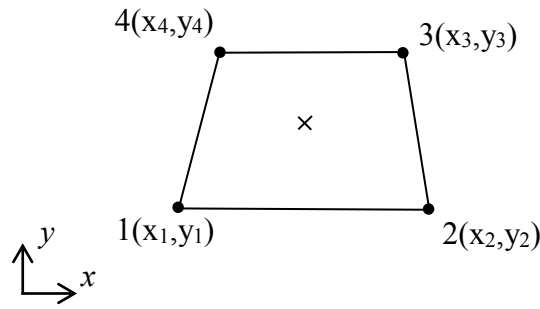
Figure 5-3. *Bilinear 4-node quadrilateral plane stress element with global coordinates used in Abaqus with a displayed reduced integration point in the middle.*

5.3 Material model

The material model in the FE analyses should be able to predict how the ice would act during an interaction. Ice has a brittle behaviour, described further in Section 3.3, which is similar to the behaviour of plain concrete. Abaqus, and many other FE programs, can describe the behaviour of concrete well and therefore a material model for concrete was used as a starting point for describing ice and its material behaviour. It was then modified, resulting in an elastic-perfectly plastic model, see Figure 5-4, with a maximum principal stress limit, equal to the tensile strength of ice, in order to predict cracks, see Table 5-2. The cracks were modelled with extended finite element method (XFEM), see Section 5.4. The damage criteria in XFEM included the fracture energy of the ice.

Table 5-2. *Summation of input values used for the material model in Abaqus.*

Input	Value
Young's modulus, E	3 500 MPa
Poisson's ratio, v	0.3
Yield stress (compressive strength), σ_c	1.4 MPa
Max principal stress (tensile strength), σ_t	0.1 MPa
Fracture energy, G_F	15 000 N/mm
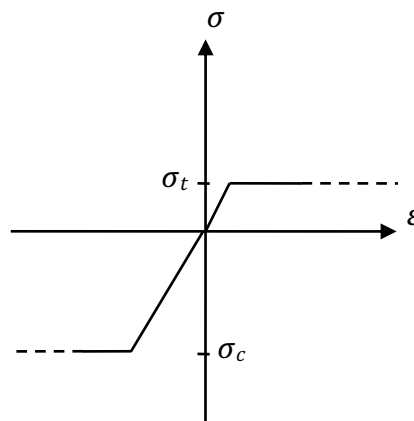
Figure 5-4. *Elastic-perfectly plastic material model of a material.*

In order to capture crushing failure of ice, an implementation of its compressive strength was needed; this was done through the plastic behaviour. In Abaqus, the inputs to the plastic model is the yield stress and the plastic strain of the material, see

Table 5-2 (SIMULIA, 2014). For ice, the yield stress could be translated to its compressive strength, σ_c, and the plastic strain, ε_{pl}, was described as an infinitely large value. The first strain value could be obtained with help of Hooke's law, using Young's Modulus and the compressive strength.

As mentioned in Section 3.1.5, Bouchat and Tremblay (2017) suggested that the tensile strength should be set to zero during modelling since ice in reality is cracked and therefore resist a very small amount of tension. However, during this study the focus was the failure and its respective load. This led to that the ice sheet required some amount of tensile strength, otherwise the ice would always fail in tension.

5.4   Extended finite element method, XFEM

One way of modelling cracks in Abaqus is by using the extended finite element method, XFEM (SIMULIA, 2014). It is a numerical technique aiming to describe the crack and its motion by using exclusively nodal data. This means that no explicit representation of the crack is needed, i.e. the crack path does not need to be represented by a vector showing the initiation and crack direction. Instead, XFEM is applied on an area and the displacement vector for the nodes within this area contains two extra terms, describing an asymptotic crack-tip function and a jump function. The crack-tip function serves to catch the singularity arising around the crack tip which initiate the crack, and the discontinuous jump function represents the instant spread of the crack through an element. These functions force the crack to progress through an entire element in one step, see Figure 5-5 a), which is done to avoid the occurrence of any stress singularity that could arise in the middle of the element, see Figure 5-5 b).

Stress singularity

a) Crack with XFEM

b) Crack which causes stress
    singularity in the middle
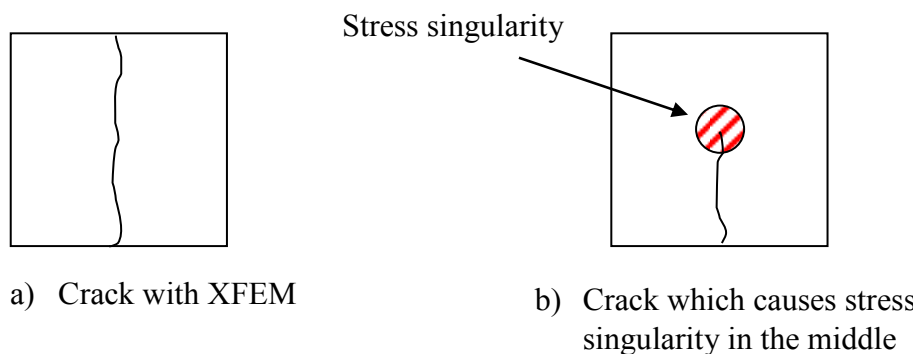
Figure 5-5.   Illustration of crack progression in an element: a) crack with XFEM b) crack which causes stress singularity.

Another aspect of XFEM is that two cracks can neither progress through the same element nor join together into one single crack. A final aspect is that one crack cannot divide into two cracks (SIMULIA, 2014). Different damage initiation criteria can be used in XFEM which is incorporated into the material properties.

In the model, the area where XFEM was assigned cracks arouse in elements which gradually fulfilled the damage criteria. This means that a larger area would result in more cracks. Like plain concrete, several cracks are not expected, instead one crack would appear and progress through the ice until global failure. In the model, this behaviour was implemented by first assigning XFEM to the whole model area to find where the stress was largest and cracks would appear, see Figure 5-6. a). Afterwards

this area was minimized, in order to compel the model to only generate one single crack within each XFEM area, see Figure 5-6. b). When the desired response with one single crack within each area was found, the stress distribution was verified so that cracks appeared where the highest tensile stresses occurred. If the response was wrong, the XFEM region was repositioned and a new verification was made.

a) Step 1: XFEM whole area.   b) Step 2: XFEM limited to two smaller areas.
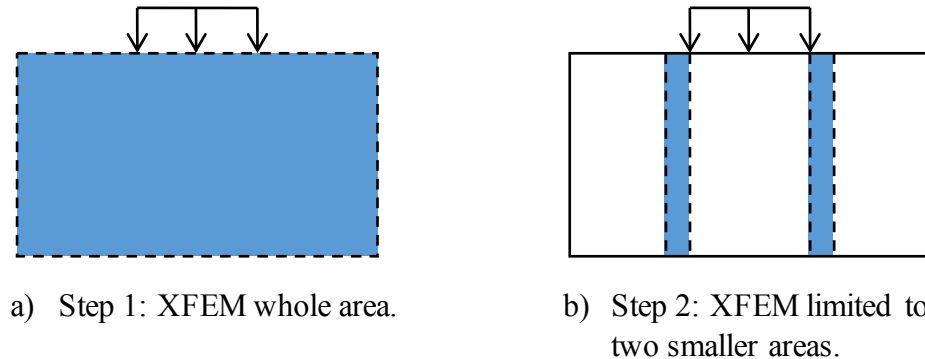
Figure 5-6.   Schematic illustration of the applied XFEM area: a) Step 1: XFEM whole area b) Step 2: XFEM limited to two smaller areas.

5.5   Solution method

In the step module, a *Static, General* procedure was used (SIMULIA, 2014). This procedure can be either linear or nonlinear and neglects time-dependent material- and inertia effects. In the analyses the nonlinear geometric effects, *Nlgeom*, can be included (SIMULIA, 2014). However, this was not chosen to be included, since the main focus were on the failure mode. At failure the deformation of the ice sheet was relatively small. To conclude, *Nlgeom* was set to off. The used solution technique were *Full Newton* with an *direct equation solver* (SIMULIA, 2014). These are default values in Abaqus *Static, General* procedure. The time period was variable and set to one for all analyses, and the chosen increments are shown in Table 5-3.

Table 5-3.   Chosen increment sizes in all analyses in Abaqus.

Increment size	Value
Initial	0.001
Minimum	$1x10^{-18}$
Maximum	0.1

5.6   Boundary conditions

In reality, the bottom boundary of the ice sheet corresponds to the far back. Since only a part of the ice sheet was modelled, the boundary conditions should simulate a continuation of the ice sheet. A continuous ice sheet would give constraint in both x- and y-direction, in the plane, as well as counteract rotations around its z-axis. Therefore, the translation in x- respective y-direction were locked as well as rotation around the z-axis. This would, in Abaqus, result in a fixed boundary condition when using CPS4R elements (SIMULIA, 2014). Fixed boundary conditions were therefore used for the bottom boundary for both Model S and Model M, see Figure 5-7 and Figure 5-8.

The sides of the ice sheet were modelled in two different ways. For Model S, the sides of the ice sheet were only locked in x-direction, in order to simulate the restraint that a continuous ice sheet would give, see Figure 5-7. Symmetry lines would give the same response since plane stress elements were used.
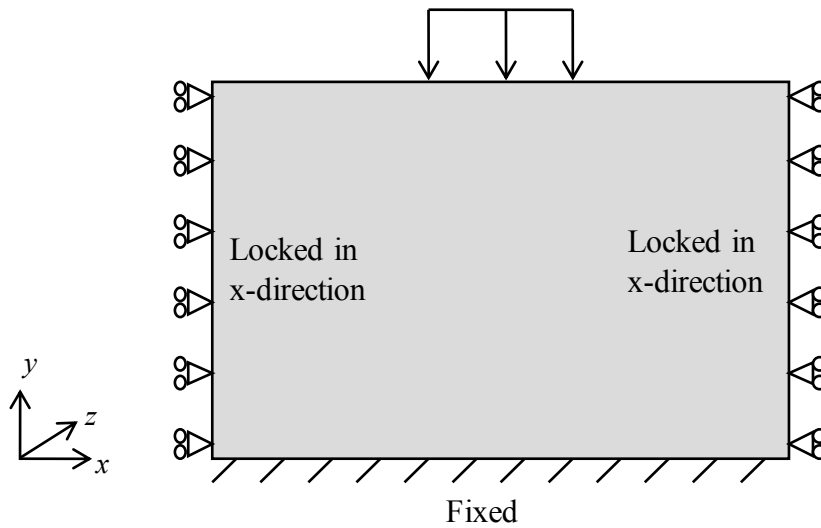
Figure 5-7.   Schematic illustration of the applied boundary conditions in Abaqus for Model S.

In Model M, symmetry lines were used on both sides to mirror the model around its side edges, see Figure 5-8. Thereby, the desired configuration in Figure 1-2 b) could be simulated and possible influence of the columns would contribute.
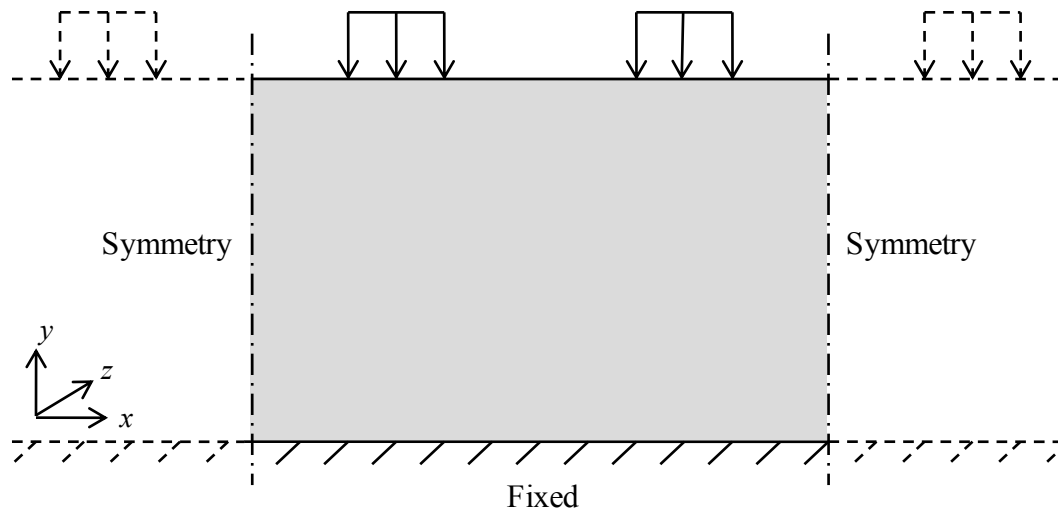
Figure 5-8.   Schematic illustration of the applied boundary conditions in Abaqus for Model M.

The columns were modelled with prescribed displacement which simulates a more realistic interaction because the stresses increase at the edges. A total displacement was given as the prescribed displacement and was then increased gradually with the chosen increments, described in Section 5.5. Since a variable increment size was used, the loading rate had irregular steps in one analysis, but also between the different analyses. A fixed increment could be used, but the computer time would then become unreasonably long since the smallest needed increment then is used for the entire analysis.

6 Analyses of Model S – single column

Model S simulated an ice sheet and its interaction with a single column, see Figure 5-1. The notations of the modelled ice sheet are presented in Figure 6-1 and its boundary conditions are displayed in Figure 5-7. The first step in the analysis were to determine the sizes of the column widths which were used in later analyses. After determination of the column widths, the heights of the modelled ice sheet was investigated, since it influence the global response. The results from the analyses were compared to analytical calculations according to guidelines, see Chapter 8.
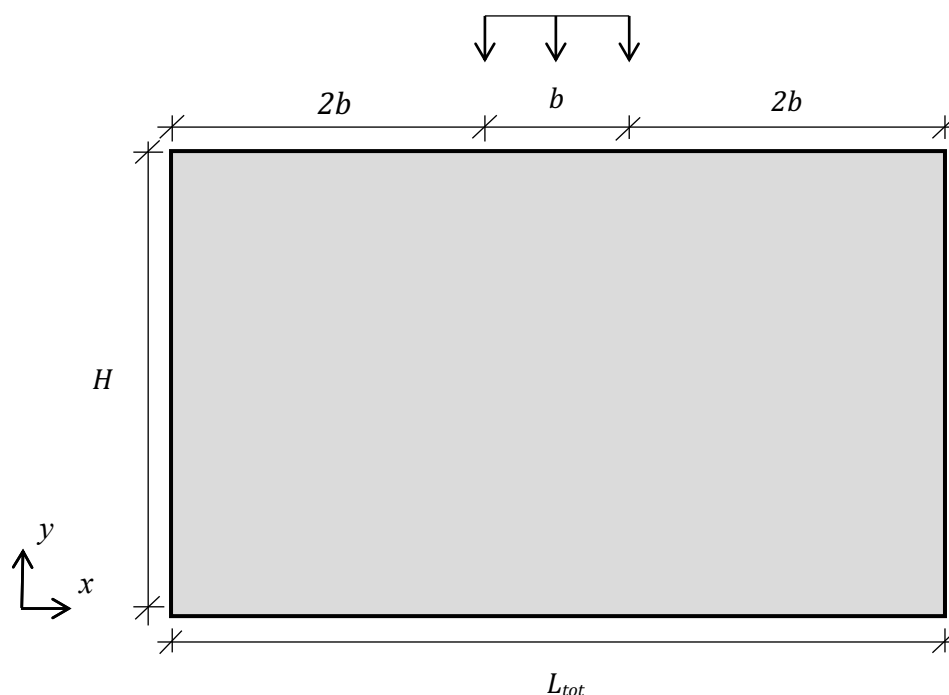
Figure 6-1.   Notations for Model S – single column.

In the analyses, the applied loads at crushing or cracking were of interest. Since displacement control was used for all analyses, there was a need for a transformation between the applied displacement at crushing or cracking to the corresponding applied load. The transformation was performed by adding the reaction forces in y-direction in all bottom nodes at all time steps. This led to a reaction force in Newton per millimetre thickness of the ice sheet, which is equal to the magnitude of an applied ice load. The load was then transformed to an equivalent pressure by dividing it with the analysed column width. This transformation enabled an easier comparison between the models.

The minimum and maximum principal stress were extracted from the top elements for all time steps in order to determine when crushing or cracking occurred. The top elements were used since they are located where the highest respectively lowest values occurred, see Figure 6-2 and Figure 6-3. As mentioned in Section 5.5, a variable time step was used which led to irregular steps between the different analyses, thus a linear relationship was assumed between the time steps. By that, the exact cracking or crushing load could be determined and compared between the models.
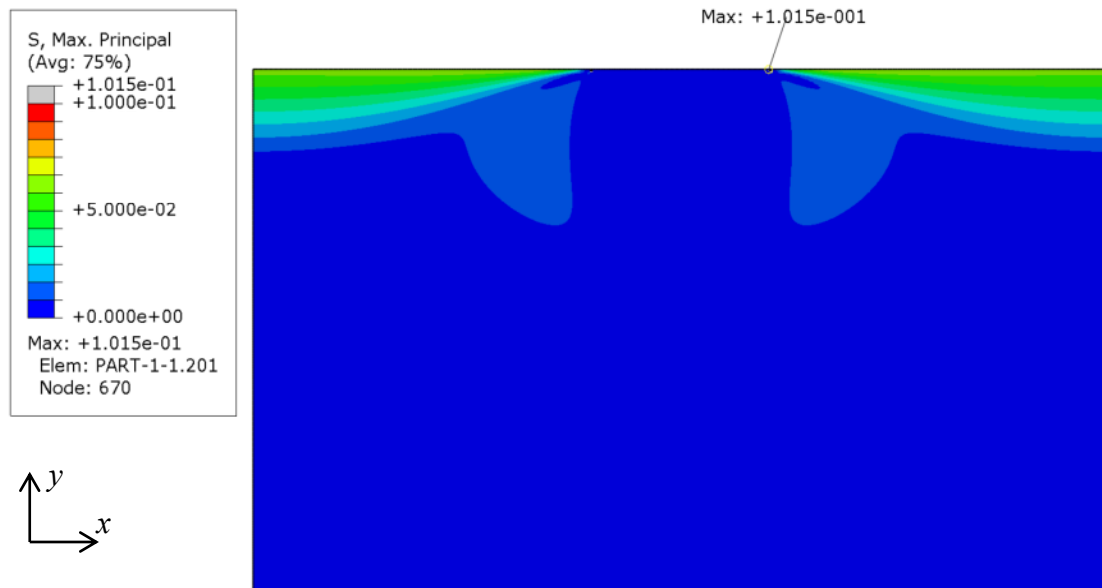
Figure 6-2.   Maximal principal stress in MPa at cracking for Model S200.

Figure 6-3.   Minimal principal stress in MPa at crushing for Model S200.

6.1   Investigation of column width, *b*

To determine which column widths, notated *b*, that would be used in further analyses, an investigation of different widths were needed. The width was varied between 200 and 1 200 millimetres, see Table 6-1. The values were chosen based on realistic sizes of columns used in marine environments[1]. The height was investigated later and kept constant to a value of 2*b*, which showed to be sufficient enough. For the notations of the dimensions in Table 6-1, see Figure 6-1.

---

[1] Emil Lindqvist (structural engineer at ÅF Infrastructure) supervising meeting March 26th 2018.

Table 6-1.   *Overview of the analysed column widths and corresponding dimensions for Model S.*

Model	Column width, b [mm]	Height, H [mm]	Total length, L_{tot} [mm]
S200	200	400	1 000
S400	400	800	2 000
S600	600	1 200	3 000
S800	800	1 600	4 000
S1200	1 200	2 400	6 000

The number of elements were modelled with a constant, but reasonable, number. This was considered to be a reasonable assumption since only the influence of different column widths were investigated and not the magnitude of the stresses.

The results from the investigations of column widths showed a nonlinear behaviour of the pressure for different column widths, see Figure 6-4. However, a linear relation was observed for column widths 400, 600 and 800 millimetres whereas the smaller and higher widths of 200 and 1 200 millimetres differed from this relation.
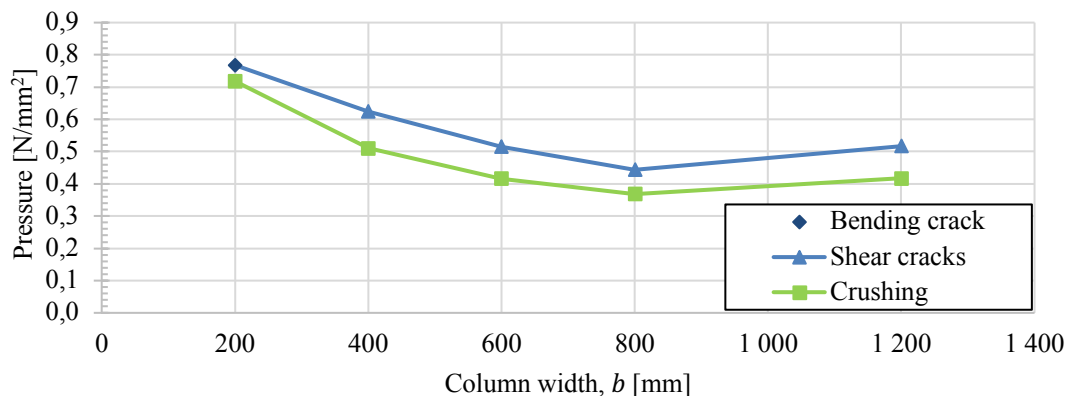
Figure 6-4.   *Applied pressure at the column versus column width for Model S.*

Some investigations were performed in order to identify why the two models, S200 and S1200, diverged from the observed linear relation. The investigations and conclusions were:

1. The total width and height of the models were sufficient enough with regard to the distribution of loads within the sheet. Both larger and smaller widths and heights were analysed and showed similar results.
2. The approach by using XFEM cracks did not influence the response of the sheet since cracking always occurred after crushing for all models, see Figure 6-4.
3. Different mesh sizes were investigated with the conclusion that the type of observed crack changed, and the magnitude of the pressure decreased slightly but no linear relation was observed. See Section 6.2 for further investigation within this subject.
4. The displayed pressure, in Figure 6-4, was extracted when local crushing or cracking occurred i.e. one element reached the fracture limit. Thereby, different behaviour might be observed if the global failure would have been included.

To summarise, no general conclusion was drawn concerning why S200 and S1200 diverged from the observed linear relation for the results of the other analyses. The applied load at crushing/cracking increased with increasing column width, but when transforming the applied load to an applied pressure, it increased for the larger column width, instead of decreased. Thus, there is a link between the applied pressure and the area of the column.

Finally, it was chosen to carry on with three different widths of the column: 200, 600 and 1200 millimetres. The column width 600 millimetres was chosen since it was in between 400 and 800 millimetres, and 200 and 1200 millimetres were chosen since they diverged from the observed linear relation. For exact values of the pressure at the event of cracking and crushing due to different column widths, see Appendix C.

6.2 Mesh convergence for Model S

The mesh convergence was carried out on each of the three column widths; Model S200, S600 and S1200 with a constant height of 2b. In the mesh convergence, the number of elements in the model were compared against the calculated applied pressure at a certain prescribed displacement. The prescribed displacement for the models was chosen right before the plastic limit occurred since the largest difference between different mesh sizes was observed there, see Figure 6-5. Pressure displacement curve showed that the plastic limit for Model S200 occurred at an applied displacement of 0.12 millimetres. Thus, 0.10 millimetre was used in the converge study of this model since it was before the plastic limit and well after both crushing and cracking. For the other two models, S600 and S1200, the same approach was implemented with resulting in that the displacement at plastic limit increased to 0.3 millimetres for Model S600 and 0.6 millimetres for Model S1200. For final mesh sizes and review of the mesh convergence studies for Model S200, S600 and S1200, see Appendix B.
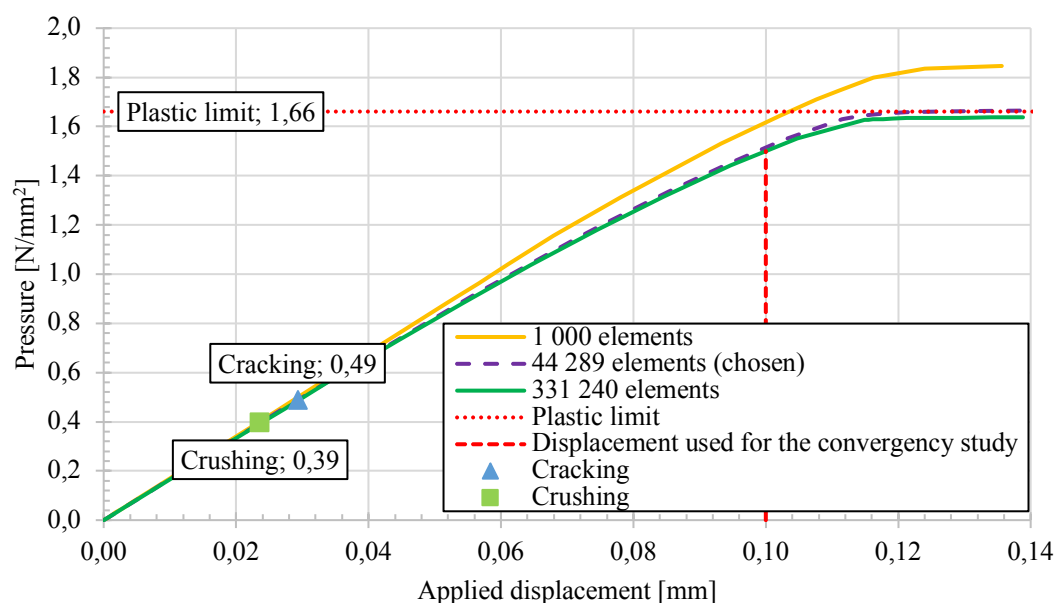
Figure 6-5.   Pressure-displacement curve for Model S200 with smallest and largest analysed number of elements as well as the pressure at crushing, cracking and plastic limit.

6.3   Height investigation of the modelled ice sheet

As mentioned above, the height of the modelled ice sheet could influence the magnitude of the pressure, and thereby also its global response. Thereby, different heights were analysed for Model S200, S600 and S1200 in order to determine a minimum required height. The minimum required height for all three models were determined with respect to its total length defining a ratio, R_1:

$$R_1 = \frac{H}{L_{tot}} \qquad\qquad (6\text{-}1)$$

The ratio, R_1, was defined to be able to transfer the minimum required height to analyses of Model M. The different heights that were analysed are presented in Table 6-2. For notations of b, H and L_{tot}, see Figure 6-1.

Table 6-2.   All heights analysed for the three different models; S200, S600 and S1200.

Model	Column width, b [mm]	Height, H [mm]	Total length, L_{tot} [mm]
S200	200	200, 300, 500, 600, 800, 1 000, 1 600	1 000
S600	600	600, 900, 1 200, 1 800, 2 400, 4 800	2 000
S1200	1 200	1 200, 1 800, 2 400, 3 600, 4 800, 7 200, 9 600	3 000

The pressure at cracking showed a change in its behaviour and different cracks appeared depending on the used number of elements. Two different crack responses were observed; bending cracks and shear cracks, see Figure 6-6.

a) Bending cracks   b) Shear cracks
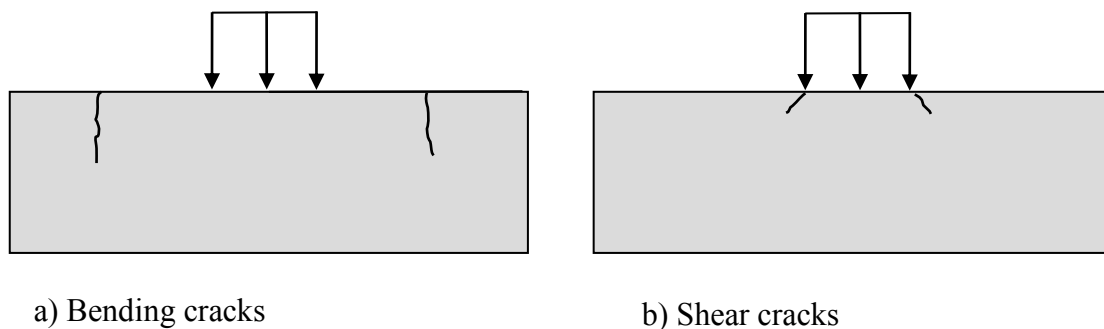
Figure 6-6.   Schematic illustration of a) Bending cracks observed in Model S, b) Shear cracks observed in Model S.

The results of the height investigation for Model S200, column width of 200 millimetres, are presented in Figure 6-7. In the figure it is seen that the cracking and crushing behaviour is constant for $R_1 \geq 0.3$, and the result can be assumed to fully converge at $R_1 = 0.6$. However, the responses differ for ratios smaller than 0.3. For these ratios, cracking occurred before crushing, which led to another global response. The cracking behaviour was also different for ratios smaller than 0.3. At this ratio, bending cracks were observed, instead of shear cracks. Bending cracks occurred for

smaller ratios, which was reasonable since it meant that the length, L_{tot}, was large, see equation (5-1). With a large length, or a small height, the sheet acts as a slender beam and the response due to bending is expected. Since the behaviour between the different crack responses was unknown, as well as when the transition takes place, a linear relation was assumed.
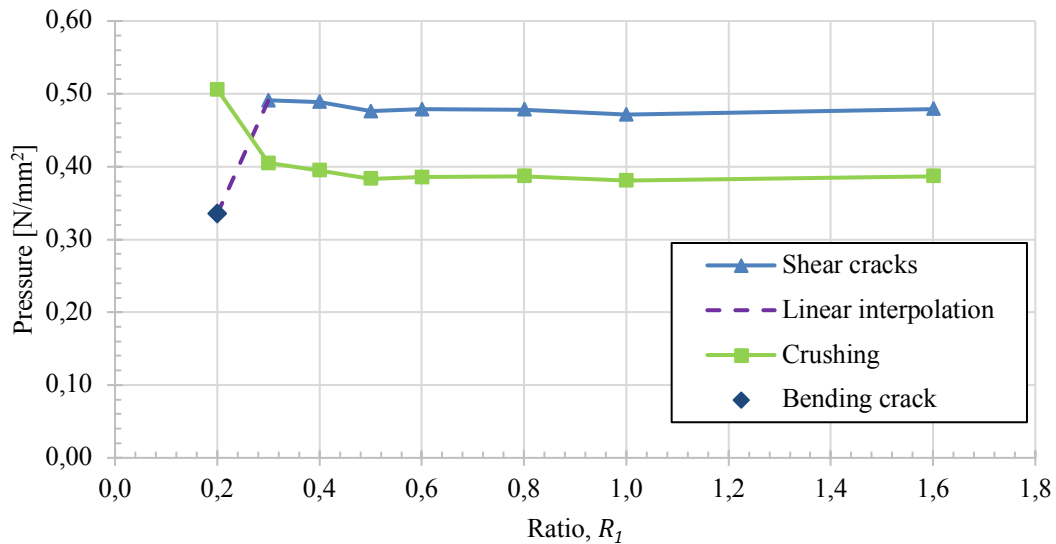
Figure 6-7.   *Height investigation for Model S200 with the pressure versus the ratio $R_1=H/L_{tot}$.*

Furthermore, the results for Model S600, column width of 600 millimetres, with different heights are displayed in Figure 6-8. Some irregularities were observed for smaller ratios. Likewise as for Model S200, the load converged at ratios larger than 0.6. The same change in cracking response was also observed, where bending cracks were seen for ratio equal to 0.2.
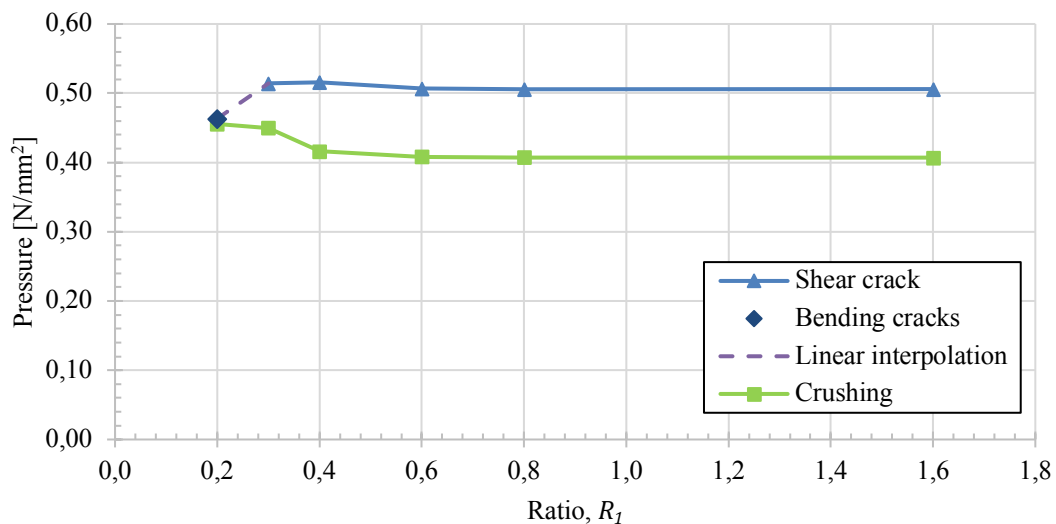
Figure 6-8.   *Height investigation for Model S600 with the pressure versus the ratio $R_1=H/L_{tot}$.*

At last, the results from the height investigation for Model S1200, column width of 1 200 millimetres, is shown in Figure 6-9. In this figure, a larger difference was observed for the smaller ratios. The larger difference could be explained by the same approach as previous; the cracking response goes from bending to shear cracks. The pressure converged at around $R_1 = 0.6$.
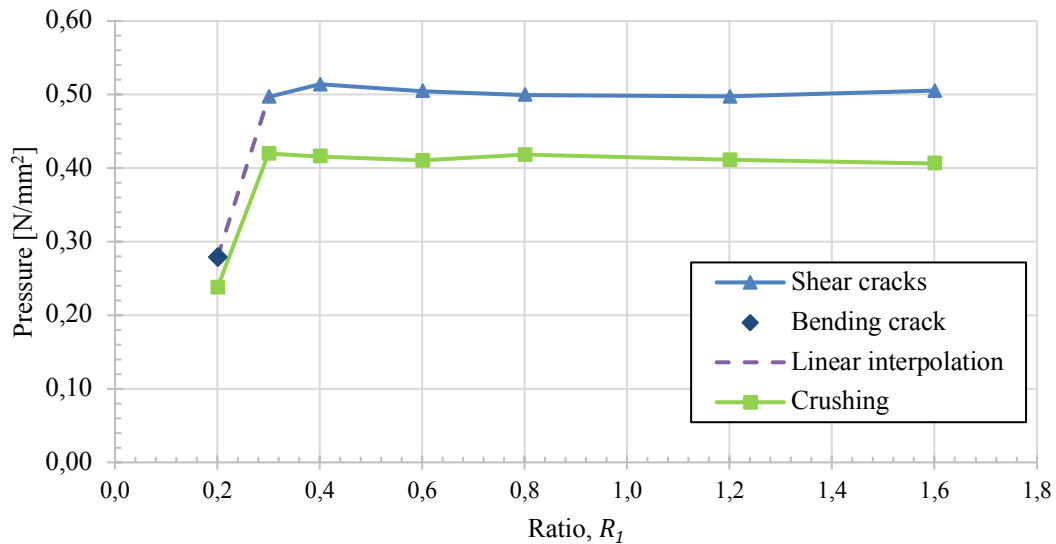
Figure 6-9.   *Height investigation for Model S1200 with the pressure versus the ratio $R_1=H/L_{tot}$.*

To summarise the results regarding pressure at cracking, all three models had the same response at ratios equal to 0.2, where bending cracks were observed, see Figure 6-10. For ratios larger than 0.2, shear cracks were instead observed at the edges of the column, see Figure 6-6 for the two crack responses. At heights where shear cracks arouse, the applied pressure was roughly constant, and the models converged at $R_1 = 0.6$. The cracking pressure for Model S200 was observed to have a constant lower value while the other two models reached larger, and more similar, values.
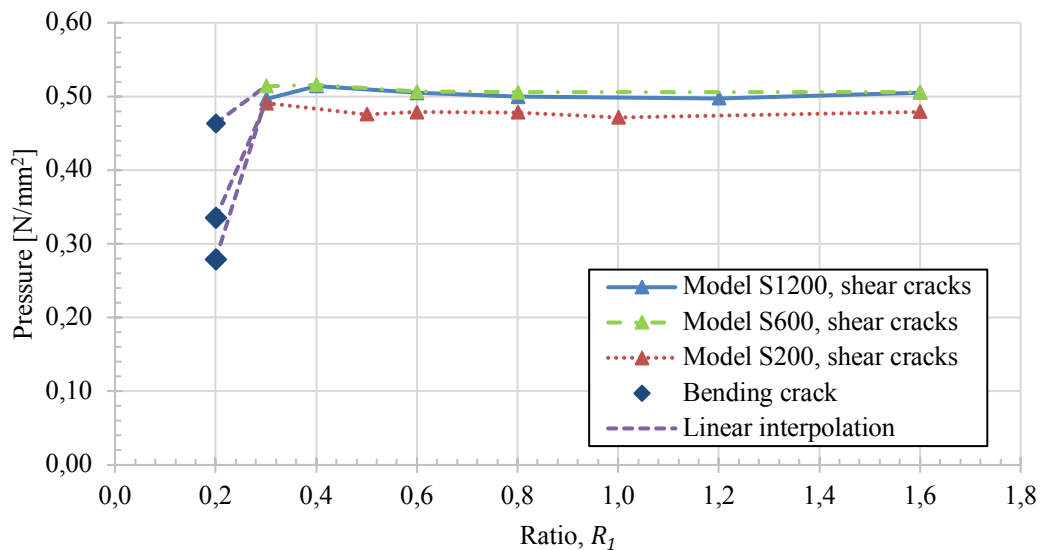
Figure 6-10.   *Pressure at cracking for Model S200, S600 and S1200, including their responses, displayed against the ratio $R_1=H/L_{tot}$.*

To summarise the results regarding pressure at crushing, the applied pressure also showed a deviation for the smallest ratios and then reached constant pressure values at a ratio of 0.6, see Figure 6-11. For crushing, the differences in magnitude between the three models at this ratio were similar to the pressure at cracking. However, the deviating pressure at $R_1 = 0.2$ showed both larger and smaller values depending on model, see Figure 6-11. The smallest model, S200, gave a higher value at this ratio while it decreased some for Model S600, and finally was much smaller for the largest model, S1200. One explanation to this behaviour could be that the stress in Model S1200 is distributed over a larger area, and therefore results in a smaller value when local crushing occurs compared to Model S200 and S600. A last aspect to consider for the crushing pressure is that crushing occurred at the elements next to where the displacement was applied, see further in Section 6.4. As the displacement increased, the crushing pressure also increased to infinity, i.e. a singular point. Results from a singular point are often excluded, but since crushing occurred there, this was the point where the shown pressure in Figure 6-11 was extracted. Therefore, some caution was needed when conclusions were drawn from the displayed crushing pressure.
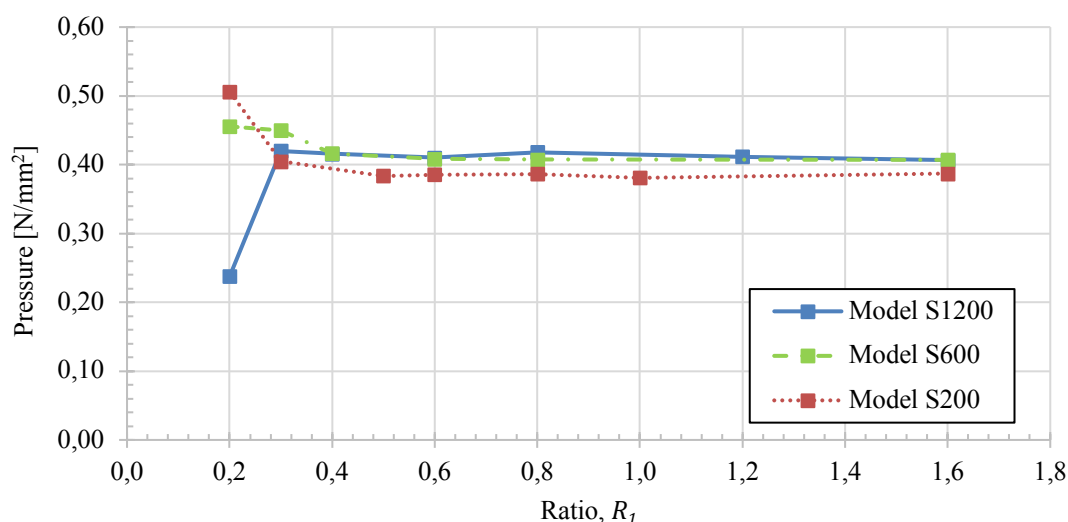
Figure 6-11. *Crushing pressure for Model S200, S600 and S1200 displayed against the ratio $R_1=H/L_{tot}$.*

Altogether, the height was assumed to be converged at $R_1 = 0.6$. This ratio was therefore used in further studies of Model S and Model M. For exact value of the pressure from Figure 6-7 to Figure 6-11, see Appendix C.

6.4 Stresses at crushing and cracking for Model S

The stress distribution of the analysed ice varied over the entire sheet. As seen in Figure 6-12, the largest minimal stresses occurred where the ice sheet interacted with the column, and resulting in crushing failure at these locations. In the models, this region represents where the displacement was applied. Therefore, it was interesting to study the stress distribution and the magnitude of the stress within this region.
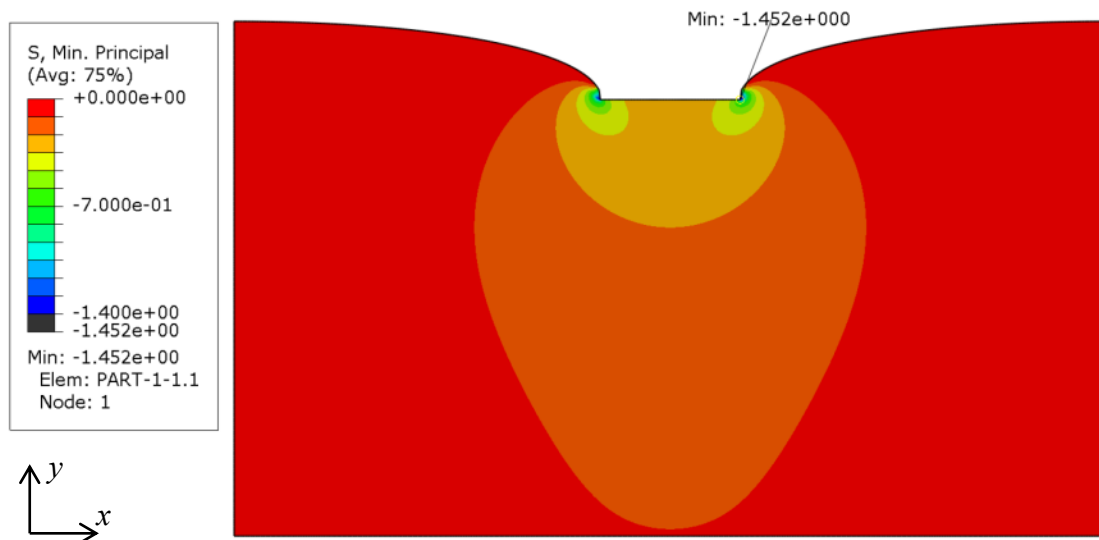
Figure 6-12.   Minimal principal stress in MPa at crushing for Model S200.

To see the local effects of the modelling choices of the column, the minimal principal stress under the column was extracted for both the prescribed displacement and for an applied load. The stress was extracted at the time step when crushing first occurred, i.e. when the minimal principal stress reached the yield stress of 1.4 MPa. The visual geometrical difference in the stress distribution and deformation between the two load modelling approaches is distinct, see Figure 6-13. For an applied load, a constant stress distribution was observed under the column and crushing occurred over the entire width. For the prescribed displacement, the stress distribution changed to only reach the crushing limit at the edges of the column.

a) Prescribed displacement
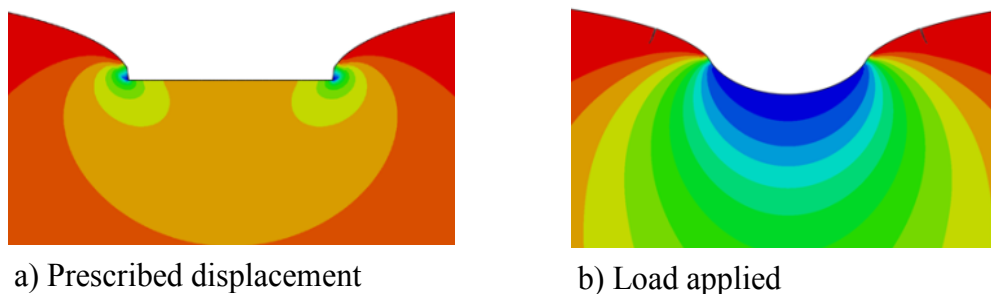
b) Load applied

Figure 6-13.   Different stress distribution at crushing for a model with a) prescribed displacement and b) load applied.

When the stress distribution for prescribed displacement is plotted in a graph, peak values were observed at the edges of the column, see Figure 6-14. Therefore, the initial crushing of the ice sheet arouse at the edges. However, when an applied load was used, instead of a prescribed displacement, the crushing strength was reached across the entire length of the column with no peak values, see Figure 6-14. Next to the column, where no displacement or load was applied, a distinct decrease in stress was visible for both approaches. Due to the differences, the modelling choices became evident for the results, see Figure 6-14. By a comparison with the graphical pictures in Figure 6-13, the results showed in the graphs become validated and together they give an overall picture.
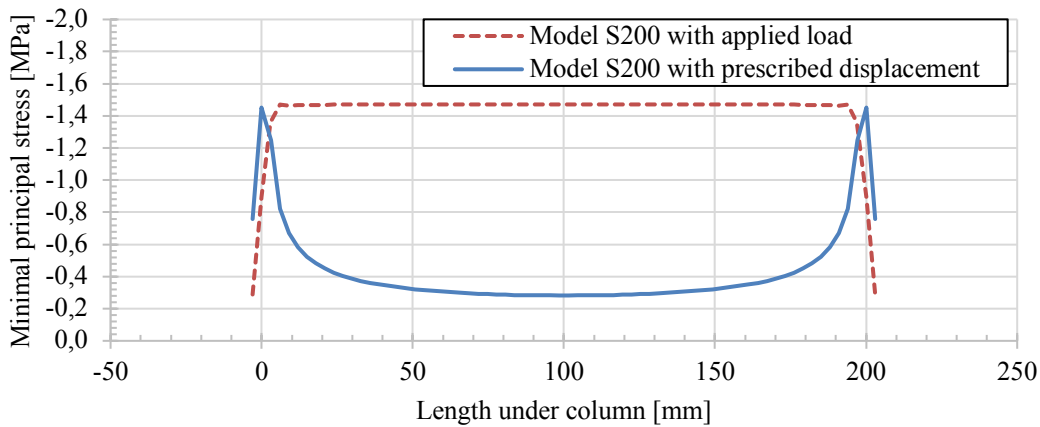
Figure 6-14. *Minimal principal stress under the column versus actual length under it for Model S200, and R₁ = 0.6.*

For Model S600 and S1200 the same behaviours were observed. With prescribed displacement, crushing was seen at the edges and with load applied the crushing strength was reached throughout the entire column width, see Figure 6-15 and Figure 6-16.
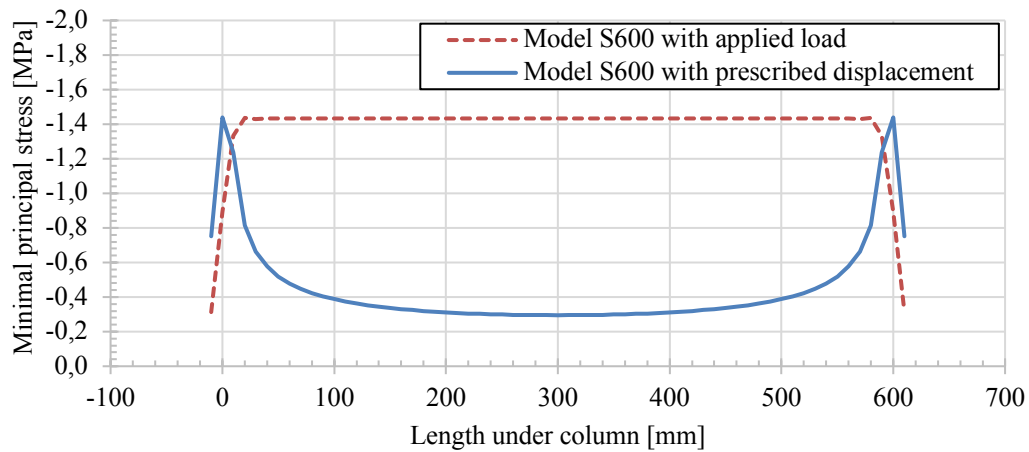
Figure 6-15. *Minimal principal stress under the column versus actual length under it for Model S600, and R₁ = 0.6.*
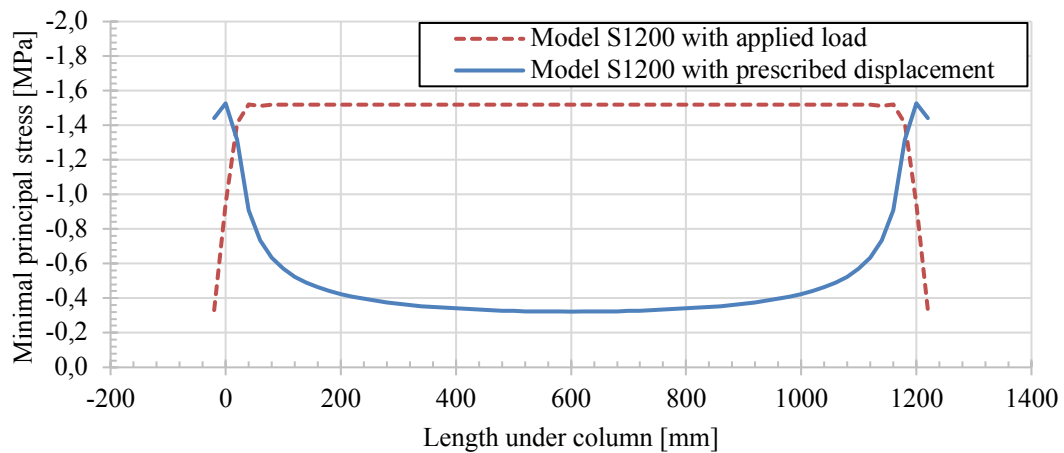
Figure 6-16. *Minimal principal stress under the column versus actual length under it for Model S1200, and R₁ = 0.6.*

The applied ice load for the two modelling approaches could be calculated from Figure 6-14, Figure 6-15 and Figure 6-16. This was done with an estimation of the area under the curves, with the help of Riemann sums. The results, displayed in Table 6-3, showed a significant difference between the load with prescribed displacement compared to the result from the analyses with applied load. This agrees with the observed and presented responses in Figure 6-13 to Figure 6-16. Equilibrium was observed in all models, but the comparison between the two approaches, load under the stress distribution curve and summation of reaction forces, generated some difference between the different models, see Table 6-3. The reason for this difference between the two approaches for prescribed displacement could be that it generated a stress peak value, and the approximation with Riemann sums therefore overestimated the load due to a large division of the length. Regarding the applied load, the difference between the two approaches instead depends on the stress spread which goes beyond the column width, and thereby excluding stresses that would contribute to a larger load.

Table 6-3.   Approximation of load per mm thickness for Model S with both prescribed displacement and with applied load at crushing.

Model	Prescribed displacement		Applied load	
	Approximated load under stress distribution curve [N per mm thickness]	Sum reaction forces in y-direction [N per mm thickness]	Approximated load under stress distribution curve [N per mm thickness]	Sum reaction forces in y-direction [N per mm thickness]
S200	89	77	282	294
S600	280	273	844	861
S1200	638	596	1 696	1823

The stress distribution in the ice sheet, and its magnitude, effect where cracks could appear. Consequently, different crack behaviours could arise; see Figure 6-6 for the two observed crack responses. Bending cracks occurred for small ratios, $R_1 \leq 0.2$, whilst shear cracks occurred for larger ratios. The shear cracks where at the edges of the column, see Figure 6-17. As seen in the figure, no other part of the ice sheet had a larger stress than maximum principal stress at cracking, 0.1 MPa. When the cracks propagated through the element, other parts of the ice sheet may reach its tensile strength and, accordingly, cracks could initiate in these parts. However, since the areas that allow cracks were limited in order to simulate the brittle behaviour of ice, no new cracks could initiate at areas outside the limited XFEM area, see Section 5.4. The result of this limitation was that cracks only initiates in areas that reach the tensile strength first and afterwards no new cracks could initiate.
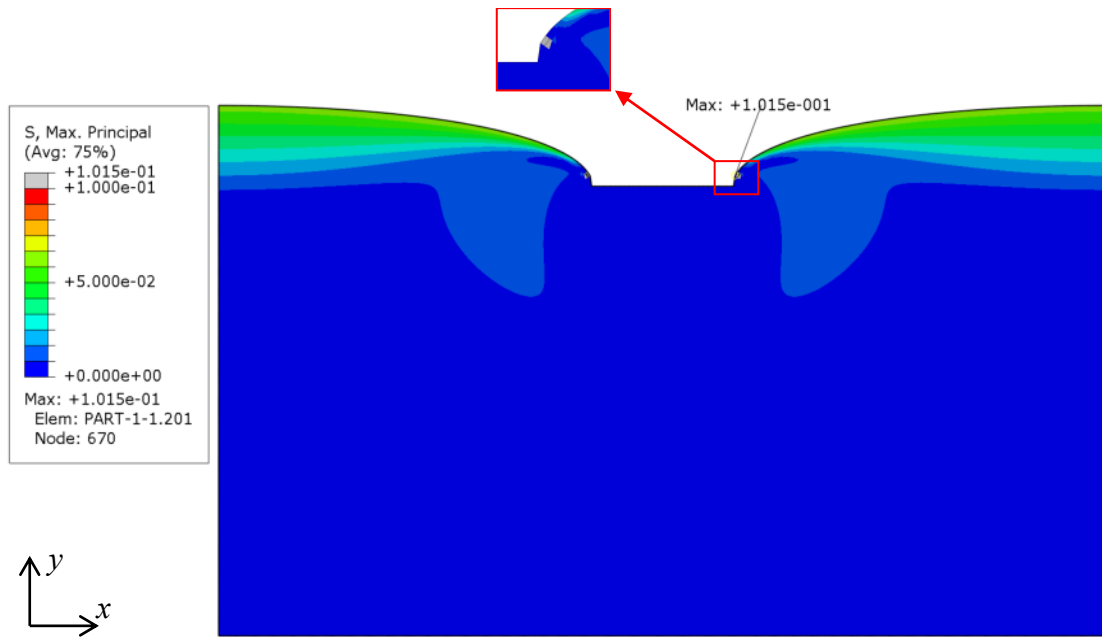
Figure 6-17. *Maximum principal stress in MPa at cracking for Model S200 with a highlighted shear crack.*

7 Analyses of Model M – multiple columns

In Model M, the ice sheet interacted with multiple columns, instead of one single column, see Figure 5-2. The notations of Model M – multiple columns are displayed in Figure 7-1. The distance between two of the columns is noted as l. Since it was of interest to compare the different analyses of Model M with each other, a new ratio was defined as:

$$R_2 = \frac{l}{b} \qquad\qquad (7\text{-}1)$$

The ratio, R_2, was varied between 1–8 for all analyses in order to include different possible configurations of columns in water. This led to a varied length and distance between the columns for all model configurations. The ratio R_1 was chosen to 0.6, according to the investigations made in Section 6.3.
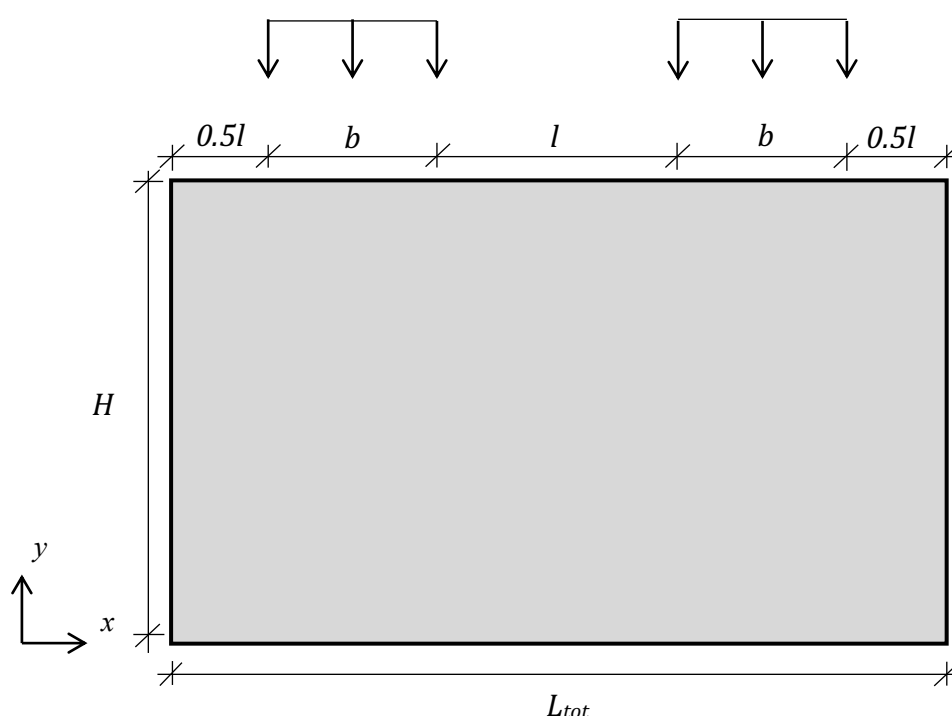
Figure 7-1. *Notations for Model M – multiple columns.*

The analysed column widths: 200, 600 and 1 200 millimetres and their respective dimensions are presented in Table 7-1, Table 7-2 and Table 7-3.

Table 7-1. *Overview of the dimensions of Model M200.*

Model	Column width, b [mm]	Ratio R_2 [-]	Distance between columns, l [mm]	Total length, L_{tot} [mm]	Total height, H [mm]
M200-1	200	1	200	800	480
M200-2	200	2	400	1 200	720
M200-4	200	4	800	2 000	1 200
M200-8	200	8	1 600	3 600	2 160

Table 7-2.　　　*Overview of the dimensions of Model M600.*

Model	Column width, *b* [mm]	Ratio *R₂* [-]	Distance between columns, *l* [mm]	Total length, *L_{tot}* [mm]	Total height, *H* [mm]
M600-1	600	1	600	2 400	1 440
M600-2	600	2	1 200	3 600	2 160
M600-4	600	4	2 400	6 000	3 600
M600-8	600	8	4 800	10 800	6 480

Table 7-3.　　　*Overview of the dimensions for Model M1200.*

Model	Column width, *b* [mm]	Ratio *R₂* [-]	Distance between columns, *l* [mm]	Total length, *L_{tot}* [mm]	Total height, *H* [mm]
M1200-1	1200	1	1 200	4 800	2 880
M1200-2	1200	2	2 400	7 200	4 320
M1200-4	1200	4	4 800	12 000	7 200
M1200-8	1200	8	9 600	21 600	12 960

7.1   Mesh convergence for Model M

All mesh convergence studies for Model M are presented in Appendix B. A summation and some major conclusion from these studies are presented in this section, but for exact values and mesh sizes as well as motivation of the convergence, see Appendix B.

In general, all models showed a high mesh dependency for the crushing and cracking pressure. Cracks occurred both as bending- and shear cracks, as seen in Figure 7-2. The convergence for the pressure at cracking showed a change in its behaviour and different cracks appeared depending on the number of elements used in the analyses.

a) Bending cracks   b) Shear cracks
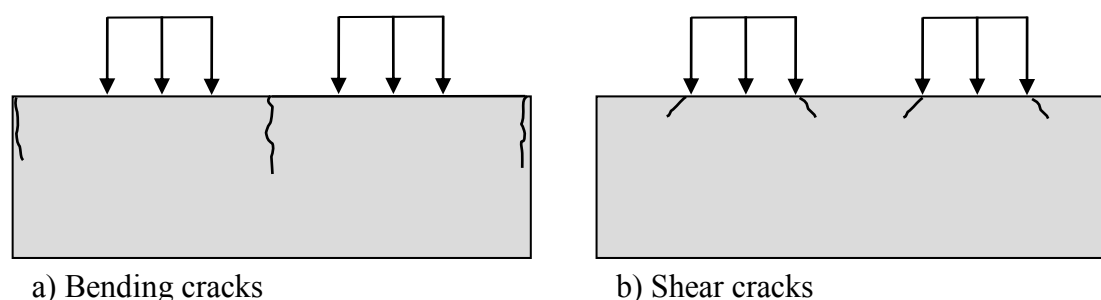
Figure 7-2.　　　*Schematic illustration of two different cracks which are initiated and propagated in the ice sheet a) bending cracks b) shear cracks.*

Common for all models was that the applied pressure, at a certain displacement, converged with fewer elements than for the pressure at crushing or cracking. Therefore, the most governing factor when determining the desirable number of elements was the applied pressure, at a certain displacement. However, the convergence for both the crushing and cracking pressure was also taken into account in the mesh convergence.

The mesh studies were intended to be performed right before the plastic limit was reached since the largest difference between different mesh sizes was observed there, see Figure 7-3. This led to that different displacement were used for all models since the plastic limit was reached at different applied displacements. Common for all mesh studies were that the chosen applied displacement was taken before the plastic limit was reached, but well after both crushing and cracking had occurred, see Figure 7-3. For the chosen convergence displacement and stress displacement curves for all models, see Appendix B.
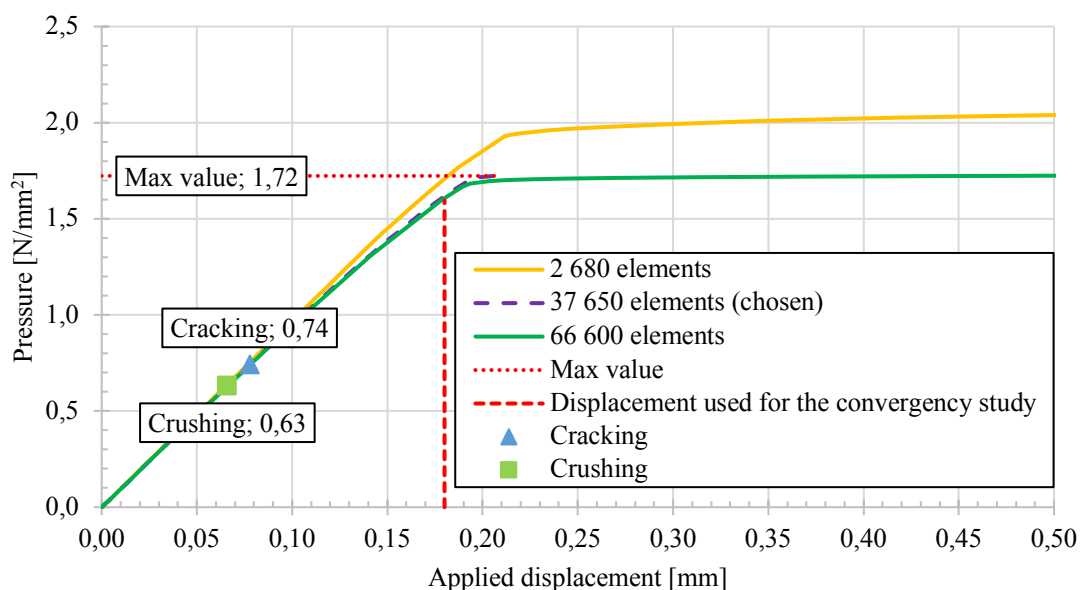
Figure 7-3. *Pressure-displacement curve for Model M200-4 with smallest and largest analysed number of elements as well as the pressure at crushing, cracking and maximum value (plastic limit).*

For two of the smallest models, M200-1 and M200-2, some difficulties were encountered with the convergence for the total analyses. The models never reached the intended prescribed displacement right before the plastic limit. The conclusion was that with a smaller mesh, a smaller prescribed displacement had to be applied to reach convergence. However, both crushing and/or cracking occurred before the analyses were aborted. Since the main focus, in all the analyses, were at the time of crushing and/or cracking the analyses were assumed to be reliable, even if the analyses was not finalised.

Another general observation was that the global response of the modelled ice sheet changed with a higher number of elements, i.e. smaller mesh size. To obtain the most correct result, the number of elements was therefore chosen where the governing failure mode was well known and did not change with more used elements.

7.2 Stresses at crushing and cracking for Model M

In this section, the stresses at the event of crushing and cracking are treated for all Model M. The general stress distribution over the entire ice sheet and stress distribution in the elements right under the columns for the different models were studied and compared. From the FE analyses, different values were extracted which later were compared with analytical calculations according to guidelines, see Chapter 8.

7.2.1 Stresses in M200

The stress distribution of Model M200-1 at the time of crushing is varying between zero and the maximum compressive stress of approximately 1.4 MPa, see Figure 7-4.
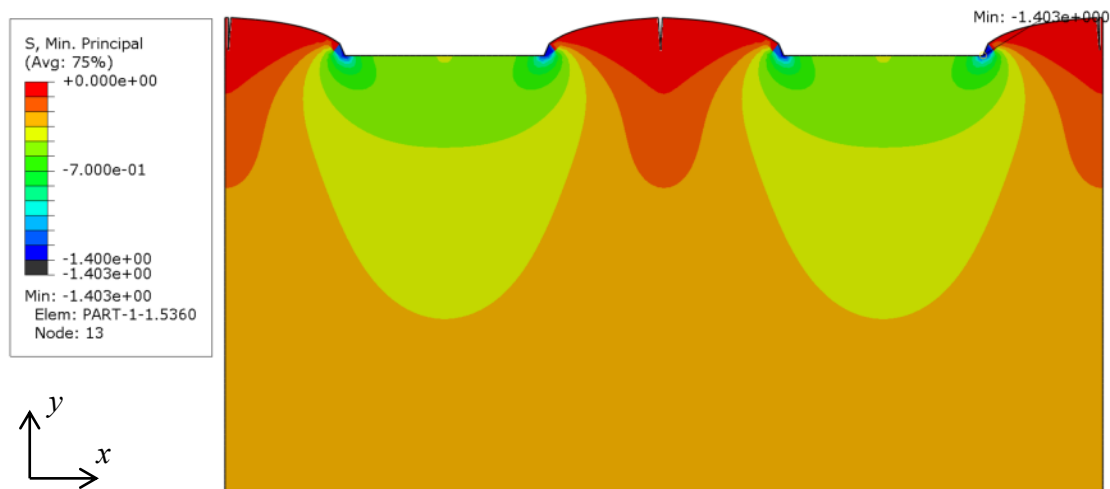
Figure 7-4.   Minimal principal stress in MPa at crushing for Model M200-1.

If the stress at the top elements were chosen and plotted in a graph, the stress distribution under the columns varied, in the same manner as for Model S. It varied with a parabolic shape with peak values where the displacement was prescribed, see Figure 7-5. The values at these locations reached the maximum allowed compressive stress of 1.4 MPa, and therefore local crushing occurred at these locations. Between the two columns and at the edges the stress was zero. In general, all Model M200 had the same appearance in their stress distribution, but with some differences in the magnitude, see Appendix E.
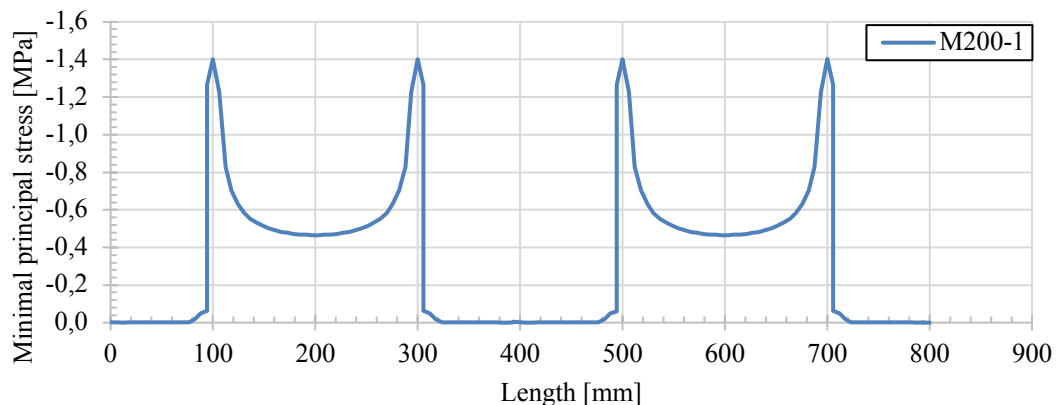
Figure 7-5.   Minimal principal stress distribution at the top elements in Model M200-1 at the time of crushing.

A more detailed stress distribution at time of crushing for all Model M200 is seen in Figure 7-6. One observation from the figure, is that with a larger ratio R_2 the more the stress distribution resembles the stress distribution which is expected for an applied load, see Section 6.4. However, for the analysed ratios was the stress distribution still parabolic with peak values at around 1.4 MPa, which was the allowed compressive strength in all analyses. The parabolic shape depends on that the sheet was analysed with a prescribed displacement and not an applied load, see Section 6.4, thus the stress distribution was not constant over the entire loading area. The diverging response of M200-8, compared to the other models, could be explained with that shear cracks were observed instead of bending cracks. Model M200-1 differed from the result by generating a higher stress, in the middle of the column, than M200-2, see Figure 7-6. This is not seen for the larger models M600 and M1200, see following sections. The difference could be that M200-1 has such small distance between the columns, thereby generating a larger magnitude of minimal principal stress. Another observation was that the decrease in stress, right outside the column, increased with a higher ratio R_2. One explanation could be the previously mentioned singular points in Section 6.4.
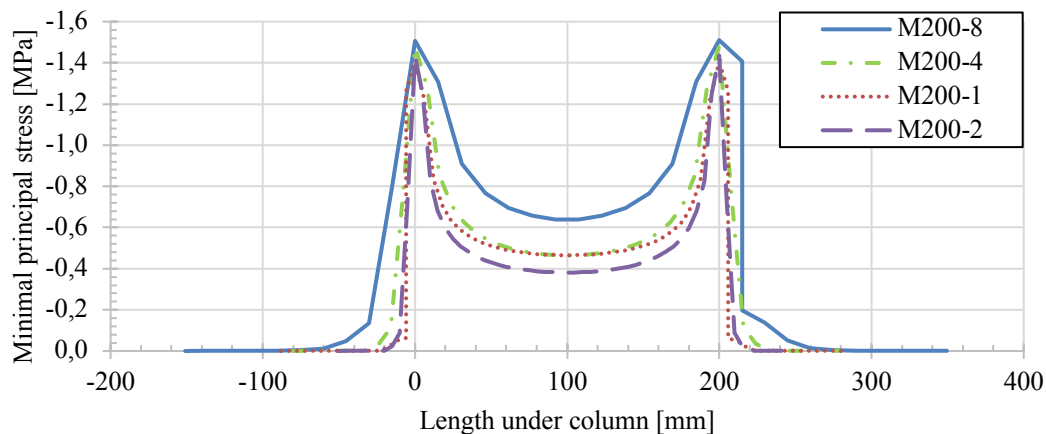
Figure 7-6.   Minimal principal stress distribution right under the left column for Model M200 at different ratios $R_2 = l/b$.

The applied load at one column for Model M200 can be calculated from each models stress distribution, which are visualised in Figure 7-6. The load was estimated as the area under the stress distribution curve, with help of Riemann sums, and was then compared to the analytical calculations, see Chapter 8.

The values were also compared to the sum of reaction forces, see Table 7-4. Model M200-4 and M200-8 showed good agreement when comparing the approximated applied pressure, as the area under the stress distribution curve, with the sum of the reaction forces. However, the two smaller models showed a higher difference that could be explained with that cracking occurred before crushing, see Figure 7-8. After cracking, the stress distribution changes in the ice sheet and since the load was based on the stresses the results for the two smallest models are not valid in this comparison. Another explanation could be the difficulties in convergence for the total analyses of these models, explained further in Section 7.1.

Table 7-4.   *Approximation of the applied load per mm thickness for Model M200 with a comparison to the applied load.*

Model	Approximated load under stress distribution curve [N per mm thickness]	Sum reaction forces in y-direction at crushing, divided on two columns [N per mm thickness]
M200-1	139	63
M200-2	118	90
M200-4	149	148
M200-8	215	212

The stress distribution at cracking for Model M200-1 is varying according to Figure 7-7. The observed cracks for this model were bending cracks that are visualised in Figure 7-7. Model M200-1, M200-2 and M200-4 had the same stress distribution, but different magnitudes. Bending cracks were also observed for these models. For Model M200-8, with a larger ratio R_2, shear cracks were observed instead, but with a similar stress distribution.
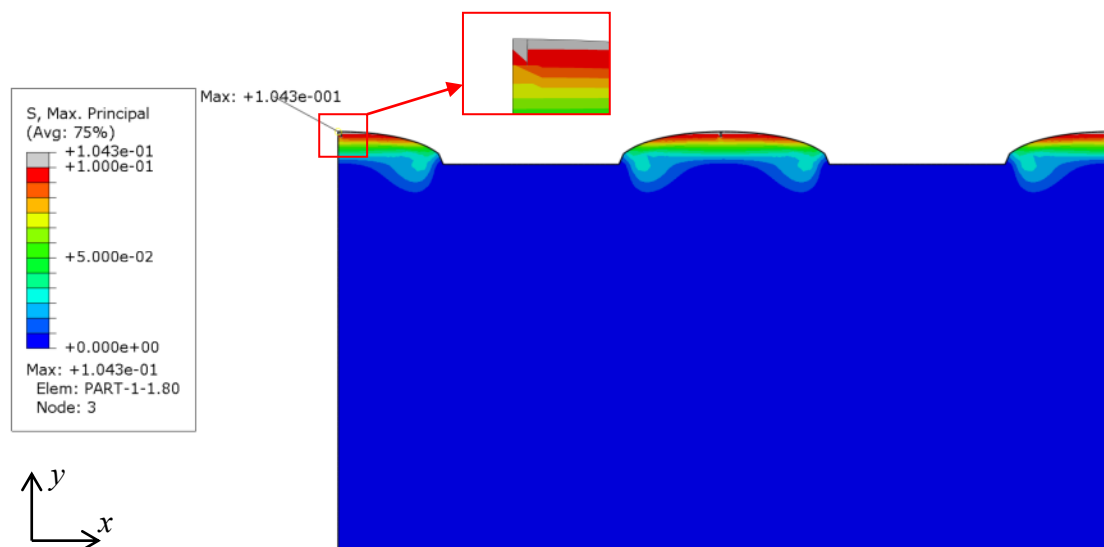
Figure 7-7.   *Maximum principal stress in MPa at cracking for Model M200-1 with a bending crack highlighted.*

To conclude, both bending and shear cracks were observed for Model M200, see Figure 7-8. For $R_2 \leq 4$ bending cracks were observed, and for $R_2 = 8$ shear cracks were observed. For $4 \leq R_2 \leq 8$, the cracking response was unknown and thereby a linear relation was assumed between the two observed responses. Exactly at which ratio the transition occurs was not investigated. Finally, a change in governing failure mode was observed at the ratio $R_2 \approx 2.8$, where it went from cracking to crushing, see Figure 7-8. This means that crushing occurred before cracking for ratios larger than ~2.8. For exact values of the ice pressure at cracking and crushing, see Appendix E.
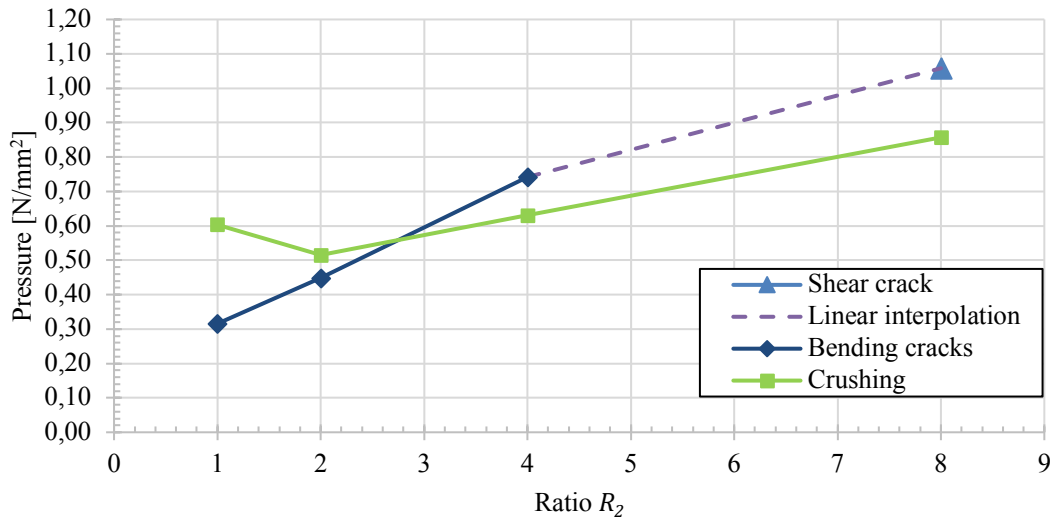
Figure 7-8.   *Cracking and crushing pressure at one column for Model M200 at different ratios*
         $R_2 = l/b$.

7.2.2   Stresses in M600

The stress distribution, at the event for crushing, for the entire ice sheet varies from zero to approximately 1.4MPa, which was set as a limit for the compressive strength of ice, see Figure 7-9.
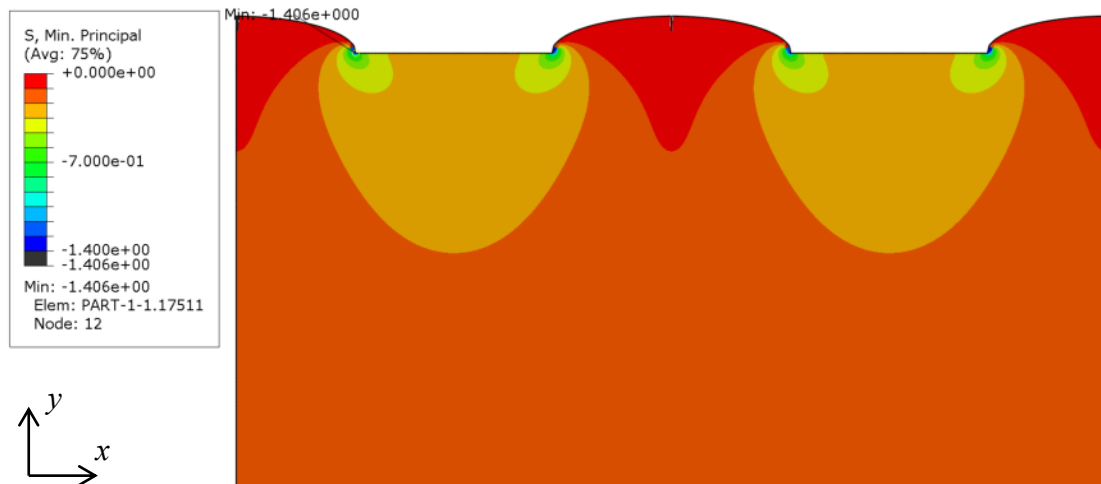
Figure 7-9.   *Minimal principal stress in MPa at crushing for Model M600-1.*

The stress distributions at the top elements, where the highest stresses occurred, were of parabolic shape under the columns and reached peak values where the displacements were applied, see Figure 7-10 for Model M600-1. At the edges and between the two columns were the stress zero, which means that it was inactive in compression at the event of local crushing. A similar visualised stress distribution can also be seen in Section 7.2 for Model M200-1. This indicates that the two models responded in the same manner with regard to compressive stresses. For the stress distribution of Model M600-2, M600-4 and M600-8, see Appendix E.
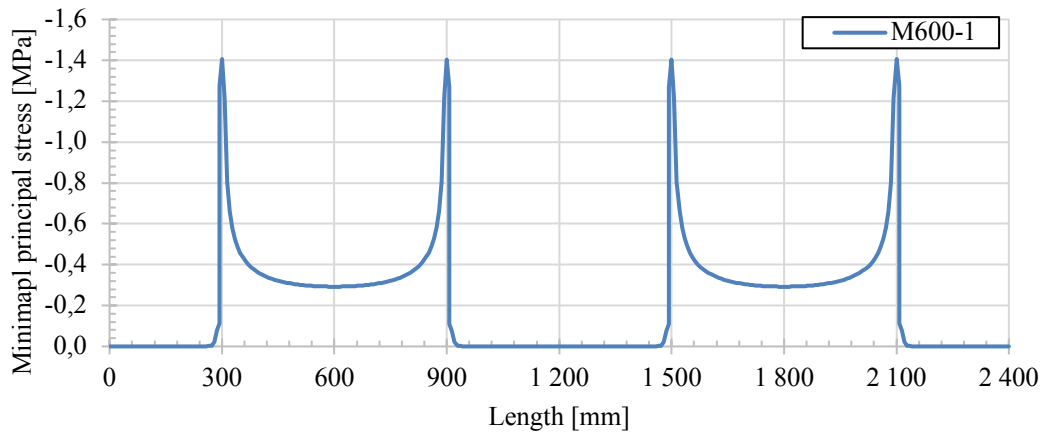
Figure 7-10.   *Minimal principal stress distribution at the top elements in Model M600-1.*

An investigation of the stress distribution right under the left column for all Models M600 showed a similar distribution as described above, see Figure 7-11. For the smaller ratios were the stress distribution very similar, but for larger ratios has the total stress magnitude increased, see Figure 7-11. The peak values for M600-2 were slightly larger, compared to the other models. One explanation could be the difference in increments between the analyses.
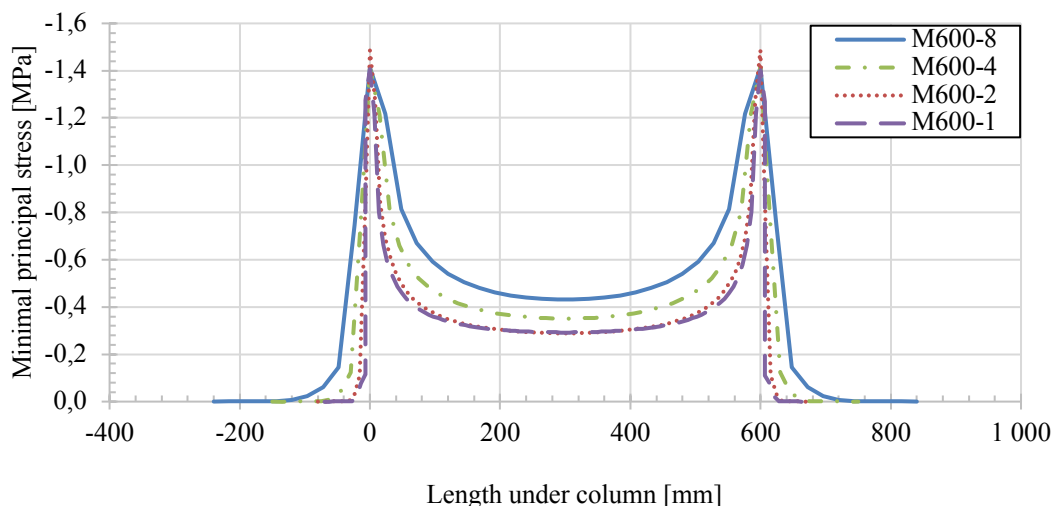
Figure 7-11.   *Minimal principal stress distribution right under the left column for Model M600 at different ratios $R_2=l/b$.*

The applied load can be estimated as the area under the curves, displayed in Figure 7-11, with the help of Riemann sums. The load was compared with analytical calculations, see Chapter 8, and the sum of the reaction forces, see Table 7-5. The three largest models showed a better agreement between the approximated applied load, under the stress distribution curve, and the sum of reaction forces. The difference between the two varied from 0.5% – 5%, whilst it for the smallest model, M600-1, showed a difference of 18%. The same explanation applies here as in Section 7.2.1, where cracking occurred before crushing and thereby changing the stress distribution, see Figure 7-12.

Table 7-5.   *Approximation of the applied load per mm thickness for Model M600 with a comparison to applied load.*

Model	App. of applied load under stress distribution curve [N per mm thickness]	Sum reaction forces in y-direction at crushing, divided on two columns [N per mm thickness]
M600-1	256	178
M600-2	266	263
M600-4	337	371
M600-8	423	463

The final response of Model M600 showed a change in governing failure mode at a ratio of ~ 1.6, see Figure 7-12. This means that for ratios larger than 1.6 was the governing failure mode crushing and for smaller ratios was the governing failure mode cracking. The observed cracks was bending cracks for ratios between 1–2 and shear cracks for ratios between 4–6, see Figure 7-12. For ratios in the range $2 < R_2 < 4$ was the cracking response unknown, thus a linear relationship was assumed between the two ratios. At which ratio the transition occurs, from bending to shear cracks, was not investigated in this study. A final conclusion from the response of Model M600 is that the crushing load increased somewhat linear for ratios larger than two. For exact values of the pressure at crushing and cracking presented in Figure 7-12, see Appendix E.
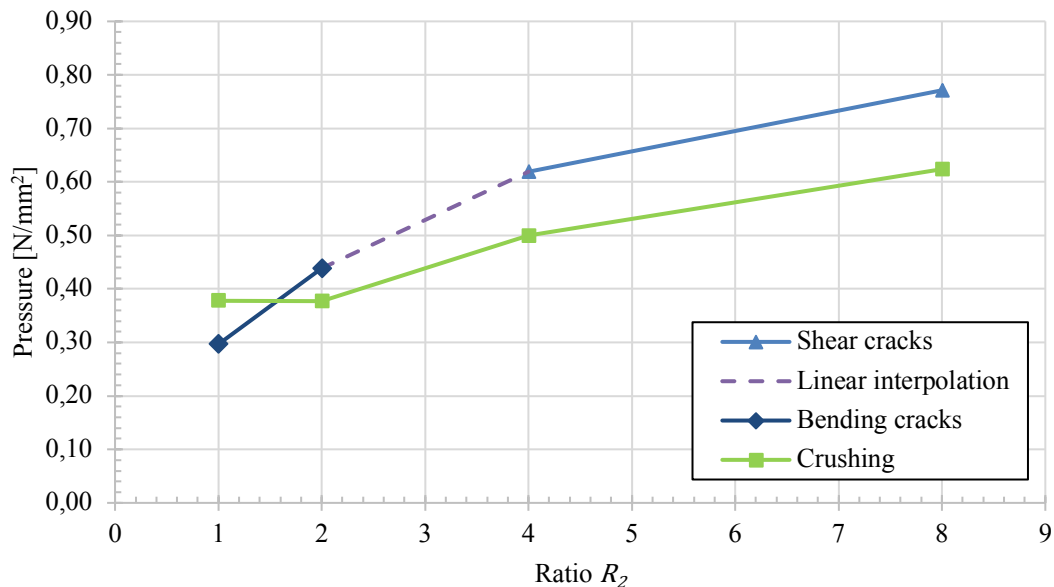
Figure 7-12.   *Cracking and crushing pressure at one column for Model M600 at different ratios $R_2 = l/b$.*

7.2.3 Stresses in M1200

The stress distribution at the event of crushing for Model M1200-1 varies according to Figure 7-13. The distribution is very similar to the distribution observed in M200-1 and M600-1. The magnitude varies from zero to 1.4MPa, which was the input value of the crushing strength of the ice.
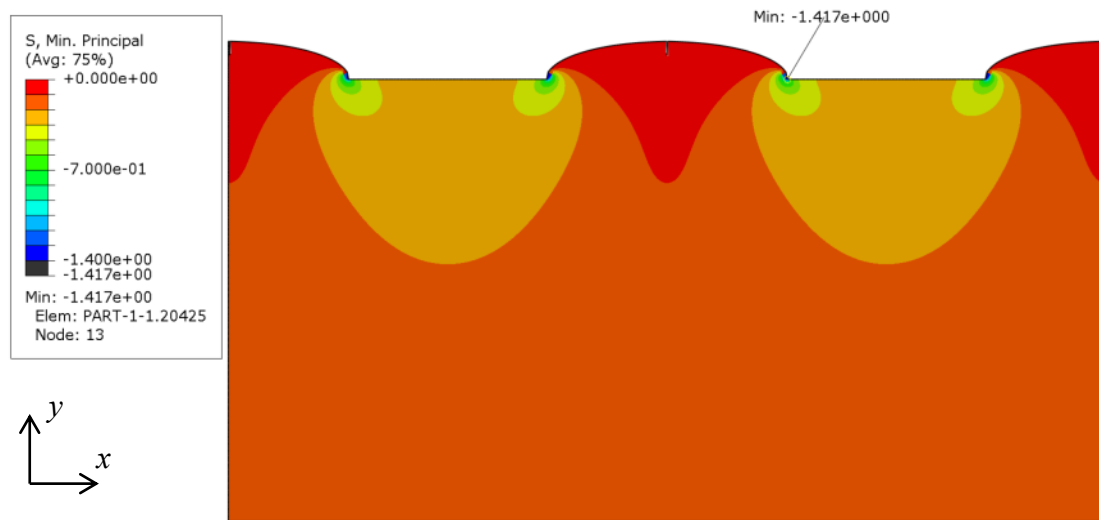
Figure 7-13.   Minimal principal stress in MPa at crushing for Model M1200-1.

The stress distribution under the columns at the event of crushing was extracted from M1200-1, see Figure 7-14. As before, the stress distribution had the same appearance as for Model M200-1 and M600-1. The stress was zero between the columns and at the edges of the ice sheet, and reached a peak values were the displacement was applied. See further in Appendix E for the stress distribution of M1200-2, M1200-4 and M1200-8. A conclusion from the stress distribution is that M200-1, M600-1 and M1200-1, has the same global response when it was subjected to an applied displacement. The peak values also reached the same magnitude, which is reasonable since they were given as input in the FE analyses.
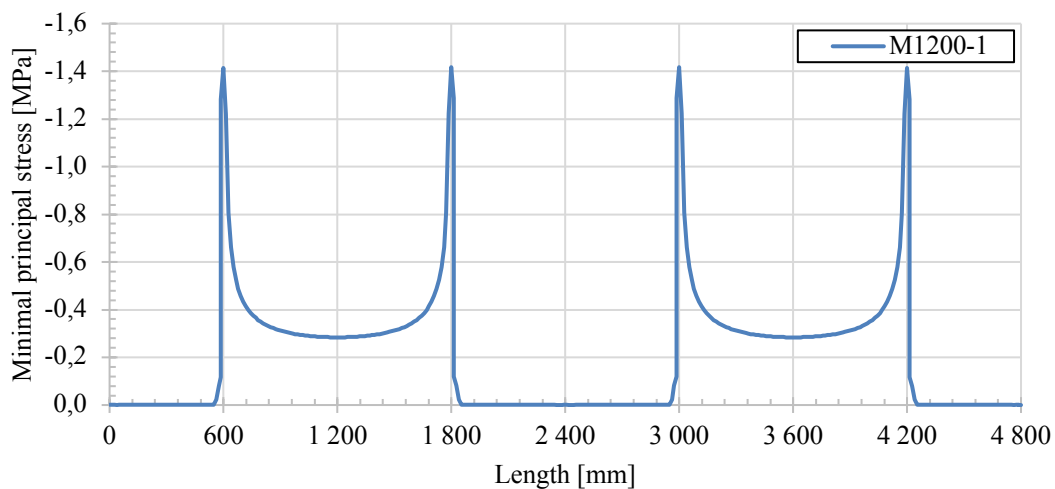
Figure 7-14.   Minimal principal stress distribution at the top elements in Model M1200-1.

The stress distributions under the left column for M1200-1 and M1200-2 were similar to each other; see Figure 7-15, while M1200-4 and M1200-8 had slightly increased, negative, values. As for Model M600, the peak values for M1200-2 was slightly larger than the rest and the same explanation could be applied for this case.
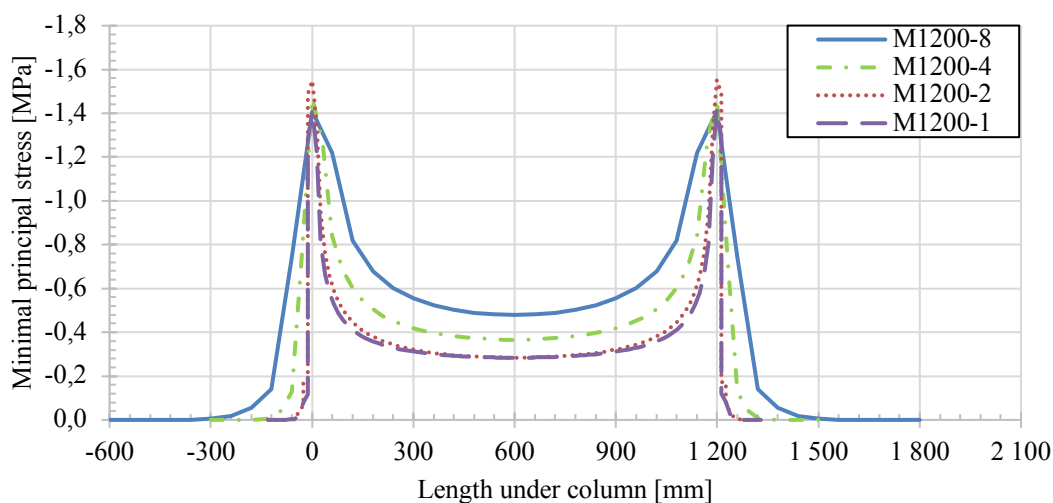
Figure 7-15. *Minimal principal stress distribution right under the left column for Model M1200 at different ratios $R_2 = l/b$.*

To be able to compare the FE values to values calculated according to Swedish guidelines was a applied load estimated with Riemann sums and the stress distribution in Figure 7-15, see Chapter 8.

The same comparison between the approximated applied load, area under the stress distribution curve, and the applied load was performed for Model M1200. As before the difference between the two calculated load were larger for the models which cracking occurred before crushing, see Table 7-6 and Figure 7-16. When crushing were the governing failure mode was the agreement good and the load could be estimated with both approaches.

Table 7-6. *Approximation of the applied load per mm thickness for Model M1200 with a comparison to applied load.*

Model	Approximation of load under stress distribution curve [N per mm thickness]	Sum reaction forces in y-direction at crushing, divided on two columns [N per mm thickness]
M1200-1	470	357
M1200-2	503	503
M1200-4	701	732
M1200-8	947	1036

For Model M1200, only bending cracks were observed for small ratios, $R_2 = 1$, see Figure 7-16. As explained before, the ice sheet reacts as a slender beam; a small ratio R_2 results in a small height and a large length. When the ratio was increased, were shear cracks only observed. A linear relationship was assumed between ratio one and two. Change in the governing failure mode occurred at ratio ~1.5, thus crushing occurred before cracking for ratios larger than ~1.5, see Figure 7-16. Another observation for Model M1200 was that for ratios larger than two were both the cracking and crushing response somewhat linear.
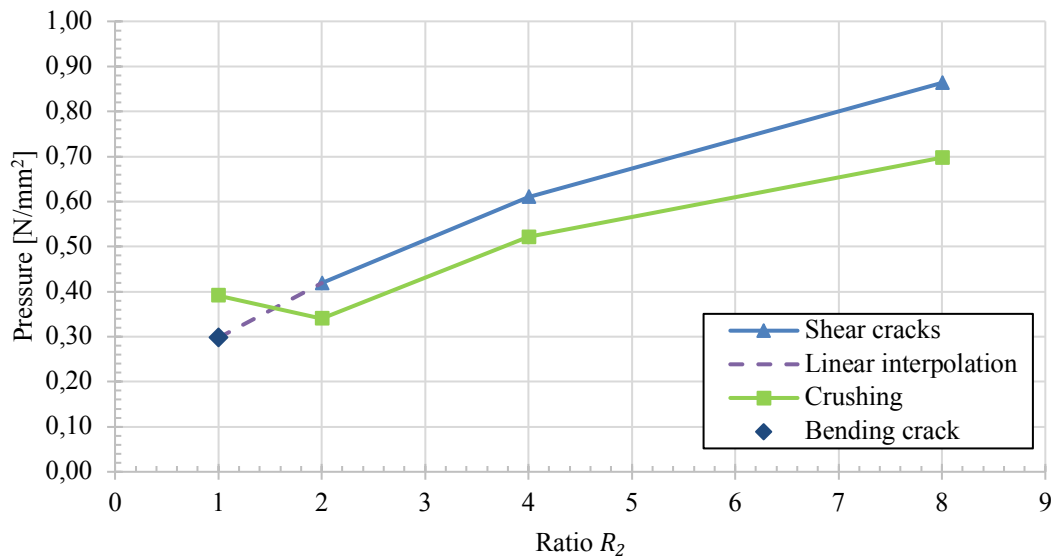
Figure 7-16.   Cracking and crushing pressure at one column for Model M1200 at different ratios $R_2=l/b$.

8 Comparison of numerical results and analytical calculations according to guidelines

In this chapter the numerical results are compared to the analytical calculated ice loads. First, a summary of the numerical results is presented, second assumptions and load cases used in the analytical calculations are treated, and finally the difference and similarities between the different ice loads are comment and discussed.

8.1 Summary of numerical results

From the FE analyses, four different values of the ice load were extracted at different types of failures. The first two loads were the pressure at local cracking and crushing, displayed previous in e.g. Figure 6-5 and Figure 7-3, multiplied with the column width and ice thickness. The third ice load was the load when the plastic limit was reached in respectively models, i.e. the highest possible load in the created model. If the plastic limit never were reached, the highest obtained load was chosen, see Appendix B for the plastic limit for all analyses.

Since the analyses with applied load resulted in an ice load corresponding to the compressive strength of ice times the interaction area, see Section 6.4, the fourth load was estimated as the theoretical maximal ice load with respect to crushing:

$$I_{max} = \sigma_c b t \tag{8-1}$$

where,
σ_c crushing strength of the ice [Pa],
b column width [m], and
t ice thickness [m].

This theoretical maximal load was calculated for both Model S and Model M, and resulted in the global capacity of the models, only reached if they would fail by crushing at "perfect" conditions.

The four ice loads created a range for each model, see Figure 8-1. The highest load was the theoretical maximal load with respect to crushing, highlighted in black, and the lowest loads were either the applied load at local crushing, in yellow, or at local cracking, in blue, see Figure 8-1. The plastic limit is also highlighted, as red, in the graph. In Appendix G, the load calculated under the stress curve at crushing in Section 6.4 and 7.2 is also included, but since it was in between the maximum and minimum values it was excluded in Figure 8-1 for a more visualized result. The exact values for all loads are also presented in Appendix G.
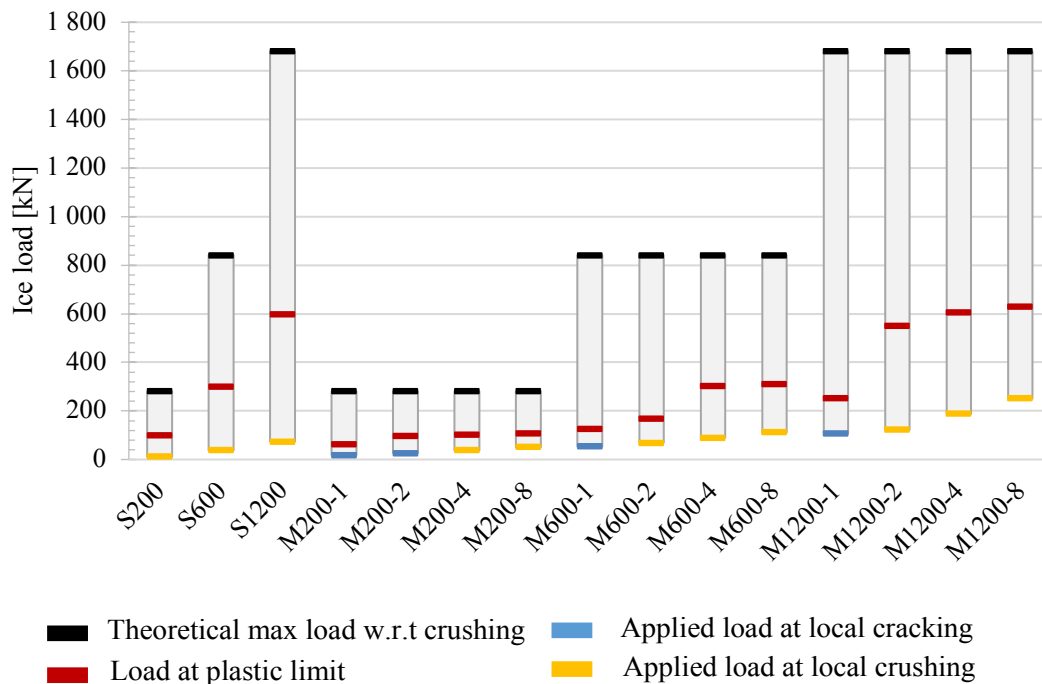
Figure 8-1.   Range of numerical results for each model with the highest and lowest values highlighted as well as the load at plastic limit. For exact values, see Appendix G.

A load higher than the crushing strength times the area, equation (8-1), would be impossible to occur and therefore the results in the upper limit are reasonable. The load at plastic limit is substantially lower, indicating that the model has lower capacity than the maximal load with respect to crushing. In reality the maximal load with regard to crushing would probably never be reached since other local failures or responses could occur before. The plastic limit could be argued to be on the safe side since the plastic limit is based on the minimal principal stress. The local stresses could therefore exceed this stress limit in the model, until global failure. The lowest load for all models were the applied load at either local cracking or local crushing. This was expected since the load was extracted when local failure in one element was reached, resulting in a lower load than for global failure. Clearly shown, in Figure 8-1, is that cracking were the governing failure mode for the smaller models, as observed in e.g. Figure 7-8 and Figure 7-12.

8.2   Analytical calculations

To be able to compare the ice loads from the Swedish guidelines with the numerical results, all ice loads were calculated with the same input values. The thickness of the ice sheet was set to 300 millimetres, according to the worst scenario at the west coast of Sweden, see Section 2.3.1. The ice load, described in Section 4.6.2, was excluded from the comparison since the ice thickness was less than 400 millimetres and the ice load should, according to that guideline, then be neglected. The columns were assumed to be quadratic with the same height, *a*, as width, *b*, with notations according to Figure 4-3.

In VV 1987:43 (Vägverket, 1987), many different suggestions were made on how to calculate the ice load for certain given conditions, see Section 4.4. The different ice loads were therefore divided into load cases to easier distinguish and compare them with each other, see Table 8-1. The load perpendicular to the water flow direction, see equation (4-1), was not included since this type of load was not investigated in the numerical analyses. In Fransson and Bergdahl (2009) an estimation of the ice load was suggested, which is based on the crushing strength of the ice. This load was also included in the comparison, see Table 8-1. Both the set ice load values in TDOK 2016:0204 (Trafikverket, 2016a) and RIDAS (RIDAS, 2012b) were also included.

Table 8-1.   Overview of load cases used in the analytical calculations.

Recommendation/standard	Load Case	Type of load	Equation
Requirement bridge design	TDOK 2016:0204	Set point load	-
Guideline for hydropower dams	RIDAS	Set distributed load	-
Ice pressure against bridge support	VV 1987:43, *LC1*	Moving ice sheet	(4-2)
	VV 1987:43, *LC2*	Larger ice sheet	(4-3)
	VV 1987:43, *LC3*	Sharp or inclined edge	(4-4)
Offshore structures	Other recommendation F&B (2009)	Horizontal ice load w.r.t. crushing strength	(4-6)

The load from TDOK 2016:0204 had a constant value of 200 kN for all models, as described in Section 0. For RIDAS the load value was chosen as 50 kN/m, according to Figure 4-5 a). The value was multiplied with the column width for the different models. For Model M, consideration was also taken to possible arching effects, explained in Section 3.3.7 and 0. The distributed load was transferred into one point load acting on each support, according to Figure 8-2. The interaction area, due to possible arching effect, consists of the column width, *b*, and the distance between the columns, *l*.
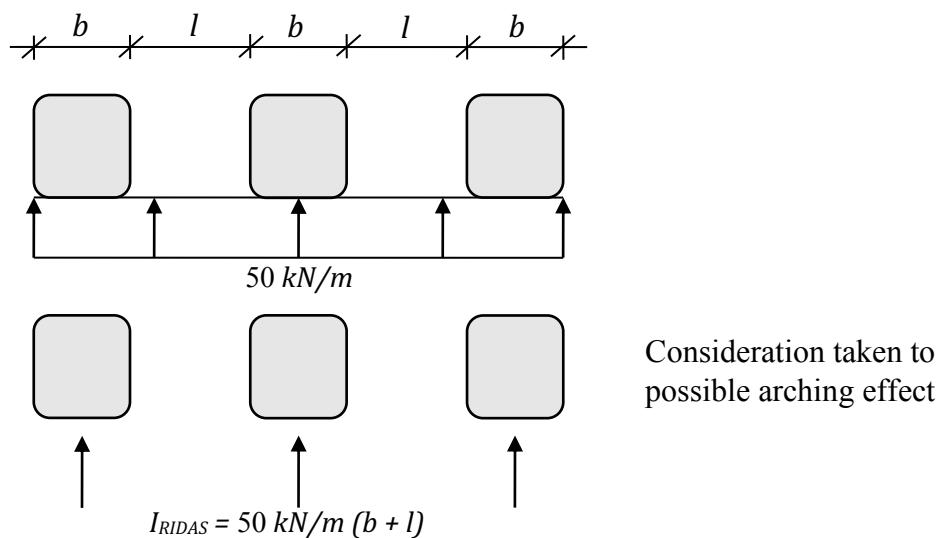
Figure 8-2.   Transformation of the ice load, according to RIDAS, with consideration to possible arching effect for Model M.

For the calculations of wind and current induced ice loads, according to equation (4-5), the ice sheet area was calculated with a range of ice loads. The wind speed was set to 26 m/s, according to the national annex in EN 1991 (2003), and the current velocity to 2 m/s which was the maximum current velocity in Kattegatt according to Fransson and Bergdahl (2009).

8.3 Estimation of ice loads induced by wind and currents

In Fransson and Bergdahl (2009), the ice load which is induced by wind or currents could be estimated according to equation (4-5). Both the current and wind velocity and the area of the ice sheet were unknown, therefore the velocities were assumed as standard values. The wind velocity was set to 26 m/s, which is the assigned wind velocity at the west coast of Sweden according to Eurocode (EN 1991). The current velocity was set to 2 m/s according to recommendations from Fransson and Bergdahl (2009). Equation (4-5) increases linearly for both the wind velocity and the current velocity, see Figure 8-3.
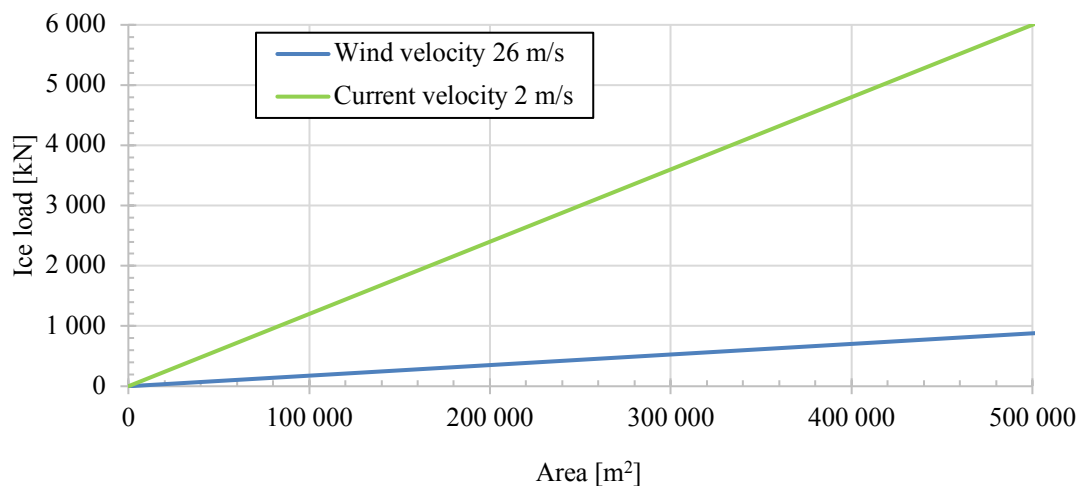
Figure 8-3.   *The ice load calculated with the wind velocity 26 m/s and the current velocity 2 m/s according to equation (4-5).*

To obtain the needed area to induce the ice loads that were obtained from the FE analyses, the minimum and maximum load from the FE analyses were used and generated a range of the area. Firstly, the one depending on the wind velocity, see Figure 8-4, and secondly the other depending on the current velocity, see Figure 8-5. The loads from the FE analyses were taken from Figure 8-21. The minimum load varied between the models and it was the applied load at either local cracking or local crushing, depending on the governing failure mode. The used maximum load were the load at plastic limit for all analyses.
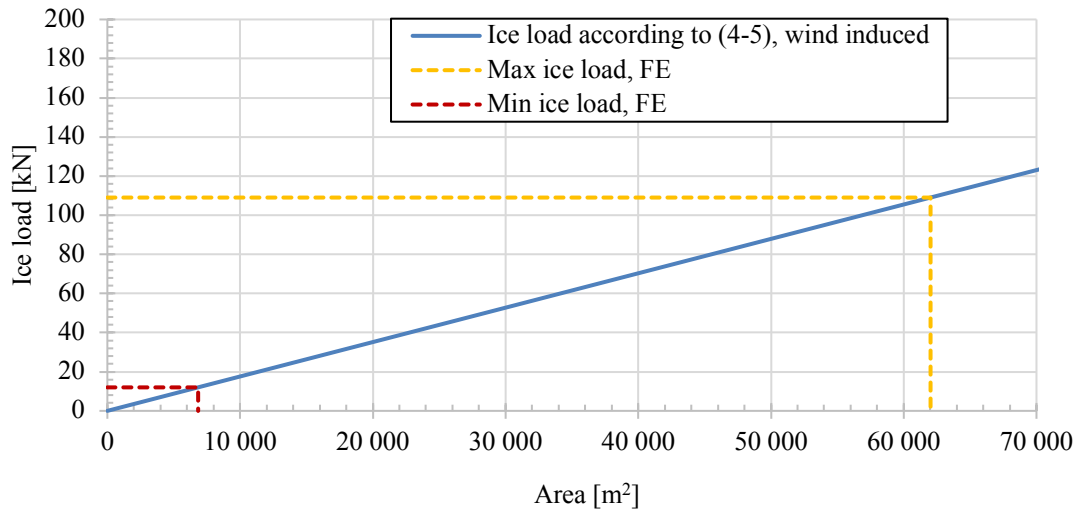
Figure 8-4. *Minimum and maximum ice loads from the FE analyses generating a range of the area to induced the same magnitude of the ice load for the models with column width b = 200mm with a wind speed of 26m/s.*
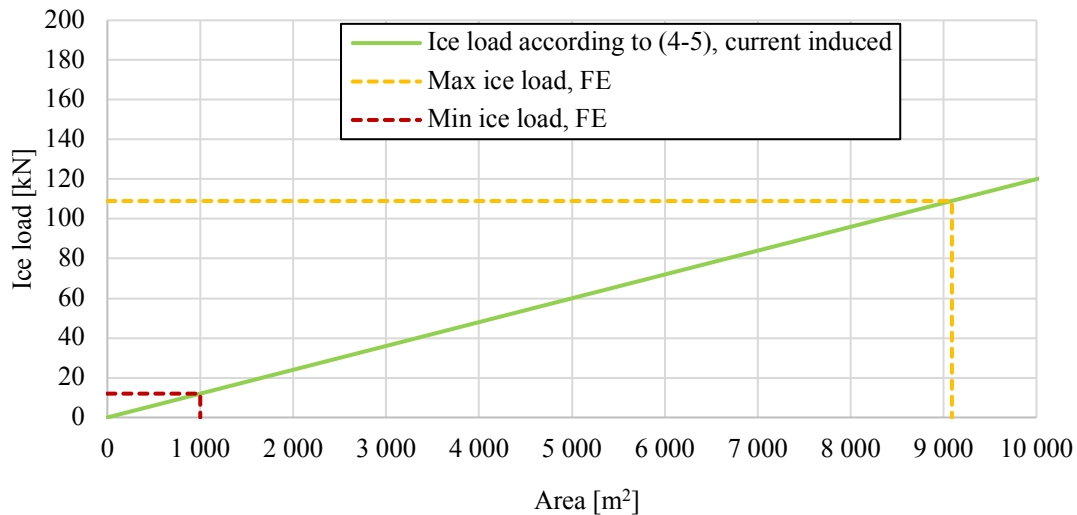
Figure 8-5. *Minimum and maximum ice loads from the FE analyses generating a range of the area to induced the same magnitude of the ice load for the models with column width b = 200mm with a current of 2m/s.*

This approach was implemented for all models, which had the same column width, b and thereby gave a range of all areas for all column widths, see Table 8-2. The maximum area were 358 500 m^2, which corresponds to around 50 soccer fields. This is a large area and not reasonable to occur at the west coast of Sweden near any kind of structure in the water. The minimum areas, especially the current induced ice loads, are more reasonable and could occur at the west cost of Sweden.

Table 8-2. *Overview of the areas which are needed to induce the same ice loads which were obtained in the FE analyses.*

Column width, b [mm]	Wind induced ice load		Current induced ice load	
	Min	Max	Min	Max
200	6 840 m^2	62 020 m^2	1 000 m^2	9 090 m^2
600	21 640 m^2	176 950 m^2	3 170 m^2	25 950m^2
1200	42 100 m^2	358 500 m^2	6 170 m^2	52 500 m^2

The ice sheet areas in between the maximal and minimal, found in Table 8-2, are unlikely to be found unbroken and homogenous. However, several ice sheets could together reach these areas. Whether equation (4-5) could be used on the studied cases or if it needs to be adjusted is not mentioned by Fransson and Bergdahl (2009).

Another aspect to consider is that these results do not involve the thickness of the ice sheet. Since the thickness affect the impact area, and thereby the load, this would probably affect the ice structure interaction more, resulting in a more important factor. It is therefore hard to draw any distinct conclusions about the areas in between the maximal and minimal areas.

8.4   Comparison for Model S

For Model S, all load cases, in Table 8-1, were included in the comparison, except VV 1987:43 *LC1* since only one column was investigated and the distance to the adjacent column was assumed to be infinitely long. The included numerical results were the applied load at local crushing or cracking and the load at plastic limit. The theoretical maximal load was also included in the comparison, but outside the numerical results since the theoretical maximal load was an conservative estimated load and not a result from the FE analyses. The performed calculations are seen in Appendix D and the numerical results are seen in Appendix G.

The scattering of results looks diverging between the different models, but the difference in percent between them is equal. Generally, it can be seen that some standards and guidelines have good agreement while some differ, see Figure 8-6. As an example, the other recommendation from Fransson och Bergdahl (2009) and the theoretical max generated consistently higher values and RIDAS generated lower ice loads compared to the numerical results.
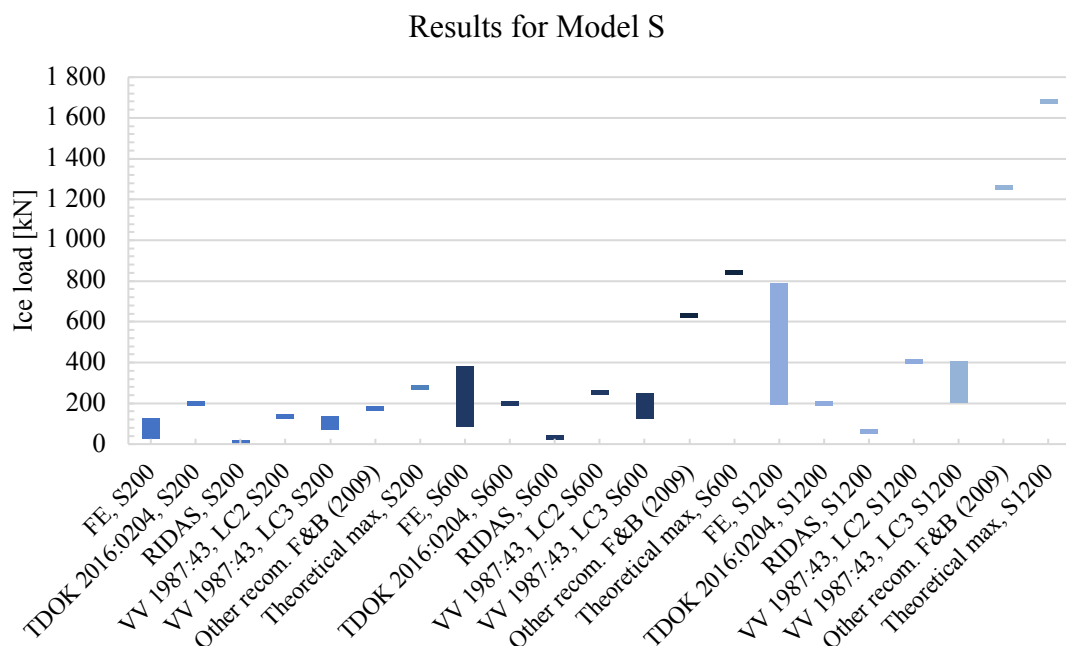
Figure 8-6.   *Range of results from the FE analyses and the analytical calculations, see Appendix D, for Model S. For exact values, see Appendix G.*

For Model S200, RIDAS was the only guideline that generated a lower value compared to the numerical results, see Figure 8-7. TDOK 2016:0204, the other recommendation from Fransson and Bergdahl (2009) and the theoretical maximal load gave higher ice loads than the FE results. *LC3* from VV1987:43 was the only ice loads that was in the range of the numerical results for Model S200.
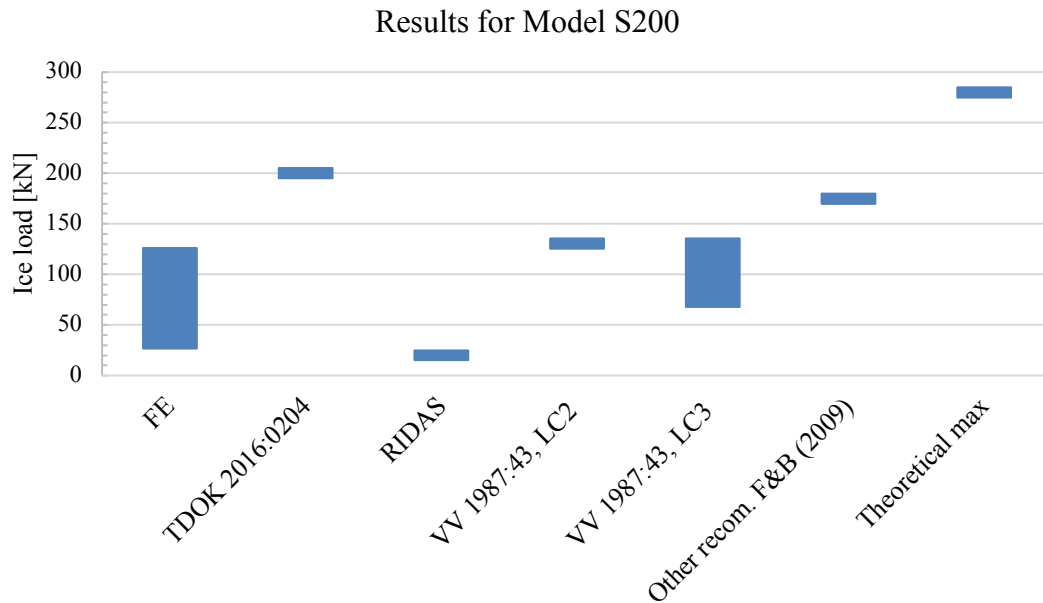
Figure 8-7. *Range of results from the FE analyses and the analytical calculations, see Appendix D, for Model S200. For exact values, see Appendix G.*

In the comparison for Model S600, the same results as for Model S200 was seen with the difference that TDOK 2016:0204 also gave good agreement with the numerical results, see Figure 8-8.
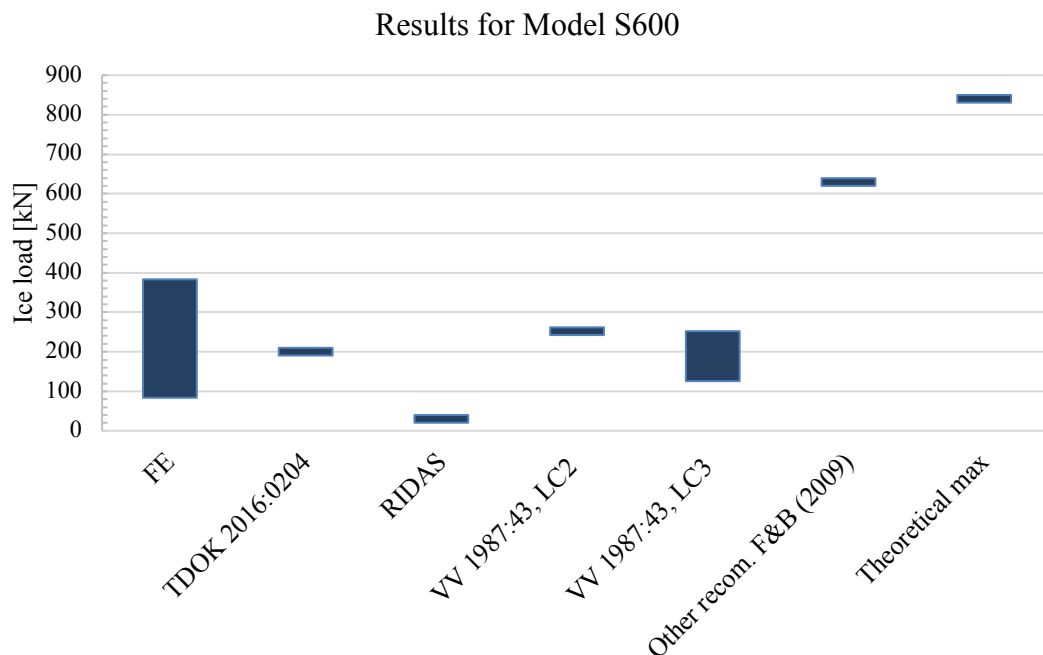
Figure 8-8. *Range of results from the FE analyses and the analytical calculations, see Appendix D, for Model S600. For exact values, see Appendix G.*

For Model S1200, TDOK 2016:0204 were in the lowest range of the FE results and *LC2* and *LC3* were in the midst to lower range of the numerical results, see Figure 8-9. RIDAS, other recommendation by Fransson and Bergdahl (2009), and the theoretical maximal load continuously generated lower respectively higher ice loads for Model S1200, as for Model S200 and S600.

Results for Model S1200
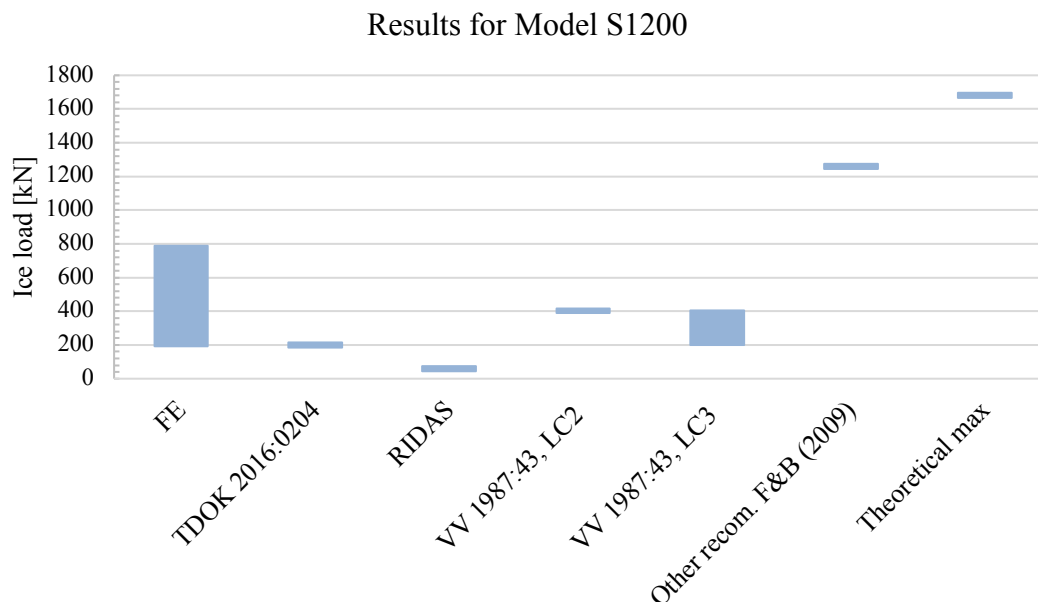
Figure 8-9.   *Range of results from the FE analyses and the analytical calculations, see Appendix D, for Model S1200. For exact values, see Appendix G.*

The difference between the FE results and the load values from the standards and guidelines for Model S are summarised in Table 8-3.

Table 8-3.   *Detailed comparison between the FE results and the calculated loads from the standards and guidelines, displayed in Figure 8-6.*

Load case	Comments
TDOK 2016:0204	Showed good agreement with S600, but was too high for S200 and too low for S1200.
RIDAS	Generated low values for all models which depends on its origin as a distributed load which is not applicable for Model S.
VV 1987:43, *LC2* Larger ice sheet	Gave good agreement with the FE results, due to that the equation is based on the crushing strength of the ice. The equation includes a shape factor that reduces the load, positioning it in the midst to higher range of the FE results.
VV 1987:43, *LC3* Sharp or inclined edge	Showed similar results as *LC2* for the same reasons, but generated a larger range because of the different investigated inclinations.
Other recom. F&B (2009) Horizontal ice load w.r.t. crushing strength	Generated larger loads than all FE results, resulting in a conservative approach. The equation is based on crushing strength, similar to *LC2* but has different shape factors and thereby generates larger loads.
Theoretical maximal load	Gave higher values for all models; thus a conservative load.

8.5 Comparison for Model M

For Model M, VV 1987:43 *LC1* was included in the comparison since the influence of the distances between the columns was of interest. The included numerical results for Model M were the applied load at local crushing or local cracking and the load at plastic limit. The complete calculations and exact values for Model M are found in Appendix F and the numerical results in Appendix G.

8.5.1 Comparison for Model M200

For Model M200, a larger part of the analytical calculated ice loads were out of the range of the FE results, see Figure 8-10. Both the theoretical maximal load, the set point load given in TDOK 2016:0204, other recommendations by Fransson and Bergdahl (2009) and VV 1987:43 *LC2* showed much higher values, resulting in a conservative approach. *LC1* in VV 1987:43, which depended on the distance to the adjacent support, was always lower than the numerical results. One reason for this deviation could be that the set distributed load, given in the recommendation, was rather low. Generally, the ice loads from the FE results increased with increasing column width.
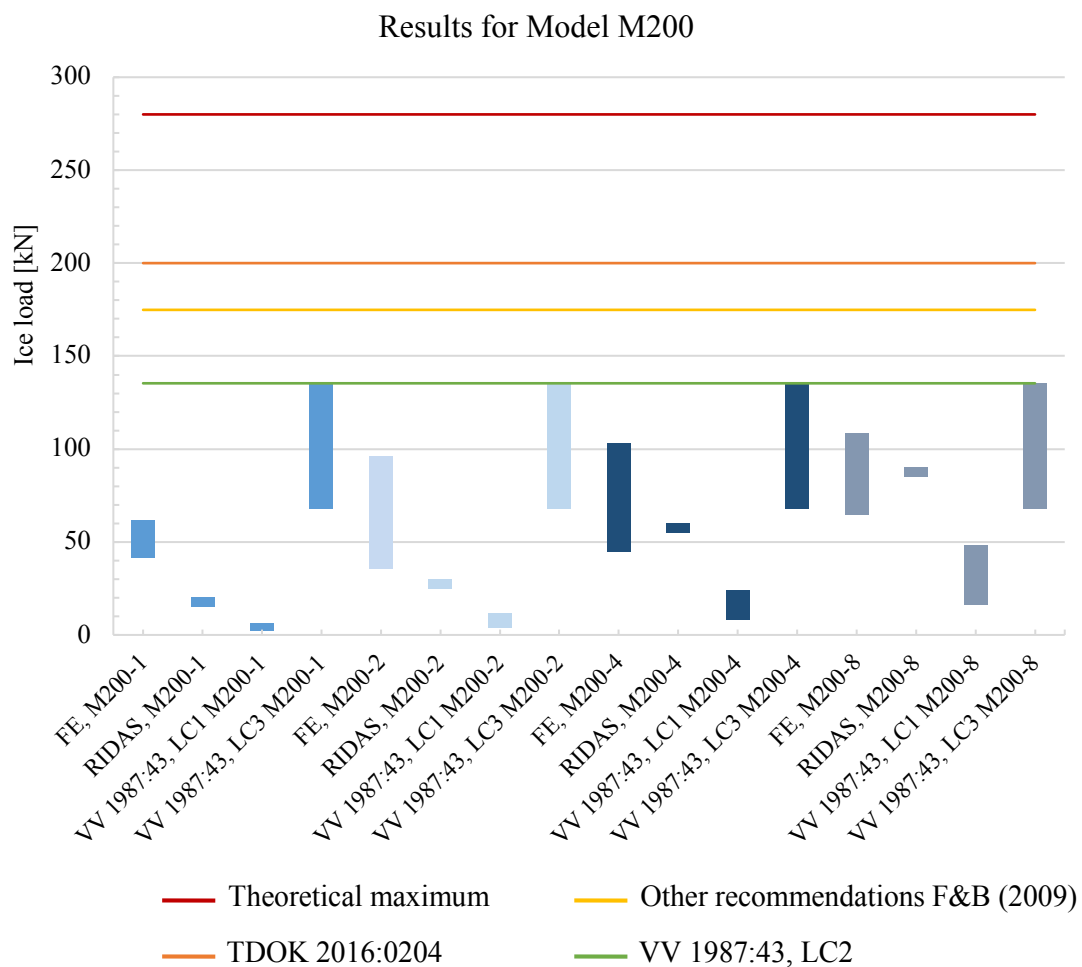
Figure 8-10. *Range of results from the FE analyses and the analytical calculations, see Appendix F, for Model M200. For exact values, see Appendix G.*

The FE results for Model M200-1 did not show any agreement with any of the analytical calculated ice loads, see Figure 8-11. RIDAS recommended value and VV 1987:43 *LC1* generated lower values and the rest of the load cases resulted in higher values. Based on the FE results, none of the load cases described in Table 8-1, could be recommended for Model M200-1.
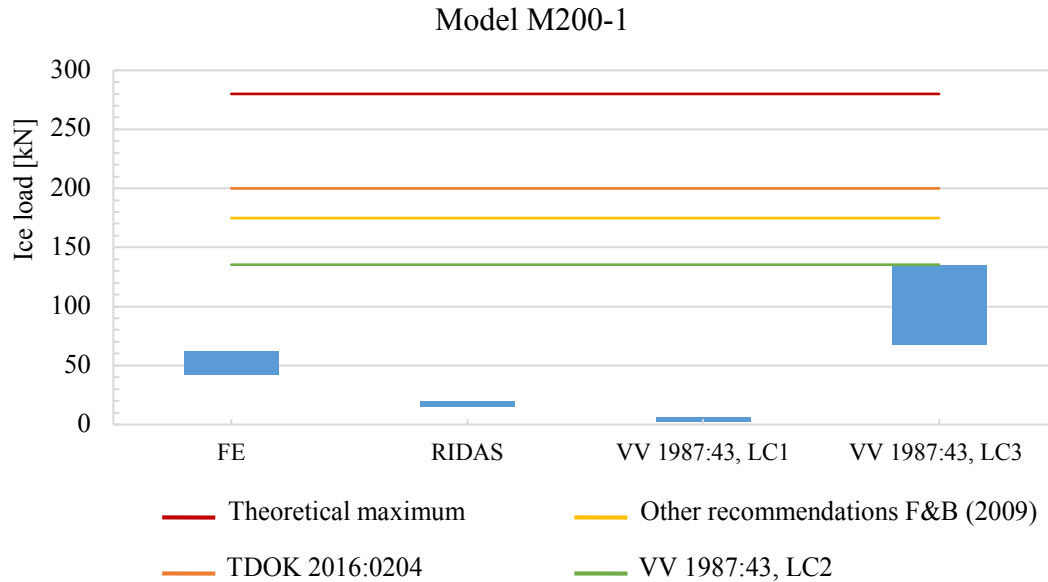
Figure 8-11.   *Range of results from the FE analyses and the analytical calculations, see Appendix F, for Model M200-1. For exact values, see Appendix G.*

Similar to Model M200-1, no agreement was observed for Model M200-2 and the numerical results, see Figure 8-12. However, the load calculated according to VV 1987:43 *LC3* was observed to be within the upper limit of the FE result.
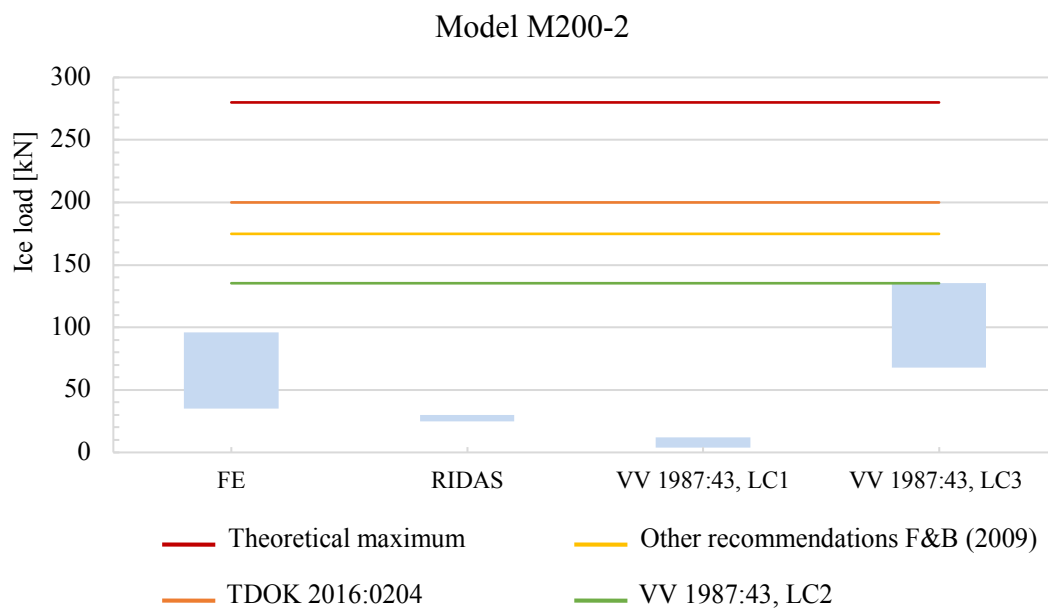
Figure 8-12.   *Range of results from the FE analyses and the analytical calculations, see Appendix F, for Model M200-2. For exact values, see Appendix G.*

The FE results for Model M200-4 also showed bad agreement with most of the analytical calculated ice loads, see Figure 8-13. Although, some agreement could be observed for the load calculated according to RIDAS as well as *LC3* according to VV 1987:43.
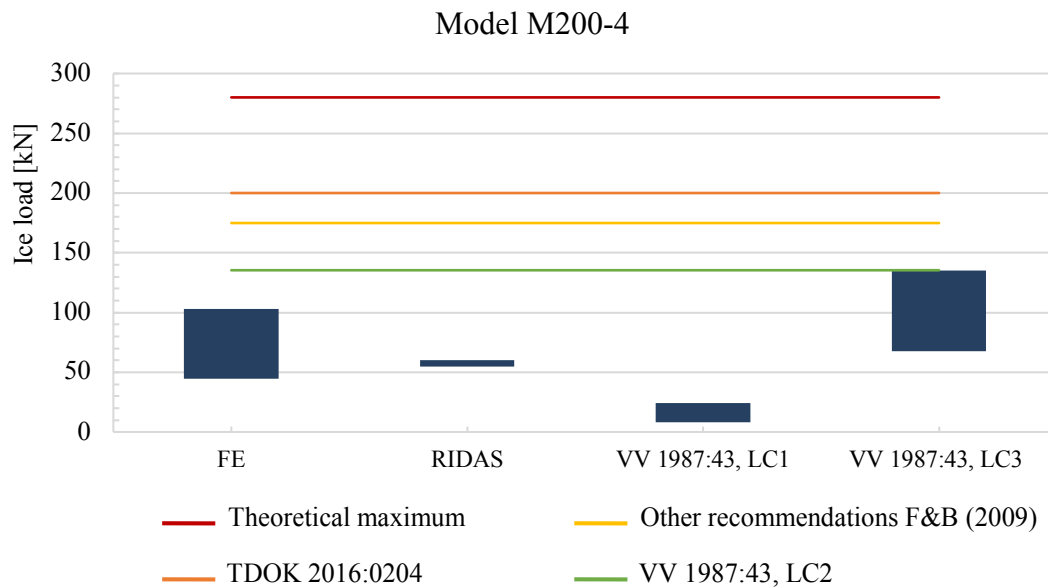
Model M200-4

Figure 8-13.   *Range of results from the FE analyses and the analytical calculations, see Appendix F, for Model M200-4. For exact values, see Appendix G.*

For Model M200-8, no agreement can be observed for the theoretical maximal load, TDOK 2016:0204, other recommendation by Fransson and Bergdahl (2009), VV 1987:43 *LC1* and *LC2*; the same observation as for the three previously models. Though, for M200-8 a better agreement was observed for RIDAS recommendation and the lower range of VV 1987:43 *LC3*.
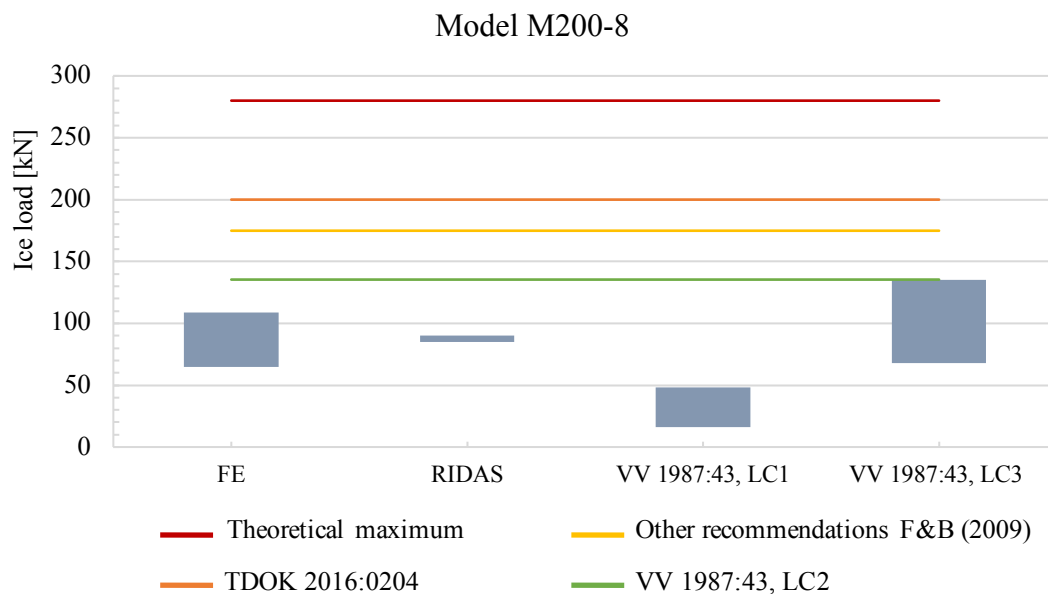
Model M200-8

Figure 8-14.   *Range of results from the FE analyses and the analytical calculations, see Appendix F, for Model M200-8. For exact values, see Appendix G.*

8.5.2 Comparison for Model M600

For Model M600, the analytical results were more gathered but still differed a lot compared to the numerical results, especially for the smaller models, see Figure 8-15. A slightly better agreement was found for the larger models. Two loads, the theoretical maximal load and the recommendation from Fransson and Bergdahl (2009), generated much higher loads, which did not agree with the rest of the ice loads. A general observation was that the set point load given in TDOK 2016:0204 agreed with the two larger models, but not with the two smaller ones.
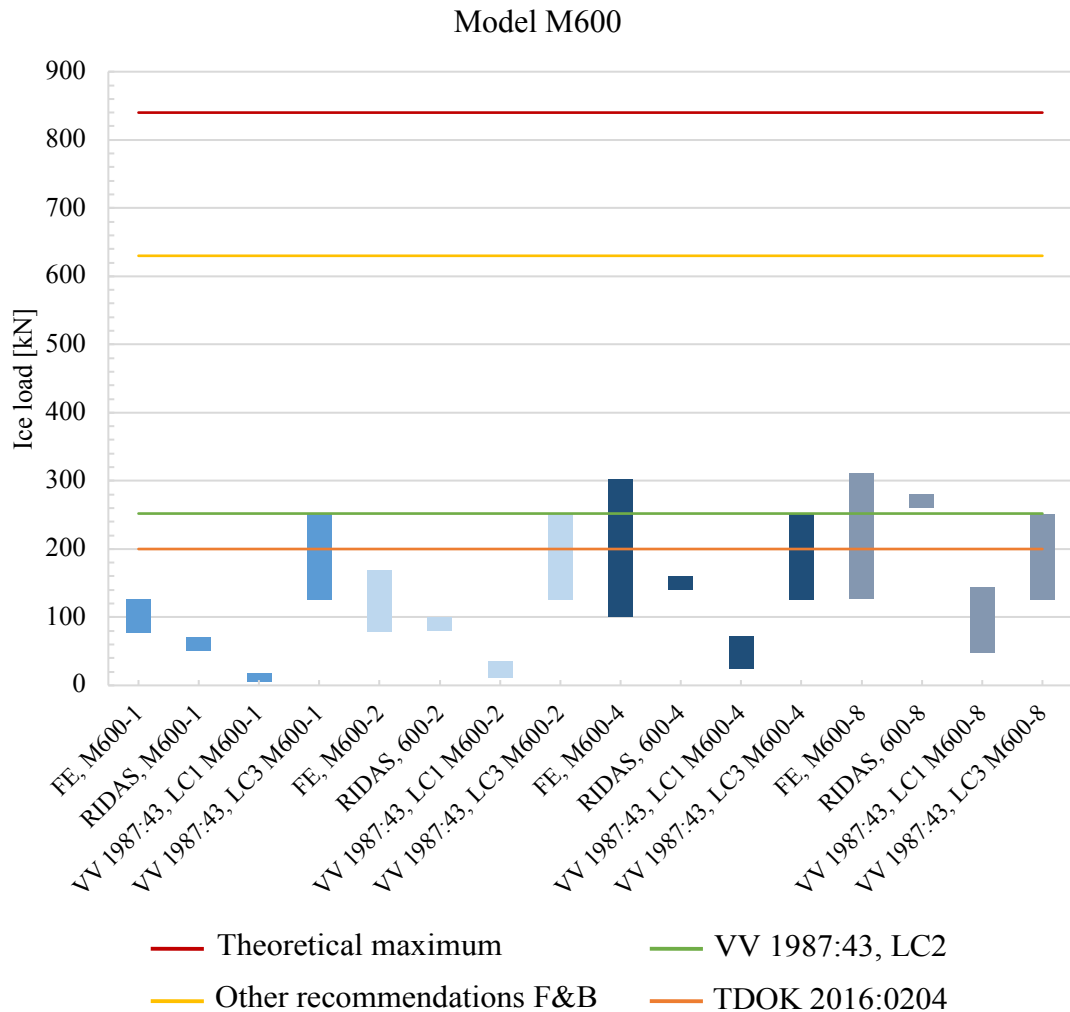
Figure 8-15.   *Range of results from the FE analyses and the analytical calculations, see Appendix F, for Model M600. For exact values, see Appendix G.*

For Model M600-1, the smallest model, no agreement could be found with any of the analytical calculated ice loads, see Figure 8-16. One contribution to this non-agreement could be that the range of the FE results was rather low, compared to the other Models M600.
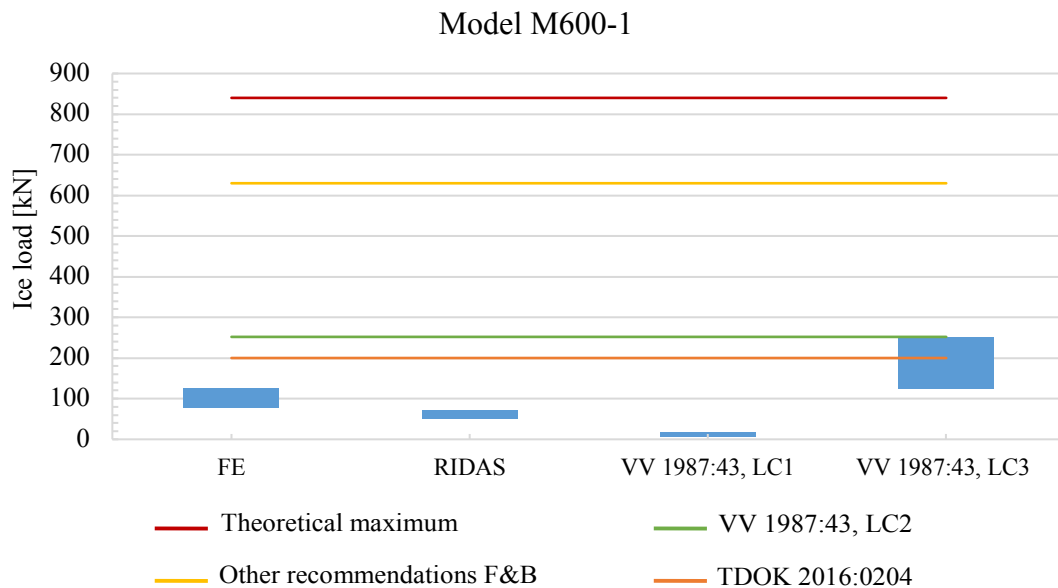
Model M600-1

Figure 8-16. *Range of results from the FE analyses and the analytical calculations, see Appendix F, for Model M600-1. For exact values, see Appendix G.*

The FE results from Model M600-2 was within the range of the recommendation according to RIDAS and in the lower range according to VV 1987:43 *LC3*, see Figure 8-17. For the rest of the analytical results no agreement could be found.
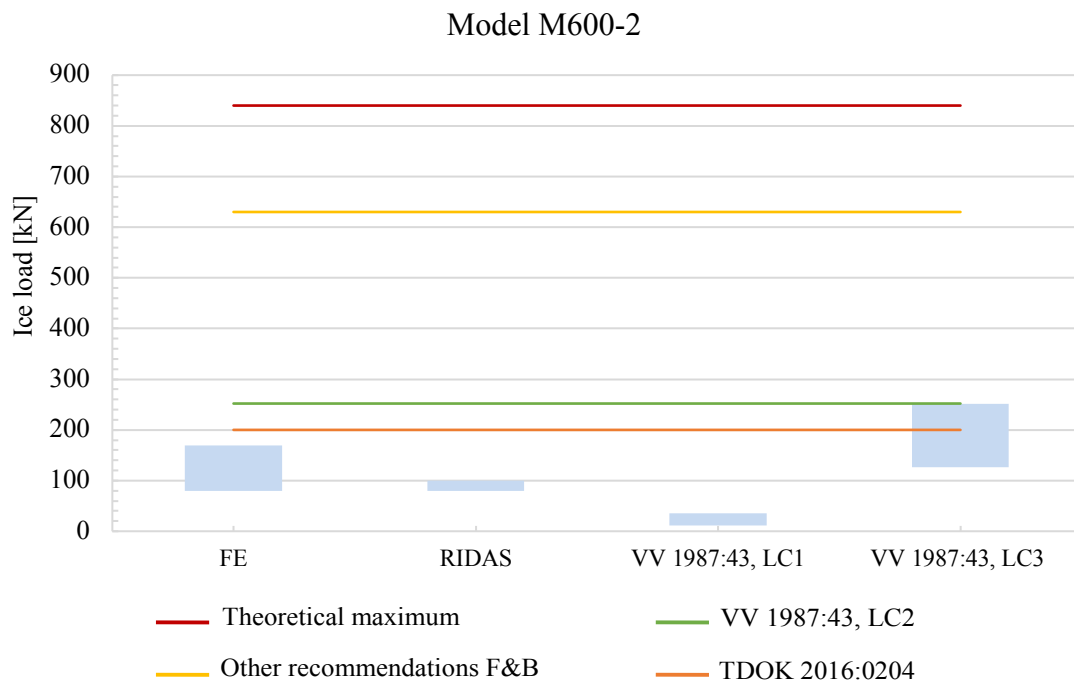
Model M600-2

Figure 8-17. *Range of results from the FE analyses and the analytical calculations, see Appendix F, for Model M600-2. For exact values, see Appendix G.*

The comparison for Model M600-4 differs from the other comparisons described above. For this model an agreement could be observed for TDOK 2016:0204, VV 1987:43 *LC2*, RIDAS and VV 1987:43 *LC3*, see Figure 8-18. However, the theoretical maximal load and other recommendation by Fransson and Bergdahl (2009) still showed a conservative value.
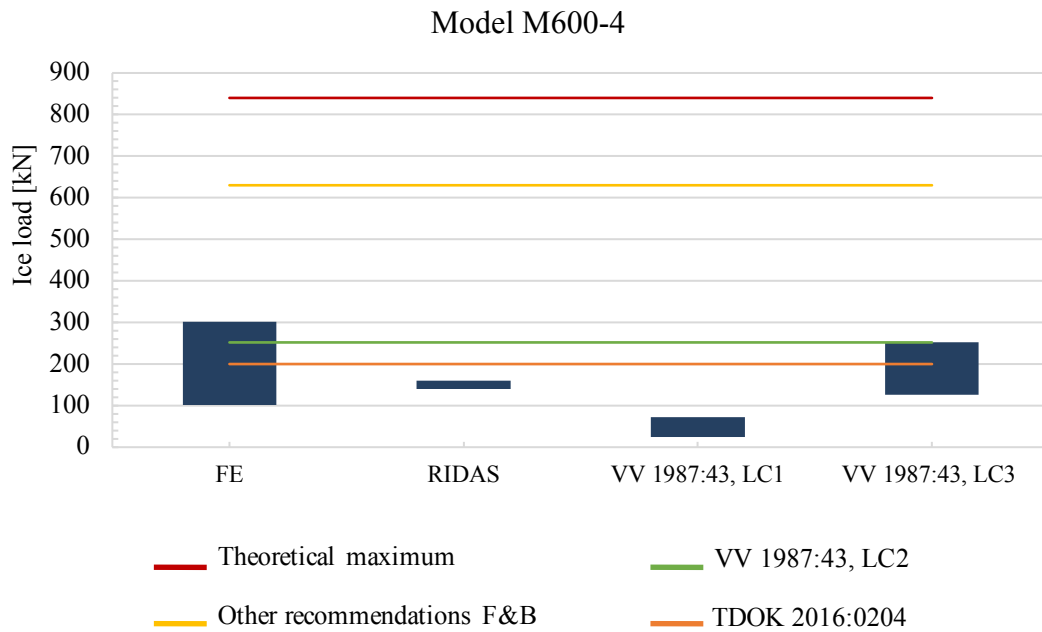
Model M600-4

Figure 8-18.   *Range of results from the FE analyses and the analytical calculations, see Appendix F, for Model M600-4. For exact values, see Appendix G.*

The same agreement, as for Model M600-4, could be observed for Model M600-8, see Figure 8-19.
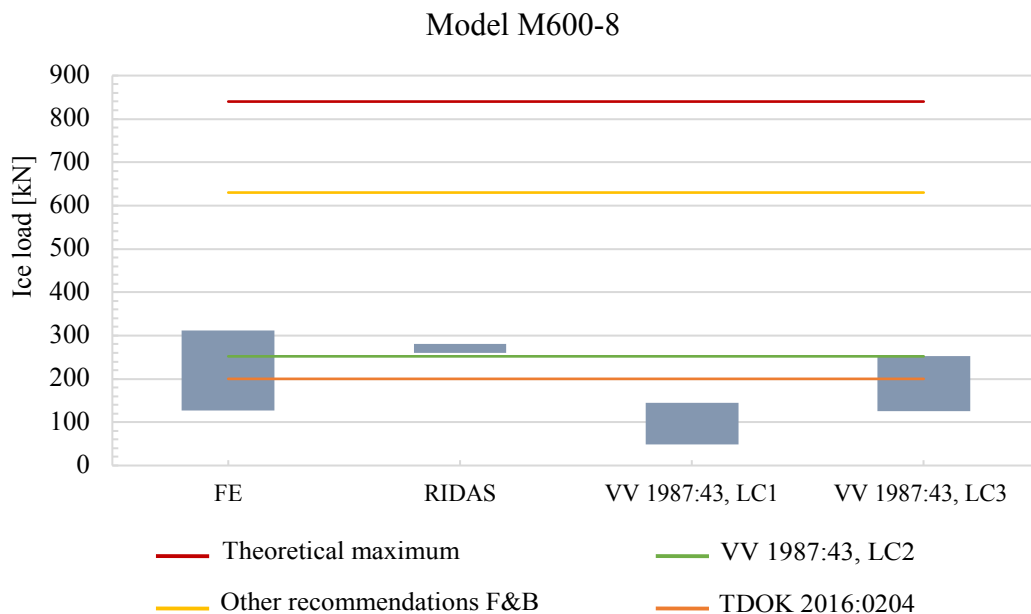
Model M600-8

Figure 8-19.   *Range of results from the FE analyses and the analytical calculations, see Appendix F, for Model M600-8. For exact values, see Appendix G.*

8.5.3   Comparison for Model M1200

For Model M1200, the values from the numerical analyses increased both in magnitude and range compared to M200 and M600, see Figure 8-20. The theoretical maximal load and other recommendation by Fransson and Bergdahl (2009) were higher than the FE results, similar as for M200 and M600. *LC1* in VV 1987:43 generated a continuously low ice load for all Model M1200, as it has previously for M200 and M600.
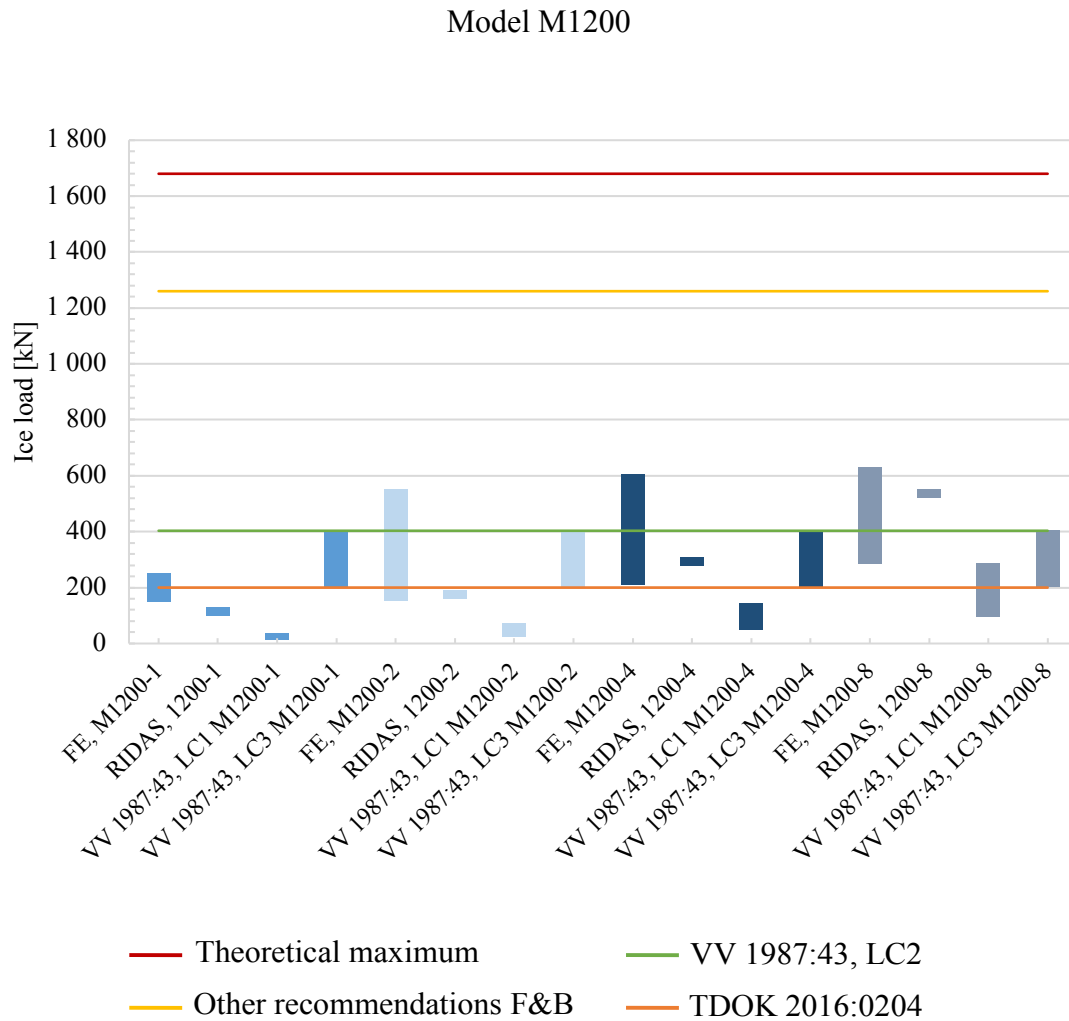
Model M1200

Figure 8-20.   Range of results from the FE analyses and the analytical calculations, see Appendix F, for Model M1200. For exact values, see Appendix G.

For Model M1200-1, only the set point load given in TDOK 2016:0204 showed a good agreement with the FE results, see Figure 8-21. The rest of the analytical calculated ice loads were either higher, e.g. VV 1987:43 *LC2*, or lower, e.g. VV 1987:43 *LC1*. This could partly be explained by the small range of FE results for M1200-1, similar to Model M600-1.
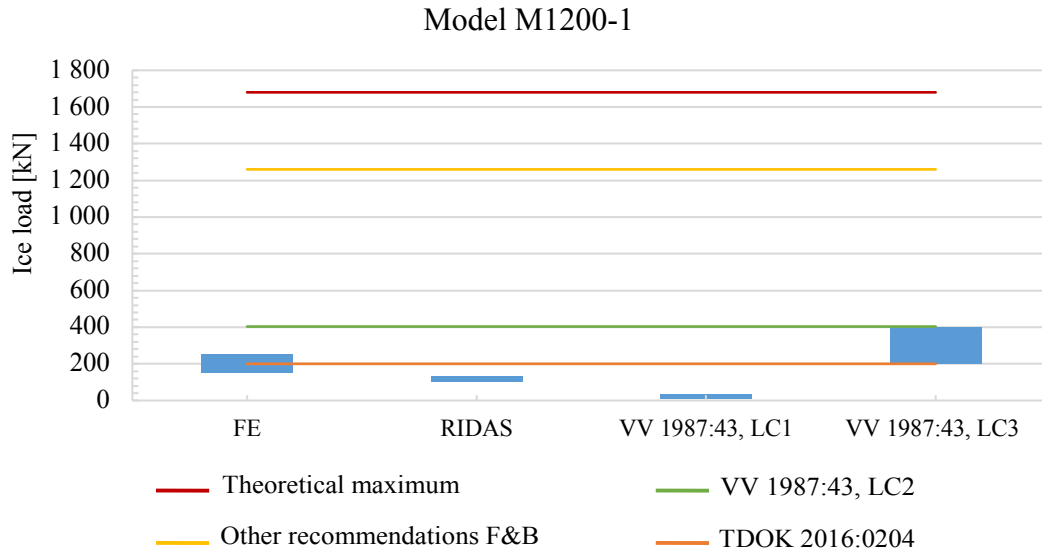
Figure 8-21.   *Range of results from the FE analyses and the analytical calculations, see Appendix F, for Model M1200-1. For exact values, see Appendix G.*

For the configuration analysed in Model M1200-2 a good agreement could be observed between the FE results and TDOK 2016:0204, VV 1987:43 *LC2* and *LC3*, see Figure 8-22. Some agreement could be observed for the set value in RIDAS, displayed in the lower range of the FE result.
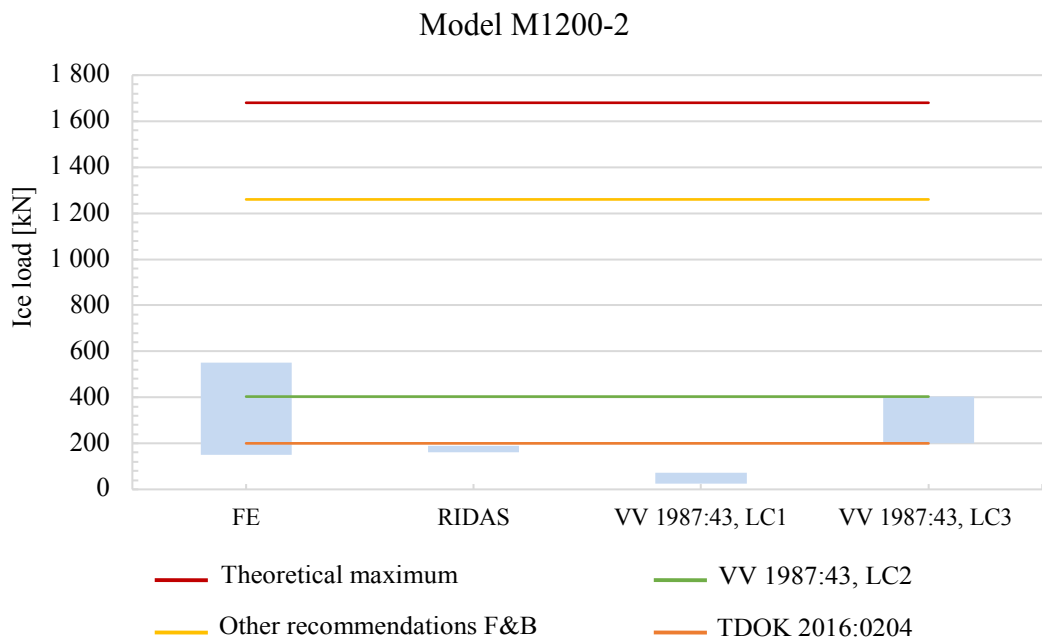
Figure 8-22.   *Range of results from the FE analyses and the analytical calculations, see Appendix F, for Model M1200-2. For exact values, see Appendix G.*

Two load cases showed a good agreement with the FE results for Model M1200-4: RIDAS and VV 1987:43 *LC2*, see Figure 8-23. Some agreement could be observed for VV 1987:43 *LC3*, but the rest of the analytical calculated ice loads were out of the range of the FE results.
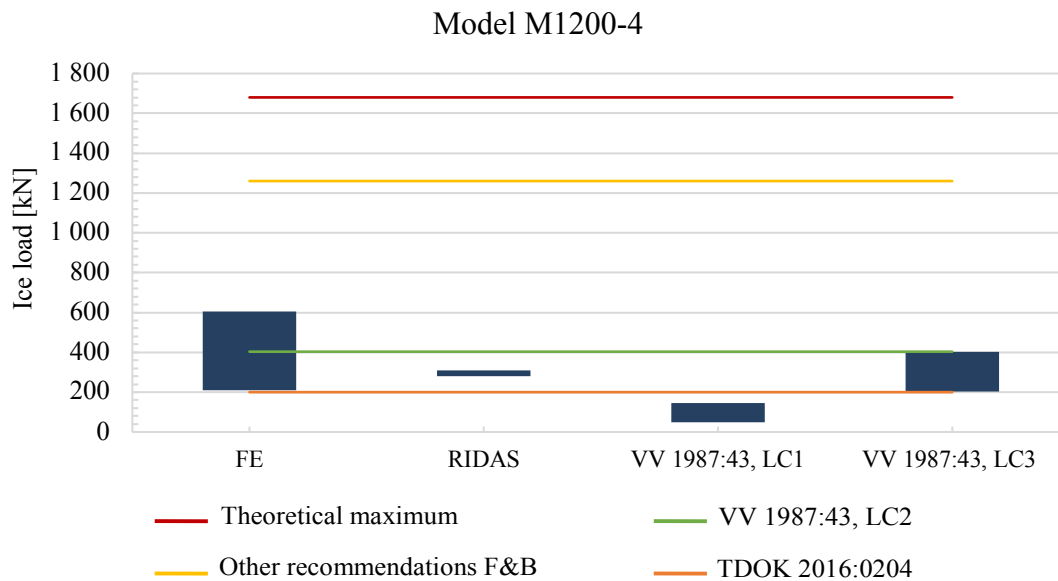
Model M1200-4

Figure 8-23.   *Range of results from the FE analyses and the analytical calculations, see Appendix F, for Model M1200-4. For exact values, see Appendix G.*

Lastly, the comparison between the FE results for Model M1200-8 and the analytical calculated ice loads resulted in a good agreement with the recommended set value in RIDAS and VV 1987:43 *LC2*. TDOK 2016:0204 and VV 1987:43 *LC1* were lower, and the theoretical maximal load and other recommendation by Fransson and Bergdahl were higher than the FE result.
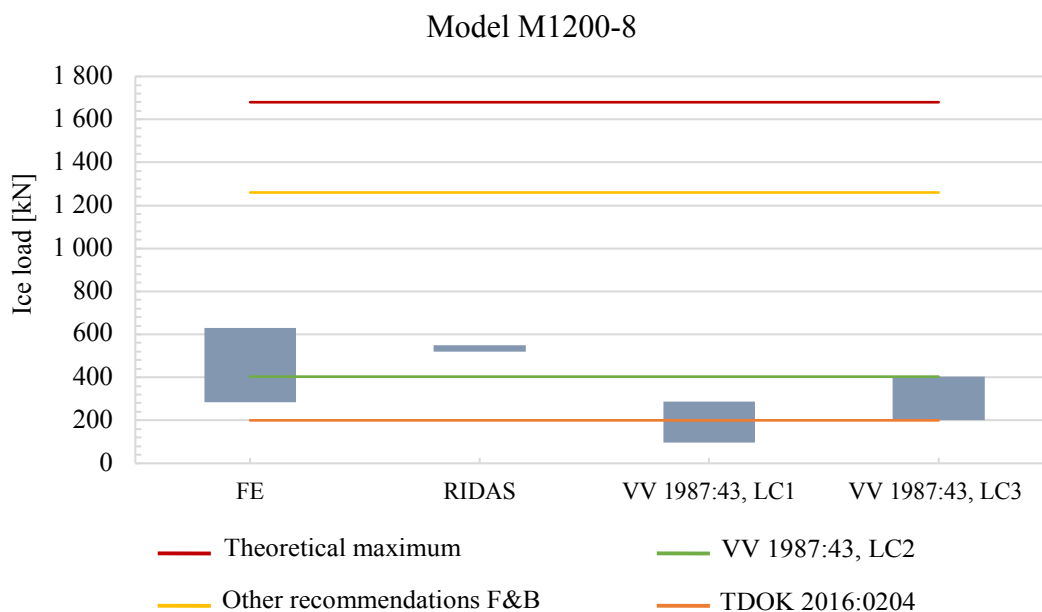
Model M1200-8

Figure 8-24.   *Range of results from the FE analyses and the analytical calculations, see Appendix F, for Model M1200-8. For exact values, see Appendix G.*

8.5.4 Summary of the comparison for Model M

The difference and similarities between the FE results and the analytical values for Model M are summarised in Table 8-4.

Table 8-4.   *Detailed comparison between the numerical results and the analytical loads from the standards and guidelines for Model M, displayed in Figure 8-10, Figure 8-15 and Figure 8-20.*

Load case	Comments
TDOK 2016:0204	According to TDOK, the ice load should be set to a constant value of 200kN. For M200, the set load value of 200kN was lower than the FE results. For M600 the load was within the FE results for the two larger models, and for M1200 the load was within the two smaller models. The conclusion is that the agreement was sporadic depending on the model size.
RIDAS	The values according to RIDAS were lower than the numerical results for the smaller models but gave good agreement for the largest models for all column widths. One reason could be the consideration to possible arching effects; increasing ice load with increasing distance between the columns.
Theoretical maximal load	The theoretical maximal load were consistently the highest load for both the analytical and the FE results, resulting in a conservative estimation.
VV 1987:43, *LC1* Moving ice sheet	*LC1* was based on a given distributed load, and did not take any specific material parameters into consideration, see equation (4-2). The ice loads were consistently smaller than all FE results, even though the load increased with increasing model size. The low set distributed load could be an explanation to the small values.
VV 1987:43, *LC2* Larger ice sheet	*LC2* was based on the crushing strength of the ice and included a shape factor to adjust the equation to different load configurations, see equation (4-3). Compared to M200 the ice loads were too high, but for M600 and M1200 the agreement was better. The smallest model for each column width agreed somewhat worse, which partly can be explained by the smaller range of results for those analyses.
VV 1987:43, *LC3* Sharp or inclined edge	*LC3* was also based on the crushing strength of the ice but was reduced with impact of inclination and sharp edges, resulting in a range. The results thereby agreed better, and were within the range of all FE results. Sometimes, higher values than the FE results were observed.
Other recommendation F&B (2009) Horizontal ice load w.r.t. crushing strength	Was calculated in the same manner as *LC2*, including the crushing strength of the ice, but with different shape factors. The obtained loads were much larger than the FE results.

9 Discussion

In this chapter the literature study is critically reviewed, followed by a discussion about the FE modelling. Finally, the FE results and the comparison with the results from the analytical calculations according to guidelines are discussed.

9.1 Discussion about the literature study

The literature review showed a wide range of research performed on ice loads all over the world, mainly in countries located in the northern hemisphere which are affected by ice during winter seasons. Parts of the literature concerning this field are from 1970th – 1980th. However, this information treats the formation of ice, its modes and behaviour during interaction with structures. Naturally, this is something that has not changed over the years, which makes the research still valid today, almost 50 years later.

All Swedish standards and guidelines, which treat ice loads, are in some way incomplete. Some standards and guidelines do not mention ice loads as an aspect to consider whereas others recommend investigating the magnitude of the ice load for each specific case. This cannot be applied in general and is therefore not durable, neither from the designers' nor the authorities' aspect.

The main guideline in Sweden when designing a bridge against ice loads is *Ice pressure against bridge supports* (Vägverket, 1987) which was written in 1987, 31 years ago (present-year 2018). An updated, or new, version of this guideline is needed not only due to the age but also to minimize the need to investigate each case separately. The input, in e.g. the equations, should be easy to determine for all loading situations, to simplify the appliance of the guideline and easily adopt it to the local conditions.

One main challenge if a completely new guideline, or standard, would be established is the design values, which now are stated in *Ice pressure against bridge supports* (Vägverket, 1987). They are based on both empirical values, measured over the years in Swedish water, and research. This means that the empirical values has been updated and adjusted to research. If a new guideline would be established, a decision needs to be taken whether empirical values or new research should be the most governing factor when estimating the ice loads.

Another challenge is the global warming which affect the recurrence time of the ice on the west coast of Sweden. As described in Section 2.3, the west coast of Sweden has been severely covered by ice 28 winter season during the last 117 years. Statistically, this means that there is 24% risk that ice will cover the west coast of Sweden and that ice loads will affect structures in water. If the risk will increase or decrease in the future is hard to tell since more extreme climate are expected.

9.2   Discussion about FE modelling

Values used in the material model were chosen, as far as possible, with respect to the west coast environment but some uncertainties remain. As an example, the tensile strength was not set to zero in the FE-analyses, resulting in a higher ice load since the ice had tension capacity. If the aim instead had been to investigate the capacity of the ice sheet, the conservative approach would be to set the tensile strength to zero.

In reality, ice has many local variations, both in properties and geometry, since it is an ever-changing material. The modelled ice in the FE analyses had a perfect geometry and did not show the inhomogeneous, anisotropic and elasto-viscoplastic behaviour that ice in reality has, but rather a simplified version. This results in a homogenous and geometrically perfect ice, which generally has higher resistance, resulting in higher ice loads. If packed ice masses were included in the FE analyses the result would be underestimated since the loads and stresses would increase due to partly increased ice thickness.

The choice of model sizes as well as the ratios R_1 and R_2, affect foremost the global response of the ice sheet but also the magnitude of the ice loads. Some analysed models were very small, e.g. M200-1, resulting in unrealistic interaction situations. The most likely result during an interaction of these sizes of ice sheets is fragmentation of the ice and an unaffected structure.

The cracks were modelled and initiated with XFEM, which has some limitations that could influence the results. One limitation with XFEM was that cracks were initiated thorough one element in the same loading step. Unfortunately, this approach led to that the models became more mesh dependant since the damage criteria involved the entire element. Parts in larger elements could locally reach the damage criterion, but globally still be within the limit. For small elements, the criterion could be fulfilled both locally and globally for a smaller prescribed displacement, resulting cracks. Consequently, the global response depends on the mesh size. With a smaller mesh, the stresses were divided into different elements leading to that cracks could arise for a lower prescribed displacement. In this study, shear cracks located in elements at the edge of the applied displacement were always observed for smaller meshes. At these locations, both compressive and tensile stresses were present, leading to a complex interpretation of the results.

9.3   Discussion about numerical results

The result, from the FE analyses, could be substantially influenced if other failure modes, than crushing and cracking, would occur at a lower ice load. Since crushing is the most common observed failure mode of an ice sheet, the result from the analyses was assumed to be reliable. The observed failure modes, in the FE-analyses, were also in agreement with Table 3-3, which states that the observed failure mode for the studied ice sheets should be crushing or gradually changing failure mode. One exception to the assumed reliable result was when the analyses generated a second failure mode i.e. crushing after cracking or cracking after crushing. The governing failure mode, either crushing or cracking, were the only failure modes from which any conclusion could be drawn. Following failures were not valid in the modelled ice sheet since the global response could not be determined. The global response could

depend on accumulation of the ice and/or continuous cracking, which not could be simulated.

The stress concentration observed at the edges of the prescribed displacement, see Section 6.4, were not investigated in detail but it was clear that it affected the response, and thereby the results, profoundly. When comparing the results from prescribed displacement and an infinitely stiff column with applied load and a weak column, both the magnitude of the load and the crack response changed. For the models with applied load, the local failure was equal to the global failure; thus generating a higher ice load which is comparable to the theoretical maximal load (crushing strength times impact area). For the models with prescribed displacement, the columns were assumed to be infinitely stiff and only local crushing were studied resulting in a lower ice load. Due to the differences, the stiffness of the column needs to be investigated and considered in further analyses of ice structure interactions. The true ice load is probably located in between the two obtained values since structures in reality are neither infinitely stiff nor infinitely weak.

A comparison of the aspect ratios of the models with previous research gave no general agreement. The aspect ratios for the analyses in this study are varying between 2/3–4 and, according to Figure 3-10, possible failure modes would then be crushing, crushing combined with spalling or radial/circumferential cracks and buckling since the analyses were performed within the brittle regime. However, the results from that particular research depends on the velocity, by the indentation rate, see Figure 3-10. Thus, it is hard to determine the correct failure mode for this study since it was analysed with a static load. Spalling and radial/circumferential cracks could not be described due to limitations in this study caused by e.g. the material model. That crushing and cracking should be observed for the modelled configurations confirms that the limitations made in this study, regarding failure modes, were reasonable.

9.4 Discussion about comparison between the FE results and analytical calculations according to guidelines

The FE analyses generated a larger ice load for larger column widths, see Figure 8-1. In the figure, it can also be seen that a larger distance between the columns resulted in an increase of the ice loads. However, the conclusion was that no relation could be drawn between the increase of the distance between the columns and the increase of the ice load. To find a relation, more column configurations need to be studied.

All analytical results showed varying agreement for the different models. One general observation in the comparison between the analytical calculations and the FE results was that the smaller models, with a smaller column width, showed less agreement than the larger models, with a larger column width. General comments on the comparison between the FE results and the different load cases is shown in Table 9-1. A more detailed explanation for each load case follows below.

Table 9-1.   Overview of the load cases used in the analytical calculations and comments on the agreement to the numerical results.

Recommendation/standard	Load Case	Comment
Requirement bridge design	TDOK 2016:0204	Sporadic agreement
Guideline for hydropower dams	RIDAS	Sporadic agreement
Ice pressure against bridge support	VV 1987:43, *LC1*	Too low value
	VV 1987:43, *LC2*	Best agreement
	VV 1987:43, *LC3*	Midst to higher range
Offshore structures	Other recommendation F&B (2009)	Too high value
-	Theoretical max load	Too high value

The two load cases that, in general, gave the best agreement were: VV 1987:43 *LC2* and *LC3* which both were based on the crushing strength of ice. However, *LC3* was based on different edge and support inclination and could thereby not be applicable on any general case. Therefore, best agreement for all configurations were VV 1987:43 *LC2* which was based on the crushing strength of the ice times a shape factor depending on the aspect ratio, see equation (4-3).

The ice load calculated according to Fransson and Bergdahl (2009) generated a much higher load than all of the other calculated ice loads and the numerical results, resulting in a very conservative load. One explanation could be that it was developed for offshore structures, which generally are subjected to higher ice loads than structures closer to the shoreline. The same conclusion, with a high and conservative ice load, could be drawn for the theoretical maximal load. Therefore, these two estimations of the ice load are not suggested to be used when estimating the ice load for the studied configurations.

RIDAS was developed for ice load acting on horizontally long structures, e.g. hydropower dams, and was not applicable on the analysed configurations, i.e. square columns. In the same manner, TDOK 2016:0204 gave a general guideline with a set value of the ice load that could be used for specific cases. In the comparison with the results from the FE analyses, some sporadic agreement were found, but no general conclusion could be drawn about the value. Therefore, a point load with a set value is not recommended to be used as a general ice load but more investigation for the specific configuration is then needed in advance. For RIDAS some agreement could be observed for the larger models, especially for Model M where the arching effect was taken into consideration, which makes the configuration more similar to a horizontally long structure.

One of the analytically calculated ice loads depended on the distance to the adjacent support, VV 1987:43 *LC1*. When comparing the value for this load case, it always generated a lower load compared to the FE results of Model M. Note that it was not compared to the FE results from Model S, as it concerns a single column interaction. One reason to the lower value could be that the set distributed load, which was suggested by Vägverket (1987), was rather low, between 10–30 kN/m. Due to the low values, this load case is not recommended to be used as an estimation of the ice load for Model M.

The analyses of the ice loads caused by wind or current, see Section 8.3, generated a large scattering of results, from reasonable to completely unreasonable ice sheet areas. The conclusion was that the thickness of the ice is a more affecting parameter of the ice load, leading to uncertainties in usage of equation (4-5). More investigations are needed to develop this equation if it should be used on the studied configurations.

It is important to keep in mind that the recommendations above can only be applied on similar or equivalent configurations that have been treated in this study. No guidance or advice about estimation of ice loads can be given for other type of configurations, structures or ice structure interactions.

10 Conclusions and further investigations

The aim of this study was to investigate how structures in the Swedish west coast marine environment are influenced by ice loads. To answer the aim, four objectives were formulated and the answer to these objectives are summarised in this chapter. Further investigations within the field of ice structure interactions are also suggested.

- **Which are the main physical properties of ice and how can ice loads be described with these?**

The behaviour of ice is very similar to the behaviour of plain concrete; can withstand compressive stresses well, but has a lower resistance to tensile stresses. Therefore, the same physical properties used to describe plain concrete can be used to describe ice loads, e.g. compressive and tensile strength. However, in contrast to plain concrete, ice can have both a brittle or a ductile response, depending mainly on the strain rate in the ice during an interaction with a structure. The real behaviour of ice is an elastic-viscoplastic behaviour. Its viscoplastic behaviour is an ongoing research subject and researchers claim that the existing constitutive models of ice, which includes the viscoplastic behaviour, are not fully reliable.

- **Which parameters affect the ice load and should be included when modelling it?**

The main parameters affecting the properties of the ice involve the formation of it, thus the conditions during its formation. The affecting conditions could be:
- type of water: sea, fresh or brackish water,
- amount of brine,
- climate in the water: e.g. temperature and currents, and
- climate in the air: e.g. temperature and wind.

The global conditions during the formation of the ice are important parameters to consider as well since it influences the type of ice formation and its strength parametres. This leads to a change in mangitude of the ice load at a possible ice structure interaction. The global parameters could be the magnitude of the water currents, type of structure and the appearance of the surroundings, e.g. if the structure is close to the shoreline or not.

To establish a finite element model of ice some strength parameters are essential, e.g. compressive and tensile strength, elastic modulus and Poisson's ratio. These parameters need to be chosen with respect to the affecting local and global conditions mentioned above. If several material parameters are included in the modelling, the true behaviour of ice could possibly be captured even better and the model would then show a more realistic interpetation of ice.

- **Can ice be modelled in a realistic way using finite element analyses in order to compare the effects of ice load on different configurations of columns?**

Ice can be modelled in a realistic way using FE analyses; the following aspects needs to be considerd:

- Include as many failure modes as possibe since they are highly dependant on each other.
- Use correct, or the most realistic input parameters: e.g. compressive and tensile strength, Young's modulus.
- Model the behaviour of the ice with a elastic-viscoplastic material model, if possible.
- Simulate a dynamic ice structure interaction.

The model used in this study captures some aspects of the behaviour of ice in a realistic way, e.g. local crushing and/or local cracking. However, the model was limited and could not describe all possible responses and failure modes during a ice structure interaction. Several important failure modes, such as accumulation of ice and bending failure, were not included in the model even though these responses are commonly observed during the studied ice structure interactions.

The material model in this study was chosen to be a elastic-perfectly plastic material model. Nevertheless, the true behaviour of ice is an elastic-viscoplastic behaviour which up untill today no researcher has suceeded to include in a material model to describe ice in a fully realistic way. Therefore, the material model used in this study was our best possible option, as it at least could describe some parts of the real response of the ice.

One challenge with modelling of ice structure interaction is the constant change of the properties of ice, both in time and at different geographical locations. In most research, one parameter is studied at a time, and the effect different parameters have on each other is lost, which is a major drawback.

- **What are the differences between modelled ice loads and the design values according to the Swedish guidelines?**

The results from the FE analyses generated a higher ice load for an increasing column width. However, the analytical calculations showed that the ice load was not only influeced by the column width, but also by different shape factors. Some design loads were based on set load values and others on the crushing strength of the ice. This resulted in a varying agreement for the different configurations.

Best agreement, between the numerical and the analytical ice loads, was found with the equations based on the crushing strength of the ice from Vägverket (1987), VV 1987:43 *LC2* and *LC3*. This agreement was reasonable, since the governing failure mode, for the majority of the analysed configurations, was crushing. However, *LC3* could not be applied in any general case since it depends on the edge and support inclination. Nevertheless, *LC2* agreed well for majority of the models; it was therefore assumed to be the best suited equation to be used for all of the studied configurations.

The values recommended by TDOK 2016:0204 and RIDAS were set load values and had an agreement for the medium sized models. Investigations of how the two recommended values could be adopted to better agree with the smaller and larger models were not performed. However, this could be an interesting subject for further research.

To further investigate ice structure interactions at the west coast of Sweden, the following investigations are suggested:

- Develop the FE model to:
    - include the elasto-viscoplastic behaviour of ice, and thereby describe the dynamic ice structure interaction,
    - describe more failure modes, e.g. bending and accumulation of ice sheet after failure,
    - include more parameters: e.g. temperature of the air and the ice, influence of the strain rate, snow condition.
- Investigate the influence of other shapes and configurations of structures e.g. circular columns, elongated structures, and the stiffness of the structures.
- Perform experimental research on the ice at the west coast of Sweden, in order to establish the material and mechanical properties of it. The results could be used as input for the FE analyses and to increase the information given in guidelines.

References

Allt om Vetenskap (2013) *Is från norr till söder*. Stockholm: Solna. Available at: http://www.alltomvetenskap.se/nyheter/fran-norr-till-soder.

Andersson, P. *et al.* (2016) *Eurokoder för dimensionering av betongdammar*. Stockholm.

Azarnejad, A. and Hrudey, T. M. (1998) 'A numerical study of thermal ice loads on structures', *Canadian Journal of Civil Engineering*, 25(3), pp. 557–568.

Bergdahl, L. (1977) *Physics of Ice and snow as Affects Thermal pressure*. Gothenburg: Chalmers University of Techonology.

Bergdahl, L. (2002) *Islaster på vindkraftverk till havs: beskrivning av mekanismer och rekommendationer för dimensionering*. Gothenburg: Chalmers University of Technology.

Bhat, S. U. *et al.* (1991) 'Failure Analysis of Impacting Ice Floes', *Journal of Offshore Mechanics and Arctic Engineering*, 113, pp. 171–178.

Blanchet, D. *et al.* (1988) 'An analysis of observed failure mechanisms for laboratory, first-year and multi-year ice', *International Association of Hydraulic Research Working Group on Ice Forces*.

Bouchat, A. and Tremblay, B. (2017) 'Using sea-ice deformation fields to constrain the mechanical strength parameters of geophysical sea ice', *Journal of Geophysical Research: Oceans*, 122(7), pp. 5802–5825.

Boverket (2016) 'Boverkets konstruktionsregler, EKS 10'. Karlskrona: Boverket.

Brinson, H. F. and Brinson, L. C. (2015) *Polymer engineering science and viscoelasticity: An introduction, Second edition, Polymer Engineering Science and Viscoelasticity: An Introduction*.

Calkins, D. J. and Ashton, G. D. (1975) 'Arching of Fragmented Ice Covers', *Canadian Journal of Civil Engineering*, 2, pp. 392–399.

Cammaert, A. . and Muggeridge, D. (1988) *Ice interaction with offshore structures*. New York: Van Nostrand Reinholdt.

Chandrasekaran, S. (2015) *Dynamic Analysis and Design of Offshore Structures*. India: Springer.

Chatterjee, M. and Chattopadhyay, A. (2017) 'Effect of moving load due to irregularity in ice sheet floating on water', *Acta Mechanica*, 228(5), pp. 1749–1765.

Cox, G. F. N. (1983) 'Thermal expansion of fresh and saline ice', 29(103), pp. 425–432.

Croasdale, K. R. (2012) 'Ice rubbling and ice interaction with offshore facilities', *Cold Regions Science and Technology*. Elsevier B.V., 76–77, pp. 37–43.

Daley, C., Tuhkuri, J. and Riska, K. (1998) 'The role of discrete failures in local ice loads', *Cold Regions Science and Technology*, 27(3), pp. 197–211.

Duval, P., Kalifa, P. and Meyssonnier, J. (1989) 'Creep constitutive equations for polycrystalline ice and effect of microcracking', *IUTAM symposium St. John's*, pp. 55–67.

EN 1991-1-3 (2003) *Eurocode 1991: Actions on structures -Part 1-3: General actions -Snow actions, European Committee for Standardization*.

EN 1991 (2003) 'Eurocode 1991: Actions on structures', *European Committee for Standardization*.

Eranti, E. and Lee, G. C. (1986) *Cold Region Structural Engineering*. Edited by J. Zseleczky and I. M. Stochmal. Mcgraw-hill book company: R. R. Donnelley & Sons, Inc.

Fransson, L. (2009) *Ice Handbook for Engineers*. Verson 1.2. Luleå: Luleå University of Technology, Institution of Civil Engineering.

Fransson, L. and Bergdahl, L. (2009) 'Recommendations for design of offshore foundations exposed to ice loads', p. 42.

Frederking, R. M. W. and Timco, G. W. (1986) *Field measurements of shear strength of columnar-grained sea ice*. Iowa City, USA: Proceedings of the 8th IAHR Symposium on Ice.

Golding, N. *et al.* (2014) 'Plastic faulting in saltwater ice', *Journal of Glaciology*, 60(221), pp. 447–452.

Goldstein, R. V., Osipenko, N. N. and Leppäranta, M. (2004) 'On the shape of the fast ice - Drift ice contact zone', *Geophysica*, 40(1–2), pp. 3–13.

Google maps (2018) 'Google maps'.

Hara, F. *et al.* (1993) 'Study on Drift Ice Control Utilizing Arch Formation of Ice Floes', II(June), pp. 6–11.

Hendrikse, H. and Metrikine, A. (2016a) 'Ice-induced vibrations and ice buckling', *Cold Regions Science and Technology*. Elsevier B.V., 131, pp. 129–141.

Hendrikse, H. and Metrikine, A. (2016b) 'Ice-induced vibrations and ice buckling', *Cold Regions Science and Technology*. Elsevier B.V., 131, pp. 129–141.

Hillerborg, A., Modéer, M. and Petersson, P. E. (1976) 'Analysis of crack formation and crack growth in concrete by means of fracture mechanics and finite elements', *Cement and Concrete Research*, 6(6), pp. 773–781.

Johnson, J. B. and Metzner, R. C. (1990a) 'Thermal Expansion Coefficients for Sea Ice', *Journal of Glaciology*, 36(124), pp. 343–349.

Johnson, J. B. and Metzner, R. C. (1990b) 'Thermal Expansion Coefficients for Sea Ice', *Journal of Glaciology*, 36(124), pp. 343–349.

Johnston, M. E., Croasdale, K. R. and Jordaan, I. J. (1998) 'Localized pressures during ice-structure interaction: relevance to design criteria', *Cold Regions Science and Technology*, 27(2), pp. 105–117.

Jordaan, I. J. (2001) 'Mechanics of ice-structure interaction', *Engineering Fracture Mechanics*, 68, pp. 1923–1960.

Jordaan, I. J. and Timco, G. W. (1988) 'Dynamics of the ice-crushing process', 34(118), pp. 318–326.

Karna, T., Frederking, R. and Shkhinek, K. (2011) 'Ice Actions in ISO 19906-Overview', *OTC Arctic Technology ...*, pp. 1–8.

Kato, K. and Sodhi, D. S. (1984) 'Ice Action on 2 Cylindrical Structures', *Journal of Energy Resources Technology-Transactions of the Asme*, 106(1), pp. 107–112.

Kolari, K., Kuutti, J. and Kurkela, J. (2009) 'FE-simulation of continuous ice failure based on model update technique', *Proceedings of the International Conference on Port and Ocean Engineering under Arctic Conditions, POAC*, 2, pp. 845–854.

Kuehn, G. A. *et al.* (1987) 'The Structure and Tensile Behavior of First Year Sea Ice and Laboratory-Grown Saline Ice', 1987(September). Available at: https://www.bsee.gov/sites/bsee.gov/files/tap-technical-assessment-program/087aa.pdf.

Lemieux, J. F. *et al.* (2016) 'Improving the simulation of landfast ice by combining tensile strength and a parameterization for grounded ridges', *Journal of Geophysical Research: Oceans*, 121(10), pp. 7354–7368.

Leppäranta, M. and Hakala, R. (1992) 'The structure and strength of first-year ice ridges in the Baltic Sea', *Cold Regions Science and Technology*, 20(3), pp. 295–311.

Lu, W. *et al.* (2016) 'Fracture of an ice floe: Local out-of-plane flexural failures versus global in-plane splitting failure', *Cold Regions Science and Technology*. Elsevier B.V., 123, pp. 1–13.

Lu, W. *et al.* (2017) 'Large Scale Simulation of Floe-Ice Fractures and Validation against Full-scale Data', *Proceeding of the 24th International Conference on Port and Ocean Engineering under Arctic Conditions*, (June).

Lu, W., Löset, S. and Lubbad, R. (2012) 'Simulating ice-sloping structure interactions with the cohesive element method', in *Proceedings of the ASME 2012 31st*. Rio de Janerio, Brazil: International Conference on Ocean, Offshore and Arctic Engineering, pp. 1–10.

Lu, W., Lubbad, R. and Løset, S. (2015a) 'In-plane fracture of an ice floe: A theoretical study on the splitting failure mode', *Cold Regions Science and Technology*. Elsevier B.V., 110, pp. 77–101.

Lu, W., Lubbad, R. and Løset, S. (2015b) 'Out-of-plane failure of an ice floe: Radial-crack-initiation-controlled fracture', *Cold Regions Science and Technology*. Elsevier B.V., 119, pp. 183–203.

Määttänen, M. P. (1991) 'Ice Interaction with Structures', *Ice-Structure Interaction*. Canada: Springer-Verlag Berlin Heidelberg.

Malm, R. *et al.* (2017). *Lastförutsättningar avseende istryck - Utveckling av en prototypgivare och möjligheter till uppdatering av svenska riktlinjer avseende islaster*. Stockholm: Energiforsk AB.

Marcellus, W. and Heuff, D. N. (1991) 'The role that fracture plays during ice failure', *Australian Road Research*, 28.

Michel, B. (1978) *Ice mechanics*. Québec: Les Presses de l'Université Laval.

Mulmule, S. V and Dempsey, J. P. (1998) 'A Viscoelastic Fictitious Crack Model for the Fracture of Sea Ice', *Mechanics of Time-Dependent Materials*, 1(1995), pp. 331–356.

Mulmule, S. V and Dempsey, J. P. (1999) 'Scale effects on sea ice fracture', *Mechanics of cohesive-frictional materials*, 4(4), pp. 505–524.

National Snow & Ice Data Center (2018) *Ice sheet*. Available at: https://nsidc.org/cryosphere/glossary/term/ice-sheet.

Olason, E. (2016) 'A dynamical model of Kara Sea land-fast ice', *Journal of Geophysical Research: Oceans*, 121(5), pp. 3141–3158.

Palmer, A. C. and Croasdale, K. (2013a) 'Broken Ice , Pressure Ridges and Ice Rubble', in *Arctic offshore engineering*. World Scientific, pp. 181–247.

Palmer, A. C. and Croasdale, K. (2013b) 'Ice Forces on Structures in the Sea', in *Arctic Offshore Engineering*. World Scientific, pp. 101–180..

Ponter, A. R. . and Cocks, A. C. . (1989) 'Creep and rupture in relation to field experiments', *IUTAM symposium St. John's*, pp. 3–18.

RIDAS (2012a) *Kraftföretagens riktlinjer för dammsäkerhet, allmän*. Stockholm: Svensk Energi, pp. 1–30.

RIDAS (2012b) *Kraftföretagens riktlinjer för dammsäkerhet - betongdammar avsnitt 7.3*' Stockholm: Svensk Energi, pp. 1–30.

Sand, B. (2008) 'Nonlinear finite element simulations of ice forces on offshore structures', p. 264. Luleå University of Technology

Sanderson, T. J. O. (1988) *Ice mechanics : risks to offshore structures*. London: Graham & Trotman.

Schulson, E. M. (2000) 'Brittle failure of ice', *Engineering fracture mechanics*, 68, pp. 1839–1887.

Schulson, E. M. and Iliescu, D. (2006) 'Brittle compressive failure of ice: Proportional straining vs proportional loading', *Journal of Glaciology*, 52(177), pp. 248–250.

Shroyer, E. L. *et al.* (2017) 'Seasonal control of Petermann Gletscher ice-shelf melt by the ocean's response to sea-ice cover in Nares Strait', *Journal of Glaciology*, 63(238), pp. 324–330.

SIMULIA (2014) *Abaqus 6.14 Online Documentation*. Dassault Systèmes Simulia.

SIMULIA (2018) *Abaqus/STANDARD*. Available at: https://www.3ds.com/products-services/simulia/products/abaqus/abaqusstandard/ (Accessed: 20 March 2018).

Sjöfartsverket (1992) *Svensk Lots Del A*. Norrköping.

Sjöfartsverket (2015) *Hållbarhetsredovisning 2015*. Norrköping. Available at: http://www.sjofartsverket.se/upload/Pdf-Gemensamma/Hallbarhetsredovisning2015_webb.pdf.

Sjöfartsverket and SMHI (2017) *Sammanfattning av isvintern och isbrytningsverksamheten 2016/2017*.

SMHI (2011a) *Största isutbredningen i Östersjön sedan 1987*. Available at: https://www.smhi.se/nyhetsarkiv/storsta-isutbredningen-i-ostersjon-sedan-1987-1.15126 (Accessed: 1 March 2018).

SMHI (2011b) *Svensk israpport*. Norrköping.

SMHI (2017a) *Pannkaksis på Västkusten*. Available at: https://www.smhi.se/nyhetsarkiv/pannkaksis-pa-vastkusten-1.28358.

SMHI (2017b) *Pannkaksis på Västkusten*.

Sodhi, D. S. (1998) 'Vertical penetration of floating ice sheets', *International Journal of Solids and Structures*. Elsevier Science Ltd, 35(31–32), pp. 4275–4294.

SOU1961:12 (1960) *Statliga belastningsbestämmelser av år 1960 för byggnadsverk*, *Library Journal*.

d Pang, S. D. (2017) 'On the Flexural Failure of Thick Ice Against Sloping Structures', *Journal of Offshore Mechanics and Arctic Engineering*, 139(4), p. 041501.

Tidlund, A. *et al.* (2017) *havet.nu*. Available at: https://www.havet.nu/index.asp?d=44 (Accessed: 12 February 2018).

Timco, G. (1987) 'Indentation and penetration of edge-loaded freshwater ice sheets in the brittle range', *Journal of Offshore Mechanics and Arctic Engineering*, 109(August).

Timco, G. W. and Frederking, R. M. W. (1996) 'A review of sea ice density', *Cold Regions Science and Technology*, 24(1), pp. 1–6.

Timco, G. W. and Weeks, W. F. (2010) 'A review of the engineering properties of sea ice', *Cold Regions Science and Technology*. Elsevier B.V., 60(2), pp. 107–129.

Trafikverket (2011) 'Trafikverkets författningssamling, TRVFS 2011:12'. Borlänge: Trafikverket, pp. 1–93.

Trafikverket (2016a) *Krav Brobyggande*. Sverige.

Trafikverket (2016b) *Råd Brobyggande*.

Tsinker, G. P. (1997) *Handbook of Port and Harbor Engineering: Geotechnical and Structural Aspects*. Edited by B. . Springer-Science+Business Media. New York: Chapman & Hall.

US Army Corps of Engineers (2006) *Engineering and design: ice engineering*, *EM 1110-2-1612 Change 3*. Washington DC.

Vägverket (1987) *Istryck mot bropelare*. 1987:43. Sweden: Vägverket.

Wang, Y. and Poh, L. H. (2017a) 'Velocity Effect on the Bending Failure of Ice Sheets Against Wide Sloping Structures', *Journal of Offshore Mechanics and Arctic Engineering*, 139(6).

Wang, Y. and Poh, L. H. (2017b) 'Velocity Effect on the Bending Failure of Ice Sheets Against Wide Sloping Structures', *Journal of Offshore Mechanics and Arctic Engineering*, 139(6), p. 061501.

Weiss, J. (2001) 'Self-affinity of fracture surfaces and implications on a possible size effect on fracture energy', *International Journal of Fracture*, 109(December), pp. 365–381.

Yasui, M., Schulson, E. M. and Renshaw, C. E. (2017) 'Experimental studies on mechanical properties and ductile-to-brittle transition of ice-silica mixtures: Young's modulus, compressive strength, and fracture toughness', *Journal of Geophysical Research: Solid Earth*, 122(8), pp. 6014–6030.

APPENDIX A
FE Modelling in Abaqus

- Create a part
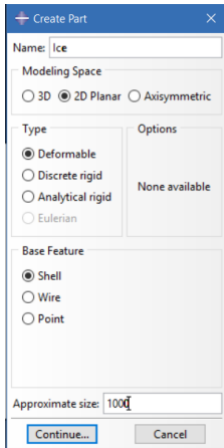
- Add material
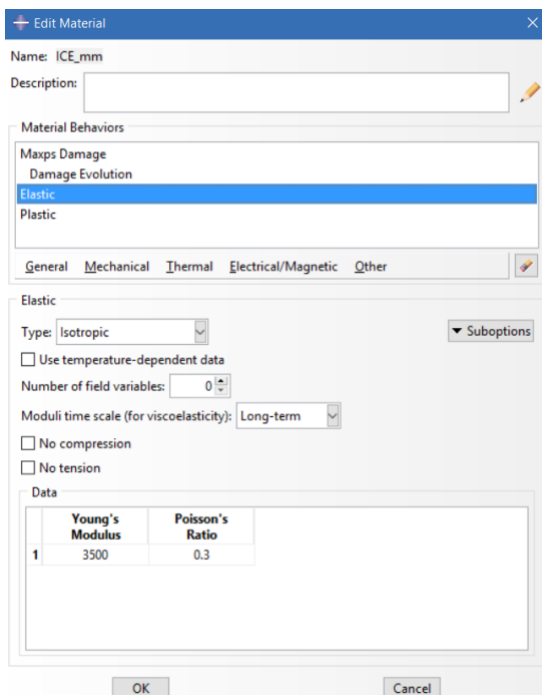
- Create a solid, homogenous section
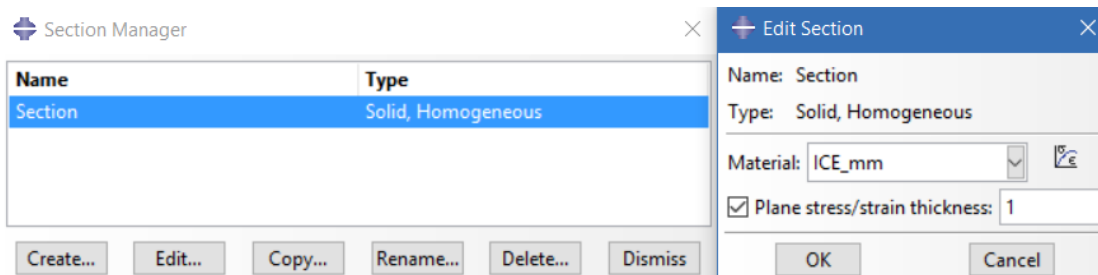
- Assign the material to that section and assemble the part that has been created

Section Assignment Manager ✕

Section Name (Type)	Material Name	Region
✔ Section (Solid, Homogeneous)	ICE_mm	(Picked)

Create...   Edit...   Delete...   Dismiss

- Create a step

Step Manager ✕

	Name	Procedure	NIgeom	Time
✔	Initial	(Initial)	N/A	N/A
✔	Step-1	Static, General	OFF	1

Create...   Edit...   Replace...   Rename...   Delete...   NIgeom...   Dismiss

Edit Step ✕

Name: Step-1
Type: Static, General

Basic | Incrementation | Other

Description:

Time period: 1

NIgeom: ⦿ Off (This setting controls the inclusion of nonlinear effects
⚬ On   of large displacements and affects subsequent steps.)

Automatic stabilization: None

☐ Include adiabatic heating effects

OK   Cancel

Edit Step ✕

Name: Step-1
Type: Static, General

Basic | Incrementation | Other

Type: ⦿ Automatic ⚬ Fixed

Maximum number of increments: 1000000

	Initial	Minimum	Maximum
Increment size:	0.001	1E-018	0.1

OK   Cancel

Edit Step ✕

Name: Step-1
Type: Static, General

Basic | Incrementation | Other

Equation Solver
Method: ⦿ Direct ⚬ Iterative
Matrix storage: ⦿ Use solver default ⚬ Unsymmetric ⚬ Symmetric
Warning: The analysis code may override your matrix storage choice.
See "STEP in the Abaqus Keywords Reference Manual.

Solution Technique
Solution technique: ⦿ Full Newton ⚬ Quasi-Newton
Number of iterations allowed before the kernel matrix is reformed: 8

Convert severe discontinuity iterations: Propagate from previous step ⌄ (Analysis produc

Default load variation with time
⚬ Instantaneous ⦿ Ramp linearly over step

OK   Cancel

2

- Edit Field Output Requests Manger
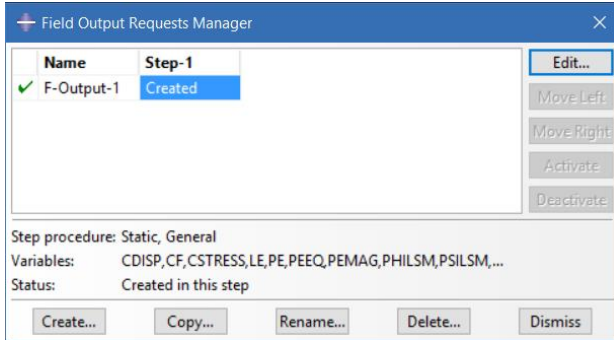
- And add following:
  o Failure/Fracture
    ▪ PHILSM, Level set value phi
    ▪ PSILSM, Level set value psi
  o State/Filed/User/Time
    ▪ STATUSXFEM, Status of xfem element
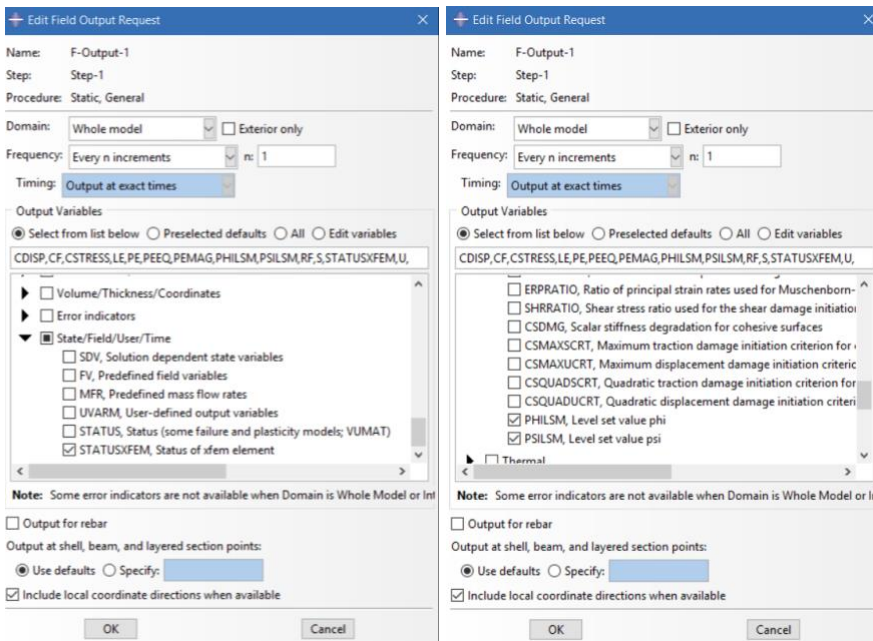
- Create XFEM area
  o Special, Crack, Manager, Create Crack, XFEM
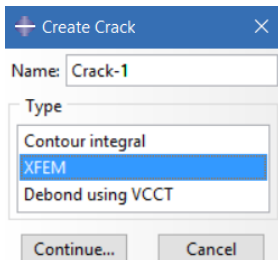
- Select the crack domain: geometric faces. Choose the assembled part
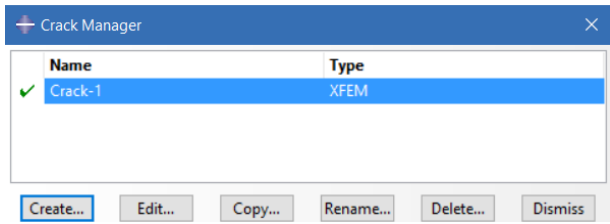
- Assign an interaction
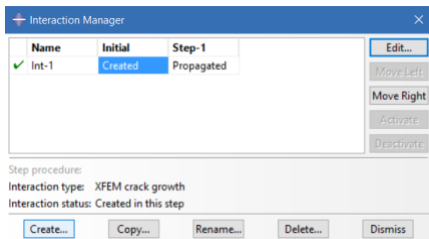
- Edit and create: XFEM crack growth. Choose Crack-1 and allow crack growth in this step.
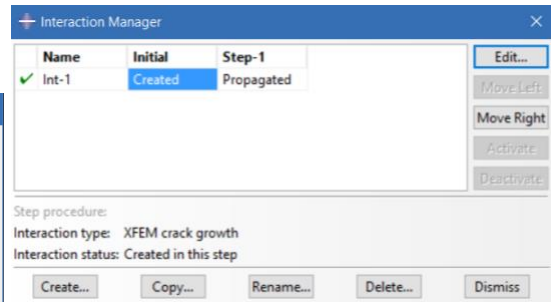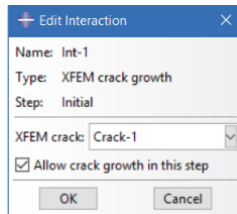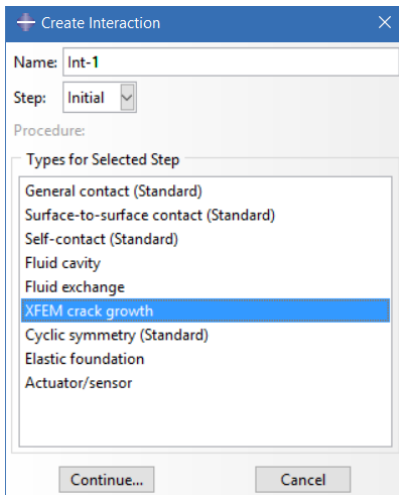
- Create boundary conditions and add a prescribed displacement according to Chapter 5.
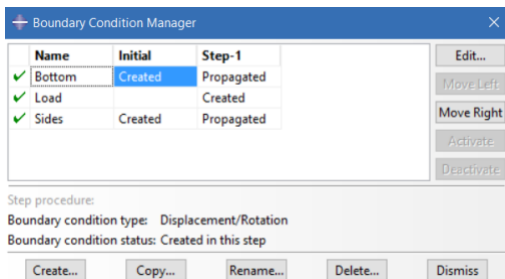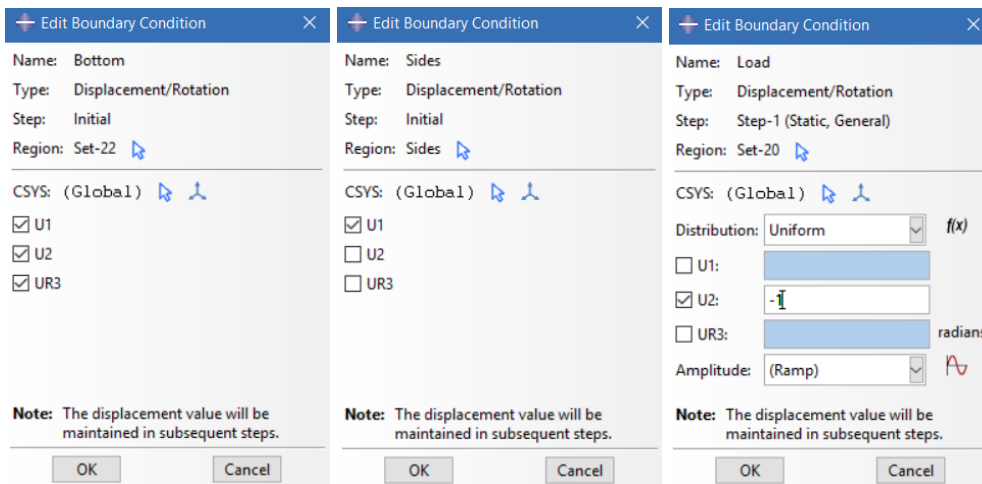
- Assign a global seeds of appropriate size and mesh the part instance. In Element Type change: Hourglass control to Enhanced from Use default.
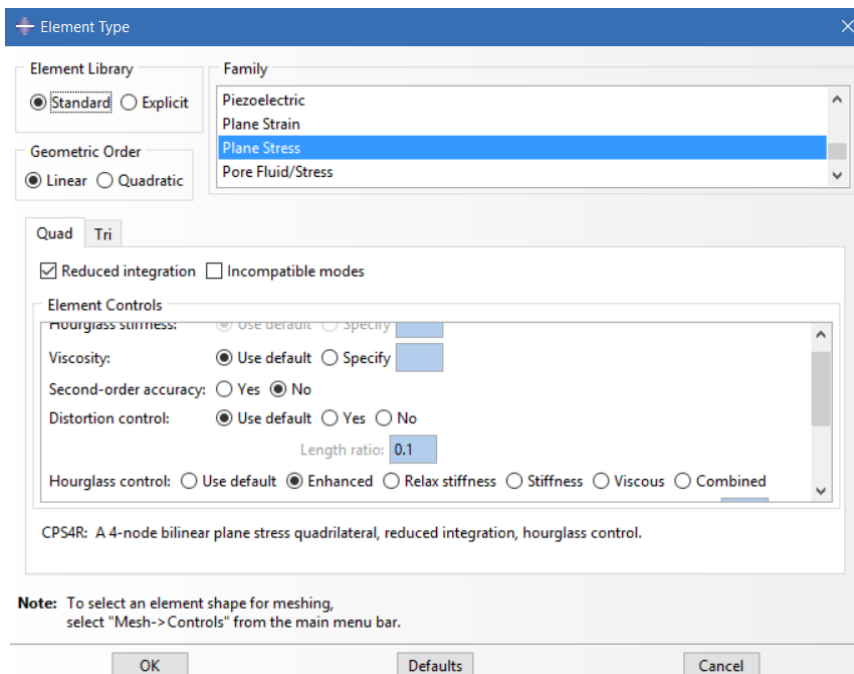
APPENDIX B

Convergence Study

B1. CONVERGENCE STUDY OF MODEL S
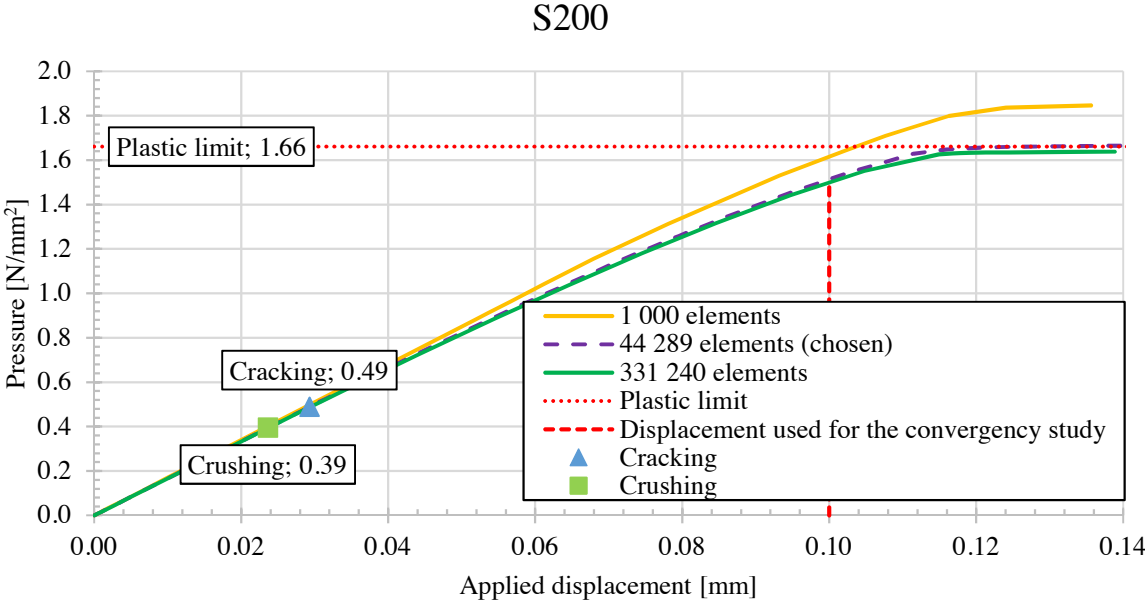
Figure B-1. *Pressure-displacement curve for Model S200 with different elements numbers and marked pressure at crushing, cracking and plasticisation.*
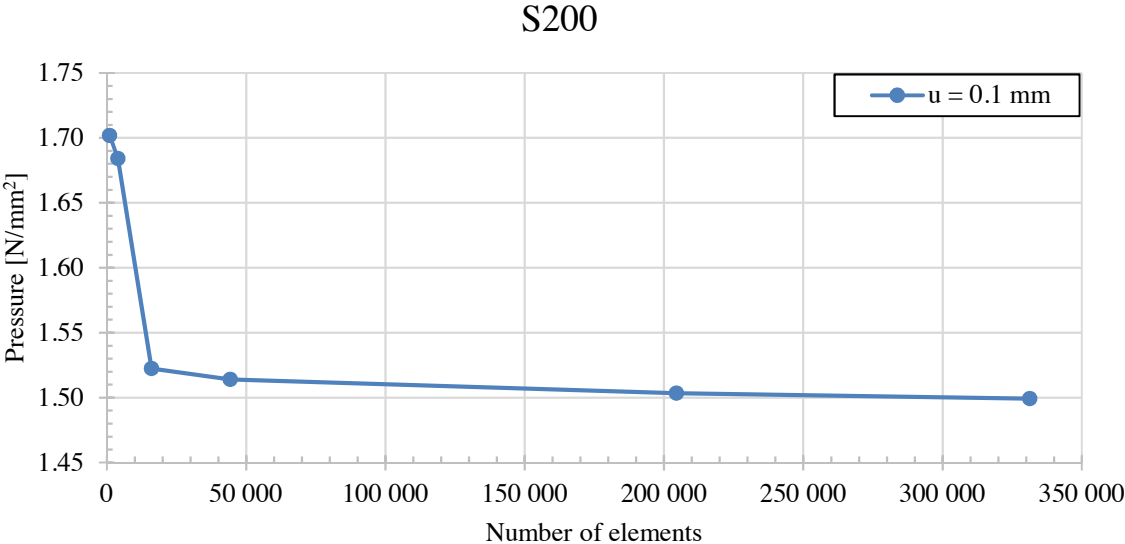
Figure B-2. *Convergence study of Model S200, where the applied fictive pressure at displacement 0.10 mm versus number of elements in the model is show*

In Table B-1 are the exact value for the diagram in Figure B-2 shown.

Table B-1.   *The result from the mesh convergence displayed in Figure B-2 for Model S200 with the further used mesh size marked.*

Mesh size [mm]	Number of elements [-]	Pressure at u = 0.10 mm [N/mm²]
20	1 000	1.70
10	4 000	1.68
5	16 000	1.52
3	**44 289**	**1.51**
1	400 000	1.50
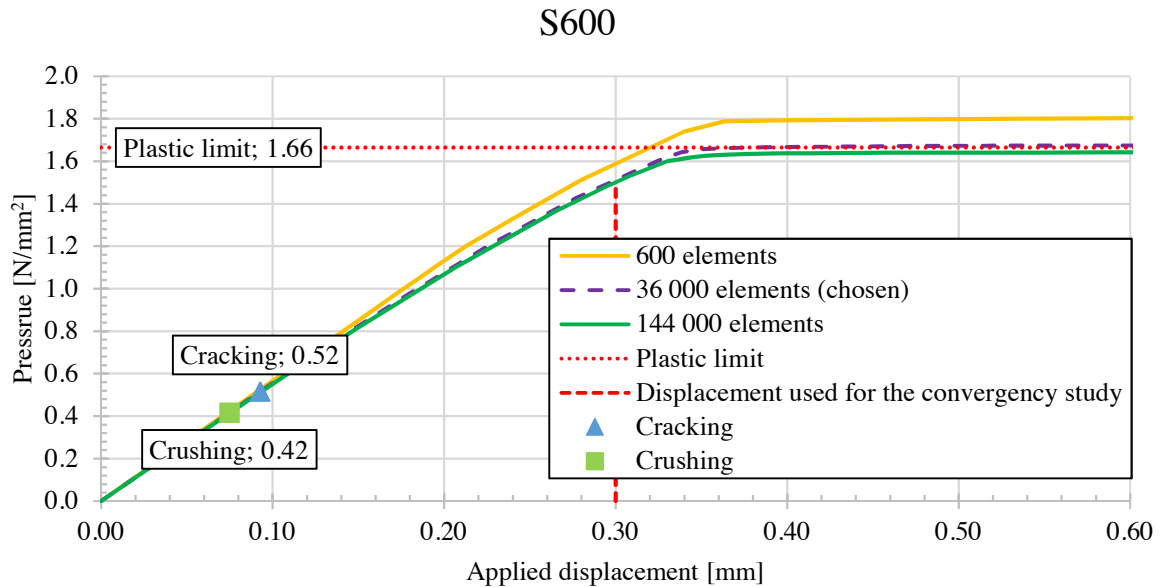
Figure B-3.   *Pressure-displacement curve for Model S600 with different elements numbers and marked pressure at crushing, cracking and plasticisation.*
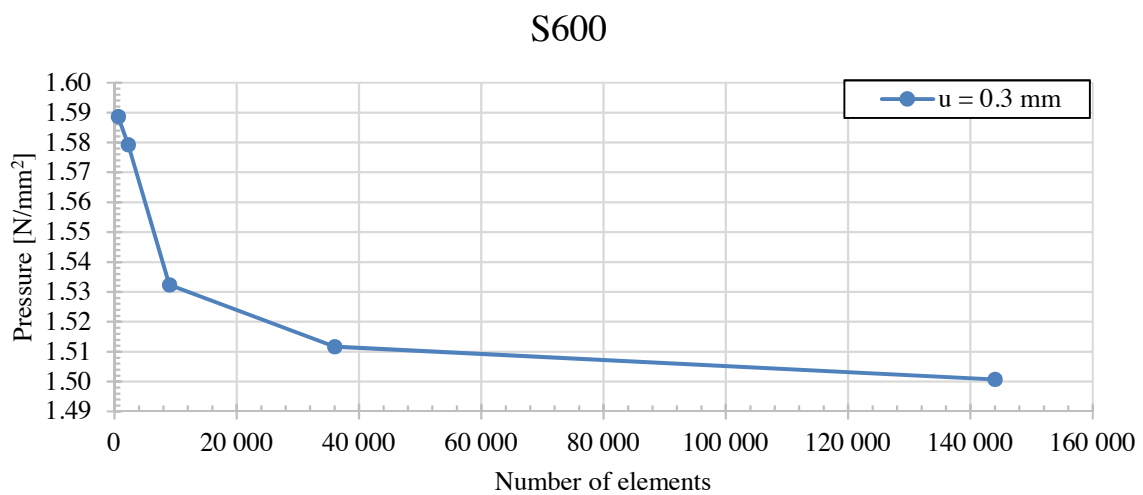
Figure B-4.   *Convergence study of Model S600, where the applied fictive pressure at displacement 0.30 mm versus number of elements in the model is shown.*

2

In Table B-2, are the exact values in Figure B-4 shown.

Table B-2.   *The result from the mesh convergence displayed in Figure A-4 for Model S600 with the further used mesh size marked.*

Mesh size [mm]	Number of elements [-]	Pressure at u = 0.30mm [N/mm²]
80	600	1.59
40	2 250	1.58
20	9 000	1.53
10	**36 000**	**1.51**
5	144 000	1.50
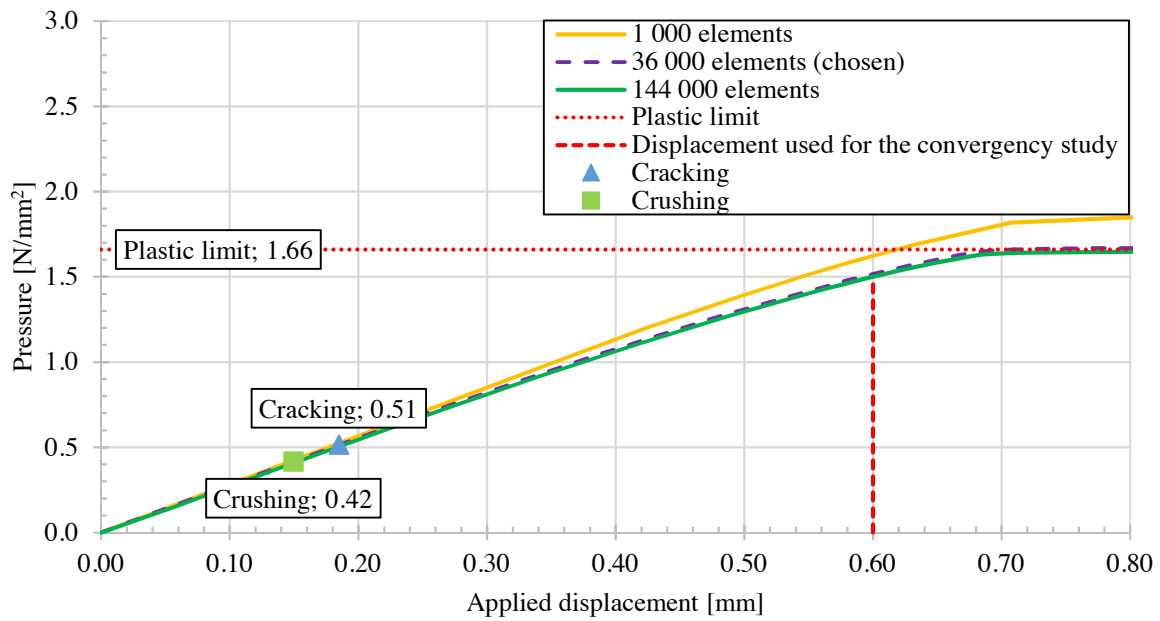
Figure B-5.   *Pressure-displacement curve for Model S1200 with different elements numbers and marked pressure at crushing, cracking and plasticisation.*
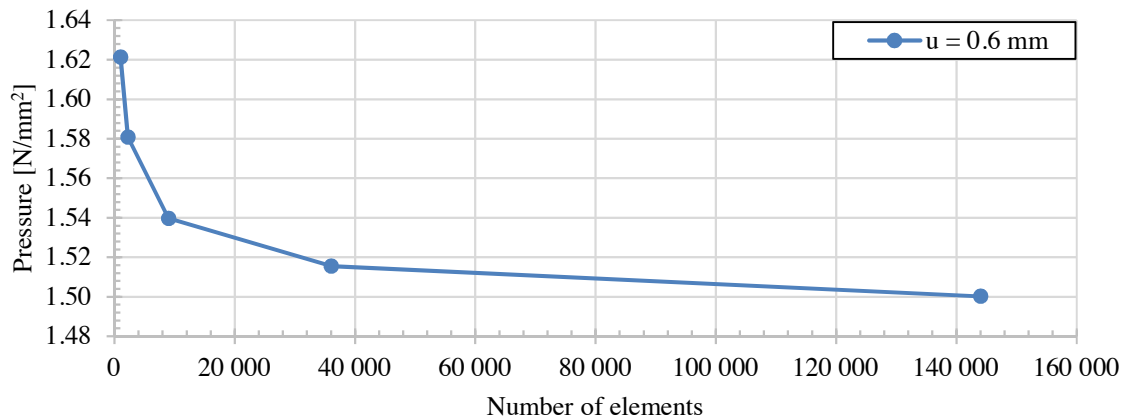
Figure B-6.   *Convergence study for Model S1200, where the applied fictive pressure at displacement 0.60 mm versus number of elements in the model is shown.*

3

In Table B-3 are the exact values in Figure B-6 shown.

Table B-3. *The result from the mesh convergence displayed in Figure A-6 for Model S1200 with the further used mesh size marked.*

Mesh size [mm]	Number of elements [-]	Pressure at u = 0.6 mm [N/mm²]
120	1 000	1.62
80	2 250	1.58
40	9 000	1.54
20	**36 000**	**1.52**
10	144 000	1.50

A summarise of the mesh sizes used, and the corresponding number of element for Model S, are presented in Table B-4. These mesh sizes were used in further analyses of Model S.

Table B-4. *A summary of the mesh sizes used and the corresponding number of elements.*

Model	Height [mm]:	Mesh size [mm]:	Number of elements [-]:
S200	400	3	44 289
S600	1200	10	36 000
S1200	2400	20	36 000

B2. CONVERGENCE STUDY OF MODEL M200

M200-1
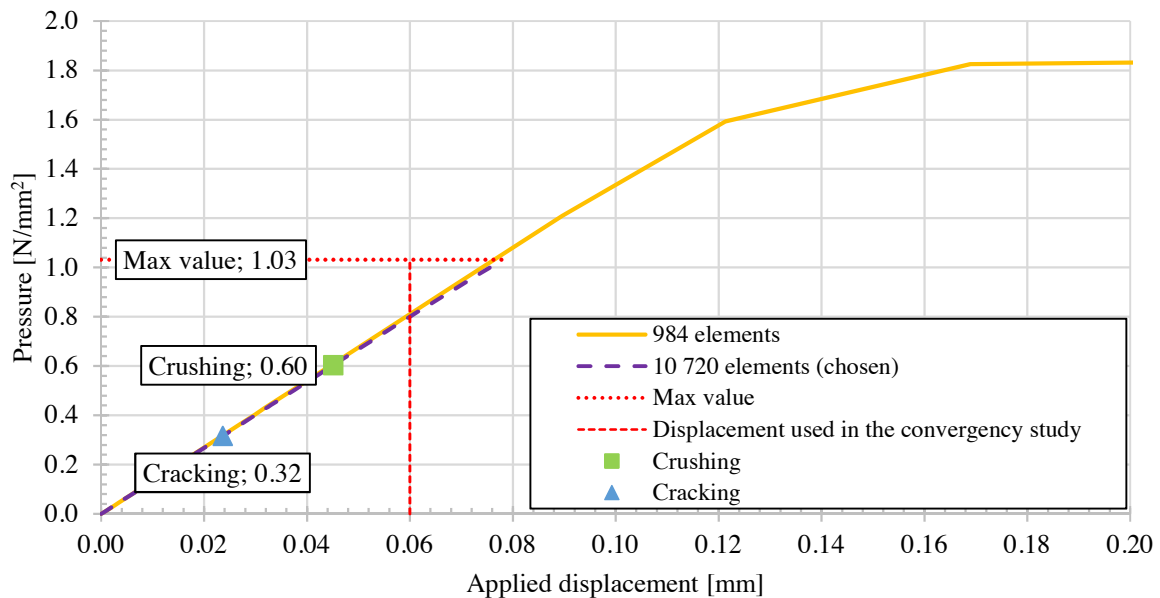
Figure B-7. *Pressure-displacement curve for Model M200-1 with different element numbers and marked pressure at crushing, cracking and plasticisation (max value).*

4
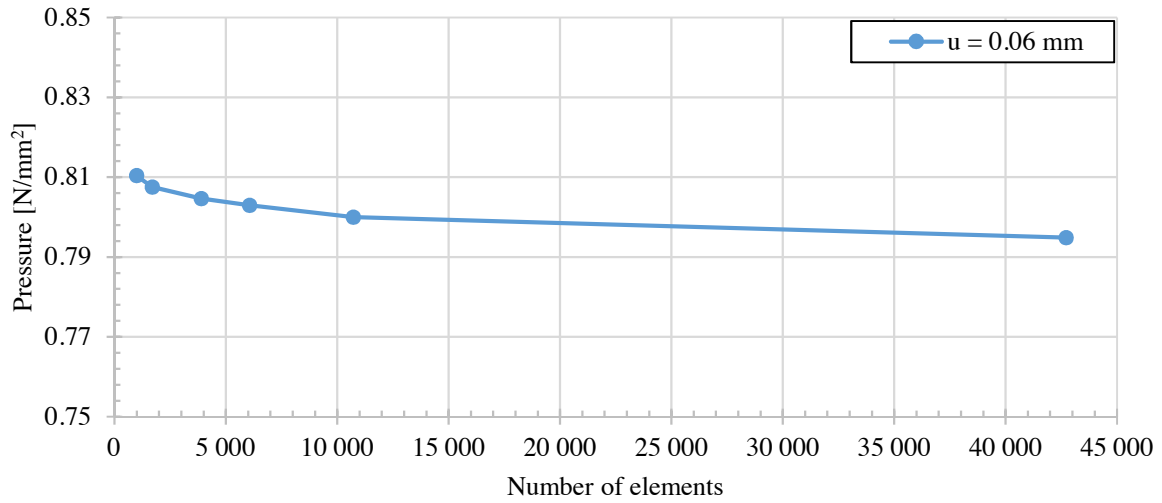
M200-1

Figure B-8. Convergence study of Model M200-1, where the applied fictive pressure at one support at displacement 0.06 mm versus number of elements in the model is shown.

M200-1
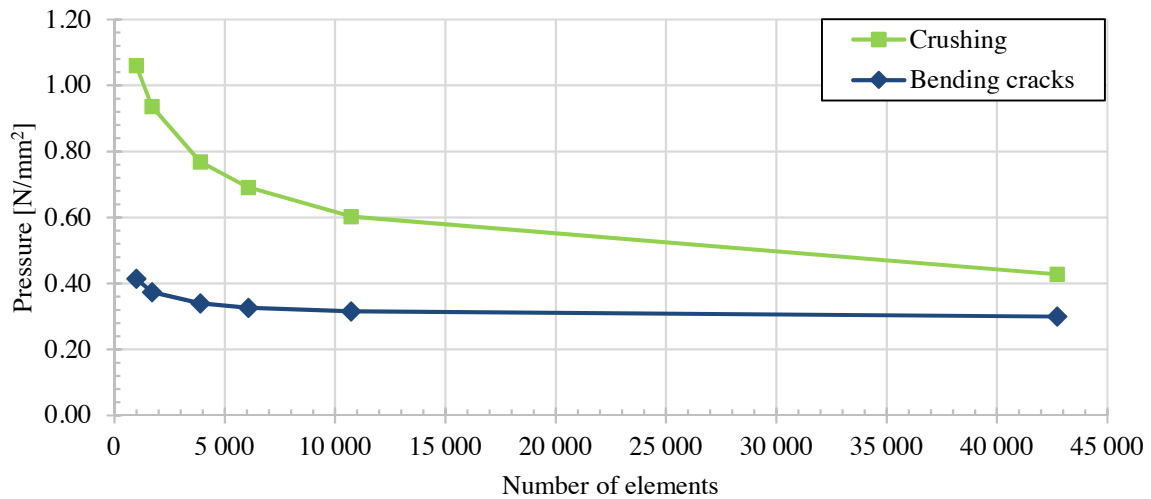
Figure B-9. The fictive applied pressure at one support versus number of elements for Model M200-1.

The exact values of the pressure and the corresponding number of elements for Model M200-1 are displayed in Table B-5.

Table B-5. Exact values for the mesh convergence of Model M200-1 with the further used mesh size marked.

Number of elements [-]	Mesh size [mm]	Pressure at one support at cracking [N/mm²]	Pressure at one support at crushing [N/mm²]	Pressure at displacement u = 0.06 mm [N/mm²]
984	20	0.41	1.06	0.81

5

1 696	15	0.37	0.94	0.81
3 888	10	0.34	0.77	0.80
10 720	**8**	**0.33**	**0.69**	**0.80**
40 000	6	0.32	0.60	0.80
42 720	3	0.30	0.43	0.79
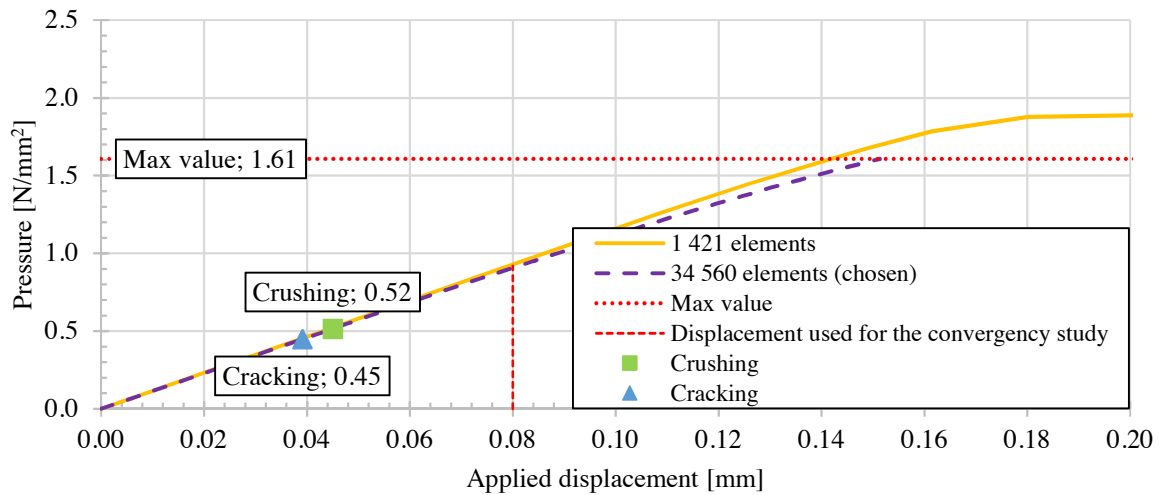
Figure B-10. *Pressure-displacement curve for Model M200-2 with different element numbers and marked pressure at crushing, cracking and plasticisation (max value).*
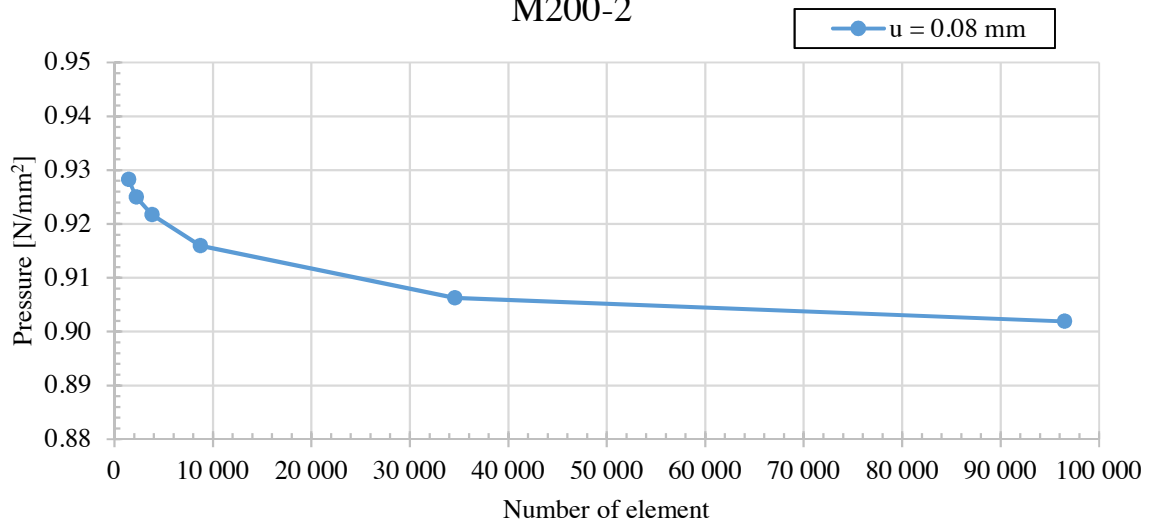
Figure B-11. *Convergence study of Model M200-2, where the applied fictive pressure at one support at displacement 0.08 mm versus number of elements in the model is shown.*
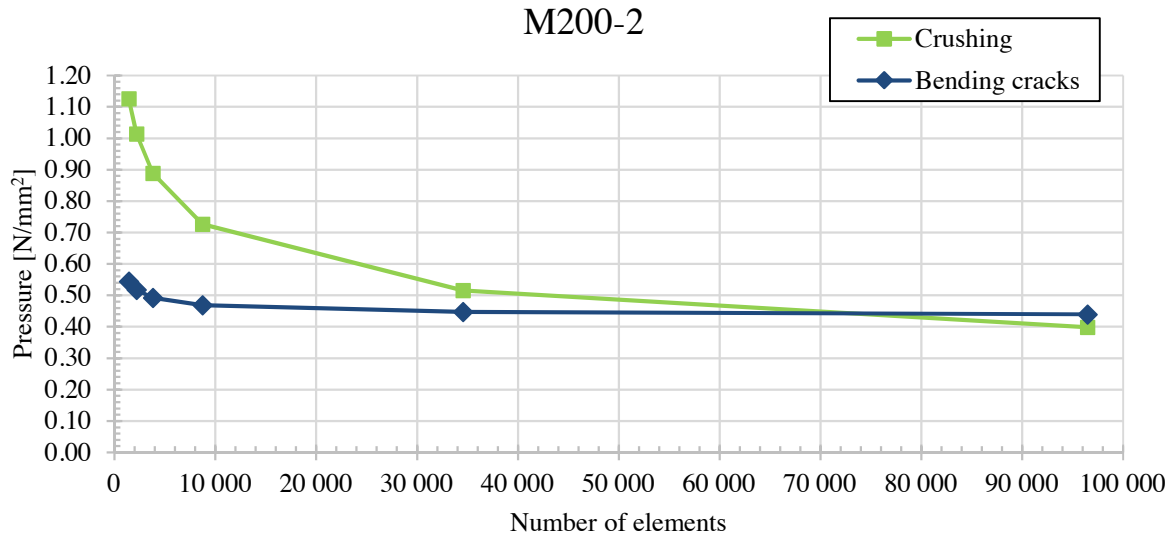
Figure B-12.   The fictive applied pressure on one support versus number of elements for Model M200-2.

The exact values of the pressures visualized in Figure B-11 and Figure A-12, for Model M200-2, are presented in Table B-6.

Table B-6.   Exact values for the mesh convergence of Model M200-2, with the further used mesh size marked.

Number of elements [-]	Mesh size [mm]	Pressure at one support at cracking [N/mm²]	Pressure at one support at crushing [N/mm²]	Pressure at displacement u = 0.08 mm [N/mm²]
1 421	25	0.54	1.13	0.93
2 196	20	0.52	1.01	0.92
3 792	15	0.49	0.89	0.92
8 712	10	0.47	0.73	0.92
34 560	**5**	**0.45**	**0.52**	**0.91**
96 480	3	0.44	0.40	0.90
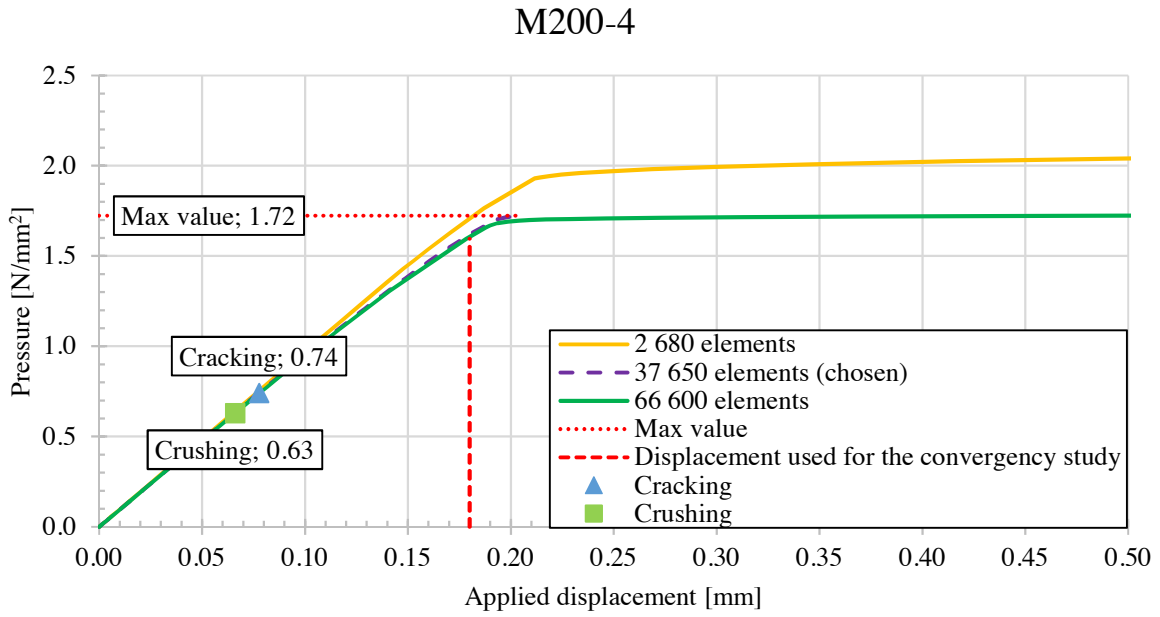
M200-4

Figure B-13. *Pressure-displacement curve for Model M200-4 with different element numbers and marked pressure at crushing, cracking and plasticisation (max value).*
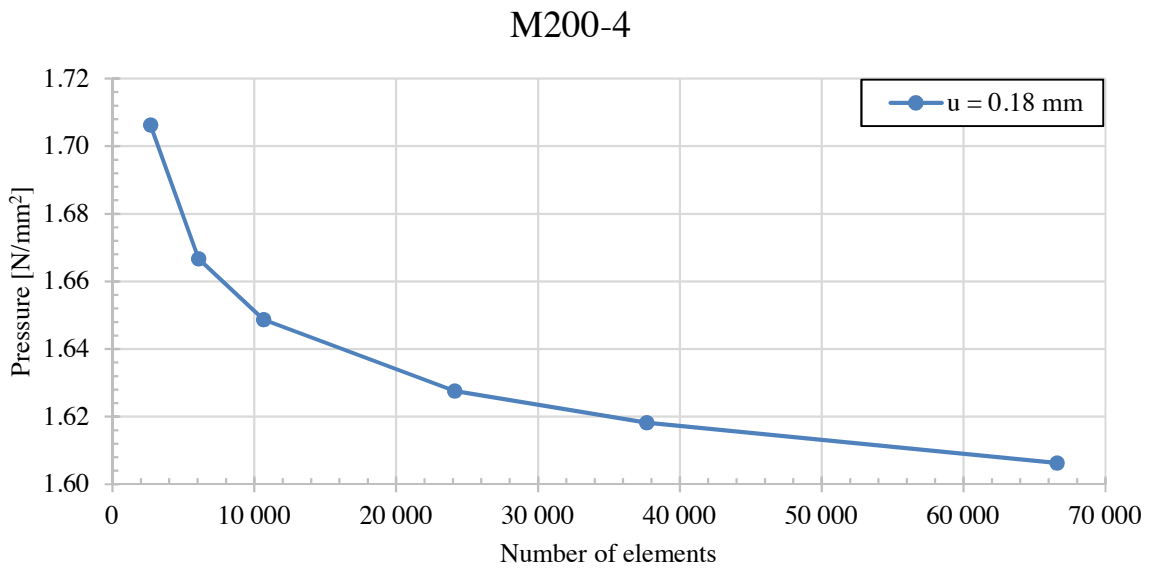
M200-4

Figure B-14. *Convergence study of Model M200-4, where the applied fictive pressure at one support at displacement 0.18 mm versus number of elements in the model is shown.*
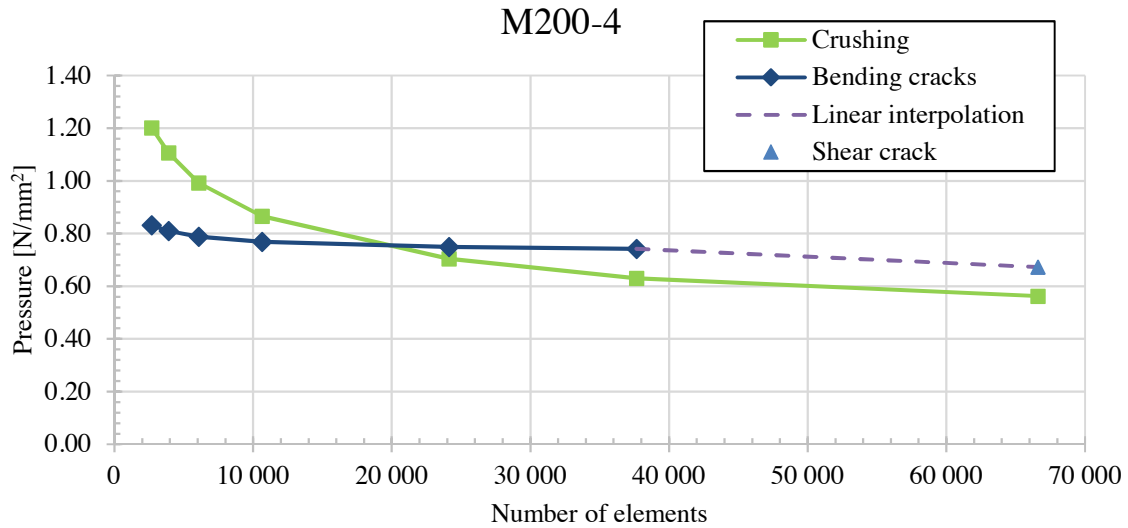
Figure B-15.   *The fictive applied pressure at one support versus number of elements for Model M200-4.*

In Table B-7 are all the exact value for the mesh convergence for Model M200-4 presented.

Table B-7.   *Exact values for the mesh convergence of Model M200-4, with the further used mesh size marked.*

Number of elements [-]	Mesh size [mm]	Pressure at one support at cracking [N/mm²]	Pressure at one support at crushing [N/mm²]	Pressure at displacement u = 0.18 mm [N/mm²]
2 680	30	0.83	1.20	1.71
3 888	25	0.81	1.11	1.65
6 060	20	0.79	0.99	1.67
10 640	15	0.77	0.87	1.65
24 120	10	0.75	0.70	1.63
37 650	**8**	**0.74**	**0.63**	**1.62**
66 600	6	0.67	0.56	1.61

9
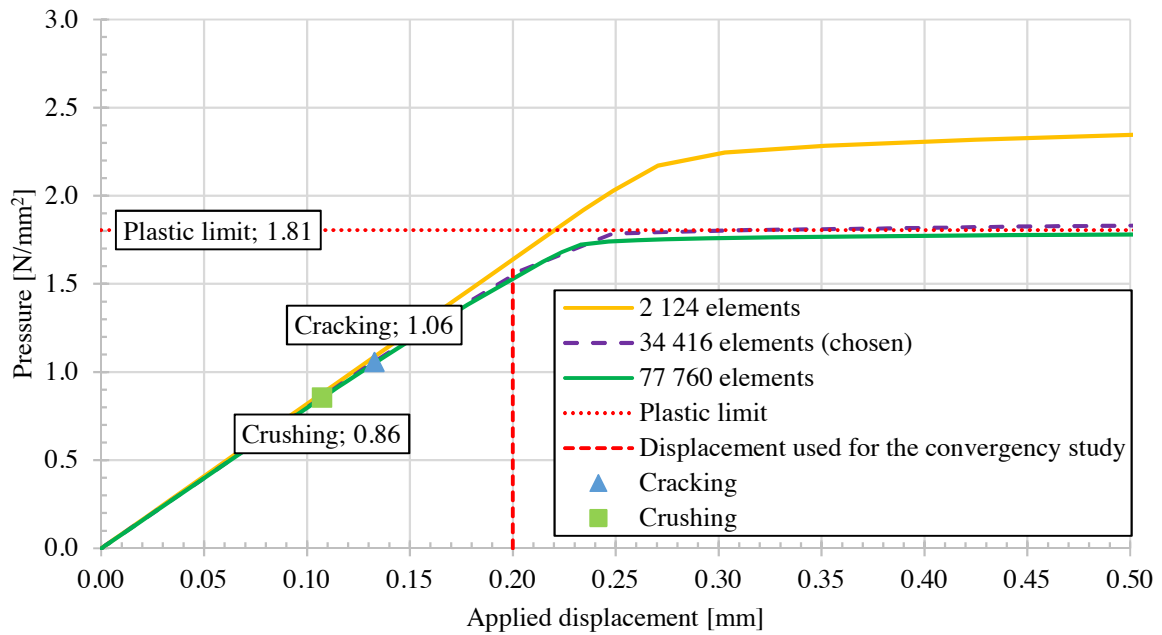
M200-8

Figure B-16. *Pressure-displacement curve for Model M200-8 with different element numbers and marked pressure at crushing, cracking and plasticisation.*

M200-8
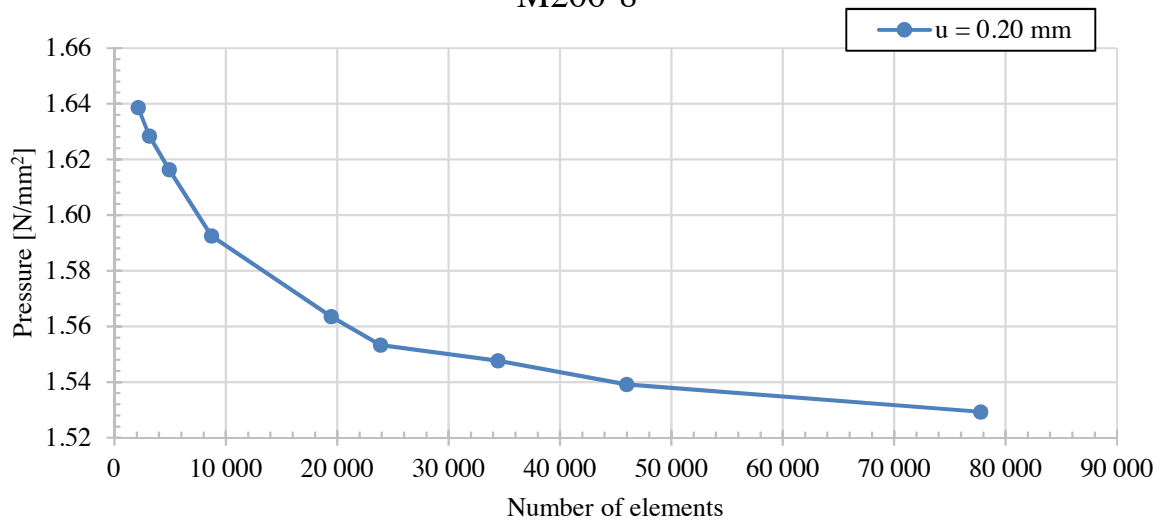
Figure B-17. *Convergence study of Model M200-8, where the applied fictive pressure at one support at displacement 0.20 mm versus number of elements in the model is shown.*
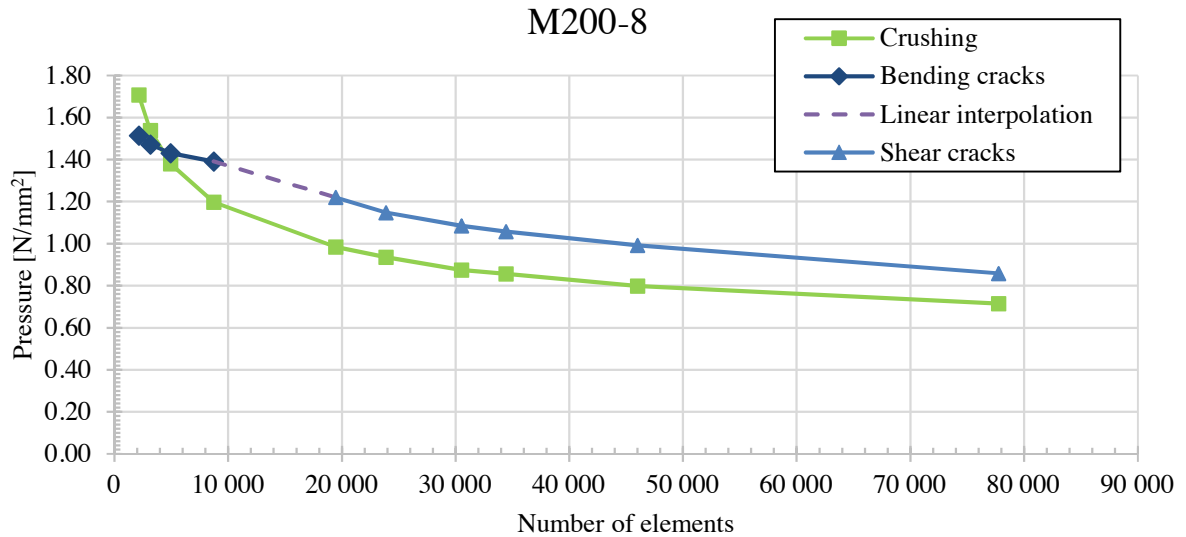
Figure A-18. *The fictive applied pressure at one support versus number of elements for Model M200-8.*

In Table B-8 are all the exact value for the mesh convergence for Model M200-8 presented.

Table B-8. *Exact values for the mesh convergence of Model M200-8, with the further used mesh size marked.*

Number of elements [-]	Mesh size [mm]	Pressure at one support at cracking [N/mm²]	Pressure at one support at crushing [N/mm²]	Pressure at displacement u = 0.20 mm [N/mm²]
2124	60	1.51	1.71	1.64
3139	50	1.47	1.54	1.63
4914	40	1.43	1.38	1.62
8712	30	1.39	1.20	1.59
19440	20	1.22	0.98	1.56
23880	18	1.15	0.94	1.55
30510	16	1.09	0.87	1.55
34416	**15**	**1.06**	**0.86**	**1.55**
45982	13	0.99	0.80	1.54
77760	10	0.86	0.71	1.53

A summarise of chosen number of elements for M200, and thereby the convergence for the models, are presented in Table B-99.

Table B-9. *Summarise of the number of elements which are used for further analyses of Model M200.*

Model	Mesh size [mm]	Number of elements [-]
M200-1	6	10 720
M200-2	5	34 560
M200-4	8	37 650
M200-8	15	34 416

B3. CONVERGENCE STUDY OF MODEL M600
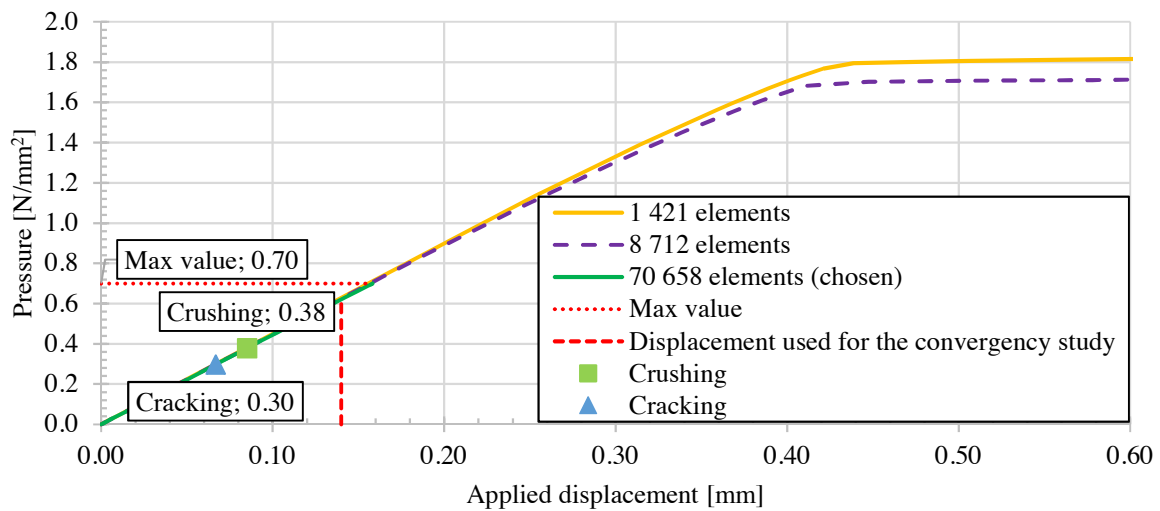
Figure B-19. *Pressure-displacement curve for Model M600-1 with different element numbers and marked pressure at crushing, cracking and plasticisation.*
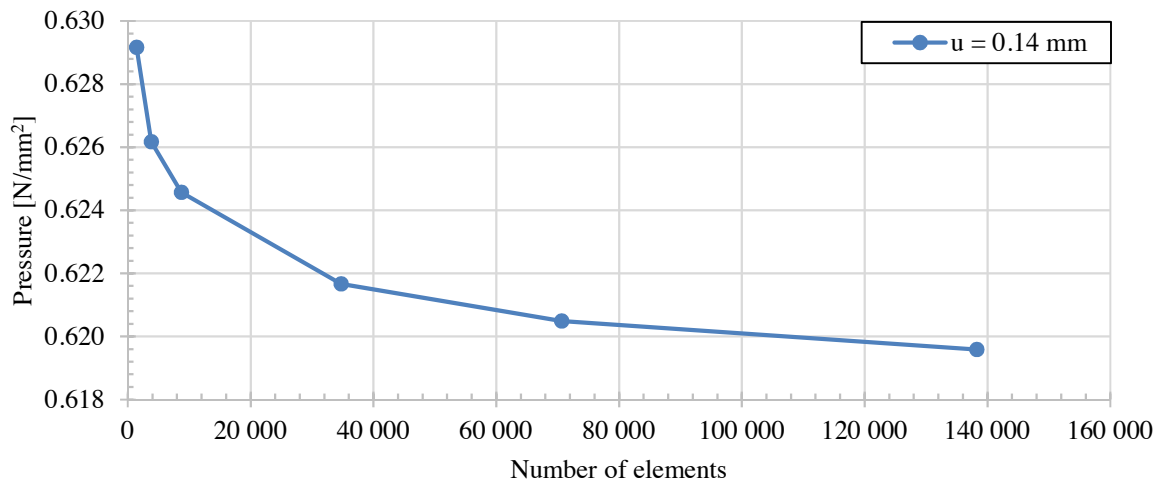
Figure B-20. *Convergence study of Model M600-1, where the applied fictive pressure at one support at displacement 0.14 mm versus number of elements in the model is shown.*

M600-1
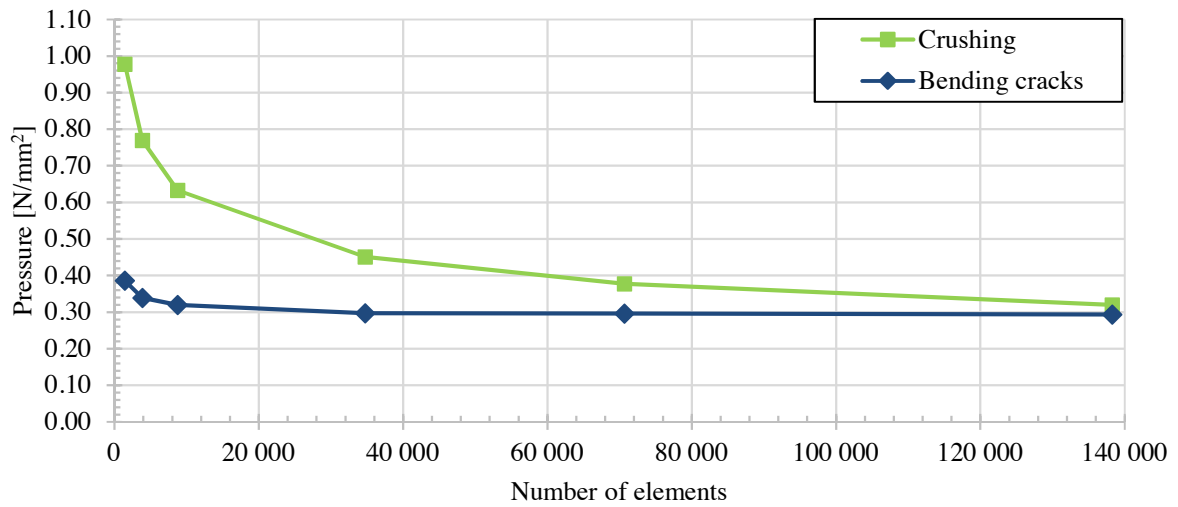
Figure B-21.   The fictive applied pressure at one support versus number of elements for Model M600-1.

In Table B-10 are all the exact value for the mesh convergence for Model M600-1 presented.

Table B-10.   Exact values for the mesh convergence of Model M600-1, with the further used mesh size marked.

Number of elements [-]	Mesh size [mm]	Pressure at one support at cracking [N/mm²]	Pressure at one support at crushing [N/mm²]	Pressure at displacement u = 0.14 mm [N/mm²]
1421	50	0.39	0.98	0.63
3840	30	0.36	0.81	0.63
8712	20	0.34	0.68	0.63
34704	10	0.30	0.45	0.62
70658	**7**	**0.30**	**0.38**	**0.62**
138240	5	0.29	0.32	0.62

13
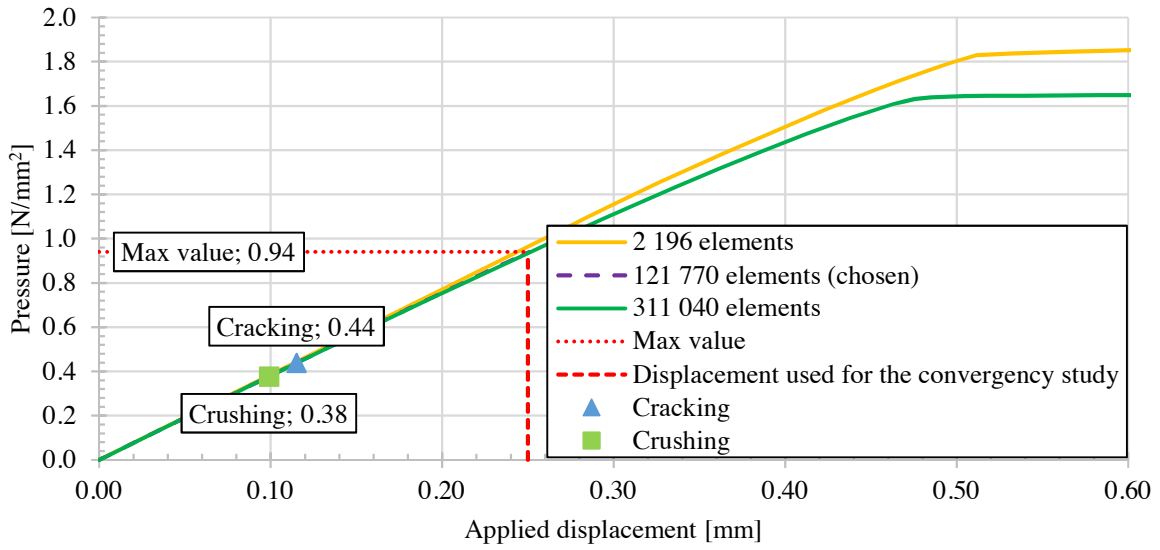
M600-2

Figure B-22. *Pressure-displacement curve for Model M600-2 with different element numbers and marked pressure at crushing, cracking and plasticisation.*

M600-2
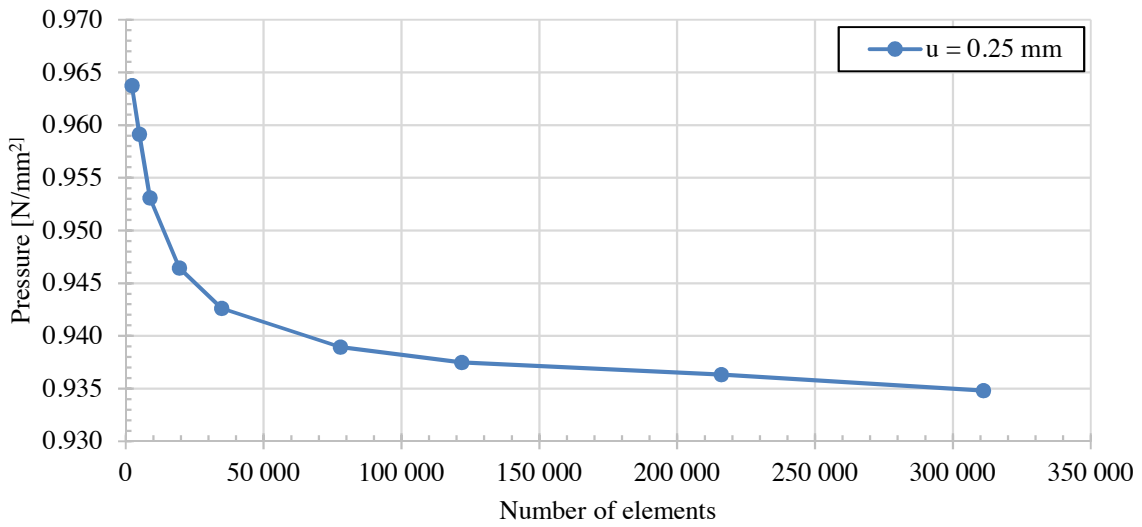
Figure B-23. *Convergence study of Model M600-2, where the applied fictive pressure at one support at displacement 0.25 mm versus number of elements in the model is shown.*
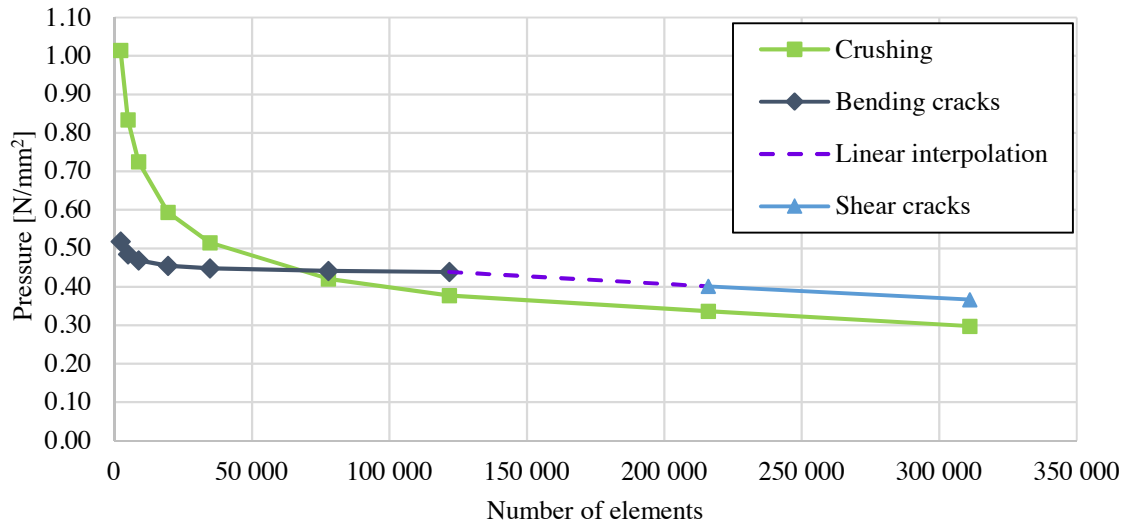
Figure B-24. *The fictive applied pressure at one support versus number of elements for Model M600-2.*

In Table B-11 are all the exact value for the mesh convergence for Model M600-2 presented.

Table B-11. *Exact values for the mesh convergence of Model M600-2, with the further used mesh size marked.*

Number of elements [-]	Mesh size [mm]	Pressure at one support at cracking [N/mm²]	Pressure at one support at crushing [N/mm²]	Pressure at displacement u = 0.18 mm [N/mm²]
2 196	60	0.52	1.01	0.96
4 914	40	0.48	0.83	0.96
8 712	30	0.47	0.73	0.95
19 440	20	0.45	0.59	0.95
34 704	15	0.45	0.51	0.94
77 760	10	0.44	0.42	0.94
121 770	**8**	**0.44**	**0.38**	**0.94**
216 000	6	0.40	0.34	0.94
311 040	5	0.37	0.30	0.93

15
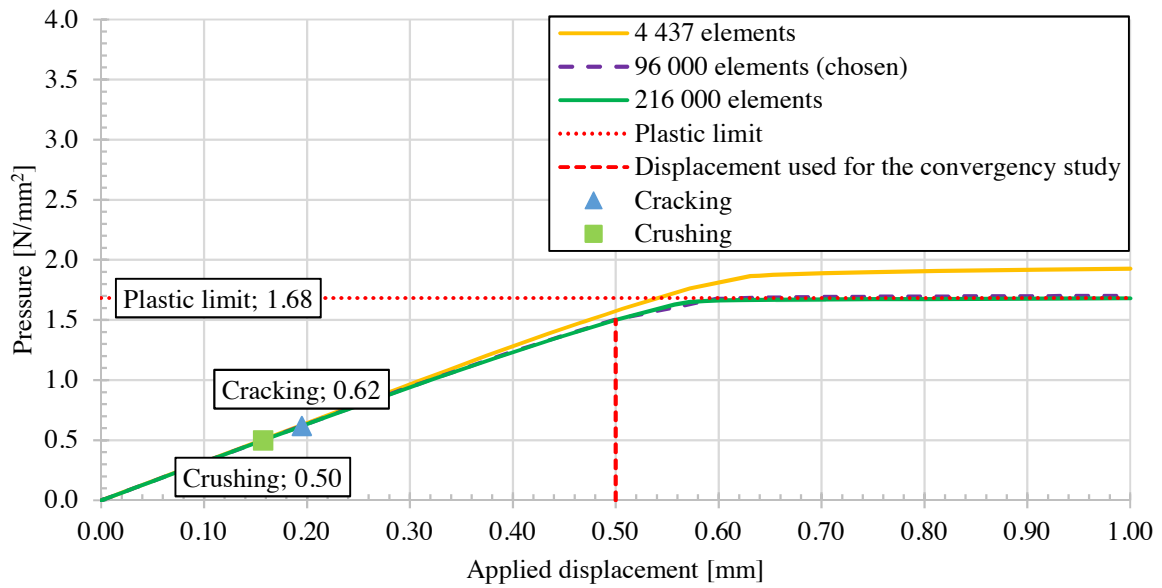
Figure B-25. *Pressure-displacement curve for Model M600-4 with different element numbers and marked pressure at crushing, cracking and plasticisation.*
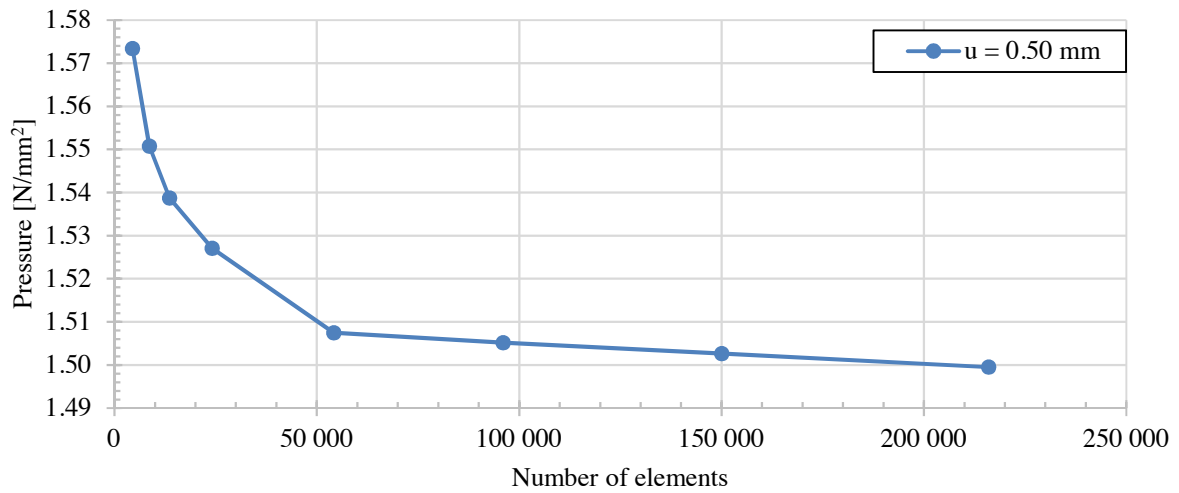
Figure B-26. *Convergence study of Model M600-4, where the applied fictive pressure at one support at displacement 0.50 mm versus number of elements in the model is shown.*
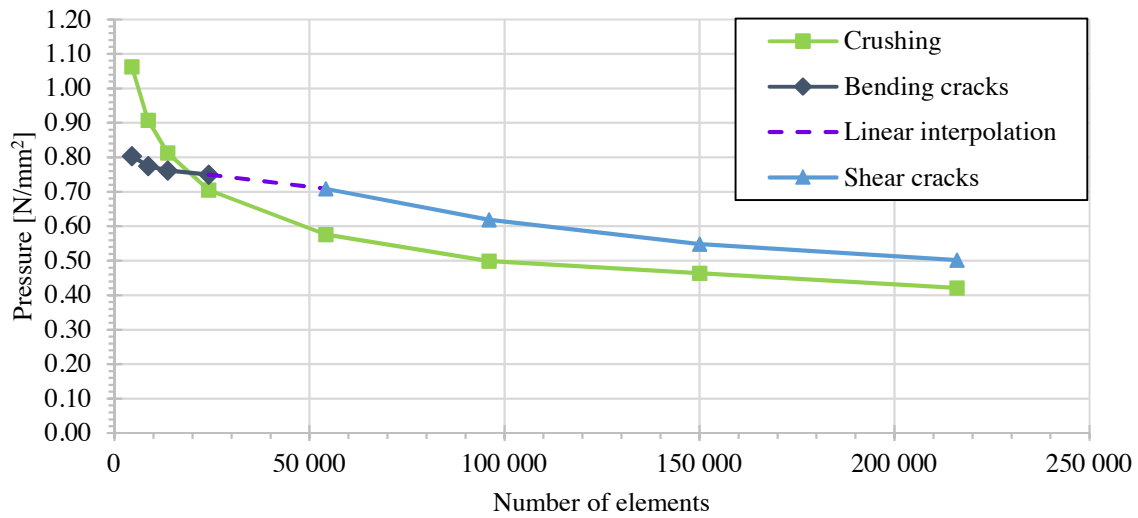
Figure B-27.   *The fictive applied pressure at one support versus number of elements for Model 600-4.*

In Table B-12 are all the exact value for the mesh convergence for Model M600-4 presented.

Table B-12.   *Exact values for the mesh convergence of Model M600-4, with the further used mesh size marked.*

Number of elements [-]	Mesh size [mm]	Pressure at one support at cracking [N/mm²]	Pressure at one support at crushing [N/mm²]	Pressure at displacement u = 0.50 mm [N/mm²]
4 437	70	0.80	1.06	1.57
8 640	50	0.78	0.91	1.55
13 590	40	0.76	0.81	1.54
24 120	30	0.75	0.70	1.53
54 180	20	0.71	0.58	1.51
96 000	**15**	**0.62**	**0.50**	**1.51**
150 000	12	0.55	0.46	1.50
216 000	10	0.50	0.42	1.50

M600-8
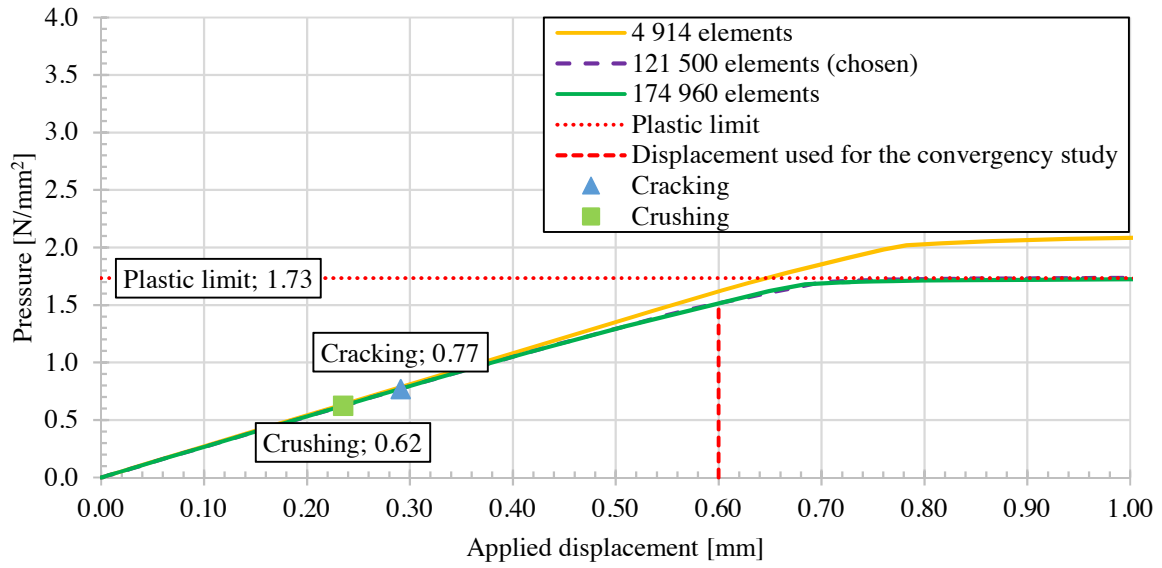
Figure B-28. *Pressure-displacement curve for Model M600-8 with different element numbers and marked pressure at crushing, cracking and plasticisation.*

M600-8
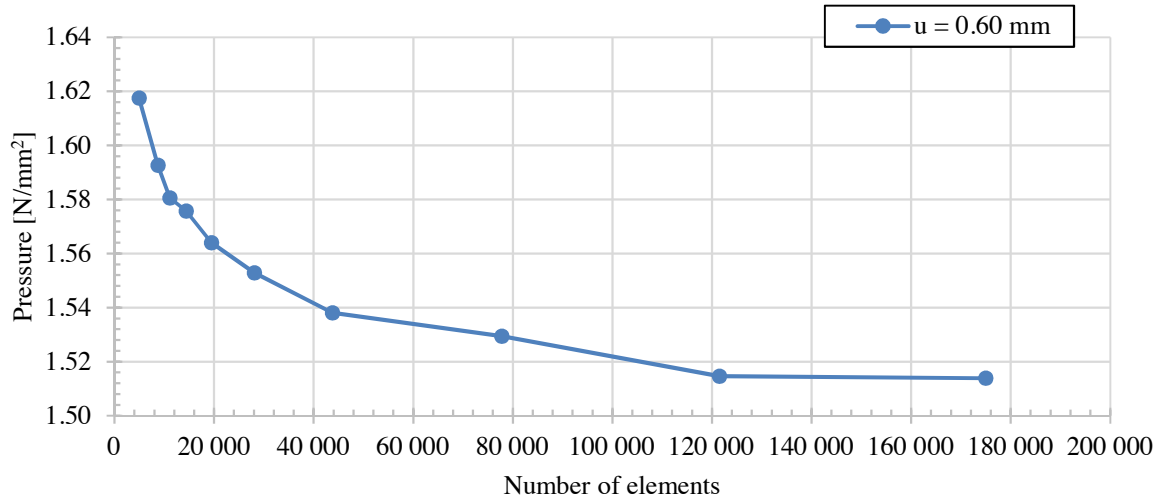
Figure B-29. *Convergence study of Model M600-8, where the applied fictive pressure at one support at displacement 0.60 mm versus number of elements in the model is shown.*
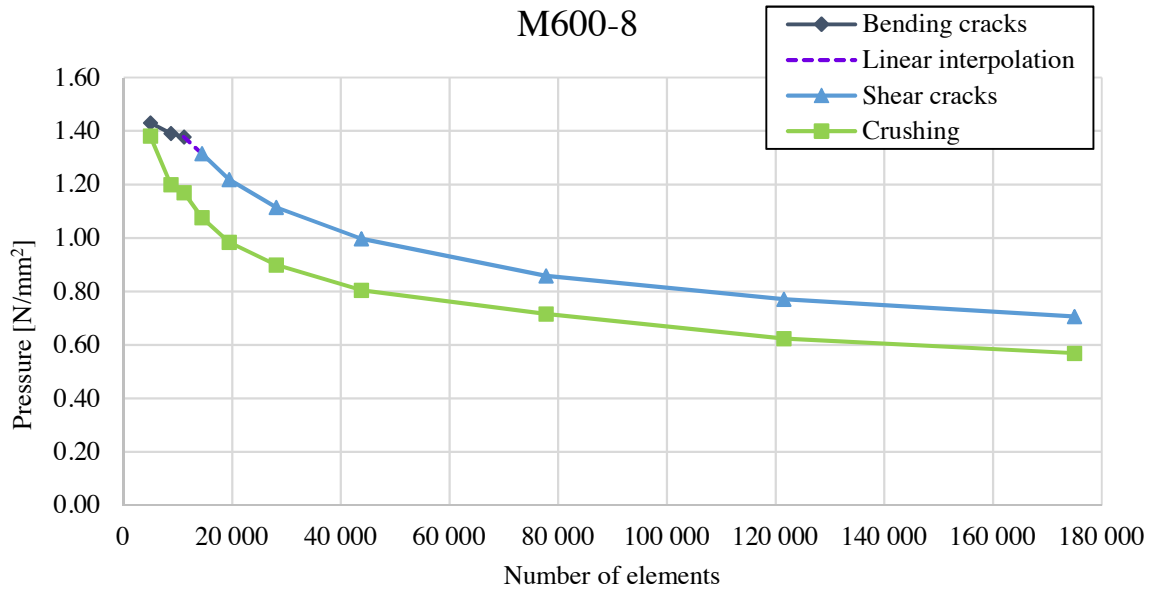
Figure B-30. *The fictive applied pressure at one support versus number of elements for Model M600-8.*

In Table B-13 are all the exact value for the mesh convergence for Model M600-8 presented.

Table B-13. *Exact values for the mesh convergence of Model M600-8, with the further used mesh size marked.*

Number of elements [-]	Mesh size [mm]	Pressure at one support at cracking [N/mm²]	Pressure at one support at crushing [N/mm²]	Pressure at displacement u = 0.60 mm [N/mm²]
4 914	120	1.43	1.38	1.62
8 712	90	1.39	1.20	1.59
11 097	80	1.38	1.17	1.58
14 415	70	1.32	1.08	1.58
19 440	60	1.22	0.98	1.56
28 080	50	1.11	0.90	1.55
43 740	40	1.00	0.80	1.54
77 760	30	0.86	0.72	1.53
121 500	**24**	**0.77**	**0.62**	**1.51**
174 960	20	0.71	0.57	1.51

19

The exact number of elements and mesh size for all M600 models, at convergence are summarised in Table B-144. The mesh sizes were used in further studies of Model M600.

Table B-14. Summary of the chosen mesh sizes and number of elements at convergence for Model M600.

Model	Mesh size [mm]	Number of elements [-]
M600-1	7	70 658
M600-2	8	121 770
M600-4	15	96 000
M600-8	24	121 500

B4. CONVERGENCE STUDY OF MODEL M1200
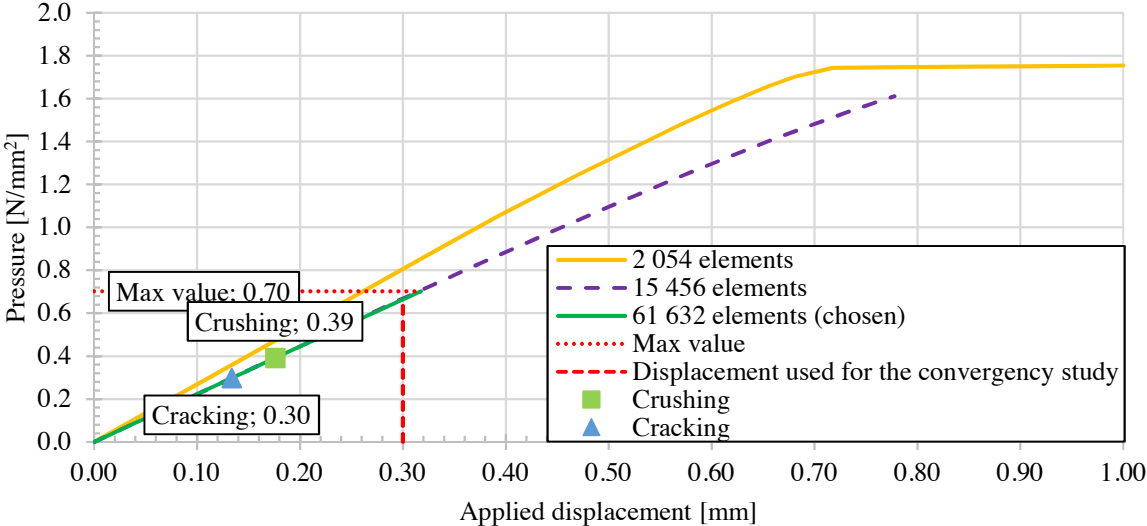
Figure B-31. Pressure-displacement curve for Model M1200-1 with different element numbers and marked pressure at crushing, cracking and plasticisation.
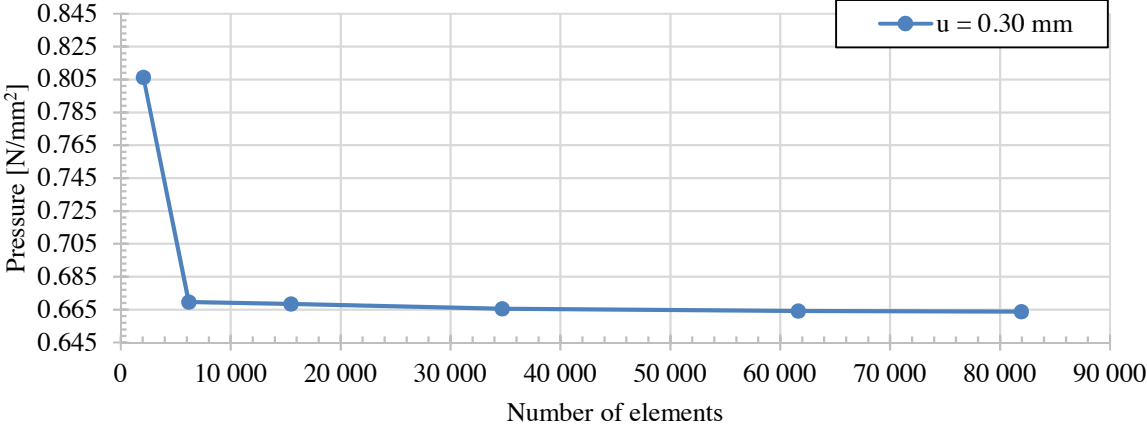
Figure B-32. Convergence study of Model M1200-1, where the applied fictive pressure at one support at displacement 0.30 mm versus number of elements in the model is shown.
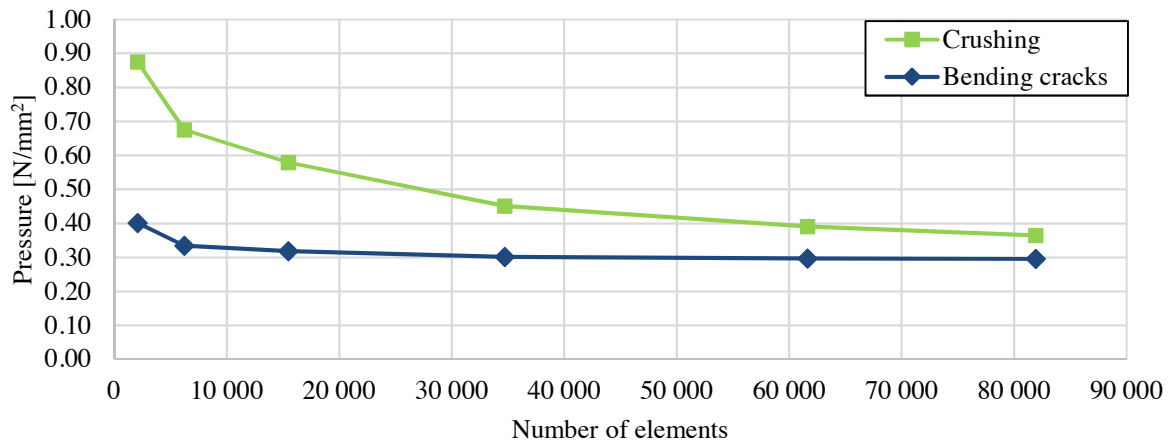
Figure B-33.   *The fictive applied pressure at one support versus number of elements for Model M1200-1.*

In Table B-15 are all the exact value for the mesh convergence for Model M1200-1 presented.

Table B-15.   *Exact values for the mesh convergence of Model M1200-1, with the further used mesh size marked.*

Number of elements [-]	Mesh size [mm]	Pressure at one support at cracking [N/mm²]	Pressure at one support at crushing [N/mm²]	Pressure at displacement u = 0.30 mm [N/mm²]
2 054	60	0.40	0.87	0.81
6 188	40	0.33	0.68	0.67
15 456	30	0.32	0.58	0.67
34 704	20	0.30	0.45	0.67
61 632	**15**	**0.30**	**0.39**	**0.66**
81 918	12	0.30	0.36	0.66

M1200-2
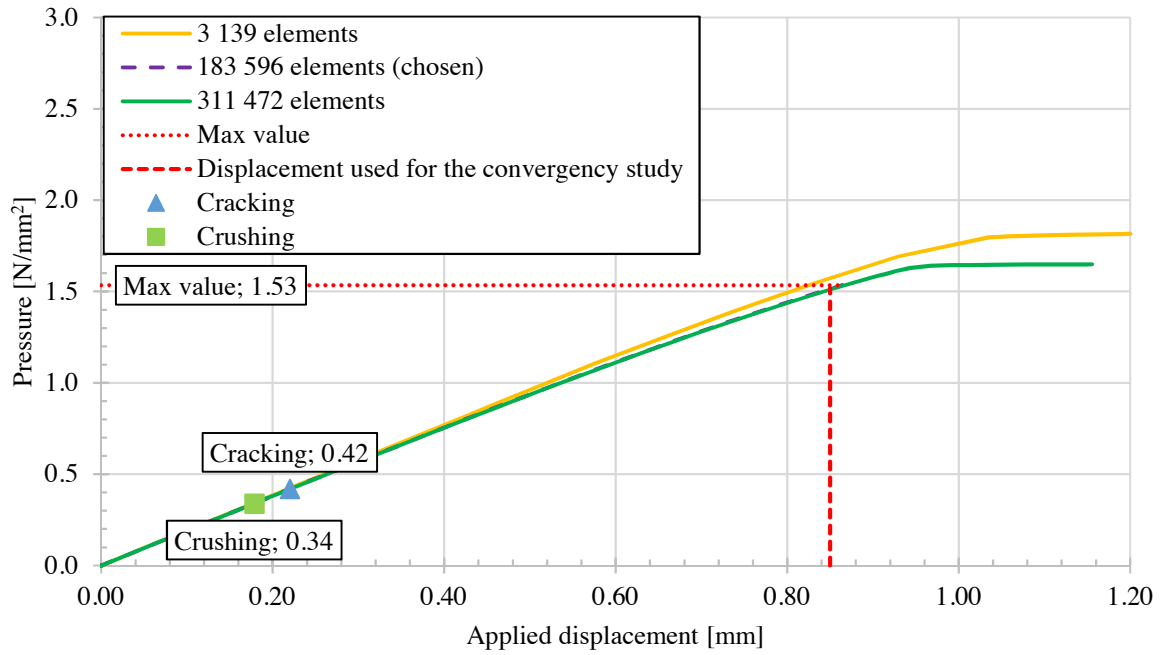
Figure B-34. *Pressure-displacement curve for Model M1200-2 with different element numbers and marked pressure at crushing, cracking and plasticisation.*

M1200-2
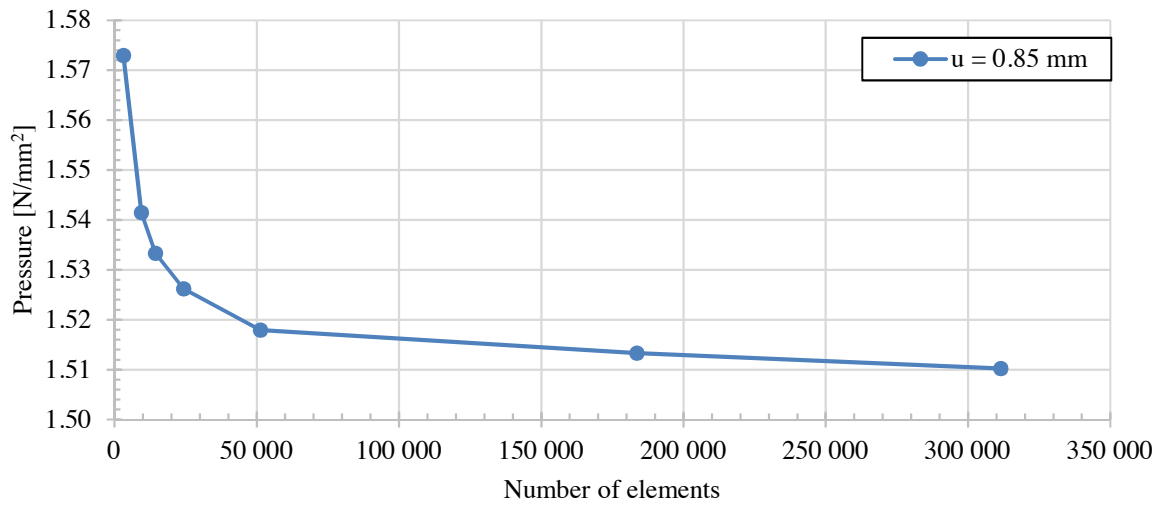
Figure B-35. *Convergence study of Model M1200-2, where the applied fictive pressure at one support at displacement 0.85 mm versus number of elements in the model is shown.*

22
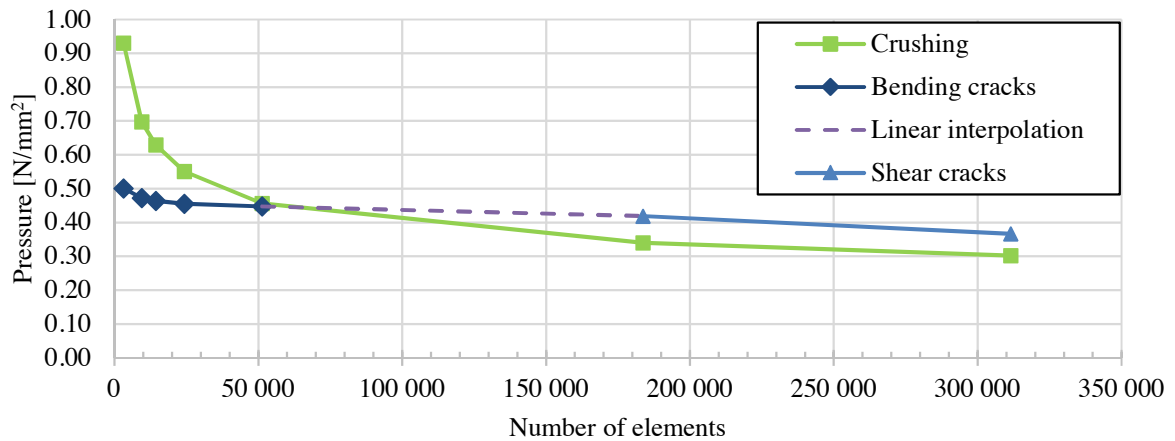
M1200-2

Figure B-36.   *The fictive applied pressure at one support versus number of elements for Model M1200-2.*

In Table B-16 are all the exact value for the mesh convergence for Model M1200-2 presented.

Table B-16.   *Exact values for the mesh convergence of Model M1200-2, with the further used mesh size marked.*

Number of elements [-]	Mesh size [mm]	Pressure at one support at cracking [N/mm²]	Pressure at one support at crushing [N/mm²]	Pressure at displacement u = 0.85 mm [N/mm²]
3 139	100	0.50	0.93	1.57
9 447	50	0.47	0.70	1.54
14 337	40	0.46	0.63	1.53
24 232	30	0.46	0.55	1.53
51 303	20	0.45	0.46	1.52
183 596	**13**	**0.42**	**0.34**	**1.51**
311 472	10	0.37	0.30	1.51
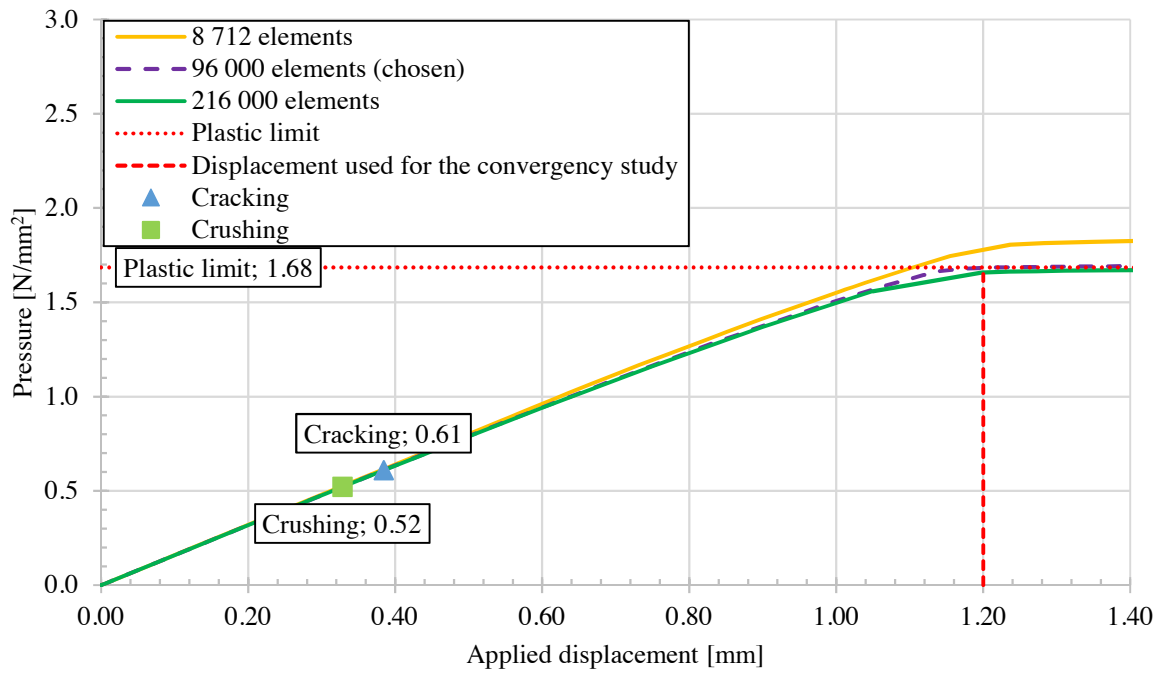
Figure B-37.   *Pressure-displacement curve for Model M1200-4 with different element numbers and marked pressure at crushing, cracking and plasticisation.*
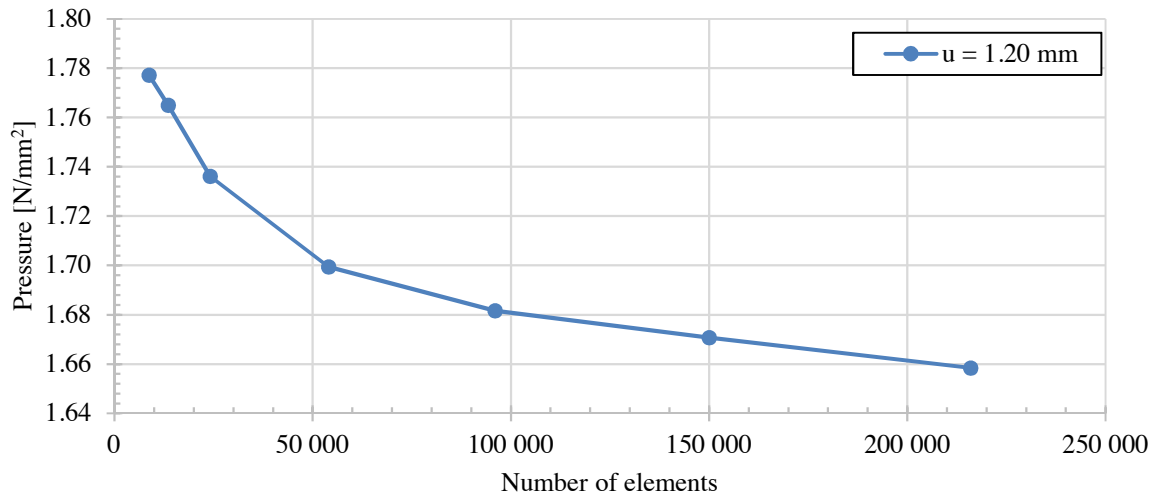
Figure B-38.   *Convergence study of Model M1200-4, where the applied fictive pressure at one support at displacement 1.20 mm versus number of elements in the model is shown.*
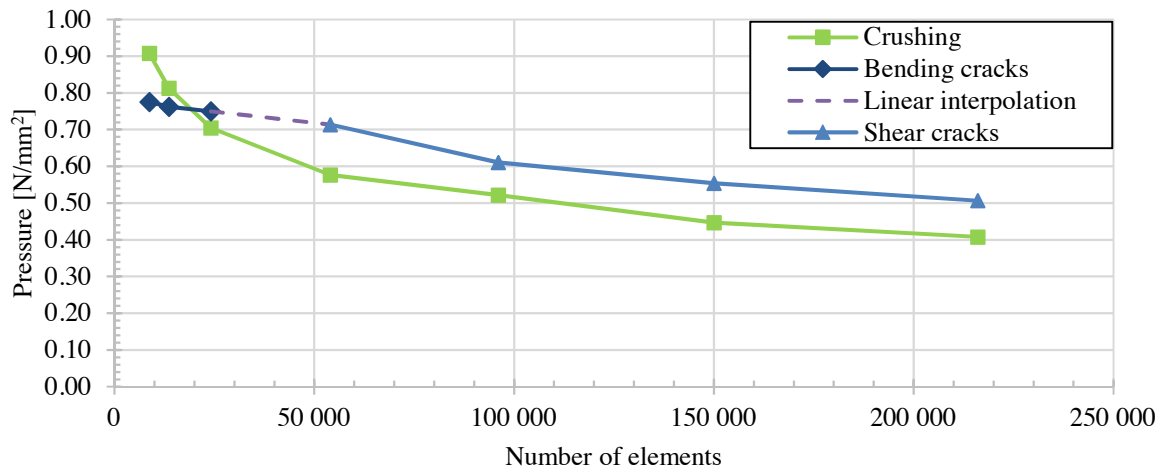
Figure B-39.   *The fictive applied pressure at one support versus number of elements for Model M1200-4.*

In Table B-17 are all the exact value for the mesh convergence for Model M1200-4 presented.

Table B-17.   *Exact values for the mesh convergence of Model M1200-4, with the further used mesh size marked.*

Number of elements [-]	Mesh size [mm]	Pressure at one support at cracking [N/mm²]	Pressure at one support at crushing [N/mm²]	Pressure at displacement u = 1.20 mm [N/mm²]
8712	100	0.78	0.91	1.78
13590	80	0.76	0.81	1.77
24120	60	0.75	0.71	1.74
54000	40	0.71	0.58	1.70
96000	**30**	**0.61**	**0.52**	**1.68**
150000	24	0.55	0.45	1.67
216000	20	0.51	0.41	1.66
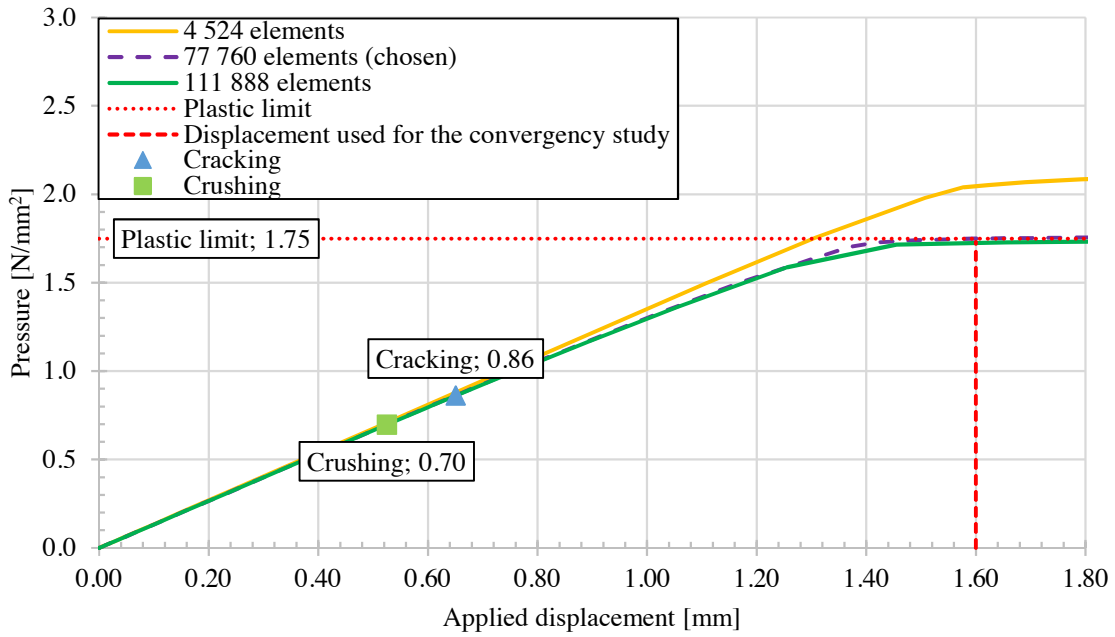
Figure B-40. *Pressure-displacement curve for Model M1200-8 with different element numbers and marked pressure at crushing, cracking and plasticisation.*
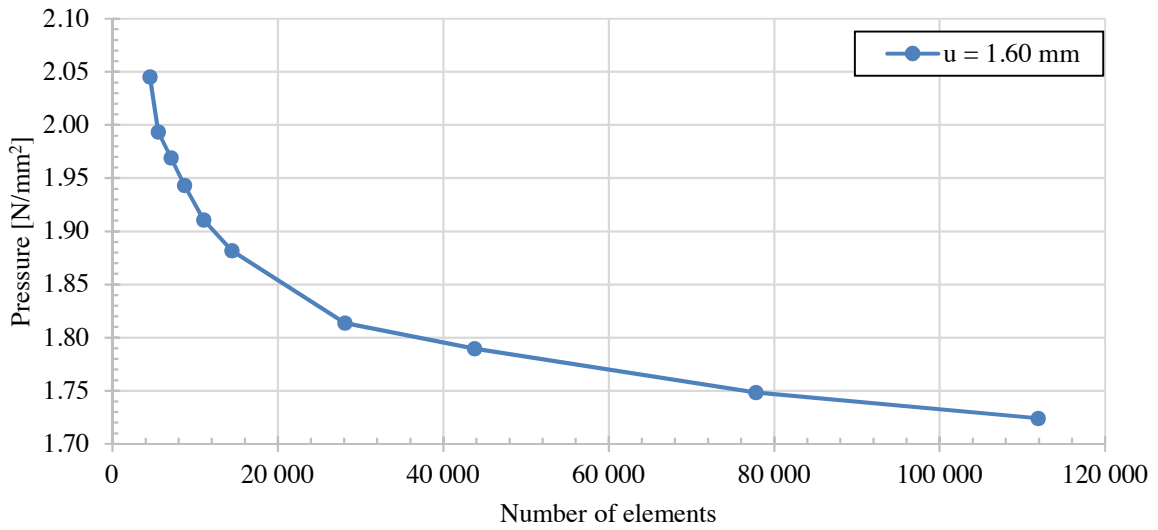
Figure B-41. *Convergence study of Model M1200-8, where the applied fictive pressure at one support at displacement 1.60 mm versus number of elements in the model is shown.*
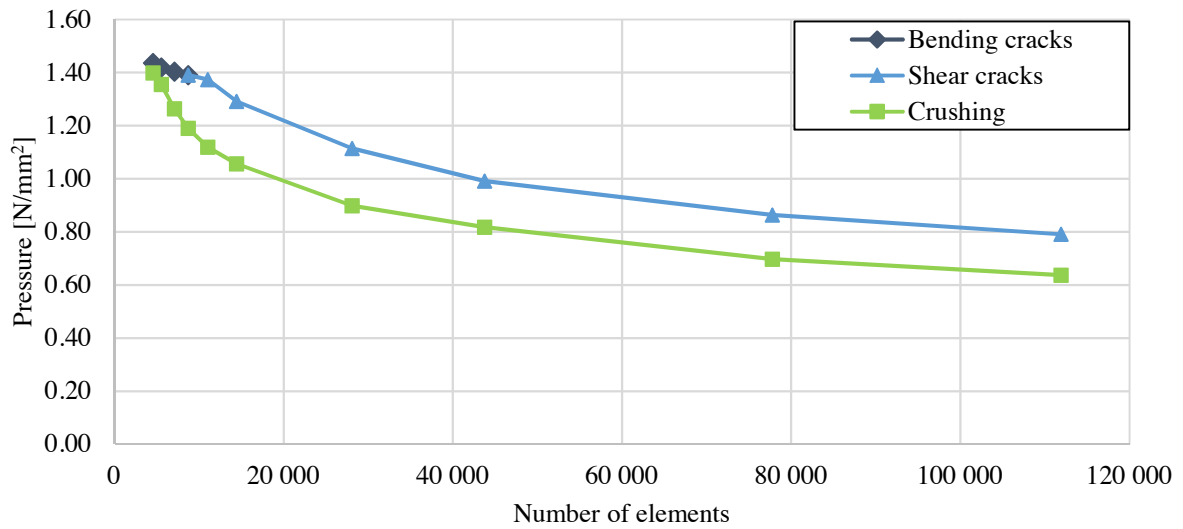
Figure B-42. *The fictive applied pressure at one support versus number of elements for Model M1200-8.*

In Table B-18 are all the exact value for the mesh convergence for Model M1200-8 presented.

Table B-18. *Exact values for the mesh convergence of Model M1200-8, with the further used mesh size marked.*

Number of elements [-]	Mesh size [mm]	Pressure at one support at cracking [N/mm²]	Pressure at one support at crushing [N/mm²]	Pressure at displacement u = 1.60 mm [N/mm²]
4 524	250	1.44	1.40	2.05
5 510	225	1.42	1.36	1.99
7 085	200	1.40	1.26	1.97
8 712	180	1.39	1.19	1.94
11 016	160	1.37	1.12	1.91
14 415	140	1.29	1.06	1.88
28 080	100	1.11	0.90	1.81
43 740	80	0.99	0.82	1.79
77 760	**60**	**0.86**	**0.70**	**1.75**
111 888	50	0.79	0.64	1.72

The final chosen number of element and mesh sizes which were used in further analyses of Model M1200 are summarized in Table B-19.

Table B-19.   *Summary of the chosen mesh sizes and number of elements at convergence for Models M1200.*

Model	Mesh size [mm]	Number of elements [-]
M1200-1	15	61 632
M1200-2	13	183 596
M1200-4	30	96 000
M1200-8	30	77 760

APPENDIX C
Results of Model S

C1. INVESTIGATION OF COLUMN WIDTH, *b*

Table C-1.   *Results from FE analyses, from the investigation of column width b, including cracking and crushing pressure and type of crack.*

Model	b [mm]	Cracking pressure [N/mm²]	Crushing pressure [N/mm²]	Type of crack
S200	200	0.77	0.72	Bending crack
S400	400	0.62	0.51	Shear crack
S600	600	0.52	0.42	Shear crack
S800	800	0.44	0.37	Shear crack
S1200	1200	0.52	0.42	Shear crack

C2. RESULTS FROM THE HEIGHT INVESTIGATION

Table C-2.   *Results from FE analyses for the height investigation of Model S200*

Height [mm]	R_1 [-]	Cracking pressure [N/mm²]	Crushing pressure [N/mm²]	Type of crack
200	0.2	0.34	0.51	Bending crack
300	0.3	0.49	0.40	Shear crack
500	0.5	0.49	0.39	Shear crack
600	0.6	0.48	0.38	Shear crack
800	0.8	0.48	0.39	Shear crack
1 000	1.0	0.48	0.39	Shear crack
1 600	1.6	0.57	0.38	Shear crack

TableC-3.   *Results from FE analyses for the height investigation of Model S600*

Height [mm]	R_1 [-]	Cracking pressure [N/mm²]	Crushing pressure [N/mm²]	Type of crack
900	0.3	0.46	0.46	Bending crack
1 200	0.4	0.51	0.45	Shear crack
1 800	0.6	0.52	0.42	Shear crack
2 400	0.8	0.51	0.41	Shear crack
4 800	1.6	0.51	0.41	Shear crack

Table C-4.   Results from FE analyses for the height investigation of Model S1200

Height [mm]	R_1 [-]	Cracking pressure [N/mm²]	Crushing pressure [N/mm²]	Type of crack
1 200	0.2	0.28	0.24	Bending crack
1 800	0.3	0.50	0.42	Shear crack
2 400	0.4	0.51	0.42	Shear crack
3 600	0.6	0.50	0.41	Shear crack
4 800	0.8	0.50	0.42	Shear crack
7 200	1.2	0.50	0.41	Shear crack
9 600	1.6	0.51	0.41	Shear crack

APPENDIX D
Analytical calculations for Model S

MODEL S200

Ice pressure against bridge supports (Vägverket, 1987)

Pressure from a larger ice sheet:

$b_{200} := 0.2m$ Column width

$a_{min} := 4m$ Minimal column height

$$a_{200} := \begin{vmatrix} b_{200} & \text{if } b_{200} > 4m \\ 4m & \text{if } b_{200} < 4m \end{vmatrix} = 4 \cdot m$$ Column height

$t := 0.3m$ Ice thickness

$ar_{200} := \dfrac{b_{200}}{t} = 0.667$ Aspect ratio

$$C_1 := \begin{pmatrix} 1.8 \\ 1.3 \\ 1.1 \\ 1.0 \\ 0.9 \\ 0.8 \end{pmatrix} \qquad ar := \begin{pmatrix} 0.5 \\ 1 \\ 1.5 \\ 2 \\ 3 \\ 4 \end{pmatrix}$$

Shape factor, C1, with respect to aspect ratio, ar

$vs := lspline(ar, C_1)$

$C_{1.200} := interp(vs, ar, C_1, ar_{200}) = 1.611$ Assuming linear relation between the coefficients

$\sigma_c := 1.4MPa$ Crushing strength of ice

$I_{2.200} := C_{1.200} \cdot \sigma_c \cdot b_{200} \cdot t = 135.361 \cdot kN$ Ice load from a larger moving ice sheet

Pressure on a sharp and/or inclined edge:

a) From above   b) From the side

$\alpha := 180 \qquad \beta := 45$

$$C_{2.200}(\alpha) := \begin{vmatrix} 0.54 & \text{if } \alpha = 45 \\ 0.59 & \text{if } \alpha = 60 \\ 0.64 & \text{if } \alpha = 75 \\ 0.69 & \text{if } \alpha = 90 \\ 0.77 & \text{if } \alpha = 120 \\ 1.00 & \text{if } \alpha = 180 \\ 1 & \text{otherwise} \end{vmatrix}$$
Shape factor with respect to sharp edge

$C_{2.200}(\alpha) = 1$

$$C_{3.200}(\beta) := \begin{vmatrix} 1.0 & \text{if } 0 \le \beta \ge 15 \\ 0.75 & \text{if } 15 < \beta \ge 30 \\ 0.5 & \text{if } 30 < \beta \ge 45 \\ 1 & \text{otherwise} \end{vmatrix}$$
Shape factor with regard to inclination

$C_{3.200}(\beta) = 0.5$

$$C_{23.200} := \begin{vmatrix} 0.5 & \text{if } C_{2.200}(\alpha) \cdot C_{3.200}(\beta) < 0.5 & = 0.5 \\ C_{2.200}(\alpha) \cdot C_{3.200}(\beta) & \text{otherwise} \end{vmatrix}$$

$I_{22.200} := C_{1.200} \cdot C_{23.200} \cdot \sigma_c \cdot b_{200} \cdot t = 67.681 \cdot kN$

Maximum ice load for a sharp and/or inclined edge

Recommendations for design of offshore foundations exposed to ice load

Maximum static ice load due to crushing

$k_1 := \begin{pmatrix} 1 \\ 0.9 \end{pmatrix}$

Column shape factor: rectangular shape
circular shape

$k_{1.200} := 1$

$k_2 := \begin{pmatrix} 0.5 \\ 1 \\ 1.5 \end{pmatrix}$

Contact factor: continuously moving ice
ice frozen to the column surface
ice locally increased around the column

$k_{2.200} := 1$

$k_{3.200} := \begin{vmatrix} 2.5 & \text{if } ar_{200} > 1 \\ \sqrt{1 + 5 \cdot ar_{200}} & \text{otherwise} \end{vmatrix} \quad = 2.082$

Aspect ratio factor

$b_{200} = 0.2\,m$

Column width

$t = 0.3\,m$

Ice thickness

$\sigma_c = 1.4 \cdot MPa$

Crushing strength of ice

$I_{h.crush} := k_{1.200} \cdot k_{2.200} \cdot k_{3.200} \cdot b_{200} \cdot t \cdot \sigma_c = 174.86 \cdot kN$

Maximum static ice load due to crushing

MODEL S600

Ice pressure against bridge supports

Pressure from a larger ice sheet:

$b_{600} := 0.6m$ Column width

$a_{min} = 4\,m$ Minimal column height

$a_{600} := \begin{vmatrix} b_{600} & \text{if } b_{600} > 4m \\ 4m & \text{if } b_{600} < 4m \end{vmatrix} = 4 \cdot m$ Column height

$t = 0.3\,m$ Ice thickness

$ar_{600} := \dfrac{b_{600}}{t} = 2$ Aspect ratio

$C_1 = \begin{pmatrix} 1.8 \\ 1.3 \\ 1.1 \\ 1 \\ 0.9 \\ 0.8 \end{pmatrix} \qquad ar = \begin{pmatrix} 0.5 \\ 1 \\ 1.5 \\ 2 \\ 3 \\ 4 \end{pmatrix}$ Shape factor, C1, with respect to aspect ratio, ar

$C_{1.600} := \text{interp}\left(vs, ar, C_1, ar_{600}\right) = 1$ Assuming linear relation between the coefficients

$\sigma_c = 1.4 \cdot MPa$ Crushing strength of ice

$I_{2.600} := C_{1.600} \cdot \sigma_c \cdot b_{600} \cdot t = 252 \cdot kN$ Ice pressure from a larger moving ice sheet

Pressure on a sharp and/or inclined edge:
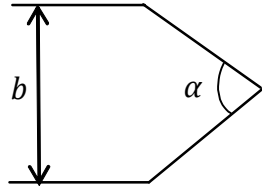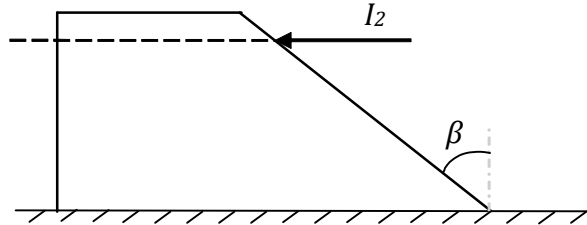
| a) From above | b) From the side |

$\alpha = 180$ $\qquad$ $\beta = 45$

$$C_{2.600}(\alpha) := \begin{cases} 0.54 & \text{if } \alpha = 45 \\ 0.59 & \text{if } \alpha = 60 \\ 0.64 & \text{if } \alpha = 75 \\ 0.69 & \text{if } \alpha = 90 \\ 0.77 & \text{if } \alpha = 120 \\ 1.00 & \text{if } \alpha = 180 \\ 1 & \text{otherwise} \end{cases}$$ $\qquad$ Shape factor with respect to sharp edge

$C_{2.600}(\alpha) = 1$

$$C_{3.600}(\beta) := \begin{cases} 1.0 & \text{if } 0 \le \beta \ge 15 \\ 0.75 & \text{if } 15 < \beta \ge 30 \\ 0.5 & \text{if } 30 < \beta \ge 45 \\ 1 & \text{otherwise} \end{cases}$$ $\qquad$ Shape factor with regard to inclination

$C_{3.600}(\beta) = 0.5$

$$C_{23.600} := \begin{cases} 0.5 & \text{if } C_{2.600}(\alpha) \cdot C_{3.600}(\beta) < 0.5 \quad = 0.5 \\ C_{2.600}(\alpha) \cdot C_{3.600}(\beta) & \text{otherwise} \end{cases}$$

$I_{22.600} := C_{1.600} \cdot C_{23.600} \cdot \sigma_c \cdot b_{600} \cdot t = 126 \cdot kN$ $\qquad$ Maximum ice pressure for a sharp and/or inclined edge

Recommendations for design of offshore foundations exposed to ice load

Maximum static ice load due to crushing

$k_1 := \begin{pmatrix} 1 \\ 0.9 \end{pmatrix}$ Column shape factor: rectangular shape
                                                     circular shape

$k_{1.600} := 1$

$k_2 := \begin{pmatrix} 0.5 \\ 1 \\ 1.5 \end{pmatrix}$ Contact factor: continuously moving ice
                                                ice frozen to the column surface
                                                ice locally increased around the column

$k_{2.600} := 1$

$k_{3.600} := \begin{vmatrix} 2.5 & \text{if } ar_{600} > 1 \\ \sqrt{1 + 5 \cdot ar_{600}} & \text{otherwise} \end{vmatrix}$ $= 2.5$ Aspect ratio factor

$b_{600} = 0.6\,m$ Column width

                                                    Ice thickness

$t = 0.3\,m$ Crushing strength of ice

$\sigma_c = 1.4 \cdot MPa$

$I_{h.crush.600} := k_{1.600} \cdot k_{2.600} \cdot k_{3.600} \cdot b_{600} \cdot t \cdot \sigma_c = 630 \cdot kN$ Maximum static ice load due to crushing

MODEL S1200

Ice pressure against bridge supports

Pressure from a larger ice sheet:

$b_{1200} := 1.2 \text{m}$ Column width

$a_{min} = 4 \text{ m}$ Minimal column height

$a_{1200} := \begin{vmatrix} b_{1200} & \text{if } b_{1200} > 4\text{m} & = 4 \cdot \text{m} \\ 4\text{m} & \text{if } b_{1200} < 4\text{m} \end{vmatrix}$ Column height

$t = 0.3 \text{ m}$ Ice thickness

$ar_{1200} := \dfrac{b_{1200}}{t} = 4$ Aspect ratio

$C_1 = \begin{pmatrix} 1.8 \\ 1.3 \\ 1.1 \\ 1 \\ 0.9 \\ 0.8 \end{pmatrix}$ $ar = \begin{pmatrix} 0.5 \\ 1 \\ 1.5 \\ 2 \\ 3 \\ 4 \end{pmatrix}$ Shape factor, C1, with respect to aspect ratio, ar

$C_{1.1200} := \text{interp}(vs, ar, C_1, ar_{1200}) = 0.8$ Assuming linear relation between the coefficients

$\sigma_c = 1.4 \cdot \text{MPa}$ Crushing strength of ice

$I_{2.1200} := C_{1.1200} \cdot \sigma_c \cdot b_{1200} \cdot t = 403.2 \cdot \text{kN}$ Ice pressure from a larger moving ice sheet

Pressure on a sharp and/or inclined edge:
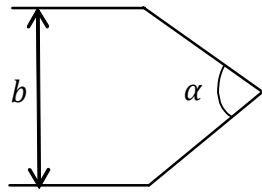
a) From above
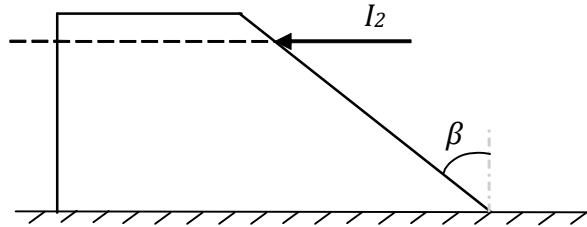
b) From the side

$\alpha = 180$ $\qquad$ $\beta = 45$

$$C_{2.1200}(\alpha) := \begin{array}{|l}
0.54 \quad \text{if } \alpha = 45 \\
0.59 \quad \text{if } \alpha = 60 \\
0.64 \quad \text{if } \alpha = 75 \\
0.69 \quad \text{if } \alpha = 90 \\
0.77 \quad \text{if } \alpha = 120 \\
1.00 \quad \text{if } \alpha = 180 \\
1 \quad \text{otherwise}
\end{array}$$ $\qquad$ Shape factor with respect to sharp edge

$C_{2.1200}(\alpha) = 1$

$$C_{3.1200}(\beta) := \begin{array}{|l}
1.0 \quad \text{if } 0 \le \beta \ge 15 \\
0.75 \quad \text{if } 15 < \beta \ge 30 \\
0.5 \quad \text{if } 30 < \beta \ge 45 \\
1 \quad \text{otherwise}
\end{array}$$ $\qquad$ Shape factor with regard to inclination

$C_{3.1200}(\beta) = 0.5$

$$C_{23.1200} := \begin{array}{|l}
0.5 \quad \text{if } C_{2.1200}(\alpha) \cdot C_{3.1200}(\beta) < 0.5 \quad = 0.5 \\
C_{2.1200}(\alpha) \cdot C_{3.1200}(\beta) \quad \text{otherwise}
\end{array}$$

$I_{22.1200} := C_{1.1200} \cdot C_{23.1200} \cdot \sigma_c \cdot b_{1200} \cdot t = 201.6 \cdot kN$

Maximum ice pressure for a sharp and/or inclined edge

Recommendations for design of offshore foundations exposed to ice load

Maximum static ice load due to crushing

$k_1 := \begin{pmatrix} 1 \\ 0.9 \end{pmatrix}$

Column shape factor: rectangular shape
                                circular shape

$k_{1.1200} := 1$

$k_2 := \begin{pmatrix} 0.5 \\ 1 \\ 1.5 \end{pmatrix}$

Contact factor: continuously moving ice
                        ice frozen to the column surface
                        ice locally increased around the column

$k_{2.1200} := 1$

$k_{3.1200} := \begin{vmatrix} 2.5 & \text{if } ar_{1200} > 1 \\ \sqrt{1 + 5 \cdot ar_{1200}} & \text{otherwise} \end{vmatrix} = 2.5$

Aspect ratio factor

Column width

$b_{1200} = 1.2\,\text{m}$

Ice thickness

$t = 0.3\,\text{m}$

Crushing strength of ice

$\sigma_c = 1.4 \cdot \text{MPa}$

$I_{h.crush.1200} := k_{1.1200} \cdot k_{2.1200} \cdot k_{3.1200} \cdot b_{1200} \cdot t \cdot \sigma_c = 1.26 \times 10^3 \cdot \text{kN}$

Maximum static ice load due to crushing

APPENDIX E
Results of Model M

E1. MODEL M200
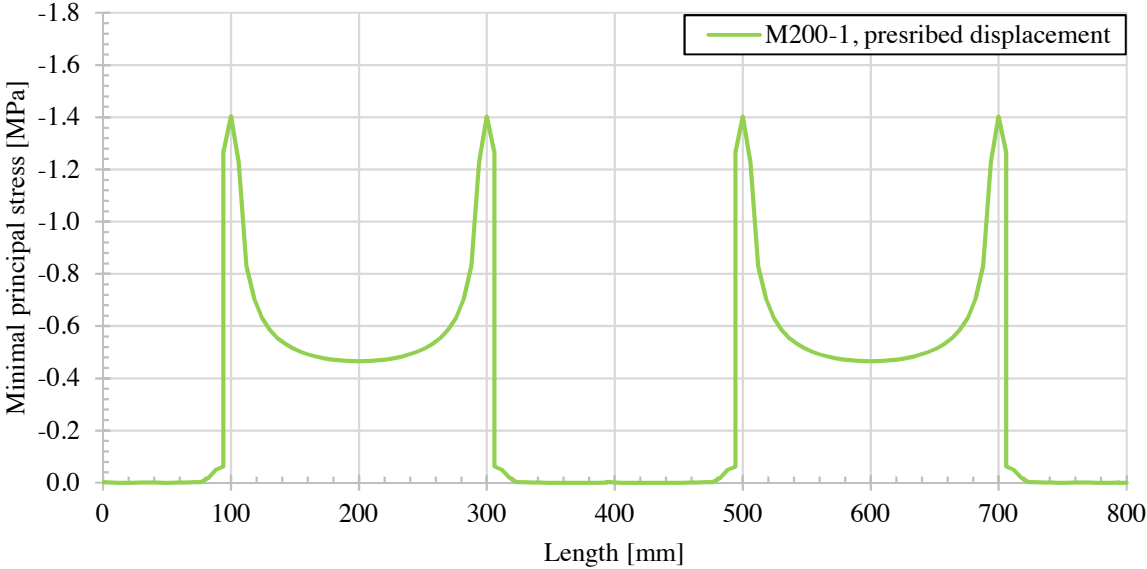
Figure E-1.   *Stress distribution in top elements of Model M200-1 with the load approach prescribed displacement.*
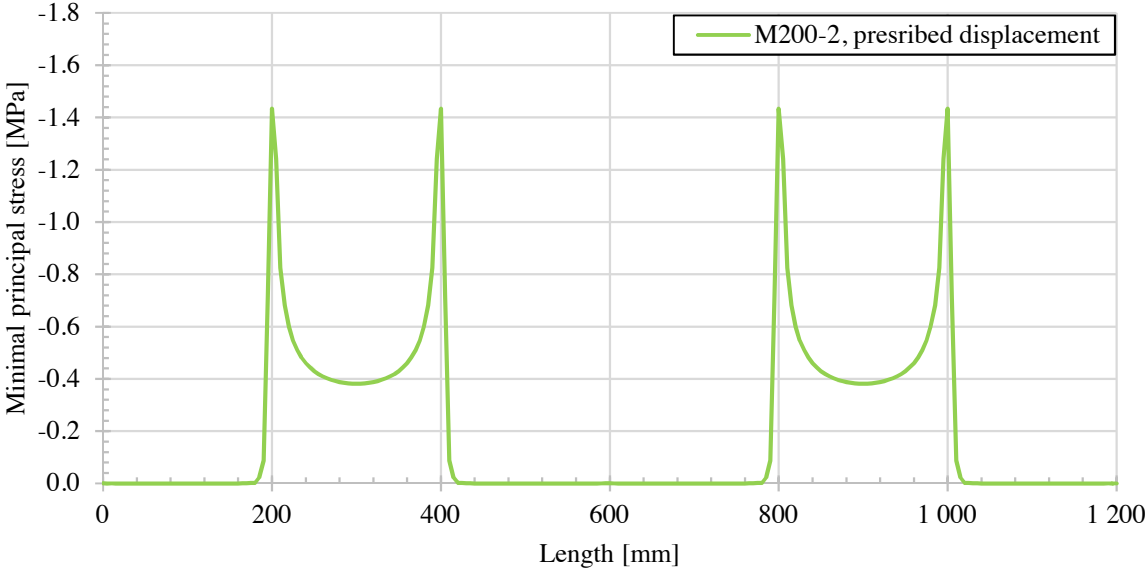
Figure E-2.   *Stress distribution in top elements of Model M200-2 with the load approach prescribed displacement.*
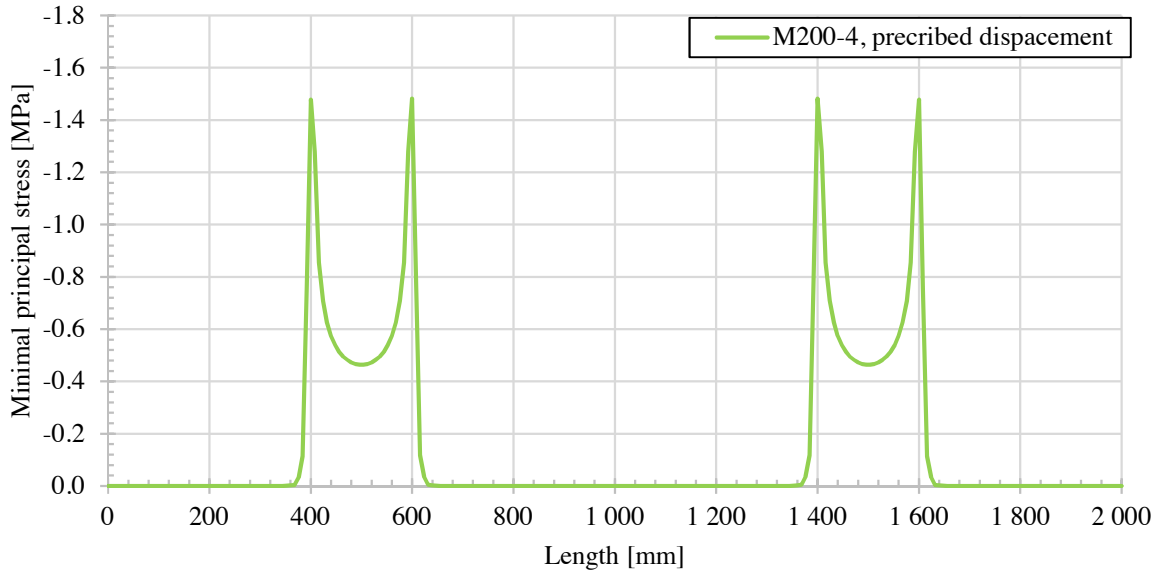
Figure E-3.   *Stress distribution in top elements of Model M200-4 with the load approach prescribed displacement.*
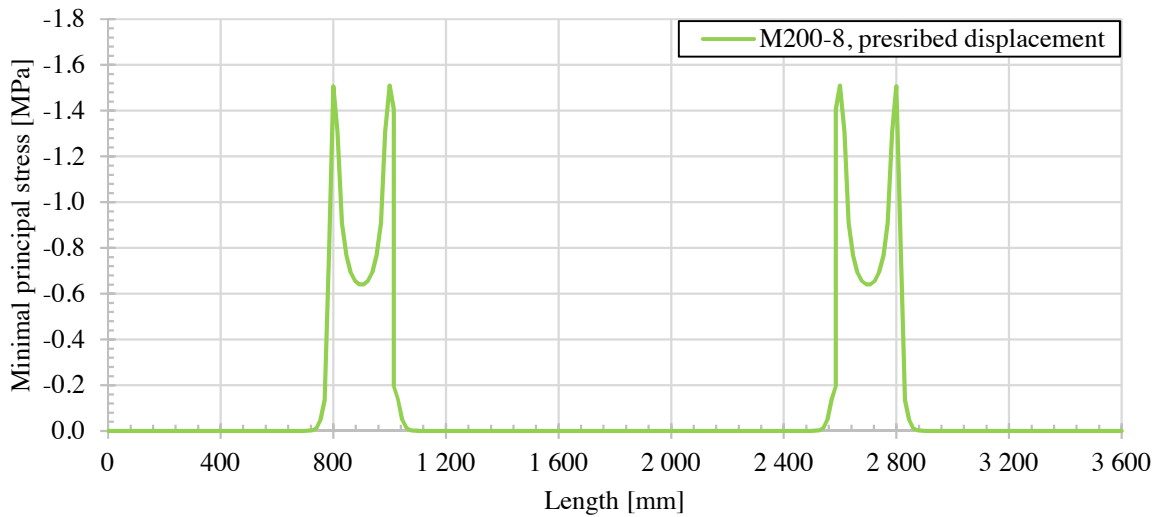
Figure E-4.   *Stress distribution in top elements of Model M200-8 with the load approach prescribed displacement.*

Table E-1.   *Results from FE analyses of the analyses of Model M200 including cracking and crushing pressure and type of observed crack.*

Model	R₂ [-]	R₁ [-]	Cracking pressure [N/mm²]	Crushing pressure [N/mm²]	Type of crack
M200-1	1	0.6	0.32	0.60	Bending crack
M200-2	2	0.6	0.45	0.52	Bending crack
M200-4	4	0.6	0.74	0.63	Bending crack
M200-8	8	0.6	1.06	0.86	Shear crack

2
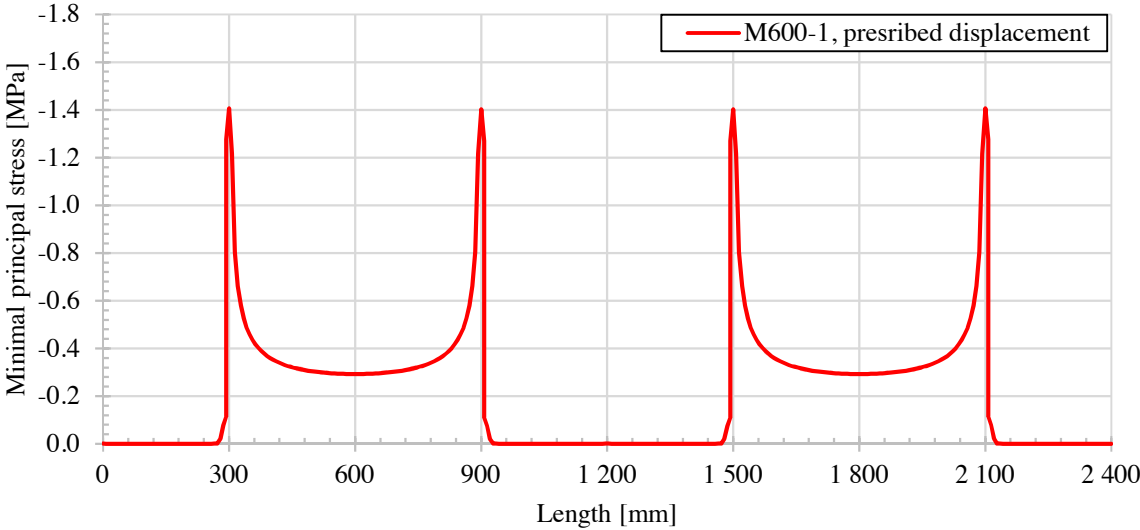
E2. MODEL M600

Figure E-5.   Stress distribution in top elements of Model M600-1 with the load approach prescribed displacement.
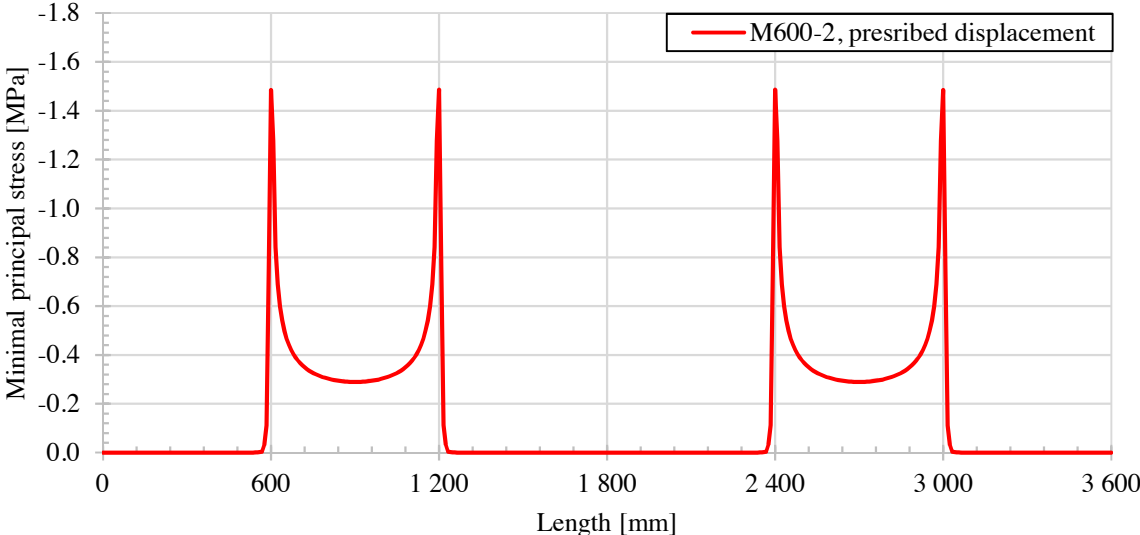
Figure E-6.   Stress distribution in top elements of Model M600-2 with the load approach prescribed displacement.
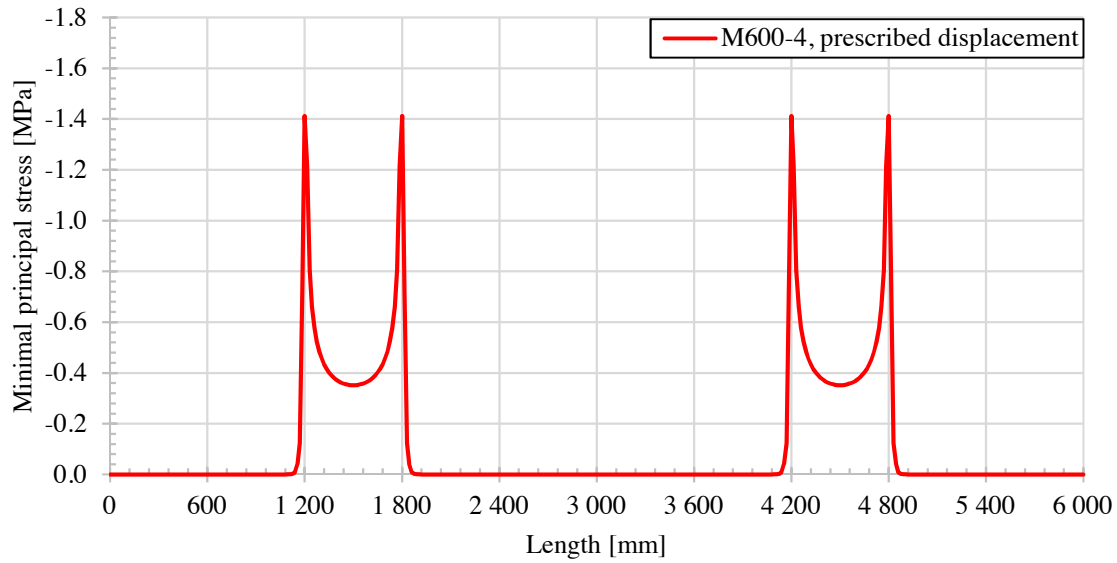
Figure E-7.   *Stress distribution in top elements of Model M600-4 with the load approach prescribed displacement.*
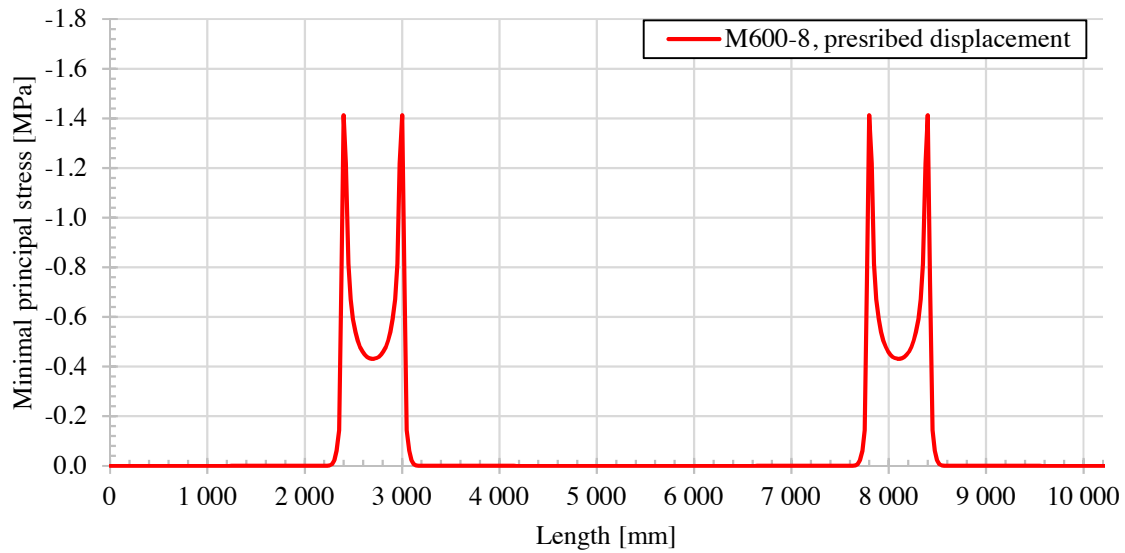
Figure E-8.   *Stress distribution in top elements of Model M600-8 with the load approach prescribed displacement.*

Table E-2.   *Results from FE analyses of the analyses of Model M600 including cracking and crushing pressure and type of observed crack.*

Model	R_2 [-]	R_1 [-]	Cracking pressure [N/mm²]	Crushing pressure [N/mm²]	Type of crack
M600-1	1	0.6	0.30	0.38	Bending crack
M600-2	2	0.6	0.44	0.38	Bending crack
M600-4	4	0.6	0.62	0.50	Shear crack
M600-8	8	0.6	0.77	0.62	Shear crack

4
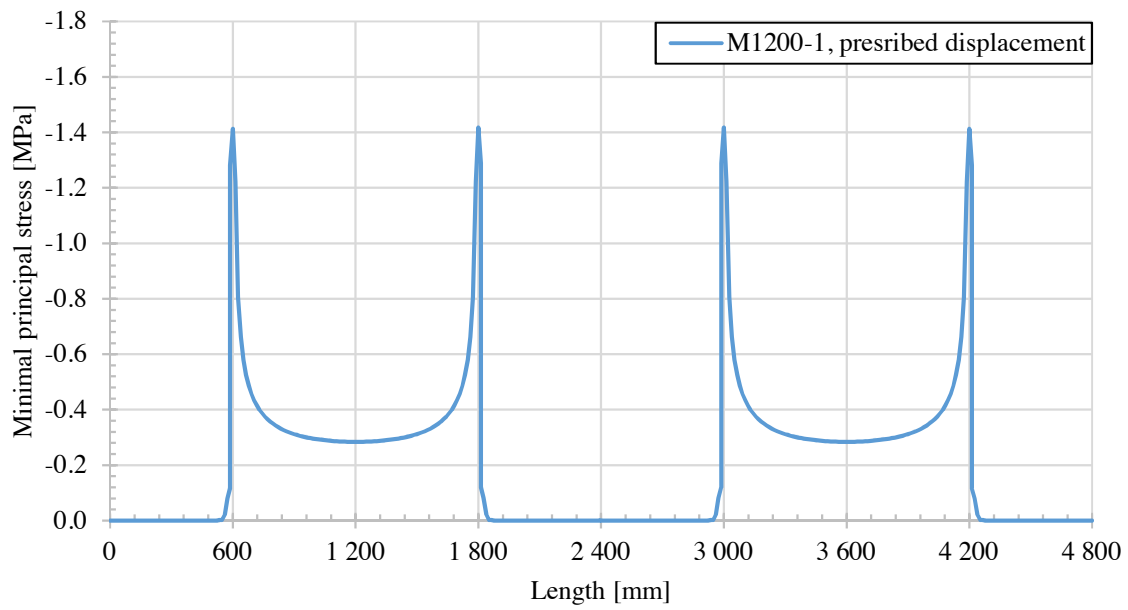
E2. MODEL M1200

Figure E-9. *Stress distribution in top elements of Model M1200-1 with the load approach prescribed displacement.*
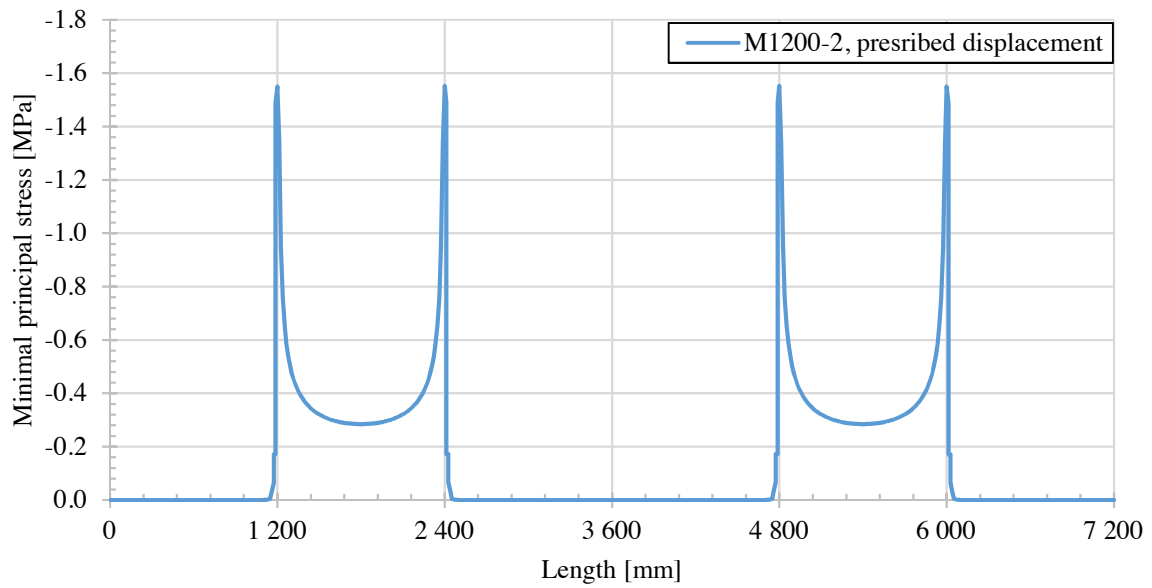
Figure E-10. *Stress distribution in top elements of Model M1200-2 with the load approach prescribed displacement.*
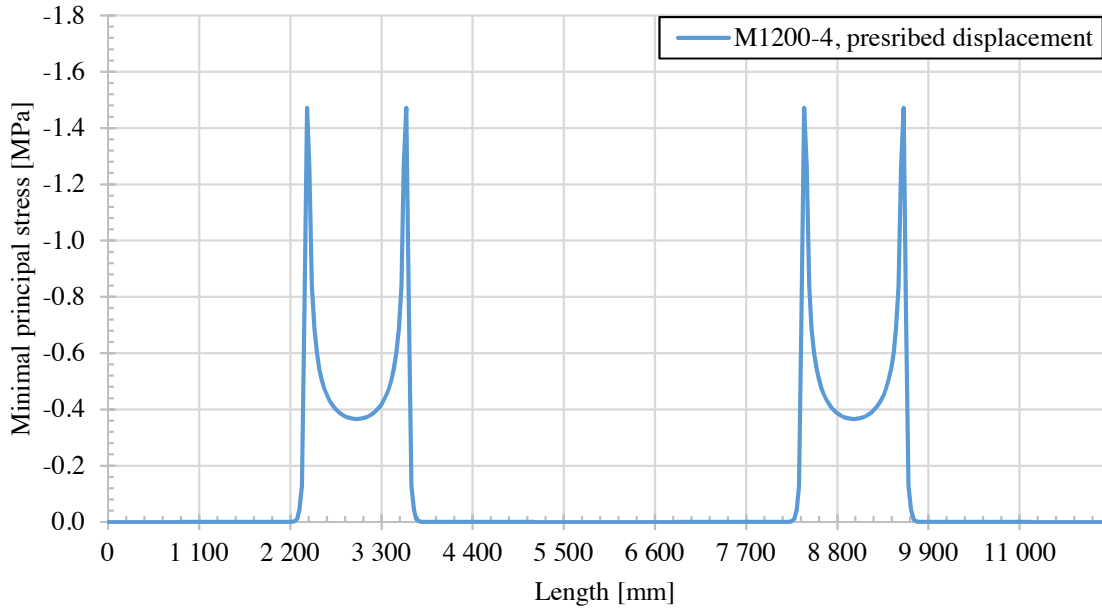
Figure E-11. *Stress distribution in top elements of Model M1200-4 with the load approach prescribed displacement.*
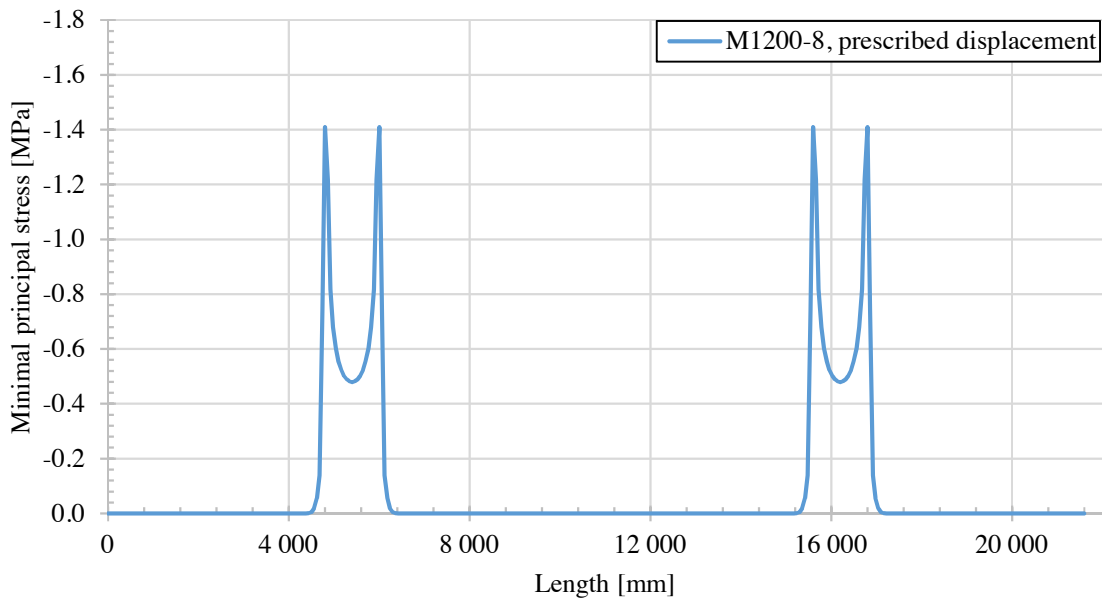
Figure E-12. *Stress distribution in top elements of Model M1200-8 with the load approach prescribed displacement.*

Table E-3. *Results from FE analyses of the analyses of Model M1200 including cracking and crushing pressure and type of observed crack.*

Model	R_2 [-]	R_1 [-]	Cracking pressure [N/mm^2]	Crushing pressure [N/mm^2]	Type of crack
M1200-1	1	0.6	0.30	0.39	Bending crack
M1200-2	2	0.6	0.42	0.34	Shear crack
M1200-4	4	0.6	0.61	0.52	Shear crack
M1200-8	8	0.6	0.86	0.70	Shear crack

6

APPENDIX F
Analytical calculations for Model M

Contents

Model M200

Ice pressure against bridge supports (Vägverket, 1987)
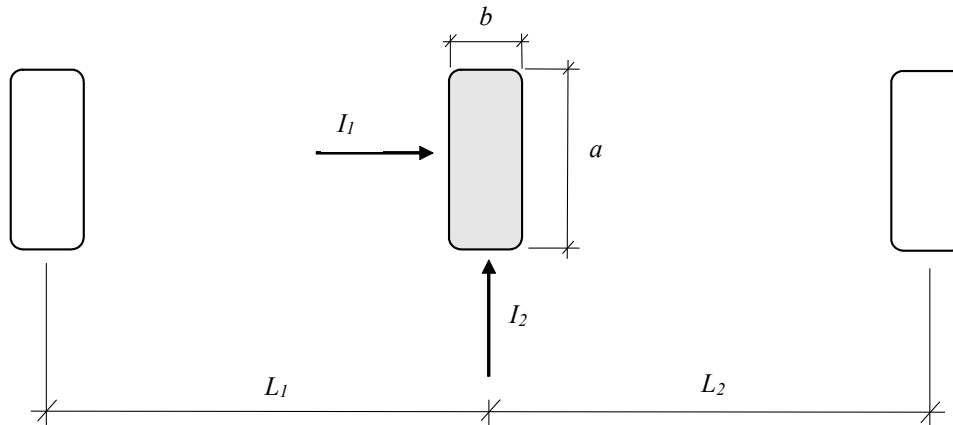
MODEL M200-1

Pressure from a moving ice sheet:

$b_{200} := 0.2m$ Column width

$a_{min} := 4m$ Minimal column height

$$a_{200} := \begin{vmatrix} b_{200} & \text{if } b_{200} > 4m & = 4 \cdot m \\ 4m & \text{if } b_{200} < 4m \end{vmatrix}$$ Column height

$L_{1.200.1} := b_{200} = 0.2\,m$ Distance to one adjacent column

$L_{2.200.1} := L_{1.200.1}$ Distance to second column, symmetry

$i_{2.min} := 10\dfrac{kN}{m}$ Minimum distributed ice load

$i_{2.max} := 30\dfrac{kN}{m}$ Maxmum distributed ice load

$$I_{2.min.200.1} := \frac{i_{2.min} \cdot (L_{1.200.1} + L_{2.200.1})}{2} = 2 \cdot kN \qquad \text{Minimum ice load from a moving ice sheet}$$

$$I_{2.max.200.1} := \frac{i_{2.max} \cdot (L_{1.200.1} + L_{2.200.1})}{2} = 6 \cdot kN \qquad \text{Maximum ice load from a moving ice sheet}$$

Pressure from a larger ice sheet:

$t := 0.3m$ Ice thickness

$$ar_{200} := \frac{b_{200}}{t} = 0.667 \qquad\qquad\qquad\qquad \text{Aspect ratio}$$

$$C_1 := \begin{pmatrix} 1.8 \\ 1.3 \\ 1.1 \\ 1.0 \\ 0.9 \\ 0.8 \end{pmatrix} \qquad ar := \begin{pmatrix} 0.5 \\ 1 \\ 1.5 \\ 2 \\ 3 \\ 4 \end{pmatrix} \qquad \begin{array}{l} \text{Shape factor, C1, with respect to aspect} \\ \text{ratio, ar} \end{array}$$

$$vs := lspline(ar, C_1)$$

$$C_{1.200} := interp(vs, ar, C_1, ar_{200}) = 1.611 \qquad \begin{array}{l} \text{Assuming linear relation between} \\ \text{the coefficients} \end{array}$$

$$\sigma_c := 1.4MPa \qquad\qquad\qquad\qquad\qquad \text{Crushing strength of the ice}$$

$$I_{2.200.1} := C_{1.200} \cdot \sigma_c \cdot b_{200} \cdot t = 135.361 \cdot kN \qquad \text{Ice load from a larger moving ice sheet}$$

Pressure on a column with a sharp and/or inclined edge:

a) From above   b) From the side

$\alpha := 180$ $\beta := 45$

$$C_{2.200}(\alpha) := \begin{vmatrix} 0.54 & \text{if } \alpha = 45 \\ 0.59 & \text{if } \alpha = 60 \\ 0.64 & \text{if } \alpha = 75 \\ 0.69 & \text{if } \alpha = 90 \\ 0.77 & \text{if } \alpha = 120 \\ 1.00 & \text{if } \alpha = 180 \\ 1 & \text{otherwise} \end{vmatrix}$$

Shape factor with respect to sharp edge

$C_{2.200}(\alpha) = 1$

$$C_{3.200}(\beta) := \begin{vmatrix} 1.0 & \text{if } 0 \le \beta \ge 15 \\ 0.75 & \text{if } 15 < \beta \ge 30 \\ 0.5 & \text{if } 30 < \beta \ge 45 \\ 1 & \text{otherwise} \end{vmatrix}$$

Shape factor with regard to inclination

$C_{3.200}(\beta) = 0.5$

$$C_{23.200} := \begin{vmatrix} 0.5 & \text{if } C_{2.200}(\alpha)\, C_{3.200}(\beta) < 0.5 & = 0.5 \\ C_{2.200}(\alpha)\, C_{3.200}(\beta) & \text{otherwise} \end{vmatrix}$$

$I_{22.200.1} := C_{1.200} \cdot C_{23.200} \cdot \sigma_c \cdot b_{200} \cdot t = 67.681 \cdot kN$

Maximum ice load for a sharp and/or inclined edge

Recommendations for design of offshore foundations exposed to ice load

Maximum static ice load due to crushing

$$k_1 := \begin{pmatrix} 1 \\ 0.9 \end{pmatrix}$$

Column shape factor: rectangular shape
                              circular shape

$$k_{1.200} := 1$$

$$k_2 := \begin{pmatrix} 0.5 \\ 1 \\ 1.5 \end{pmatrix}$$

Contact factor: continuously moving ice
                          ice frozen to the column surface
                          ice locally increased around the column

$$k_{2.200} := 1$$

$$k_{3.200} := \begin{vmatrix} 2.5 & \text{if } ar_{200} > 1 \\ \sqrt{1 + 5 \cdot ar_{200}} & \text{otherwise} \end{vmatrix} \quad = 2.082$$

Aspect ratio factor

$$b_{200} = 0.2\,m$$

Column width

Ice thickness

$$t = 0.3\,m$$

Crushing strength of ice

$$\sigma_c = 1.4 \cdot MPa$$

$$I_{h.crush} := k_{1.200} \cdot k_{2.200} \cdot k_{3.200} \cdot b_{200} \cdot t \cdot \sigma_c = 174.86 \cdot kN$$

Maximum static ice load due to crushing

MODEL M200-2

Pressure from a moving ice sheet:

$L_{1.200.2} := b_{200} \cdot 2 = 0.4\,m$ Distance to one adjacent column

$L_{2.200.2} := L_{1.200.2}$ Distance to second column, symmetry

$i_{2.min} = 10 \cdot \dfrac{kN}{m}$ Minimum distributed ice load

$i_{2.max} = 30 \cdot \dfrac{kN}{m}$ Maxmum distributed ice load

$I_{2.min.200.2} := \dfrac{i_{2.min} \cdot \left(L_{1.200.2} + L_{2.200.2} \right)}{2} = 4 \cdot kN$ Minimum ice load from a moving ice sheet

$I_{2.max.200.2} := \dfrac{i_{2.max} \cdot \left(L_{1.200.2} + L_{2.200.2} \right)}{2} = 12 \cdot kN$ Maximum ice load from a moving ice sheet

Pressure from a larger ice sheet:

$I_{2.200.2} := I_{2.200.1} = 135.361 \cdot kN$ Ice load from a larger moving ice sheet

Pressure on a column with a sharp and/or inclined edge:

$I_{22.200.2} := I_{22.200.1} = 67.681 \cdot kN$ Maximum ice load for a column with a sharp and/or inclined edge

Maximum static ice load due to crushing

$I_{h.crush} = 174.86 \cdot kN$ Maximum static ice load due to crushing

MODEL M200-4

Pressure from a moving ice sheet:

$L_{1.200.4} := b_{200} \cdot 4 = 0.8\,m$ Distance to one adjacent column

$L_{2.200.4} := L_{1.200.4}$ Distance to second column, symmetry

$i_{2.min} = 10 \cdot \dfrac{kN}{m}$ Minimum distributed ice load

$i_{2.max} = 30 \cdot \dfrac{kN}{m}$ Maxmum distributed ice load

$I_{2.min.200.4} := \dfrac{i_{2.min} \cdot \left(L_{1.200.4} + L_{2.200.4}\right)}{2} = 8 \cdot kN$ Minimum ice load from a moving ice sheet

$I_{2.max.200.4} := \dfrac{i_{2.max} \cdot \left(L_{1.200.4} + L_{2.200.4}\right)}{2} = 24 \cdot kN$ Maximum ice load from a moving ice sheet

Pressure from a larger ice sheet:

$I_{2.200.4} := I_{2.200.1} = 135.361 \cdot kN$ Ice load from a larger moving ice sheet

Pressure on a column with a sharp and/or inclined edge:

$I_{22.200.4} := I_{22.200.1} = 67.681 \cdot kN$ Maximum ice load for a column with
                                                               a sharp and/or inclined edge

Maximum static ice load due to crushing

$I_{h.crush} = 174.86 \cdot kN$ Maximum static ice load due to crushing

MODEL M200-8

Pressure from a moving ice sheet:

$L_{1.200.8} := b_{200} \cdot 8 = 1.6\,\text{m}$

Distance to one adjacent column

$L_{2.200.8} := L_{1.200.8}$

Distance to second column, symmetry

$i_{2.min} = 10 \cdot \dfrac{\text{kN}}{\text{m}}$

Minimum distributed ice load

$i_{2.max} = 30 \cdot \dfrac{\text{kN}}{\text{m}}$

Maxmum distributed ice load

$I_{2.min.200.8} := \dfrac{i_{2.min} \cdot \left(L_{1.200.8} + L_{2.200.8}\right)}{2} = 16 \cdot \text{kN}$ Minimum ice load from a moving ice sheet

$I_{2.max.200.8} := \dfrac{i_{2.max} \cdot \left(L_{1.200.8} + L_{2.200.8}\right)}{2} = 48 \cdot \text{kN}$ Maximum ice load from a moving ice sheet

Pressure from a larger ice sheet:

$I_{2.200.8} := I_{2.200.1} = 135.361 \cdot \text{kN}$

Ice pressure from a larger moving ice sheet

Pressure on a column with a sharp and/or inclined edge:

$I_{22.200.8} := I_{22.200.1} = 67.681 \cdot \text{kN}$

Maximum ice load for a column with
a sharp and/or inclined edge

Maximum static ice load due to crushing

$I_{h.crush} = 174.86 \cdot \text{kN}$

Maximum static ice load due to crushing

Model M600

Ice pressure against bridge supports (Vägverket, 1987)
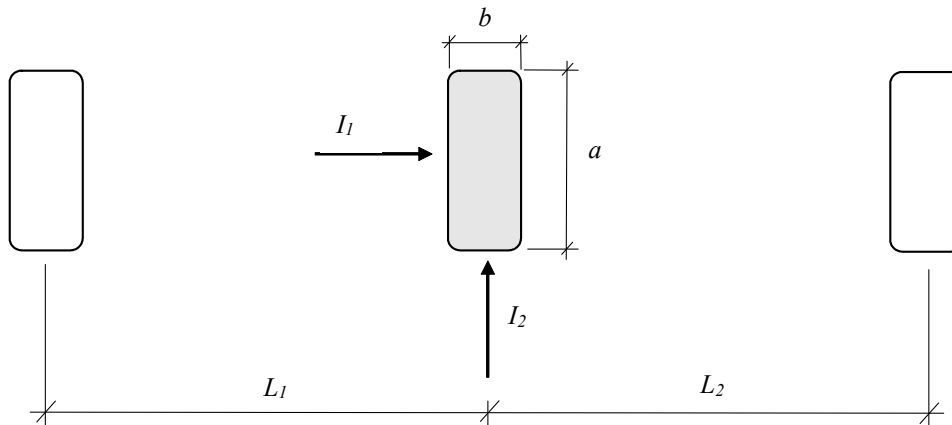
MODEL M600-1

Pressure from a moving ice sheet:

$b_{600} := 0.6m$ Column width

$a_{min} := 4m$ Minimal column height

$$a_{600} := \begin{vmatrix} b_{600} & \text{if } b_{600} > 4m & = 4 \cdot m \\ 4m & \text{if } b_{600} < 4m \end{vmatrix}$$ Column height

$L_{1.600.1} := b_{600} = 0.6\,m$ Distance to one adjacent column

$L_{2.600.1} := L_{1.600.1}$ Distance to second column, symmetry

$i_{2.min} := 10\dfrac{kN}{m}$ Minimum distributed ice load

$i_{2.max} := 30\dfrac{kN}{m}$ Maxmum distributed ice load

$$I_{2.min.600.1} := \frac{i_{2.min} \cdot \left(L_{1.600.1} + L_{2.600.1}\right)}{2} = 6 \cdot kN$$ Minimum ice load from a moving ice sheet

$$I_{2.max.600.1} := \frac{i_{2.max} \cdot \left(L_{1.600.1} + L_{2.600.1}\right)}{2} = 18 \cdot kN$$ Maximum ice load from a moving ice sheet

Pressure from a larger ice sheet:

$t := 0.3m$ Ice thickness

$$ar_{600} := \frac{b_{600}}{t} = 2$$ Aspect ratio

$$C_1 := \begin{pmatrix} 1.8 \\ 1.3 \\ 1.1 \\ 1.0 \\ 0.9 \\ 0.8 \end{pmatrix} \qquad ar := \begin{pmatrix} 0.5 \\ 1 \\ 1.5 \\ 2 \\ 3 \\ 4 \end{pmatrix}$$ Shape factor, C1, with respect to aspect ratio, ar

$vs := lspline(ar, C_1)$

$C_{1.600} := interp(vs, ar, C_1, ar_{600}) = 1$ Assuming linear relation between the coefficients

$\sigma_c := 1.4MPa$ Crushing strength of the ice

$I_{2.600.1} := C_{1.600} \cdot \sigma_c \cdot b_{600} \cdot t = 252 \cdot kN$ Ice load from a larger moving ice sheet

Pressure on a column with a sharp and/or inclined edge:
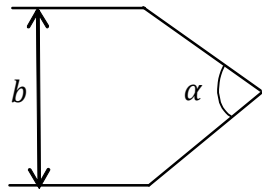
a) From above
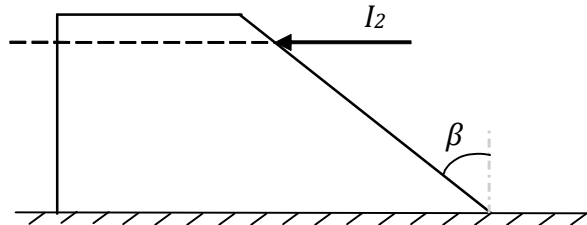
b) From the side

$\alpha := 45 \qquad \beta := 0$

$$C_{2.600}(\alpha) := \begin{cases} 0.54 & \text{if } \alpha = 45 \\ 0.59 & \text{if } \alpha = 60 \\ 0.64 & \text{if } \alpha = 75 \\ 0.69 & \text{if } \alpha = 90 \\ 0.77 & \text{if } \alpha = 120 \\ 1.00 & \text{if } \alpha = 180 \\ 1 & \text{otherwise} \end{cases}$$

Shape factor with respect to sharp edge

$C_{2.600}(\alpha) = 0.54$

$$C_{3.600}(\beta) := \begin{cases} 1.0 & \text{if } 0 \le \beta \ge 15 \\ 0.75 & \text{if } 15 < \beta \ge 30 \\ 0.5 & \text{if } 30 < \beta \ge 45 \\ 1 & \text{otherwise} \end{cases}$$

Shape factor with regard to inclination

$C_{3.600}(\beta) = 1$

$$C_{23.600} := \begin{cases} 0.5 & \text{if } C_{2.600}(\alpha)\,C_{3.600}(\beta) < 0.5 \quad = 0.54 \\ C_{2.600}(\alpha)\,C_{3.600}(\beta) & \text{otherwise} \end{cases}$$

$I_{22.600.1} := C_{1.600} \cdot C_{23.600} \cdot \sigma_c \cdot b_{600} \cdot t = 136.08 \cdot \text{kN}$

Maximum ice load for a sharp and/or inclined edge

Recommendations for design of offshore foundations exposed to ice load

Maximum static ice load due to crushing

$k_1 := \begin{pmatrix} 1 \\ 0.9 \end{pmatrix}$

Column shape factor: rectangular shape
                               circular shape

$k_{1.600} := 1$

$k_2 := \begin{pmatrix} 0.5 \\ 1 \\ 1.5 \end{pmatrix}$

Contact factor: continuously moving ice
                    ice frozen to the column surface
                    ice locally increased around the column

$k_{2.600} := 1$

$k_{3.600} := \begin{vmatrix} 2.5 & \text{if } ar_{600} > 1 \\ \sqrt{1 + 5 \cdot ar_{600}} & \text{otherwise} \end{vmatrix} = 2.5$

Aspect ratio factor

$b_{600} = 0.6\,m$

Column width

Ice thickness

$t = 0.3\,m$

Crushing strength of ice

$\sigma_c = 1.4 \cdot MPa$

$I_{h.crush} := k_{1.600} \cdot k_{2.600} \cdot k_{3.600} \cdot b_{600} \cdot t \cdot \sigma_c = 630 \cdot kN$

Maximum static ice load due to crushing

MODEL M600-2

Pressure from a moving ice sheet:

$L_{1.600.2} := b_{600} \cdot 2 = 1.2 \, m$ Distance to one adjacent column

$L_{2.600.2} := L_{1.600.2}$ Distance to second column, symmetry

$i_{2.min} = 10 \cdot \dfrac{kN}{m}$ Minimum distributed ice load

$i_{2.max} = 30 \cdot \dfrac{kN}{m}$ Maxmum distributed ice load

$I_{2.min.600.2} := \dfrac{i_{2.min} \cdot \left(L_{1.600.2} + L_{2.600.2} \right)}{2} = 12 \cdot kN$ Minimum ice load from a moving ice sheet

$I_{2.max.600.2} := \dfrac{i_{2.max} \cdot \left(L_{1.600.2} + L_{2.600.2} \right)}{2} = 36 \cdot kN$ Maximum ice load from a moving ice sheet

Pressure from a larger ice sheet:

$I_{2.600.2} := I_{2.600.1} = 252 \cdot kN$ Ice load from a larger moving ice sheet

Pressure on a column with a sharp and/or inclined edge:

$I_{22.600.2} := I_{22.600.1} = 136.08 \cdot kN$ Maximum ice load for a column with a sharp and/or inclined edge

Maximum static ice load due to crushing

$I_{h.crush} = 630 \cdot kN$ Maximum static ice load due to crushing

MODEL M600-4

Pressure from a moving ice sheet:

$L_{1.600.4} := b_{600} \cdot 4 = 2.4\,\text{m}$

Distance to one adjacent column

$L_{2.600.4} := L_{1.600.4}$

Distance to second column, symmetry

$i_{2.min} = 10 \cdot \dfrac{\text{kN}}{\text{m}}$

Minimum distributed ice load

$i_{2.max} = 30 \cdot \dfrac{\text{kN}}{\text{m}}$

Maxmum distributed ice load

$I_{2.min.600.4} := \dfrac{i_{2.min} \cdot \left(L_{1.600.4} + L_{2.600.4} \right)}{2} = 24 \cdot \text{kN}$ Minimum ice load from a moving ice sheet

$I_{2.max.600.4} := \dfrac{i_{2.max} \cdot \left(L_{1.600.4} + L_{2.600.4} \right)}{2} = 72 \cdot \text{kN}$ Maximum ice load from a moving ice sheet

Pressure from a larger ice sheet:

$I_{2.600.4} := I_{2.600.1} = 252 \cdot \text{kN}$

Ice load from a larger moving ice sheet

Pressure on a column with a sharp and/or inclined edge:

$I_{22.600.4} := I_{22.600.1} = 136.08 \cdot \text{kN}$

Maximum ice load for a column with
a sharp and/or inclined edge

Maximum static ice load due to crushing

$I_{h.crush} = 630 \cdot \text{kN}$

Maximum static ice load due to crushing

MODEL M600-8

Pressure from a moving ice sheet:

$L_{1.600.8} := b_{600} \cdot 8 = 4.8\,m$ Distance to one adjacent column

$L_{2.600.8} := L_{1.600.8}$ Distance to second column, symmetry

$i_{2.min} = 10 \cdot \dfrac{kN}{m}$ Minimum distributed ice load

$i_{2.max} = 30 \cdot \dfrac{kN}{m}$ Maxmum distributed ice load

$I_{2.min.600.8} := \dfrac{i_{2.min} \cdot \left(L_{1.600.8} + L_{2.600.8}\right)}{2} = 48 \cdot kN$ Minimum ice load from a moving ice sheet

$I_{2.max.600.8} := \dfrac{i_{2.max} \cdot \left(L_{1.600.8} + L_{2.600.8}\right)}{2} = 144 \cdot kN$ Maximum ice load from a moving ice sheet

Pressure from a larger ice sheet:

$I_{2.600.8} := I_{2.600.1} = 252 \cdot kN$ Ice pressure from a larger moving ice sheet

Pressure on a column with a sharp and/or inclined edge:

$I_{22.600.8} := I_{22.600.1} = 136.08 \cdot kN$ Maximum ice load for a column with a sharp and/or inclined edge

Maximum static ice load due to crushing

$I_{h.crush} = 630 \cdot kN$ Maximum static ice load due to crushing

Model M1200

Ice pressure against bridge supports (Vägverket, 1987)
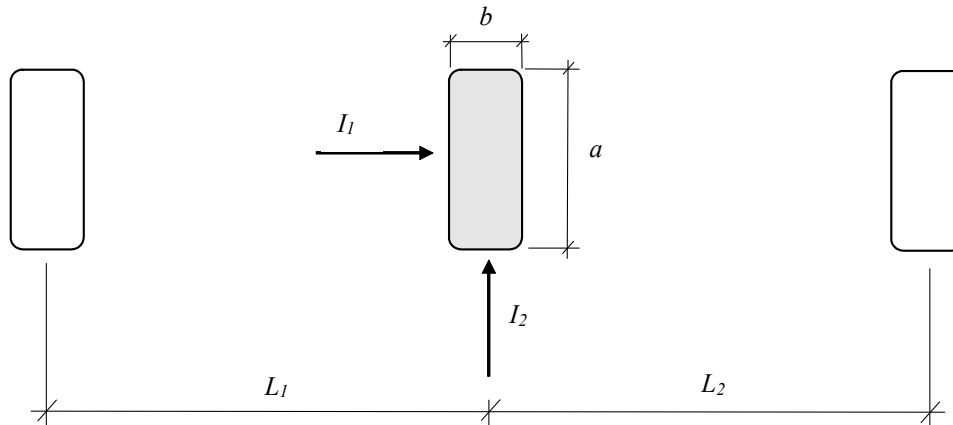
MODEL M1200-1

Pressure from a moving ice sheet:

$b_{1200} := 1.2m$

Column width

$a_{min} := 4m$

Minimal column height

$a_{1200} := \begin{vmatrix} b_{1200} & \text{if } b_{1200} > 4m & = 4 \cdot m \\ 4m & \text{if } b_{1200} < 4m \end{vmatrix}$

Column height

$L_{1.1200.1} := b_{1200} = 1.2\,m$

Distance to one adjacent column

$L_{2.1200.1} := L_{1.1200.1}$

Distance to second column, symmetry

$i_{2.min} := 10 \dfrac{kN}{m}$

Minimum distributed ice load

$i_{2.max} := 30 \dfrac{kN}{m}$

Maxmum distributed ice load

$$I_{2.min.1200.1} := \frac{i_{2.min} \cdot \left(L_{1.1200.1} + L_{2.1200.1}\right)}{2} = 12 \cdot kN \quad \text{Minimum ice load from a moving ice sheet}$$

$$I_{2.max.1200.1} := \frac{i_{2.max} \cdot \left(L_{1.1200.1} + L_{2.1200.1}\right)}{2} = 36 \cdot kN \quad \text{Maximum ice load from a moving ice sheet}$$

Pressure from a larger ice sheet:

$t := 0.3m$ Ice thickness

$$ar_{1200} := \frac{b_{1200}}{t} = 4 \quad \text{Aspect ratio}$$

$$C_1 := \begin{pmatrix} 1.8 \\ 1.3 \\ 1.1 \\ 1.0 \\ 0.9 \\ 0.8 \end{pmatrix} \qquad ar := \begin{pmatrix} 0.5 \\ 1 \\ 1.5 \\ 2 \\ 3 \\ 4 \end{pmatrix}$$

Shape factor, C1, with respect to aspect ratio, ar

$$vs := lspline\left(ar, C_1\right)$$

$$C_{1.1200} := interp\left(vs, ar, C_1, ar_{1200}\right) = 0.8$$

Assuming linear relation between the coefficients

$\sigma_c := 1.4MPa$ Crushing strength of the ice

$$I_{2.1200.1} := C_{1.1200} \cdot \sigma_c \cdot b_{1200} \cdot t = 403.2 \cdot kN \quad \text{Ice load from a larger moving ice sheet}$$

Pressure on a column with a sharp and/or inclined edge:
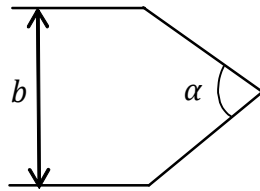
a) From above
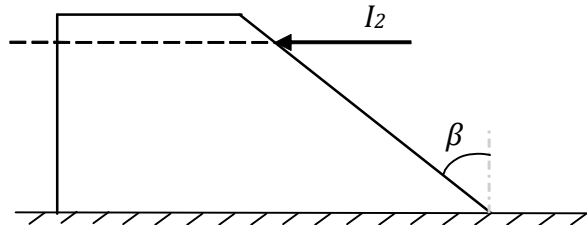
b) From the side

$\alpha := 45$　　　　$\beta := 35$

$$C_{2.1200}(\alpha) := \begin{vmatrix} 0.54 & \text{if } \alpha = 45 \\ 0.59 & \text{if } \alpha = 60 \\ 0.64 & \text{if } \alpha = 75 \\ 0.69 & \text{if } \alpha = 90 \\ 0.77 & \text{if } \alpha = 120 \\ 1.00 & \text{if } \alpha = 180 \\ 1 & \text{otherwise} \end{vmatrix}$$　　Shape factor with respect to sharp edge

$C_{2.1200}(\alpha) = 0.54$

$$C_{3.1200}(\beta) := \begin{vmatrix} 1.0 & \text{if } 0 \le \beta \ge 15 \\ 0.75 & \text{if } 15 < \beta \ge 30 \\ 0.5 & \text{if } 30 < \beta \ge 45 \\ 1 & \text{otherwise} \end{vmatrix}$$　　Shape factor with regard to inclination

$C_{3.1200}(\beta) = 0.75$

$$C_{23.1200} := \begin{vmatrix} 0.5 & \text{if } C_{2.1200}(\alpha)\,C_{3.1200}(\beta) < 0.5 & = 0.5 \\ C_{2.1200}(\alpha)\,C_{3.1200}(\beta) & \text{otherwise} \end{vmatrix}$$

$I_{22.1200.1} := C_{1.1200} \cdot C_{23.1200} \cdot \sigma_c \cdot b_{1200} \cdot t = 201.6 \cdot kN$　　Maximum ice load for a sharp and/or inclined edge

Recommendations for design of offshore foundations exposed to ice load

Maximum static ice load due to crushing

$k_1 := \begin{pmatrix} 1 \\ 0.9 \end{pmatrix}$

$k_{1.1200} := 1$

$k_2 := \begin{pmatrix} 0.5 \\ 1 \\ 1.5 \end{pmatrix}$

$k_{2.1200} := 1$

$k_{3.1200} := \begin{vmatrix} 2.5 & \text{if } ar_{1200} > 1 \\ \sqrt{1 + 5 \cdot ar_{1200}} & \text{otherwise} \end{vmatrix} = 2.5$

$b_{1200} = 1.2\,m$

$t = 0.3\,m$

$\sigma_c = 1.4 \cdot MPa$

Column shape factor: rectangular shape
                                     circular shape

Contact factor: continuously moving ice
                         ice frozen to the column surface
                         ice locally increased around the column

Aspect ratio factor

Column width

Ice thickness

Crushing strength of ice

$I_{h.crush} := k_{1.1200} \cdot k_{2.1200} \cdot k_{3.1200} \cdot b_{1200} \cdot t \cdot \sigma_c = 1.26 \times 10^3 \cdot kN$

Maximum static ice load due to crushing

MODEL M1200-2

Pressure from a moving ice sheet:

$L_{1.1200.2} := b_{1200} \cdot 2 = 2.4\,m$

Distance to one adjacent column

$L_{2.1200.2} := L_{1.1200.2}$

Distance to second column, symmetry

$i_{2.min} = 10 \cdot \dfrac{kN}{m}$

Minimum distributed ice load

$i_{2.max} = 30 \cdot \dfrac{kN}{m}$

Maxmum distributed ice load

$I_{2.min.1200.2} := \dfrac{i_{2.min} \cdot \left(L_{1.1200.2} + L_{2.1200.2}\right)}{2} = 24 \cdot kN$ Minimum ice load from a moving ice sheet

$I_{2.max.1200.2} := \dfrac{i_{2.max} \cdot \left(L_{1.1200.2} + L_{2.1200.2}\right)}{2} = 72 \cdot kN$ Maximum ice load from a moving ice sheet

Pressure from a larger ice sheet:

$I_{2.1200.2} := I_{2.1200.1} = 403.2 \cdot kN$

Ice load from a larger moving ice sheet

Pressure on a column with a sharp and/or inclined edge:

$I_{22.1200.2} := I_{22.1200.1} = 201.6 \cdot kN$

Maximum ice load for a column with
a sharp and/or inclined edge

Maximum static ice load due to crushing

$I_{h.crush} = 1.26 \times 10^3 \cdot kN$

Maximum static ice load due to crushing

MODEL M1200-4

Pressure from a moving ice sheet:

$L_{1.1200.4} := b_{1200} \cdot 4 = 4.8\,m$

Distance to one adjacent column

$L_{2.1200.4} := L_{1.1200.4}$

Distance to second column, symmetry

$i_{2.min} = 10 \cdot \dfrac{kN}{m}$

Minimum distributed ice load

$i_{2.max} = 30 \cdot \dfrac{kN}{m}$

Maxmum distributed ice load

$I_{2.min.1200.4} := \dfrac{i_{2.min} \cdot \left(L_{1.1200.4} + L_{2.1200.4}\right)}{2} = 48 \cdot kN$ Minimum ice load from a moving ice sheet

$I_{2.max.1200.4} := \dfrac{i_{2.max} \cdot \left(L_{1.1200.4} + L_{2.1200.4}\right)}{2} = 144 \cdot kN$ Maximum ice load from a moving ice sheet

Pressure from a larger ice sheet:

$I_{2.1200.4} := I_{2.1200.1} = 403.2 \cdot kN$

Ice load from a larger moving ice sheet

Pressure on a column with a sharp and/or inclined edge:

$I_{22.1200.4} := I_{22.1200.1} = 201.6 \cdot kN$

Maximum ice load for a column with
a sharp and/or inclined edge

Maximum static ice load due to crushing

$I_{h.crush} = 1.26 \times 10^3 \cdot kN$

Maximum static ice load due to crushing

MODEL M1200-8

Pressure from a moving ice sheet:

$L_{1.1200.8} := b_{1200} \cdot 8 = 9.6 \, m$ Distance to one adjacent column

$L_{2.1200.8} := L_{1.1200.8}$ Distance to second column, symmetry

$i_{2.min} = 10 \cdot \dfrac{kN}{m}$ Minimum distributed ice load

$i_{2.max} = 30 \cdot \dfrac{kN}{m}$ Maxmum distributed ice load

$I_{2.min.1200.8} := \dfrac{i_{2.min} \cdot \left(L_{1.1200.8} + L_{2.1200.8}\right)}{2} = 96 \cdot kN$ Minimum ice load from a moving ice sheet

$I_{2.max.1200.8} := \dfrac{i_{2.max} \cdot \left(L_{1.1200.8} + L_{2.1200.8}\right)}{2} = 288 \cdot kN$ Maximum ice load from a moving ice sheet

Pressure from a larger ice sheet:

$I_{2.1200.8} := I_{2.1200.1} = 403.2 \cdot kN$ Ice pressure from a larger moving ice sheet

Pressure on a column with a sharp and/or inclined edge:

$I_{22.1200.8} := I_{22.1200.1} = 201.6 \cdot kN$ Maximum ice load for a column with a sharp and/or inclined edge

Maximum static ice load due to crushing

$I_{h.crush} = 1.26 \times 10^3 \cdot kN$ Maximum static ice load due to crushing

APPENDIX G
Comparison between the analytical calculations and the numerical results

G1.   NUMERICAL RESULTS FROM THE FE ANALYSES

Table G-1.   Results from the FE analyses for all models.

Model	Applied load at local cracking [kN]	Applied load at local crushing [kN]	Crushing load, under stress distribution curve [kN]	Theoretical max load w.r.t. crushing [kN]	Load at plastic limit [kN]
S200	29	12	27	280	100
S600	91	38	84	840	299
S1200	182	74	192	1680	598
M200-1	19	36	42	280	62
M200-2	27	31	35	280	96
M200-4	45	38	45	280	103
M200-8	64	51	65	280	109
M600-1	53	68	77	840	126
M600-2	79	68	80	840	169
M600-4	111	90	101	840	302
M600-8	139	112	127	840	311
M1200-1	107	141	149	1680	252
M1200-2	151	122	151	1680	551
M1200-4	220	188	210	1680	605
M1200-8	311	251	284	1680	630
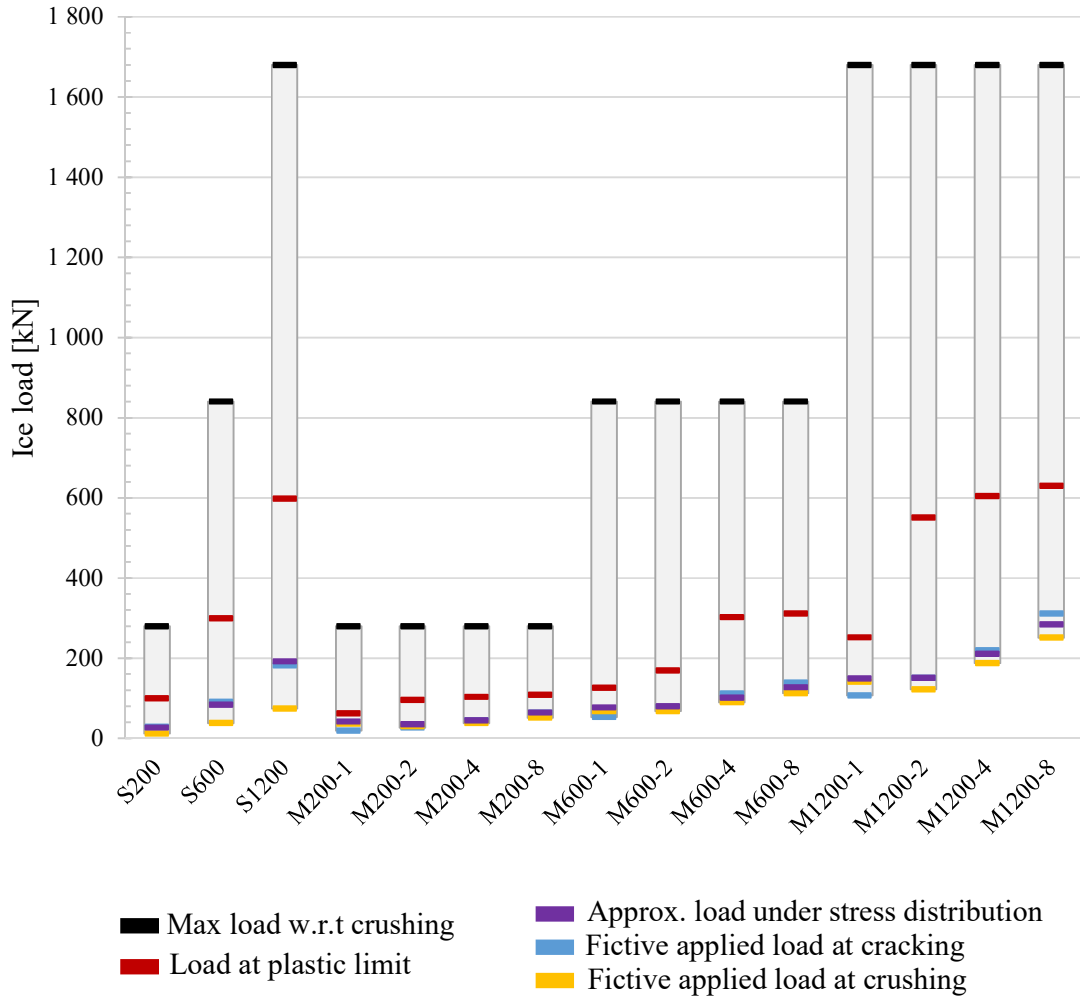
Figure G-1.   *The range of numerical results from the FE analyses for each model, from Table G-1.*

G2. RESULTS FROM MODEL S

Table G-2. *Results from the FE analyses, according to Table G-1, and calculations according to guidelines, see Appendix D, for Model S.*

		S200[kN]	S600[kN]	S1200[kN]
FE results	Fictive applied load at local cracking	29	91	182
	Fictive applied load at local crushing	12	38	74
	Load at plastic limit	100	299	598
Theoretical max load w.r.t. crushing		280	840	1680
TDOK 2016:0204 (Trafikverket, 2016a, 2016b)		200	200	200
RIDAS (RIDAS, 2012b)		10	30	60
Other recom. (Fransson and Bergdahl, 2009)	Maximum static force due to crushing	175	360	1260
VV 1987:43, *LC2*	Larger ice sheet	135	252	403
VV 1987:43, *LC3*	Sharp and inclined edge, $\alpha=180$ $\beta=0$	135	252	403
	$\alpha=45$ $\beta=0$	73	136	218
	$\alpha=180$ $\beta=45$	68	126	202

G3. RESULTS FROM MODEL M200

The same output from FE analyses, as for Model S, was extracted for Model M200. The result together with the calculations from the guidelines are shown in Table G-3.

Table G-3.   *Results from the FE analyses, according to Table G-1, and calculations according to standards, see Appendix F, for Model M200.*

		M200-1 [kN]	M200-2 [kN]	M200-4 [kN]	M200-8 [kN]
FE results	Fictive applied load at local cracking	19	27	45	64
	Fictive applied load at local crushing	36	31	38	51
	Load at plastic limit	62	96	103	109
Theoretical max load w.r.t. crushing		280	280	280	280
TDOK 2016:0204 (Trafikverket, 2016a, 2016b)		200	200	200	200
RIDAS (RIDAS, 2012b)		10	10	10	10
Other recom. (Fransson and Bergdahl, 2009)	Maximum static force due to crushing	175	175	175	175
VV 1987:43, *LC1*	Moving ice sheet, minimum	2	4	8	16
	Moving ice sheet, maximum	6	12	24	48
VV 1987:43, *LC2*	Larger ice sheet	135	135	135	135
VV 1987:43, *LC3*	Sharp and inclined edge, α=180 β=0	135	135	135	135
	α=45 β=0	73	73	73	73
	α=180 β=45	68	68	68	68

G4. RESULTS FROM MODEL M600

Table G-4. *Results from the FE analyses, according to Table G-1, and calculations according to standards, see Appendix F, for Model M600.*

		M600-1 [kN]	M600-2 [kN]	M600-4 [kN]	M600-8 [kN]
FE results	Fictive applied load at local cracking	53	79	111	139
	Fictive applied load at local crushing	68	68	90	112
	Load at plastic limit	126	169	302	311
Theoretical max load w.r.t. crushing		480	480	480	480
TDOK 2016:0204 (Trafikverket, 2016a, 2016b)		200	200	200	200
RIDAS (RIDAS, 2012b)		30	30	30	30
Other recom. (Fransson and Bergdahl, 2009)	Maximum static force due to crushing	630	630	630	630
VV 1987:43, *LC1*	Moving ice sheet, minimum	6	12	24	48
	Moving ice sheet, maximum	18	36	72	144
VV 1987:43, *LC2*	Larger ice sheet	252	252	252	252
VV 1987:43, *LC3*	Sharp and inclined edge, $\alpha=180\ \beta=0$	252	252	252	252
	$\alpha=45\ \beta=0$	136	136	136	136
	$\alpha=180\ \beta=45$	126	126	126	126

G5. RESULTS FROM MODEL M1200

Table G-5. *Results from the FE analyses, according to Table G-1, and calculations according to standards, see Appendix F, for Model M1200.*

		M1200-1 [kN]	M1200-2 [kN]	M1200-4 [kN]	M1200-8 [kN]
FE results	Fictive applied load at local cracking	107	151	220	311
	Fictive applied load at local crushing	141	122	188	251
	Load at plastic limit	252	551	605	630
Theoretical max load w.r.t. crushing		1680	1680	1680	1680
TDOK 2016:0204 (Trafikverket, 2016a, 2016b)		200	200	200	200
RIDAS (RIDAS, 2012b)		60	60	60	60
Other recom. (Fransson and Bergdahl, 2009)	Maximum static force due to crushing	1260	1260	1260	1260
VV 1987:43, *LC1*	Moving ice sheet, minimum	12	24	48	96
	Moving ice sheet, maximum	36	72	144	288
VV 1987:43, *LC2*	Larger ice sheet	403	403	403	403
VV 1987:43, *LC3*	Sharp and inclined edge, $\alpha=180$ $\beta=0$	403	403	403	403
	$\alpha=45$ $\beta=0$	218	218	218	218
	$\alpha=180$ $\beta=45$	201	201	201	201